

# 495: Mechanical Properties of Soft Materials

Department of Materials Science and Engineering  
Northwestern University

April 20, 2022

## Contents

<b>1</b>	<b>Course Description</b>	<b>6</b>
<b>2</b>	<b>Introduction</b>	<b>7</b>
<b>3</b>	<b>Stress and Strain</b>	<b>9</b>
3.1	Tensor Representation of Stress . . . . .	9
3.2	Tensor Transformation Law . . . . .	11
3.3	Principal Stresses . . . . .	16
3.4	Strain . . . . .	25
3.5	Deformation Modes . . . . .	29
3.6	Representative Moduli . . . . .	35
3.7	Speed of Sound . . . . .	35
<b>4</b>	<b>Matrix Representation</b>	<b>37</b>
4.1	Compliance matrix . . . . .	37
4.2	Stiffness Matrix . . . . .	38
4.3	Symmetry Requirements . . . . .	38
<b>5</b>	<b>Amorphous Polymers</b>	<b>46</b>
5.1	End-to-end Vector . . . . .	47
5.2	1D Random Walk . . . . .	47
5.3	Average of a Function . . . . .	48
5.4	Averages for Random Walks . . . . .	50
5.5	3D Random Walks . . . . .	51
<b>6</b>	<b>Rubber Elasticity</b>	<b>55</b>
6.1	Molecular Deformation . . . . .	55
6.2	Free energy of a stretched rubber . . . . .	57
6.3	Free energy change due to deformation . . . . .	57

6.4	Shear deformation of an elastomer . . . . .	59
6.5	Uniaxial deformation of an elastomer . . . . .	60
<b>7</b>	<b>Finite (Large) Strain</b>	<b>62</b>
<b>8</b>	<b>Viscoelasticity</b>	<b>63</b>
8.1	Intro to Time-Dependent Behavior . . . . .	63
8.2	Shear Relaxation Modulus . . . . .	68
8.3	Boltzmann Superposition Principle . . . . .	69
8.4	Idealized Relaxation Curves . . . . .	71
8.5	Temperature Dependence . . . . .	73
8.6	Relationships between $G^*(\omega)$ and $G(t)$ . . . . .	74
8.7	Torsional Resonator . . . . .	76
8.8	Viscoelastic Models . . . . .	78
8.9	Time-Temp. Shifting . . . . .	85
<b>9</b>	<b>The Glass Transition</b>	<b>89</b>
9.1	Free volume . . . . .	89
9.2	Enthalpy and Heat Capacity . . . . .	93
9.3	DSC . . . . .	93
<b>10</b>	<b>Contact Mechanics</b>	<b>95</b>
10.1	Sign conventions . . . . .	95
10.2	Flat Punch Indentation . . . . .	96
10.3	Energy Release Rate . . . . .	98
10.4	Contact of Paraboloids . . . . .	107
10.5	Indentation with Berkovich Trips . . . . .	110
<b>11</b>	<b>Fracture</b>	<b>113</b>
11.1	Fracture Modes . . . . .	113
11.2	Stress Concentrations . . . . .	114
11.3	Stress Intensity Factor . . . . .	115
11.4	Fracture condition . . . . .	118
11.5	General relationship between $K$ and $\mathcal{G}$ . . . . .	119
11.6	Some Specific Geometries . . . . .	120
11.7	Fracture Toughness of Materials . . . . .	124
<b>12</b>	<b>Yield Behavior</b>	<b>127</b>
12.1	Yield Surfaces . . . . .	127
12.2	Localized Deformation . . . . .	130
<b>13</b>	<b>Weibull Analysis of Failure</b>	<b>135</b>
<b>14</b>	<b>Deformation of Polymers</b>	<b>138</b>
<b>15</b>	<b>Case Study: Triblock Gels</b>	<b>147</b>

15.1	Introduction	147
15.2	Gelcasting	148
15.3	Solid/Liquid Transition	149
15.4	Glass Transition	152
15.5	Gel Modulus	155
15.6	Hydrogels: Water as the Solvent	156
<b>16</b>	<b>Creep Behavior</b>	<b>161</b>
16.1	Linear Creep	161
16.2	Nonlinear Creep	162
16.3	Use of empirical, analytic expressions	163
16.4	Eyring Model of Steady State Creep	164
<b>17</b>	<b>495 Problems</b>	<b>168</b>
17.1	Course Organization	168
17.2	The Stress Tensor	168
17.3	Strains	169
17.4	Typical Moduli	169
17.5	Matrix Representation of Stress and Strains	169
17.6	Rubber Elasticity	171
17.7	Viscoelasticity	172
17.8	Contact Mechanics	176
17.9	Nanoindentation	177
17.10	Fracture Mechanics	179
17.11	Weibull Statistics	181
17.12	Yield Criteria	182
17.13	Nonlinear Viscoelasticity and Creep	184
17.14	Polymer Swelling	185
<b>A</b>	<b>Synthetic Polymers</b>	<b>187</b>
A.1	What is a Polymer	187
A.2	Classification Scheme	187
A.3	Understanding Polymer Chemistry	189
<b>B</b>	<b>Polymerization Reactions</b>	<b>193</b>
B.1	Step-Growth	193
B.2	Interfacial Polymerizations	195
<b>C</b>	<b>Non-Linear Step Growth</b>	<b>198</b>
C.1	Gelation	198
C.2	Prepolymers	198
C.3	Corothers Theory	199
<b>D</b>	<b>Chain-Growth</b>	<b>203</b>
D.1	Mechanisms	203
D.2	Reactive Species	204

D.3	Initiation . . . . .	204
D.4	Termination . . . . .	205
D.5	Intramolecular Chain Transfer . . . . .	208
D.6	Dienes . . . . .	209
D.7	Living Polymerizations . . . . .	211
D.8	Tacticity . . . . .	211
D.9	Crosslinking . . . . .	212
<b>E</b>	<b>Common Polymers</b>	<b>214</b>
E.1	Add. to a Double Bond . . . . .	214
E.2	Ring Opening . . . . .	220
E.3	Step Growth . . . . .	221
E.4	Copolymers . . . . .	224
<b>F</b>	<b>Chain Dimensions</b>	<b>227</b>
F.1	General Considerations . . . . .	227
F.2	Freely Jointed Chain Model . . . . .	229
F.3	Freely Rotating Chain Model . . . . .	229
F.4	Bond Angle Restrictions . . . . .	231
F.5	Characteristic Ratio . . . . .	232
F.6	Self-Avoiding Random Walks . . . . .	234
<b>G</b>	<b>Semicrystalline Polymers</b>	<b>235</b>
G.1	Structural Hierarchy in Semicrystalline Polymers . . . . .	235
G.2	The Structural Repeat Unit . . . . .	235
G.3	Helix Formation . . . . .	236
G.4	Crystalline unit cells . . . . .	238
G.5	Single Crystal Stiffness . . . . .	240
G.6	Chain Folding . . . . .	241
G.7	Spherulitic morphologies . . . . .	243
G.8	Birefringence . . . . .	245
G.9	Growth of a Lamellar Crystallite . . . . .	246
G.10	Density . . . . .	248
<b>H</b>	<b>Solutions and Blends</b>	<b>250</b>
H.1	Chemical Potentials . . . . .	251
H.2	Ideal Entropy of Mixing for Polymers . . . . .	254
H.3	Idealized Enthalpy of Mixing . . . . .	255
H.4	Flory-Huggins . . . . .	259
H.5	Binodal and Spinodal . . . . .	260
H.6	Critical Point . . . . .	262
H.7	Spinodal Decomposition . . . . .	263
H.8	Phase Diagrams . . . . .	264
H.9	Chemical Potentials . . . . .	265
H.10	Osmotic Pressure . . . . .	268
H.11	Equilibrium Swelling . . . . .	276

**Nomenclature**

**281**

# 1 Course Description

A course on the mechanical properties of soft materials, designed for first year graduate students in Materials Science and related disciplines. Not recommended for students who have already taken MatSCI 332. Topics include matrix and tensor representations of stress and strain, including extensions to large strains, contact mechanics, fracture mechanics, yield, deformation and time dependent behavior. Applications of these concepts to polymeric materials is emphasized.



**Figure 2.1:** An example of a 'soft' material.

## 2 Introduction

Since the title of this book contains the term 'Soft Materials', it makes sense to define what we really mean by 'soft'. Here are two ways to think about it:

1. Soft Materials have Low Elastic Moduli.

By 'low' we mean significantly lower than the moduli of crystalline metals and ceramics. The jellyfish shown in Fig. 2.1 is obviously 'soft' in this sense. Metals and ceramics typically have moduli in the range of 100 MPa (see Fig. 2.2). While the strength of metals can be adjusted by a variety of mechanisms that affect the nature of dislocation motion in these systems, the modulus is set by the nature of the interatomic potentials and there nothing that can really be done to significantly affect the modulus of a given material. Polymers are different, however, and have a much broader range of elastic moduli. The stiffest of these (Kevlar<sup>TM</sup> for example) have elastic moduli in at least one direction that are comparable to the modulus of steel.

2. Thermal Fluctuations Matter in Soft Materials.

At a molecular level, the relevant energy scale that determines a variety of important properties is the thermal energy,  $k_B T$ , where  $k_B$  is Boltzmann's constant and  $T$  is the absolute temperature. If different molecular arrangements within a material differ in energy by an amount that of the order of  $k_B T$  or less, than these different arrangements will all be experienced by the material. When the free energy of a material is dominated by the entropy associated with the accessibility of these different arrangements, it is possible to calculate the elastic properties of the material from the molecular structure with considerable accuracy.

**Exercise:** How high above the earth's surface must a single oxygen molecule be lifted in order for its gravitational potential energy to be increased by  $k_B T$ ?

**Solution:** The gravitational potential energy is  $mgh$ , where  $m$  is the mass of the object,  $g$  is the gravitational acceleration ( $9.8 \text{ m/s}^2$ ) and  $h$  is height. The

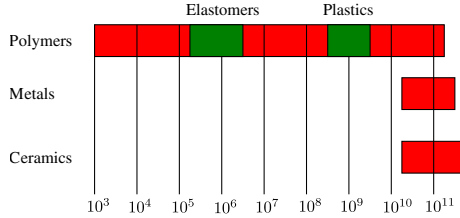


**Figure 2.2:** Range of Young's moduli (Pa) for different materials classes.

mass of a single  $O_2$  molecule is obtained by dividing the molecular weight in g/mole by Avogadro's number:

$$m = 32 \left( \frac{\text{g}}{\text{mole}} \right) \left( \frac{\text{mole}}{6.02 \times 10^{23}} \right) = 5.3 \times 10^{-23} \text{ g} = 5.3 \times 10^{-26} \text{ kg}$$

The conversion to kg illustrates the first point that we want to make with this simple calculation: **Don't mix units and convert everything to SI units (m-kg-s) to keep yourself sane and avoid unit errors.** Boltmann's constant,  $k_B$  needs to be in SI units as well:

$$k_B = 1.38 \times 10^{-23} \text{ J/K}$$

Now we just need to equate  $k_B T$  to  $mgh$ , using something reasonable for the absolute temperature,  $T$ . I'll use  $T=300$  K to get the following:

$$h = \frac{k_B T}{mg} = \frac{(1.38 \times 10^{-23} \text{ J/K}) (300 \text{ K})}{(5.3 \times 10^{-26} \text{ kg}) (9.8 \text{ m/s}^2)} = 8000 \text{ m} = 8 \text{ km}$$

The full oxygen partial pressure is given proportional to  $\exp(-mgh/k_B T)$ , so this value of  $h$  is the altitude where the oxygen pressure is a factor of  $e$  (2.7) less than the value at sea level.



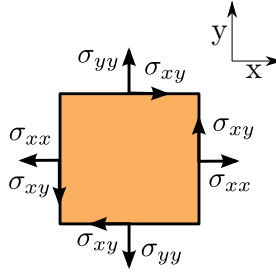


Figure 3.1: 2-dimensional stress tensor

### 3 Stress and Strain

The mechanical properties of a material are defined in terms of the strain response of material after a certain stress is applied. In order to properly understand mechanical properties, we have to have a good understanding of stress and strain, so that's where we begin.

**Some Notes on Notation:** There are different ways to represent scalar quantities, vectors and matrices. Here's how we do it in this text:

- Scalar quantities are straight up symbols, like  $P_1$ ,  $\sigma_{12}$ , etc.
- Vectors are indicated with an arrow over the symbol, like  $\vec{P}$ .
- Unit vectors are indicated with a caret above the symbol, like  $\hat{n}$ .
- Matrices are enclosed in square brackets, like  $[\sigma]$

#### 3.1 Tensor Representation of Stress

The **stress** applied to an object, which we denote as  $\sigma_{ij}$  or  $[\sigma]$  is the force acting over an area of an object, divided by the area over which this force is acting. Note note that  $[\sigma]$  is a matrix with individual components,  $\sigma_{ij}$  specified by the indices  $i$  and  $j$ . These indices have the following significance:

- $i$ : surface normal ( $i = x, y, z$ )
- $j$ : direction of force ( $j = x, y, z$ )

To obtain the **Engineering stress**,  $[\sigma^{\text{eng}}]$ , we use the undeformed areas of the stress-free object to obtain the stress tensor, whereas the true stress (which is

what we generally mean when we write  $[\sigma]$ ) we use the actual areas in the as-stressed state.

The stress matrix is a **tensor**, which means that it obeys the coordinate transformation laws describe below. In two dimensions it has the following form:

$$[\sigma] = \begin{bmatrix} \sigma_{xx} & \sigma_{xy} \\ \sigma_{yx} & \sigma_{yy} \end{bmatrix} \quad (3.1)$$

The stress tensor must be symmetric, with  $\sigma_{xy} = \sigma_{yx}$ . If this were not the case, the torques on the volume element shown above in Figure 3.1 would not balance, and the material would not be in static equilibrium. As a result the two dimensional stress state is specified by three components of the stress tensor:

- 2 normal stresses,  $\sigma_{xx}$ ,  $\sigma_{yy}$ . These are referred to as 'normal' stresses because the force acts perpendicular to the plane that it is referred to.
- A single shear stress,  $\sigma_{xy}$ .

In three dimensions we add a  $z$  axis to the existing  $x$  and  $y$  axes, so the stress state is defined by a symmetric 3x3 tensor. The full stress tensor can be used to define the stresses acting on any given plane. To simplify the notation a bit we label the three orthogonal directions by numbers (1, 2 and 3) instead of letters ( $x$ ,  $y$  and  $z$ ). The stress tensor gives the components of the force ( $P_1$ ,  $P_2$  and  $P_3$ ) acting on a given plane. The plane is specified by the orientation of the unit vector,  $\hat{n}$  that is perpendicular to the plane. This vector has components  $n_1$ ,  $n_2$  and  $n_3$  in the 1, 2 and 3 directions, respectively. It's a 'unit' vector because the length of the vector is 1, i.e.  $(n_1^2 + n_2^2 + n_3^2)^{1/2} = 1$ . The relationship between  $\vec{P}$ ,  $\sigma$  and  $\vec{n}$  is as follows:

$$\begin{bmatrix} P_1 \\ P_2 \\ P_3 \end{bmatrix} = A \begin{bmatrix} \sigma_{11} & \sigma_{12} & \sigma_{13} \\ \sigma_{12} & \sigma_{22} & \sigma_{23} \\ \sigma_{13} & \sigma_{23} & \sigma_{33} \end{bmatrix} \begin{bmatrix} n_1 \\ n_2 \\ n_3 \end{bmatrix} \quad (3.2)$$

or in more compact matrix notation:

$$\vec{P} = A [\sigma] \hat{n} \quad (3.3)$$

Here  $A$  is the total cross sectional area of the plane that we are interested in. (If you need a refresher on matrix multiplication, the Wikipedia page on Matrix Multiplication ([https://en.wikipedia.org/wiki/Matrix\\_multiplication](https://en.wikipedia.org/wiki/Matrix_multiplication)) [1] is very helpful).

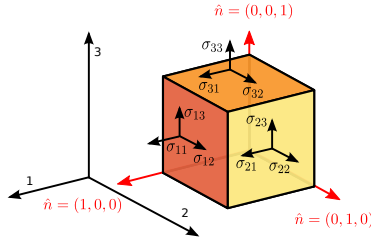


**Figure 3.2:** 3 dimensional stress tensor

In graphical form the relationship is as shown in Figure 3.2. Like the 2-dimensional stress tensor mentioned above, the 3-dimensional stress tensor must also be symmetric in order for static equilibrium to be achieved. There are therefore 6 independent components of the three-dimensional stress tensor:

- 3 normal stresses,  $\sigma_{11}$ ,  $\sigma_{22}$  and  $\sigma_{33}$ , describing stresses applied perpendicular to the 1, 2 and 3 faces of the cubic volume element.
- 3 shear stresses:  $\sigma_{12}$ ,  $\sigma_{23}$  and  $\sigma_{13}$ .

The three dimensional stress tensor is a  $3 \times 3$  matrix with 9 elements (though only 6 are independent), corresponding to the three stress components acting on each of the three orthogonal faces of cube in the Cartesian coordinate system used to define the stress components. The 1 face has  $n_1=1$ ,  $n_2 = 0$  and  $n_3 = 0$ . By setting  $\vec{n} = (1, 0, 0)$  in Eq. 3.2, we get the following for the stresses acting on the 1 face of the volume element:

$$\begin{aligned} P_1/A &= \sigma_{11} \\ P_2/A &= \sigma_{12} \\ P_3/A &= \sigma_{13} \end{aligned} \tag{3.4}$$

Equivalent expressions can be obtained for the stresses acting on the 2 and 3 faces, by setting  $\vec{n} = (0, 1, 0)$  and  $\vec{n} = (0, 0, 1)$ , respectively.

### 3.2 Tensor Transformation Law

The stress experienced by a material does not depend on the coordinate system used to define the stress state. The stress tensor will look very different if we chose a different set of coordinate axes to describe it, however, and it is important to understand how changing the coordinate system changes the stress tensor. We begin in this section by describing the procedure for obtaining the

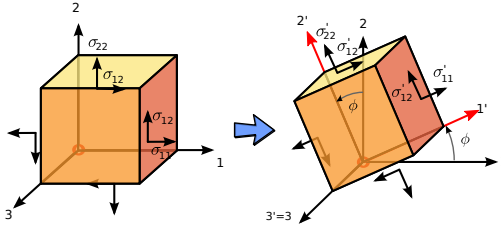


**Figure 3.3:** Rotation of coordinate system. The coordinate system is rotated by  $\theta$  about the 3 axis, transforming the 1 axis to  $1'$  and the 2 axis to  $2'$ .

stress tensor that emerges from a given change in the coordinate system. We then describe the method for obtaining a specific set of coordinate axis which gives a diagonalized tensor where only normal stresses are present (Section 3.3).

### 3.2.1 Specification of the Transformation Matrix

In general, we consider the case where our 3 axes (which we refer to simply as axes 1, 2 and 3) are moved about the origin to define a new set of coordinate axes that we refer to as  $1'$ ,  $2'$  and  $3'$ . As an example, consider the simple counterclockwise rotation around the 3 axis by an angle  $\phi$ , shown schematically in Figure 3.3. In general, the relative orientation of the transformed (rotated) and untransformed coordinate axes are given by a set of 9 angles between the 3 untransformed axes and the three transformed axes. In our notation we specify these angles as  $\theta_{ij}$ , where  $i$  specifies the transformed axes ( $1'$ ,  $2'$  or  $3'$ ) and  $j$  specifies the untransformed axis (1, 2 or 3). In our simple example, the angle between the 1 and  $1'$  axes is  $\phi$ , so  $\theta_{11} = \phi$ . The angle between the 2 and  $2'$  axes is also  $\phi$ , so  $\theta_{22} = \phi$ . The 3 axis remains unchanged in our rotation example, so  $\theta_{33} = 0$ . The  $3/3'$  axis remains perpendicular to the  $1, 1'$ ,  $2, 2'$  axes, so we have  $\theta_{31} = \theta_{32} = \theta_{13} = \theta_{23} = 90^\circ$ . Finally, we see that the angle between the  $1'$  and the 2 axis is  $90 - \phi$  ( $\theta_{12} = 90 - \phi$ ) and the angle between the  $2'$  and 1 axis is  $90 + \phi$  ( $\theta_{21} = 90 + \phi$ ). The full  $[\theta]$  matrix in this case is as follows:

$$[\theta] = \begin{bmatrix} \phi & 90 - \phi & 90 \\ 90 + \phi & \phi & 90 \\ 90 & 90 & 0 \end{bmatrix} \quad (3.5)$$

Note that the  $[\theta]$  matrix is NOT symmetric ( $\theta_{ij} \neq \theta_{ji}$ ), so you always need to make sure the first index,  $i$ , (denoting the row in the  $[\theta]$  matrix) corresponds to the transformed axes, and the second index,  $j$  (denoting the column in the  $[\theta]$  matrix) corresponds to the original, untransformed axes.

### 3.2.2 Expressions for the Stress Components

Once we specify all the different components of  $[\theta]$ , we can use the following general expression to obtain the stresses in the new (primed) coordinate system as a function of the stresses in the original coordinate system:

$$\sigma'_{ij} = \sum_{k,l} \cos \theta_{jk} \cos \theta_{il} \sigma_{kl} \quad (3.6)$$

For each component of the stress tensor, we have to sum 9 individual terms (all combinations of  $k$  and  $l$  from 1 to 3). For example,  $\sigma'_{12}$  is given as follows:

$$\begin{aligned} \sigma'_{12} = & \cos \theta_{21} \cos \theta_{11} \sigma_{11} + \cos \theta_{21} \cos \theta_{12} \sigma_{12} + \cos \theta_{21} \cos \theta_{13} \sigma_{13} + \\ & \cos \theta_{22} \cos \theta_{11} \sigma_{21} + \cos \theta_{22} \cos \theta_{12} \sigma_{22} + \cos \theta_{22} \cos \theta_{13} \sigma_{23} + \\ & \cos \theta_{23} \cos \theta_{11} \sigma_{31} + \cos \theta_{23} \cos \theta_{12} \sigma_{32} + \cos \theta_{23} \cos \theta_{13} \sigma_{33} \end{aligned} \quad (3.7)$$

The calculation is breathtakingly tedious if we do it all by hand, so it makes sense to automate this and do the calculation via computer, in our case with Python. In this example we'll start with a simple stress state corresponding to uniaxial extension in the 1 direction, with the following untransformed stress tensor:

$$[\sigma] = \begin{bmatrix} 5 \times 10^6 & 0 & 0 \\ 0 & 0 & 0 \\ 0 & 0 & 0 \end{bmatrix} \quad (3.8)$$

Suppose we want to obtain the stress tensor in the transformed coordinate system obtained from a  $45^\circ$  counterclockwise rotation around the  $z$  axis. The rotation matrix is given by Eq. 3.5, with  $\phi = 45^\circ$ . The following Python code solves for the full transformed tensor, with  $\sigma_{ij}$  given by Eq. 3.8 and  $[\theta_{ij}]$  given by Eq. 3.5 with  $\phi = 45^\circ$ :

```

1 #!/usr/bin/env python3
2 # -*- coding: utf-8 -*-
3
4 import numpy as np
5
6 sig=np.zeros((3, 3))  ## create stress tensor and set to zero
7 sig[0, 0] = 5e6; # this is the only nonzero component
8
9 sigp=np.zeros((3, 3)) # initialize rotated stresses to zero
10
11 phi = 45
12
13 theta = [[phi,90-phi,90], [90+phi,phi,90], [90,90,0]]

```

```
[[2500000. 2500000. 0.]
 [2500000. 2500000. 0.]
 [ 0. 0. 0.]]
```

Figure 3.4: Output generated by rotate45.py.

```
14 theta = np.deg2rad(theta) # trig functions need angles in
    radians
15 for i in [0, 1, 2]:
16     for j in [0, 1, 2]:
17         for k in [0, 1, 2]:
18             for l in [0, 1, 2]:
19                 sigp[i,j]=sigp[i,j]+np.cos(theta[i,k])*np.cos(
                    theta[j,l])*sig[k,l]
20
21 print(sigp) # display the transformed tensor components
```

We use Python because it is free, powerful, and quite easy to learn especially if you have experience with a similarly-structured programming environment like MATLAB. Various Python code examples are included in this text, and are presented as examples of how to do some useful things in Python.

The output generated by the Python code is shown in Figure 3.4, and corresponds to the following result:

$$[\sigma'] = \begin{bmatrix} 2.5 \times 10^6 & -2.5 \times 10^6 & 0 \\ -2.5 \times 10^6 & 2.5 \times 10^6 & 0 \\ 0 & 0 & 0 \end{bmatrix} \quad (3.9)$$

Note the following:

- The normal stresses in the 1 and 2 directions are equal to one another.
- The transformed shear stress in the 1-2 plane is half the original tensile stress.
- The sum of the normal stresses (the sum of the diagonal components of the stress tensor) is unchanged by the coordinate transformation

### 3.2.3 An Easier Way: Transformation by Direct Matrix Multiplication

A much easier way to do the transformation is to use a little bit of matrix math. The approach we use is described in a very nice web page put together by Bob

McGinty[2]: A transformation matrix,  $Q_{ij}$ , is obtained by taking the cosines of all of these angles describing the relationship between the transformed and untransformed coordinate axes:

$$[\mathbf{Q}] = \cos[\theta] \quad (3.10)$$

For the simple case of rotation about the z axis, the angles are given by Eq. 3.5, so that  $[\mathbf{Q}]$  is given as:

$$[\mathbf{Q}] = \begin{bmatrix} \cos \phi & \cos(90 - \phi) & \cos 90 \\ \cos(90 + \phi) & \cos \phi & \cos 90 \\ \cos 90 & \cos 90 & \cos 0 \end{bmatrix} = \begin{bmatrix} \cos \phi & \sin \phi & 0 \\ -\sin \phi & \cos \phi & 0 \\ 0 & 0 & 1 \end{bmatrix} \quad (3.11)$$

The transformed stress is now obtained by the following simple matrix multiplication:

$$[\sigma'] = [\mathbf{Q}] [\sigma] [\mathbf{Q}]^T \quad (3.12)$$

where the  $[\mathbf{Q}]^T$  is the transpose of  $[\mathbf{Q}]$ :

$$Q^T(i, j) = Q(j, i) \quad (3.13)$$

For the rotation by  $\phi$  around the z axis,  $[\mathbf{Q}]^T$  is given by the following:

$$[\mathbf{Q}]^T = \begin{bmatrix} \cos \phi & -\sin \phi & 0 \\ \sin \phi & \cos \phi & 0 \\ 0 & 0 & 1 \end{bmatrix} \quad (3.14)$$

Equation 3.12 is much easier to deal with than Eq. 3.7. The Python code to take a uniaxial stress state and rotate the coordinate system by  $45^\circ$  about the 3 axis looks like this if we base it on Eq. 3.12:

```

1 import numpy as np
2
3 # create stress tensor with all zero elements
4 sig = np.zeros((3,3))
5
6 # set first one element to be nonzero (one of the normal stresses)
7 sig[0][0] = 5e6
8
9 #set the rotation angle
10 phi = 45
11
12 # define the rotation matrix in degrees
13 theta = np.array([[phi, 90+phi, 90], [90-phi, phi, 90], [90, 90, 0]])

```

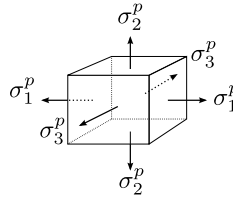


Figure 3.5: Principal Stresses

```

14
15 # now put all the direction cosines in Q
16 Q = np.cos(np.radians(theta))
17
18 # calculate the transpose of Q
19 QT = np.transpose(Q)
20
21 # now multiply everything together
22 # note that we use the @ sign to multiply matrices in python
23 sigp = np.round(Q@sig@QT)
24
25 # print the result
26 print(sigp)

```

Running this script gives the output shown in Figure 3.4, *i.e.* we obtain exactly the same result we obtained by using Eq. 3.7.

### 3.3 Principal Stresses

Any stress state (true stress) can be written in terms of three principal stresses  $\sigma_1^p$ ,  $\sigma_2^p$  and  $\sigma_3^p$ , applied in three perpendicular directions as illustrated in Figure 3.5. Note that we still need 6 independent parameters to specify a stress state: the 3 principal stresses, in addition to three parameters that specify the orientation of the principal axes. The stress tensor depends on our definition of the axes, but it is always possible to choose the axes so that all of the shear components of the stress tensor vanish, so that the stress tensor looks like the following:

$$[\sigma] = \begin{bmatrix} \sigma_1^p & 0 & 0 \\ 0 & \sigma_2^p & 0 \\ 0 & 0 & \sigma_3^p \end{bmatrix} \quad (3.15)$$

In order to gain some insight into the points mentioned above, it is useful to consider a range of rotation angles, and not just a single rotation angle of  $45^\circ$ . One way to do this is to use the symbolic math capability of Python (or



your other favorite software) to obtain the full stress tensor as a function of the rotation angle. We'll use the principal axes to define our untransformed state, and transform to a new set of axes by rotating counterclockwise by an angle  $\phi$  around the 3 axis. We want to calculate

$[\sigma']$  from Eqs.3.11 and 3.12 as we did before, but we leave  $\phi$  as an independent variable. We use the following python script to do this:

```

1  # mohr_circle.py
2  # Mohr's circle derivation
3  from sympy import symbols, Matrix, cos, pi, simplify, preview
4
5  # specify the principal stresses S
6  sig1p, sig2p, sig3p = symbols(['sigma_1^p', 'sigma_2^p', 'sigma_3
   ^p'])
7  sig = Matrix([[sig1p, 0, 0], [0, sig2p, 0], [0, 0, sig3p]])
8
9  # now specify the rotation angle
10 phi = symbols('phi')
11
12 # specify the theta matrix
13 theta=Matrix([[phi,pi/2-phi,pi/2], [pi/2+phi,phi,pi/2],[pi/2,pi
   /2,0]])
14
15 # take the cosine of all the elements in the matrix to get Q
16 Q=theta.applyfunc(cos)
17
18 # get the transpose of the matrix
19 QT=Q.transpose()
20
21 # now do the matrix multiplication to get the transformed matrix
22 sigp=Q*sig*QT
23
24 # now simplify and show the output
25 exp1 = simplify(sigp)
26 preview(exp1, filename='../figures/sympy_mohr_exp1.svg')
27
28 # define the center (C) and radius (R) of the circle
29 R, C = symbols(['R', 'C'])
30
31 # now we rewrite in terms of center and radius and simplify again
32 sigp = sigp.subs([(sig1p, C+R), (sig2p, C-R)])
33 exp2 = simplify(sigp)
34
35 # now save the exp1 and exp2 as image files
36 preview(exp1, viewer = 'file', filename = '../figures/
   sympy_mohr_exp1.png')
37 preview(exp2, viewer = 'file', filename = '../figures/
   sympy_mohr_exp2.png')

```

This results in the following expression for  $[\sigma']$  (exp1, generated in line 26 of mohr\_circle.py).

$$\begin{bmatrix} \sigma_1^p \cos^2(\phi) + \sigma_2^p \sin^2(\phi) & \frac{(-\sigma_1^p + \sigma_2^p) \sin(2\phi)}{2} & 0 \\ \frac{(-\sigma_1^p + \sigma_2^p) \sin(2\phi)}{2} & \sigma_1^p \sin^2(\phi) + \sigma_2^p \cos^2(\phi) & 0 \\ 0 & 0 & \sigma_3^p \end{bmatrix}$$

This is not yet a very illuminating result, but it is the basis for the Mohr circle construction, which provides a very useful way to visualize two dimensional stress states. This construction is described in more detail in the following Section.

### 3.3.1 Mohr's Circle Construction

The Mohr circle is a graphical construction that can be used to describe a two dimensional stress state. A two dimensional stress state is specified by two principal stresses,  $\sigma_1^p$  and  $\sigma_2^p$ , and by the orientation of the principal axes. The Mohr circle is drawn with a radius,  $R$ , of  $\sigma_1^p - \sigma_2^p$ , centered at  $C = (\sigma_1^p + \sigma_2^p) / 2$  on the horizontal axis. We can use these values of  $R$  and  $C$  as the independent variables in the expression for  $\sigma'$  that we obtained from our python script. This substitution is made in lines 30-34 of `mohr_circle.py`, and leads to the following expression for  $[\sigma']$  (exp2 from line 34):

$$\begin{bmatrix} C - 2R \sin^2(\phi) + R & -R \sin(2\phi) & 0 \\ -R \sin(2\phi) & C - 2R \cos^2(\phi) + R & 0 \\ 0 & 0 & \sigma_3^p \end{bmatrix}$$

Python has taken us almost as far as we need to go, but it doesn't seem to be smart enough to use the following two trigonometric identities:

$$\begin{aligned} 1 - 2 \sin^2 \phi &= \cos(2\phi) \\ 1 - 2 \cos^2 \phi &= -\cos(2\phi) \end{aligned} \quad (3.16)$$

Substituting these into the expression for  $[\sigma']$  gives our final result:

$$[\sigma'] = \begin{bmatrix} C + R \cos(2\phi) & -R \sin(2\phi) & 0 \\ -R \sin(2\phi) & C - R \cos(2\phi) & 0 \\ 0 & 0 & \sigma_3^p \end{bmatrix} \quad (3.17)$$

In the Mohr circle construction normal stresses ( $\sigma_N$ ) are plotted on the x axis and the shear component of the stress tensor ( $\tau$ ) is plotted on the y axis. For a two dimensional stress state in the 1-2 plane the circle is defined by two points:  $(\sigma_{11}, \sigma_{12})$  and  $(\sigma_{22}, -\sigma_{12})$ . In our current example the stress state in

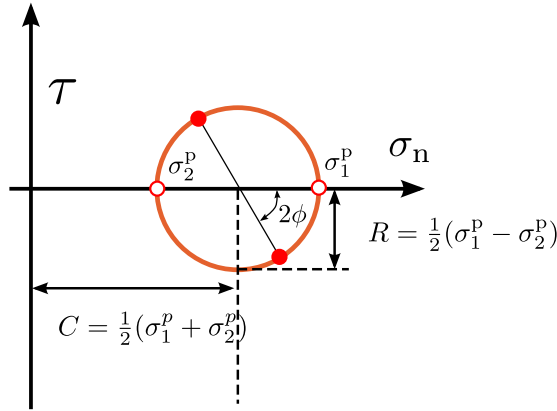


Figure 3.6: Mohr's circle construction.

the untransformed axes is represented by the open symbols in Figure 3.6, *i.e.* by the points  $(\sigma_1^p, 0)$  and  $(\sigma_2^p, 0)$ . In the transformed axes the stress state is represented by the solid circles in Figure 3.6. From Eq. 3.17 it is evident that the relationship between the two different representations of the stress state is obtained by a rotation along circle by  $2\phi$ . Whether this rotation is clockwise or counterclockwise depends on the sign convention in the definition of the shear stress. We're not going to worry about it here, but you can refer to the [Mohr's Circle Wikipedia article](#)[3] for the details (see the Section on the sign convention).

The Mohr circle construction can only be applied for a two dimensional meaning that there are no shear stresses with a component in the direction of the rotation axis. There can be a normal stress in the third direction, as in our example above, because this normal stress is simply superposed on the 2d stress state. In general, there are three principal stresses,  $\sigma_1^p$ ,  $\sigma_2^p$  and  $\sigma_3^p$ , and we can draw the Mohr circle construction with any combination of these 3 stresses. We end up with 3 different circles, as shown in Figure 3.7. Note that the convention is that  $\sigma_1^p$  is the largest principal stress and that  $\sigma_3^p$  is the smallest principal stress, *i.e.*  $\sigma_1^p > \sigma_2^p > \sigma_3^p$ . An important result is that the largest shear stress,  $\tau_{max}$ , is given by the difference between the largest principal stress and the smallest one:

$$\tau_{max} = \frac{1}{2} (\sigma_1^p - \sigma_3^p) \quad (3.18)$$

This maximum shear stress is an important quantity, because it determines when a material will deform plastically (much more on this later). In order

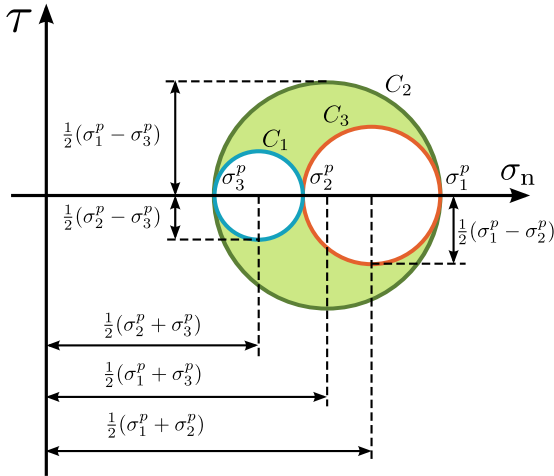


Figure 3.7: Three-dimensional Mohr's Circle.

to determine this maximum shear stress, we need to first Figure out what the principal stresses are. In some cases this is easy. In a uniaxial tensile test, one of the principals stresses is the applied stress, and the other two principal stresses are equal to zero.

The individual Mohr's circles in Figure 3.7 correspond to rotations in the around the individual principal axes. Circle  $C_1$  corresponds to rotation around the direction in which  $\sigma_1^p$  is directed,  $C_2$  corresponds to rotation around the direction in which  $\sigma_2^p$  is directed, and  $C_3$  corresponds to rotation around the direction in which  $\sigma_3^p$  is directed. A consequence of this is that is always possible to use the Mohr's circle construction to determine the principal stresses if there is only one non-zero shear stress.

**Exercise:** Determine the maximum shear stress for the following stress state:

$$[\sigma] = \begin{bmatrix} 3 & 0 & 2 \\ 0 & 3 & 0 \\ 2 & 0 & 5 \end{bmatrix} \text{ MPa} \quad (3.19)$$

**Solution:** We can handle this one without using a computer. There is only one non-zero shear stress ( $\sigma_{13}$ ), so we can determine the principals stresses in

the following manner:

1. One of the three principal stresses is the normal stress in the direction that does not involve either of the directions in the nonzero shear stress. Since the non-zero shear stress in our example is  $\sigma_{13}$ , one of the principal stresses is  $\sigma_{22}=3$  MPa.
2. Now we draw a Mohr circle construction using the two normal stresses and the non-zero shear stress, in this case  $\sigma_{11}$ ,  $\sigma_{33}$  and  $\sigma_{13}$ . Mohr's circle is centered at the the average of these two normal stresses, in our case at  $C = (\sigma_{11} + \sigma_{33}) / 2 = 4$  MPa.

3. Determine the radius of the circle,  $R$ , is given as:

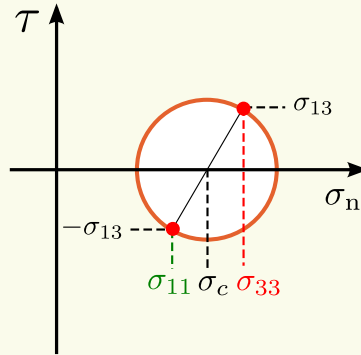
$$R = \sqrt{(\sigma_{33} - \sigma_c)^2 + \sigma_{13}^2} = \sqrt{(5 - 4)^2 + \sigma_{13}^2} = 2.24 \text{ MPa}$$

4. The principal stresses are given by the intersections of the circle with the horizontal axis:

$$\sigma^p = C \pm R = 6.24 \text{ MPa}, 1.76 \text{ MPa}$$

The third principal stress is 3 MPa, as we already determined.

5. The maximum shear stress is half the difference between the largest principal stress (6.64 MPa) and the smallest one (1.76), or 2.24 MPa.



### 3.3.2 Critical Resolved Shear Stress for Uniaxial Tension

As an example of the Mohr circle construction we can consider the calculation of the resolved shear stress on a sample in a state of uniaxial tension. The Mohr's circle representation of the stress state is shown in Figure 3.8. The resolved shear stress,  $\tau_{rSS}$ , for sample in uniaxial tension is given by the following expression:

$$\tau_{rss} = \sigma_1^p \cos \phi \cos \lambda \quad (3.20)$$

where  $\sigma_1^p$  is the applied tensile stress,  $\phi$  is the angle between the tensile axis and a vector normal to the plane of interest, and  $\lambda$  is the angle between the tensile axis and the direction of the shear stress. This shear stress has to be in the plane itself, so for a 2-dimensional sample  $\lambda + \phi = 90^\circ$ . This means we can rewrite Eq. 3.20 in the following way:

$$\tau_{rss} = \sigma_1^p \cos \phi \cos (90^\circ - \phi) \quad (3.21)$$

We can use the identities  $\cos (90 - \phi) = \sin \phi$  and  $\sin (2\phi) = 2 \sin \phi \cos \phi$  to obtain the following:

$$\tau_{rss} = \frac{\sigma_1^p}{2} \sin (2\phi) \quad (3.22)$$

We can get the same thing from the Mohr's circle construction to redefine the axes by a rotation of  $\phi$ . The shear stress is simply the radius of the circle ( $\phi_1^p/2$  in this case) multiplied by  $\sin (2\phi)$ . Mohr's circle also gives us the normal stresses:

$$\begin{aligned} \sigma_{11} &= \frac{\sigma_1^p}{2} + \frac{\sigma_1^p}{2} \cos (2\phi) \\ \sigma_{22} &= \frac{\sigma_1^p}{2} - \frac{\sigma_1^p}{2} \cos (2\phi) \end{aligned} \quad (3.23)$$

The untransformed 2-dimensional stress tensor looks like this:

$$[\sigma] = \begin{bmatrix} \sigma_1^p & 0 \\ 0 & 0 \end{bmatrix} \quad (3.24)$$

The transformed stress tensor (after rotation by  $\phi$  to give the resolved shear stress) looks like this:

$$[\sigma'] = \begin{bmatrix} \frac{\sigma_1^p}{2} + \frac{\sigma_1^p}{2} \cos (2\phi) & \frac{\sigma_1^p}{2} \sin (2\phi) \\ \frac{\sigma_1^p}{2} \sin (2\phi) & \frac{\sigma_1^p}{2} - \frac{\sigma_1^p}{2} \cos (2\phi) \end{bmatrix} \quad (3.25)$$

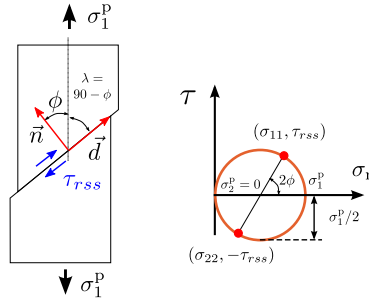


**Figure 3.8:** Mohr's circle construction and calculation of the resolved shear stress for a 2-dimensional sample in uniaxial extension.

### 3.3.3 Principal Stress Calculation

Principal stresses can easily be calculated for any stress state just by obtaining the eigenvalues of the stress tensor. In addition, the orientation of the principal axes (the coordinate system for which there are no off-diagonal components in the stress tensor). If you need a refresher on what eigenvalues and eigenvectors actually are, take a look at the appropriate Wikipedia page ([http://en.wikipedia.org/wiki/Eigenvalues\\_and\\_eigenvectors](http://en.wikipedia.org/wiki/Eigenvalues_and_eigenvectors)). We'll use Python to do this, using the 'eig' command.

To illustrate, we'll start with the stress state specified by Eq. 3.9. which we got by starting with a simple uniaxial extension in the 1 direction, and rotating the coordinate system by  $45^\circ$  about the 3 axis. The MATLAB script to do this is very simple and is as follows:

```

1  #!/usr/bin/env python3
2  # -*- coding: utf-8 -*-
3
4  import numpy as np
5
6  # write down the stress tensor that we need to diagonalize
7  sig=1e6*np.array([[2.5,2.5,0],[2.5,2.5,0],[0,0,0]])
8
9  # get the eigen values and eigen vectors
10 [principalstresses, directions]=np.linalg.eig(sig)
11
12 # the columns in 'directions' correspond to the dot product of
13 the
14 # principal axes with the original coordinate system
15 # The rotation angles are obtained by calculating the inverse
16 cosines
17 theta=np.arccos(directions)*180/(np.pi)
18
19 # print the results (or just look at them in the variable
20 explorer in Spyder)
21 print ('theta=\n', theta)
22 print ('principal stresses=\n', principalstresses)

```

```

theta=
[[ 45. 135. 90.]
 [ 45.  45. 90.]
 [ 90. 90.  0.]]
principal stresses=
[5.00000000e+06 4.65661287e-10 0.00000000e+00]

```

Figure 3.9: Output generated by principal\_stress\_calc.py.

Here's the output generated by this script:

3 principal axes returned as column vectors. In this case there is a single normal stress, acting in a direction midway between the original  $x$  and  $y$  axes. The original uniaxial stress state is recovered in this example, as it should be. To summarize:

- Principal Stresses: Eigenvalues of the stress tensor
- Principal Stress directions: Eigenvectors of the stress tensor

### 3.3.4 Stress Invariants

Some quantities are invariant to choice of axes. The most important one is the **hydrostatic pressure**,  $p$ , given by summing the diagonal components of the stress tensor and dividing by 3:

$$p = -\frac{1}{3}(\sigma_{11} + \sigma_{22} + \sigma_{33}) = -\frac{1}{3}(\sigma_1^p + \sigma_2^p + \sigma_3^p) \quad (3.26)$$

The negative sign appears because a positive pressure is compressive, but positive stresses are tensile. The hydrostatic pressure is closely related to a quantity referred to as the 'first **stress invariant**',  $I_1$ :

$$I_1 = \sigma_{11} + \sigma_{22} + \sigma_{33} \quad (3.27)$$

The second and third stress invariants,  $I_2$  and  $I_3$ , are also independent of the way the axes are defined:

$$I_2 = \sigma_{11}\sigma_{22} + \sigma_{22}\sigma_{33} + \sigma_{33}\sigma_{11} - \sigma_{12}^2 - \sigma_{13}^2 - \sigma_{23}^2 \quad (3.28)$$

$$I_3 = \sigma_{11}\sigma_{22}\sigma_{33} - \sigma_{11}\sigma_{23}^2 - \sigma_{22}\sigma_{13}^2 - \sigma_{33}\sigma_{12}^2 + 2\sigma_{12}\sigma_{13}\sigma_{23} \quad (3.29)$$



It's not obvious at first that each of these quantities are invariant to the choice of coordinate axes. As a check, we can start with a general tensor, rotate the coordinate system through a full 180 degrees, and plot the value of an invariant as a function of a the rotation angle,  $\phi$ . The following python code does this for  $I_2$ :

```

1 import numpy as np
2 import matplotlib.pyplot as plt
3
4 # create a function that multiplies the transforms a stress
5 # tensor sig by a rotation of phi about the Z axis,
6 # and returns the vaalue of I2
7
8 def I2_calc(phi):
9     sig = np.array([[3, 5, 4], [5, 2, 9], [4, 9, 6]])
10    theta = np.array([[phi, 90+phi, 90], [90-phi, phi, 90], [90, 90, 0]])
11    Q = np.cos(np.radians(theta))
12    QT = np.transpose(Q)
13    sigp = Q@sig@QT
14    I2 = (sigp[0][0]*sigp[1][1]+sigp[1][1]*sigp[2][2]+sigp[2][2]*
15         sigp[0][0] -
16         sigp[0][1]**2 - sigp[1][2]**2 -sigp[0][2]**2)
17    return I2
18
19 # vectorize the function so we can input an array of phi values
20 vI2 = np.vectorize(I2_calc)
21
22 # now calculate I2 over a range of phi values
23 phi = np.linspace(0, 180, 100)
24 I2vals = vI2(phi)
25
26 # now make the plot
27 plt.close('all')
28 fig, ax = plt.subplots(1,1, figsize=(3,3), constrained_layout=
29 True)
30 ax.plot(phi, I2vals, '-')
31 ax.set_xlabel(r'$\phi$ (deg)')
32 ax.set_ylabel(r'$I_2$')
33
34 # save the plot
35 fig.savefig('../figures/I2plot.svg')

```

This results in the very boring plot shown in Figure 3.10, indicating that  $I_2$  really is invariant to the definition of the coordinate axes.

### 3.4 Strain

There are 3 related definitions of the strain:

1. Engineering strain
2. Tensor strain

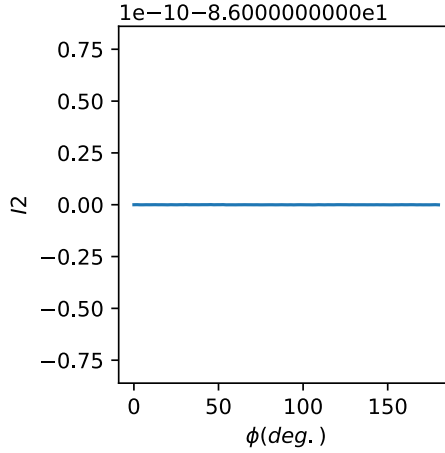


**Figure 3.10:** Plot of  $I_2$  as a function of the axis rotation angle for a generic 3d stress state, calculated from `I2_invariant_check.py`.

### 3. Generalized strain (large deformations, also referred to as ‘finite strain’)

Each of these definitions of strain describe the way different points an object move relative to one another when the material is deformed. Consider two points  $P_1$  and  $P_2$ , separated initially by the increments  $x_1, x_2$  and  $x_3$  along the 1, 2 and 3 directions. After the deformation is applied, these points move by the following amounts, as illustrated in Figure 3.11:

- $P_1$  moves by an amount  $\vec{u} = (u_1, u_2, u_3)$
- $P_2$  moves by  $\vec{u} + d\vec{u} = (u_1 + du_1, u_2 + du_2, u_3 + du_3)$

#### 3.4.1 Small Strains

Strain describes how much farther point to moved in three different directions, as a function of how far  $P_2$  was from  $P_1$  initially. For small strains we can ignore higher order terms in a Taylor expansion for  $du$ ,  $dv$  and  $dw$  and maintain only the first, partial derivative terms as follows:

$$\begin{aligned}
 du_1 &= \frac{\partial u_1}{\partial x_1} dx + \frac{\partial u_1}{\partial x_2} dy + \frac{\partial u_1}{\partial x_3} dz \\
 du_2 &= \frac{\partial u_2}{\partial x_1} dx + \frac{\partial u_2}{\partial x_2} dy + \frac{\partial u_2}{\partial x_3} dz \\
 du_3 &= \frac{\partial u_3}{\partial x_1} dx + \frac{\partial u_3}{\partial x_2} dy + \frac{\partial u_3}{\partial x_3} dz
 \end{aligned} \tag{3.30}$$

The three normal components of the strain correspond to the change in the displacement in a given direction corresponds to a change in initial separation between the points of interest in the same direction:

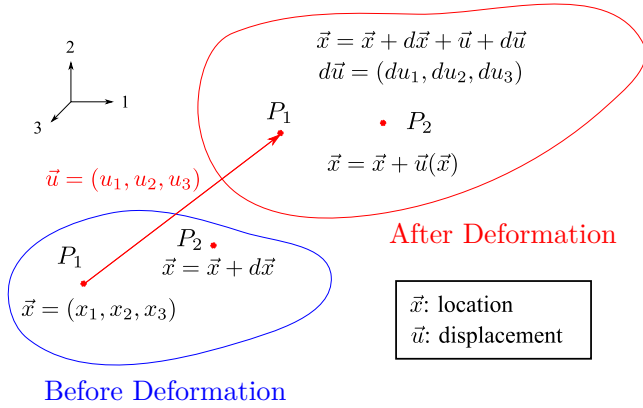


**Figure 3.11:** Location of two points,  $P_1$  and  $P_2$ , before and after an applied deformation.

$$\begin{aligned}
 e_{11} &= \frac{\partial u_1}{\partial x_1} \\
 e_{22} &= \frac{\partial u_2}{\partial x_2} \\
 e_{33} &= \frac{\partial u_3}{\partial x_3}
 \end{aligned}
 \tag{3.31}$$

The engineering shear strains are defined as follows:

$$\begin{aligned}
 e_{23} &= \frac{\partial u_3}{\partial x_2} + \frac{\partial u_2}{\partial x_3} \\
 e_{13} &= \frac{\partial u_1}{\partial x_3} + \frac{\partial u_3}{\partial x_1} \\
 e_{12} &= \frac{\partial u_1}{\partial x_2} + \frac{\partial u_2}{\partial x_1}
 \end{aligned}
 \tag{3.32}$$

Note: shear strains are often represented by the lower case Greek gamma to distinguish them from normal strains:

$$\gamma_{12} \equiv e_{12}; \gamma_{23} \equiv e_{23}; \gamma_{13} = e_{13}
 \tag{3.33}$$

### 3.4.2 Tensor Shear Strains

Engineering strains relate two vectors to one another ( $\vec{x}$  and  $\vec{u}$ ), just as a tensor does, but the transformation law between different coordinate systems is not obeyed for the engineering strains. For this reason the engineering strains are NOT tensor strains. Fortunately, all we need to do to change engineering strains to tensor strains is to divide the shear components by 2. In our notation we use  $e$  to indicate engineering strain and  $\epsilon$  to indicate tensor strains. The tensor normal strains are exactly the same as the engineering normal strains:

$$\begin{aligned}
 \epsilon_{11} &= e_{11} \\
 \epsilon_{22} &= e_{22} \\
 \epsilon_{zz} &= e_{zz}
 \end{aligned}
 \tag{3.34}$$

Engineering shear strains ( $e_{yz}$ ,  $e_{xz}$ ,  $e_{zy}$ ) are divided by two to give tensor shear strains:

$$\begin{aligned}
 \epsilon_{23} &= e_{23}/2 \\
 \epsilon_{13} &= e_{13}/2 \\
 \epsilon_{12} &= e_{12}/2
 \end{aligned}
 \tag{3.35}$$

Note that the tensor strains must be used in coordinate transformations (axis rotation, calculation of principal strains,  $e_1^p$ ,  $e_2^p$ ,  $e_3^p$ ).

### 3.4.3 Generalized Strain

We can also define the strain by considering a cube of side  $\ell$  that is deformed into a parallelepiped with dimensions of (along principal strain axes). After deformation, the cube has dimensions of  $\lambda_1\ell$ ,  $\lambda_2\ell$ ,  $\lambda_3\ell$ . Alternatively, a sphere of radius  $r_0$  is deformed into an ellipsoid with principal axes of  $\lambda_1r_0$ ,  $\lambda_2r_0$  and  $\lambda_3r_0$ , as shown in Figure 3.12. The quantities  $\lambda_1, \lambda_2, \lambda_3$  are **extension ratios**, and are related to the principal strains as follows:

$$\begin{aligned}
 \lambda_1 &= 1 + e_1^p \\
 \lambda_2 &= 1 + e_2^p \\
 \lambda_3 &= 1 + e_3^p
 \end{aligned}
 \tag{3.36}$$

The true strains,  $e_1^t$ , are obtained as by taking the natural log of the relevant extension ratio. For example, for a uniaxial tensile test, the true strain in the tensile direction (assumed to be the 1 direction here) is:

$$e_1^t = \ln(\lambda_1)
 \tag{3.37}$$

This expression for the true strain can be obtained by recognizing that the incremental strain is always given by the fractional increase in length  $d\ell/\ell$ , where  $\ell$  is the current length of the material as it is being deformed. If the initial length is  $\ell_0$  and the final, deformed length is  $\ell_f$ , then the total true strain,  $e_1^{true}$  is obtained by integrating the incremental strains accumulated throughout the entire deformation history:

$$e_1^t = \int_{\ell_0}^{\ell_f} \frac{d\ell}{\ell} = \ln \ell \Big|_{\ell_0}^{\ell_f} = \ln \left( \frac{\ell_f}{\ell_0} \right) = \ln \lambda_1
 \tag{3.38}$$

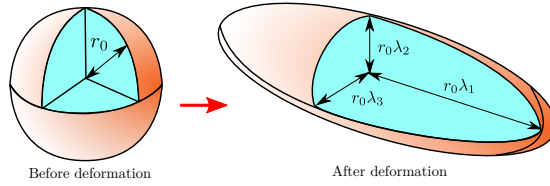


**Figure 3.12:** Unit sphere deformed into a strain ellipsoid with dimensions of  $\lambda_1, \lambda_2, \lambda_3$ .

The extension ratios provide a useful description of the strain for both small and large values of the strain. A material with isotropic mechanical properties has the same coordinate axes for the principal stresses and the principal strains.

A more detailed description of generalized strain, with a lot of relevant matrix math, is provided in the Wikipedia article on finite strain theory ([https://en.wikipedia.org/wiki/Finite\\_strain\\_theory](https://en.wikipedia.org/wiki/Finite_strain_theory)). If you come across concepts like the **Cauchy-Green deformation tensor** or the **Finger deformation tensor**, this article provides a useful introduction (but prepared for a lot of matrix math). These concepts appear in a range of useful description of mechanical response, including many in the biomedical field (muscle actuation, deformation of skin, etc).

## 3.5 Deformation Modes

Now that we've formally defined stress and strain we can give some specific examples where these definitions are used, and begin to define some elastic constants. We'll begin with the two most fundamental deformation states: simple shear and hydrostatic compression. These are complementary strain states - for an isotropic material simple shear changes the shape but not the volume, and hydrostatic compression changes the volume but not the shape. We'll eventually show that for an isotropic material there are only two independent elastic constants, so if we know how an isotropic material behaves in response to these two stress states, we have a complete understanding of the elastic properties of the material.

### 3.5.1 Simple Shear

**Simple shear** is a two dimensional strain state, which means that one of the principal strains is zero (or one of the principal extension ratios is 1).

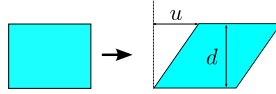


Figure 3.13: Schematic representation of simple shear.

The stress tensor looks like this:

$$[\sigma] = \begin{bmatrix} 0 & \sigma_{12} & 0 \\ \sigma_{12} & 0 & 0 \\ 0 & 0 & 0 \end{bmatrix} \quad (3.39)$$

From the definition of the engineering shear strain (Eq. 3.32) we have:

$$e_{12} = \frac{u}{d} \quad (3.40)$$

We need to divide the engineering shear strains by 2 to get the tensor strains, so we get the following:

$$[\epsilon] = \begin{bmatrix} 0 & e_{12}/2 & 0 \\ e_{12}/2 & 0 & 0 \\ 0 & 0 & 0 \end{bmatrix} \quad (3.41)$$

We're generally going to use engineering strains and not tensor strains, so we generally don't need to worry about the factor of two. The exception is when we want to use a coordinate transformation to find the principal strains. To do this we use a procedure exactly analogous to the procedure described in Section 3.3, but we need to make sure we are using the tensor strains when we do the calculation.

The **shear modulus** is simply the ratio of the shear stress to the shear strain.

$$G \text{ (shear modulus)} = \frac{\sigma_{12}}{e_{12}} \quad (3.42)$$

Note that the volume of the material is not changed, but it's shape has. In very general terms we can view the shear modulus of a material as a measure of its resistance to a change in shape under conditions where the volume remains constant.

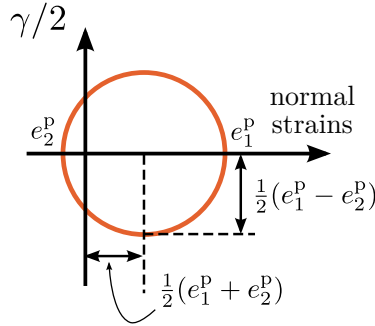


Figure 3.14: Mohr's circle construction for SMALL strains.

### 3.5.2 Simple Shear and the Mohr's Circle Construction for Strains

Mohr's circle for strain looks just like Mohr's circle for stress, provided that we use the appropriate tensor components. That means that we need to plot  $e_{12}/2$  on the vertical axis and the normal strains on the horizontal axis, as shown in Figure 3.14 (where we have used the common notation for the simple shear geometry, with  $e_{xy} = \gamma$ ). One thing that we notice from this plot is that  $\gamma$  is simply given by the difference between the two principal strains:

$$\gamma = e_1^p - e_2^p = \lambda_1 - \lambda_2 \quad (3.43)$$

For simple shear this relationship is valid, even for large strains, even though there are other aspects of the Mohr's circle construction that no longer work at large strains. The primary difficulty is that the frame of reference for the strained and unstrained case are not the same. In general, strains rotate the frame of reference by an amount that we don't want to worry about for the purposes of this course. For small strains typically obtained in metals or ceramics (with strain amplitudes of a few percent or less) we don't need to worry about this rotation, but it can become important for polymeric systems that undergo very large strains prior to failure. However, if all we want a measure of the shear strain in the material, we can still use Eq. 3.43, regardless of how large the principal strains (and corresponding extension ratios) actually are.

I

### 3.5.3 Torsion

An important geometry for characterizing the shear properties of soft materials is the torsional geometry shown in Figure 3.15. In this material a cylindrical or disk-shaped material is twisted about an axis of symmetry. The material

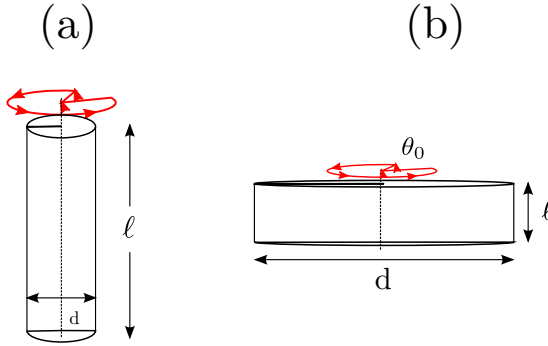


Figure 3.15: Fiber torsion.

could be a long, thin fiber (Figure 3.15a) or a flat disk sandwiched between two plates (Figure 3.15b). We obtain the shear modulus by looking at the torsional stiffness of material, *i.e.*, the Torque,  $T$ , required to rotate the top and bottom of the fiber by an angle  $\theta_0$ .

We define a cylindrical system with a  $z$  axis along the fiber axis. The other axes in this coordinate system are the distance  $r$  from this axis of symmetry, and the angle  $\theta$  around the  $z$  axis. The shear strain in the  $\theta - z$  plane depends only on  $r$ , and is given by:

$$e_{\theta z} = r \frac{d\theta}{dz} = r \frac{\theta_0}{\ell} \quad (3.44)$$

The corresponding shear stress is obtained by multiplying by the shear modulus,  $G$ :

$$\sigma_{\theta z} = Gr\theta_0 / \ell \quad (3.45)$$

We integrate the shear stress to give the torque,  $T$ :

$$T = \int_0^{d/2} r\sigma_{\theta z} 2\pi r dr = \frac{\pi G\theta_0 d^4}{32\ell} \quad (3.46)$$

This geometry is commonly used in an oscillatory mode, where  $\theta$  is oscillated at a specified frequency. In this case the torque response is obtained by using the dynamic shear modulus,  $G^*$  (defined in the section on viscoelasticity) in place of  $G$ .



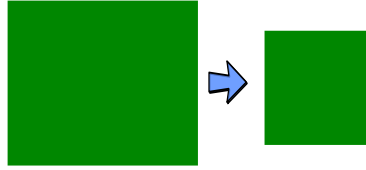


Figure 3.16: Hydrostatic Compression.

### 3.5.4 Hydrostatic Compression

The **bulk compressive modulus**,  $K_b$ , of a material describes its resistance to a change in density. Formally, it is defined in terms of the dependence of the volume of the material on the hydrostatic pressure,  $p$ :

$$K_b = -V \frac{dp}{dV} \quad (3.47)$$

The hydrostatic stress state corresponds to the stress state where there are no shear stresses, and each of the normal stresses are equal. Compressive stresses are defined as negative, whereas a compressive pressure is positive, so the stress state for hydrostatic compression looks like this:

$$\sigma = \begin{bmatrix} -p & 0 & 0 \\ 0 & -p & 0 \\ 0 & 0 & -p \end{bmatrix} \quad (3.48)$$

where  $p$  is the **hydrostatic pressure**.

### 3.5.5 Uniaxial Extension

Uniaxial extension corresponds to the application of a normal stress along one direction, which we define here as the 3 direction so that the stress tensor looks like this:

$$\sigma = \begin{bmatrix} 0 & 0 & 0 \\ 0 & 0 & 0 \\ 0 & 0 & \sigma_{33} \end{bmatrix} \quad (3.49)$$

We can measure two separate strains from this experiment: the longitudinal strain in the same direction that we apply the stress, and the transverse strain,  $e_{22}$ , measured in the direction perpendicular to the applied stress (we'll assume

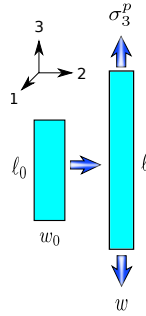


Figure 3.17: Uniaxial tensile deformation.

that the sample is isotropic in the 1-2 plane, so  $e_{11} = e_{22}$ . The strains are given by the fractional changes in the length and width of the sample:

$$e_{33} = \frac{\Delta \ell}{\ell_0} \quad (3.50)$$

$$e_{22} = \frac{\Delta w}{w} \quad (3.51)$$

From these strains we can define **Young's modulus**,  $E$ , and **Poisson's ratio**,  $\nu$ :

$$E = \sigma_{33} / e_{33} \quad (3.52)$$

$$\nu = -e_{22} / e_{33} \quad (3.53)$$

### 3.5.6 Longitudinal Compression

A final deformation state that we will consider is longitudinal compression. In this state all of the compression is in one direction, which we will specify as the 3 direction. The strains in the other two direction are constrained to be zero, so the strain state is as follows:

$$e = \begin{bmatrix} 0 & 0 & 0 \\ 0 & 0 & 0 \\ 0 & 0 & e_{33} \end{bmatrix}$$

Note that the strain state is similar to that of uniaxial extension or compression (Figure 3.17), but in the current case we have a single nonzero strain instead of a single non-zero stress. Finite values of  $\sigma_{11}$  and  $\sigma_{22}$  must exist in order for sample in order for this strain state to be maintained, but we're not going to

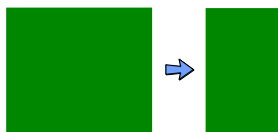


**Figure 3.18:** Longitudinal Compression

**Table 3.1:** Representative elastic moduli for different materials.

Material	$G$ (Pa)	$K_b$ (Pa)
Air	0	$1.0 \times 10^5$
Water	0	$2.2 \times 10^9$
Jello	$\approx 10^4$	$2.2 \times 10^9$
Plastic	$\approx 10^9$	$\approx 2 \times 10^9$
Steel	$8 \times 10^{10}$	$1.6 \times 10^{11}$

worry about those for now. Instead, we'll use the following relationship for the longitudinal elastic modulus,  $E_\ell$  which is the ratio of  $\sigma_{33}$  to  $e_{33}$  for this strain state. Note that this deformation state changes both the shape and volume of the material, so  $E_\ell$  involves both  $G$  and  $K_b$ :

$$E_\ell = \frac{\sigma_{33}}{e_{33}} = K_b + \frac{4}{3}G \quad (3.54)$$

### 3.6 Representative Moduli

A few typical values for  $G$  and  $K$  are listed in Table on this page. Liquids do not have a shear modulus, but they do have a bulk modulus.

### 3.7 Case Study: Speed of Sound

The speed of sound, or **sound velocity**,  $V_{sound}$ , is actually a mechanical property. It is related to a modulus,  $M$ , in the following way:

$$V_{sound} = \sqrt{\frac{M}{\rho}} \quad (3.55)$$

Here  $\rho$  is the density of the material. The modulus that we need to use depends on the type of sound wave that is propagating. The two most common are a shear wave and a longitudinal compressional wave:

- Longitudinal compressional wave:  $M = E_\ell$
- Shear wave:  $M = G$

In a liquid or gas (like air),  $G = 0$  and shear waves cannot propagate. In this case there is a single sound velocity obtained by setting  $M = K_b$ . For an ideal gas:

$$P = \frac{n}{V}RT \quad (3.56)$$

If the compression is applied slowly enough so that the temperature of the gas can equilibrate, we have:

$$K_b = -V \frac{dP}{dV} = \frac{n}{V}RT = P \quad (3.57)$$

So we expect that for a gas, the compressive modulus just equal to the pressure. The situation is a bit more complicated for gas, since we need to use the adiabatic modulus, which is about 40% higher than the pressure itself. (For a detailed explanation, see the Wikipedia article on the speed of sound ([http://en.wikipedia.org/wiki/Speed\\_of\\_sound](http://en.wikipedia.org/wiki/Speed_of_sound))[4]. The brief explanation is that for sound propagation, the derivative in Eq. 3.57 needs to be evaluated at constant entropy and not constant temperature, because the sound oscillation is so fast that the heat does not have time to escape). With  $\rho=1.2 \text{ kg/m}^3$  and  $K = 1.4 \times 10^5 \text{ Pa}$ , we end up with a sound velocity of 344 m/s.

**Table 4.1:** Definition of the matrix components of stress and strain.

Engineering stress	Matrix Stress	Engineering Strain	Matrix Strain
$\sigma_{11}$	$\sigma_1$	$e_{11}$	$e_1$
$\sigma_{22}$	$\sigma_2$	$e_{22}$	$e_2$
$\sigma_{33}$	$\sigma_3$	$e_{33}$	$e_3$
$\sigma_{23}$	$\sigma_4$	$e_{23}$	$e_4$
$\sigma_{13}$	$\sigma_5$	$e_{13}$	$e_5$
$\sigma_{12}$	$\sigma_6$	$e_{12}$	$e_6$

## 4 Matrix representation of Stress and Strain

As usual, we begin by replacing the directions ( $x$ ,  $y$ , and  $z$ ) with numbers:  $x \rightarrow 1$ ,  $y \rightarrow 2$ ,  $z \rightarrow 3$ . Once we do this we have 6 stress components, and six strain components. We then number these components from 1-6, so that 1, 2 and 3 are the normal components and 4, 5 and 6 are the shear components. We do this for both stress and strain as shown in Table 4.1.

A series of elastic constants relate the stresses to the strains. We can do calculations in either of the following two ways:

1. Start with a column vector consisting of the 6 elements of an applied stress, and use the compliance matrix to calculate the strains.
2. Start with a column vector consisting of the 6 elements of an applied strain, and use the stiffness matrix to calculate the stresses.

In each case we use a  $6 \times 6$  matrix to relate two 6-element column vectors to one another. The procedure in each case is outlined below.

### 4.1 Compliance matrix

$$\begin{bmatrix} e_1 \\ e_2 \\ e_3 \\ e_4 \\ e_5 \\ e_6 \end{bmatrix} = \begin{bmatrix} s_{11} & s_{12} & s_{13} & s_{14} & s_{15} & s_{16} \\ s_{21} & s_{22} & s_{23} & s_{24} & s_{25} & s_{26} \\ s_{31} & s_{32} & s_{33} & s_{34} & s_{35} & s_{36} \\ s_{41} & s_{42} & s_{43} & s_{44} & s_{45} & s_{46} \\ s_{51} & s_{52} & s_{53} & s_{54} & s_{55} & s_{56} \\ s_{61} & s_{62} & s_{63} & s_{64} & s_{65} & s_{66} \end{bmatrix} \begin{bmatrix} \sigma_1 \\ \sigma_2 \\ \sigma_3 \\ \sigma_4 \\ \sigma_5 \\ \sigma_6 \end{bmatrix} \quad (4.1)$$

The matrix must be symmetric, with  $s_{ij} = s_{ji}$ , so there are a maximum of 21 independent compliance coefficients:

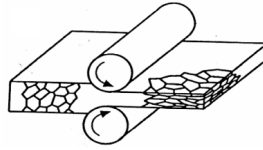


Figure 4.1: Schematic representation of an extruded sheet.

$$\begin{bmatrix} e_1 \\ e_2 \\ e_3 \\ e_4 \\ e_5 \\ e_6 \end{bmatrix} = \begin{bmatrix} s_{11} & s_{12} & s_{13} & s_{14} & s_{15} & s_{16} \\ s_{12} & s_{22} & s_{23} & s_{24} & s_{25} & s_{26} \\ s_{13} & s_{23} & s_{33} & s_{34} & s_{35} & s_{36} \\ s_{14} & s_{24} & s_{34} & s_{44} & s_{45} & s_{46} \\ s_{15} & s_{25} & s_{35} & s_{45} & s_{55} & s_{56} \\ s_{16} & s_{26} & s_{36} & s_{46} & s_{56} & s_{66} \end{bmatrix} \begin{bmatrix} \sigma_1 \\ \sigma_2 \\ \sigma_3 \\ \sigma_4 \\ \sigma_5 \\ \sigma_6 \end{bmatrix} \quad (4.2)$$

Note that the compliance coefficients have the units of an inverse stress ( $\text{Pa}^{-1}$ ).

## 4.2 Stiffness Matrix

The stiffness matrix ( $c$ ) is the inverse of compliance matrix (note the somewhat confusing notation in that the compliance matrix is  $s$  and the stiffness is  $c$ , backwards from what you might expect). The stiffness coefficients have units of stress.

$$\begin{bmatrix} \sigma_1 \\ \sigma_2 \\ \sigma_3 \\ \sigma_4 \\ \sigma_5 \\ \sigma_6 \end{bmatrix} = \begin{bmatrix} c_{11} & c_{12} & c_{13} & c_{14} & c_{15} & c_{16} \\ c_{12} & c_{22} & c_{23} & c_{24} & c_{25} & c_{26} \\ c_{13} & c_{23} & c_{33} & c_{34} & c_{35} & c_{36} \\ c_{14} & c_{24} & c_{34} & c_{44} & c_{45} & c_{46} \\ c_{15} & c_{25} & c_{35} & c_{45} & c_{55} & c_{56} \\ c_{16} & c_{26} & c_{36} & c_{46} & c_{56} & c_{66} \end{bmatrix} \begin{bmatrix} e_1 \\ e_2 \\ e_3 \\ e_4 \\ e_5 \\ e_6 \end{bmatrix} \quad (4.3)$$

## 4.3 Symmetry requirements on the compliance (or stiffness) matrix.

### 4.3.1 Orthorhombic symmetry

Extruded polymer sheets, like the one shown schematically in Figure 4.1 have orthorhombic symmetry, with different elastic properties in the extrusion, thickness and width directions. These materials have orthorhombic symmetry.

For materials with orthorhombic symmetry, the principal axes of stress and strain are identical, and all compliance components relating a shear strain ( $e_4$ ,  $e_5$  or  $e_6$ ) to normal stresses ( $\sigma_1, \sigma_2$  or  $\sigma_3$ ) or to another shear stress must be zero. The stiffness matrix is as shown in Eq. 4.4 below, and there are 9 independent elastic constants. These 9 elastic constants can be identified as follows:

- $E_1 = 1/s_{11}$ ,  $E_2 = 1/s_{22}$  and  $E_3 = 1/s_{33}$ , Young's moduli for extension in the 1, 2 and 3 directions, respectively.
- $G_1 = 1/s_{44}$ ,  $G_2 = 1/s_{55}$  and  $G_3 = 1/s_{66}$ , Shear moduli for shear in the planes perpendicular to the 1, 2 and 3 directions, respectively.
- $s_{12}$ ,  $s_{13}$  and  $s_{23}$ , which relate stresses in one direction to strains in the perpendicular direction.

$$\begin{bmatrix} e_1 \\ e_2 \\ e_3 \\ e_4 \\ e_5 \\ e_6 \end{bmatrix} = \begin{bmatrix} s_{11} & s_{12} & s_{13} & 0 & 0 & 0 \\ s_{12} & s_{22} & s_{23} & 0 & 0 & 0 \\ s_{13} & s_{23} & s_{33} & 0 & 0 & 0 \\ 0 & 0 & 0 & s_{44} & 0 & 0 \\ 0 & 0 & 0 & 0 & s_{55} & 0 \\ 0 & 0 & 0 & 0 & 0 & s_{66} \end{bmatrix} \begin{bmatrix} \sigma_1 \\ \sigma_2 \\ \sigma_3 \\ \sigma_4 \\ \sigma_5 \\ \sigma_6 \end{bmatrix} \quad (4.4)$$

### 4.3.2 Fiber Symmetry

For a material with fiber symmetry, one of the axes is unique (in this case the 3 axis) and the material is isotropic in the orthogonal plane. Since the 1 and 2 axes are identical, there are now 5 independent elastic constants  $s_{33}$ ,  $s_{13}$ ,  $s_{44}$ ,  $s_{11}$ ,  $s_{12}$ :

$$\begin{bmatrix} e_1 \\ e_2 \\ e_3 \\ e_4 \\ e_5 \\ e_6 \end{bmatrix} = \begin{bmatrix} s_{11} & s_{12} & s_{13} & 0 & 0 & 0 \\ s_{12} & s_{11} & s_{13} & 0 & 0 & 0 \\ s_{13} & s_{13} & s_{33} & 0 & 0 & 0 \\ 0 & 0 & 0 & s_{44} & 0 & 0 \\ 0 & 0 & 0 & 0 & s_{44} & 0 \\ 0 & 0 & 0 & 0 & 0 & 2(s_{11} - s_{12}) \end{bmatrix} \begin{bmatrix} \sigma_1 \\ \sigma_2 \\ \sigma_3 \\ \sigma_4 \\ \sigma_5 \\ \sigma_6 \end{bmatrix} \quad (4.5)$$

Examples of materials with fiber symmetry include the following:

1. Many liquid crystalline polymers (e.g. Kevlar).
2. Materials after cold drawing (plastic deformation to high strains, carried out below the glass transition temperature or melting temperature of the material.)

To better understand the significance of the 5 elastic constants for fiber symmetry, it is useful to consider the types of experiment we would need to conduct to measure each of them for a cylindrical fiber. The necessary experiments are described below.

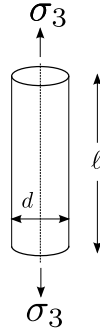


Figure 4.2: Fiber extension.

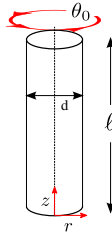


Figure 4.3: Fiber torsion.

**Fiber extension along 3 direction: measurement of  $s_{33}$  and  $s_{13}$**  We obtain  $s_{33}$  and  $s_{13}$  by performing a tensile test along the fiber axis (the 3 direction) as shown in Figure 4.2. The strain in the 3 direction is given by the fractional change in the length of the fiber after application of the load, and the strains in the 1 and 2 directions are given by the fractional changes in the diameter of the fiber:

$$e_3 = \Delta\ell/\ell; \quad e_1 = e_2 = \Delta d/d \quad (4.6)$$

We then obtain  $s_{33}$  and  $s_{13}$  from Eq. 4.5, recalling that  $\sigma_3$  is the only non-zero stress component in this situation:

$$\begin{aligned} s_{33} &= e_{33}/\sigma_3 \\ s_{13} &= e_1/\sigma_3 \end{aligned} \quad (4.7)$$

**Fiber Torsion: Measurement of  $s_{44}$**  We obtain the shear modulus by looking at the torsional stiffness of the fiber, *i.e.*, the torque,  $T$ , required to rotate the top and bottom of the fiber by an angle  $\theta_0$ , as illustrated in Figure 4.3

We define a cylindrical system with a  $z$  axis along the fiber axis. The other axes in this coordinate system are the distance  $r$  from this axis of symmetry, and the



angle  $\theta$  around the  $z$  axis. The shear strain in the  $\theta - z$  plane depends only on  $r$ , and is given by :

$$e_{\theta z} = r \frac{d\theta}{dz} = r \frac{\theta_0}{\ell} \quad (4.8)$$

The corresponding shear stress is obtained by multiplying by the shear modulus,  $G$  characterizing deformation in the 1-2 and 2-3 planes:

$$\sigma_{\theta z} = Gr\theta_0/\ell \quad (4.9)$$

We integrate the shear stress to give the torque,  $T$ :

$$T = \int_0^{d/2} r\sigma_{\theta z} 2\pi r dr = \frac{\pi G\theta_0 d^4}{32\ell} \quad (4.10)$$

So once we know the torsional stiffness of the fiber (the relationship between the applied  $T$  and  $\theta_0$ ) we know the shear modulus,  $G$ . This shear modulus is simply the inverse of  $s_{44}$ :

$$G = \frac{1}{s_{44}} \quad (4.11)$$

### 4.3.3 Fiber compression in 1-2 plane: determination of $s_{11}$ and $s_{12}$

The last two elastic constants for a material with fiber symmetry can be determined from an experiment where the fiber is confined between two surfaces and compressed as shown in Figure 4.4. The elastic constants can be determined by measuring the width of the contact region between the fiber and the confining surface. If the confining surfaces are much stiffer than the fiber itself, then this contact width,  $2b$ , is determined by the elastic deformation of the material in the 1-2 plane. If there is no friction between the fiber and the confining surfaces the fiber is allowed to extend in the 3 direction as it is compressed and the contact width is given by the following expression:

$$b^2 = \frac{2Fd_0 s_{11}}{\ell} \quad (4.12)$$

where  $P$  is the force applied to the fiber,  $d_0$  is its undeformed diameter and  $\ell$  is its length.

A practical situation that is often observed is that friction between the fiber and confining surfaces keeps the fiber length from increasing, so the strain in

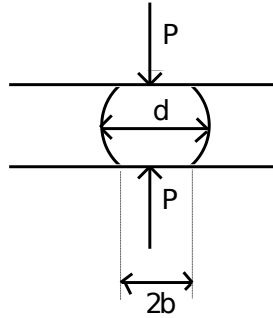


**Figure 4.4:** Transverse deformation of a fiber.

the three direction must be zero. If we express the stress state in terms of the principle stresses in 1 and 2 directions, we have the following from Eq. 4.5:

$$e_3 = s_{13} (\sigma_1^p + \sigma_2^p) + s_{33}\sigma_3 \quad (4.13)$$

Setting  $e_3$  to zero in this equation gives the following for  $\sigma_3$ :

$$\sigma_3 = \frac{-s_{13}}{s_{33}} (\sigma_1^p + \sigma_2^p) \quad (4.14)$$

A consequence of this stress is that the frictionless expression for  $b$  gets modified to the following:

$$b^2 = \frac{2Fd_0}{\ell} \left( s_{11} - \frac{s_{13}^2}{s_{33}} \right) \quad (4.15)$$

The remaining constant,  $s_{12}$ , is determined from a measurement of  $d/d_0$ , the ratio of the fiber width at the midplane to the original width of the fiber. This relationship is complicated, and involves several of the different elastic constants.

$$\frac{d}{d_0} = f(P, s_{11}, s_{13}, s_{33}, s_{12}) \quad (4.16)$$

#### 4.3.4 Cubic Symmetry

For a material with cubic symmetry the 1,2 and 3 axes are all identical to one another, and we end up with 3 independent elastic constants:

$$\begin{bmatrix} e_1 \\ e_2 \\ e_3 \\ e_4 \\ e_5 \\ e_6 \end{bmatrix} = \begin{bmatrix} s_{11} & s_{12} & s_{12} & 0 & 0 & 0 \\ s_{12} & s_{11} & s_{12} & 0 & 0 & 0 \\ s_{12} & s_{12} & s_{11} & 0 & 0 & 0 \\ 0 & 0 & 0 & s_{44} & 0 & 0 \\ 0 & 0 & 0 & 0 & s_{44} & 0 \\ 0 & 0 & 0 & 0 & 0 & s_{44} \end{bmatrix} \begin{bmatrix} \sigma_1 \\ \sigma_2 \\ \sigma_3 \\ \sigma_4 \\ \sigma_5 \\ \sigma_6 \end{bmatrix} \quad (4.17)$$

### 4.3.5 Isotropic systems

For an isotropic material all axes are equivalent, and the properties are invariant to any rotation of the coordinate axes. In this case there are two independent elastic constants, and the compliance matrix looks like this:

$$\begin{bmatrix} e_1 \\ e_2 \\ e_3 \\ e_4 \\ e_5 \\ e_6 \end{bmatrix} = \begin{bmatrix} s_{11} & s_{12} & s_{12} & 0 & 0 & 0 \\ s_{12} & s_{11} & s_{12} & 0 & 0 & 0 \\ s_{12} & s_{12} & s_{11} & 0 & 0 & 0 \\ 0 & 0 & 0 & 2(s_{11} - s_{12}) & 0 & 0 \\ 0 & 0 & 0 & 0 & 2(s_{11} - s_{12}) & 0 \\ 0 & 0 & 0 & 0 & 0 & 2(s_{11} - s_{12}) \end{bmatrix} \begin{bmatrix} \sigma_1 \\ \sigma_2 \\ \sigma_3 \\ \sigma_4 \\ \sigma_5 \\ \sigma_6 \end{bmatrix} \quad (4.18)$$

The requirement that the material properties be invariant with respect to any rotation of the coordinate axes results in the requirement that  $s_{44} = 2(s_{11} - s_{12})$ , so there are two independent elastic constants. The shear modulus,  $G$ , Young's modulus  $E$  and Poisson's ratio,  $\nu$  are given as follows:

$$G = 1/2(s_{11} - s_{12}); \quad E = 1/s_{11}; \quad \nu = -s_{12}/s_{11} \quad (4.19)$$

**Bulk Modulus for an Isotropic Material** The bulk modulus,  $K_b$ , of a material describes its resistance to a change in volume (or density) when we apply a hydrostatic pressure,  $p$ . It is defined in the following way:

$$K_b = -V \frac{dP}{dV} \quad (4.20)$$

The stress state in this case is as follows:

$$\sigma = \begin{bmatrix} -p & 0 & 0 \\ 0 & -p & 0 \\ 0 & 0 & -p \end{bmatrix} \quad (4.21)$$

From the compliance matrix (Eq. 4.18) we get  $e_1 = e_2 = e_3 = -p(s_{11} + 2s_{12})$ . The change in volume,  $\Delta V$  can be written in terms of the three principal extension ratios,  $\lambda_1, \lambda_2$  and  $\lambda_3$ :

$$\frac{\Delta V}{V_0} = \frac{V}{V_0} - 1 = \lambda_1 \lambda_2 \lambda_3 - 1 = (1 + e_1)(1 + e_2)(1 + e_3) - 1 \approx e_1 + e_2 + e_3 \quad (4.22)$$

Now we use the fact that for small  $x$ ,  $(1 + x)^3 \approx 1 + 3x$ , so we have:

$$\frac{\Delta V}{V_0} = e_1 + e_2 + e_3 = -3p(s_{11} + 2s_{12}) \quad (4.23)$$

Recognizing that the derivative  $dP/dV$  in the definition of  $K_b$  can be written as the limit of  $p/\Delta V$  for very small  $p$  allows us to obtain the expression we want for  $K_b$ :

$$K_b = \lim_{p \rightarrow 0} \frac{-p}{\Delta V/V_0} = \frac{1}{3(s_{11} + 2s_{12})} \quad (4.24)$$

**Relationship between the Isotropic Elastic Constants:** Because there are only two independent elastic constants for an isotropic system  $E$  and  $\nu$  can be expressed in terms of some combination of  $K_b$  and  $G$ . For  $E$  the relevant relationship is as follows.

$$E = \frac{9G}{3 + G/K_b} = 2G(1 + \nu) \quad (4.25)$$

We can also equate the two expressions for  $G$  in Eq. 4.25 to get the following expression for  $\nu$ :

$$\nu = \frac{3 - 2G/K_b}{6 + 2G/K_b} \quad (4.26)$$

Note that if  $K_b \gg G$ ,  $E \approx 3G$  and  $\nu \approx 0.5$ .

### 4.3.6 Relationship between Stiffness Matrix and Compliance Matrix

The stiffness matrix is the inverse of the compliance matrix. The relationships between the individual coefficients is quite complicated, unless there is a lot of symmetry. It's not too bad for the isotropic case, in which case we can use symbolic python to do the inversion. Here's the code:

```

1 from sympy import symbols, Matrix, preview
2 # specify two independent elements of s for an isotropic material
3 s11, s12 = symbols(['s_11', 's_12'])
4
5 # define the matrix
6 s = Matrix([[s11, s12, s12, 0,0,0],
7             [s12,s11,s12,0,0,0],
8             [s12,s12,s11,0,0,0],
9             [0,0,0,2*(s11-s12),0,0],
10            [0,0,0,0,2*(s11-s12),0],
11            [0,0,0,0,0,2*(s11-s12)]])
12
13 # now invert the matrix
14 c=s.inv()
15 preview(c, viewer = 'file', filename = '../figures/sympy_c.png')

```

This gives the output shown here:

$$\begin{bmatrix}
 \frac{s_{11}+s_{12}}{s_{11}^2+s_{11}s_{12}-2s_{12}^2} & -\frac{s_{12}}{s_{11}^2+s_{11}s_{12}-2s_{12}^2} & -\frac{s_{12}}{s_{11}^2+s_{11}s_{12}-2s_{12}^2} & 0 & 0 & 0 \\
 -\frac{s_{12}}{s_{11}^2+s_{11}s_{12}-2s_{12}^2} & \frac{s_{11}+s_{12}}{s_{11}^2+s_{11}s_{12}-2s_{12}^2} & -\frac{s_{12}}{s_{11}^2+s_{11}s_{12}-2s_{12}^2} & 0 & 0 & 0 \\
 -\frac{s_{12}}{s_{11}^2+s_{11}s_{12}-2s_{12}^2} & -\frac{s_{12}}{s_{11}^2+s_{11}s_{12}-2s_{12}^2} & \frac{s_{11}+s_{12}}{s_{11}^2+s_{11}s_{12}-2s_{12}^2} & 0 & 0 & 0 \\
 0 & 0 & 0 & \frac{1}{2s_{11}-2s_{12}} & 0 & 0 \\
 0 & 0 & 0 & 0 & \frac{1}{2s_{11}-2s_{12}} & 0 \\
 0 & 0 & 0 & 0 & 0 & \frac{1}{2s_{11}-2s_{12}}
 \end{bmatrix}$$

Note that the stiffness matrix has the same symmetry as the compliance matrix, as it must:

$$\begin{bmatrix} \sigma_1 \\ \sigma_2 \\ \sigma_3 \\ \sigma_4 \\ \sigma_5 \\ \sigma_6 \end{bmatrix} = \begin{bmatrix} c_{11} & c_{12} & c_{12} & 0 & 0 & 0 \\ c_{12} & c_{11} & c_{12} & 0 & 0 & 0 \\ c_{12} & c_{12} & c_{11} & 0 & 0 & 0 \\ 0 & 0 & 0 & G & 0 & 0 \\ 0 & 0 & 0 & 0 & G & 0 \\ 0 & 0 & 0 & 0 & 0 & G \end{bmatrix} \begin{bmatrix} e_1 \\ e_2 \\ e_3 \\ e_4 \\ e_5 \\ e_6 \end{bmatrix} \tag{4.27}$$

Comparison of Eq. 4.27 to the output from symbolic\_cmatrix.py gives the following:

$$G = \frac{1}{2(s_{11} - s_{12})}; \quad c_{11} = \frac{s_{11} + s_{12}}{s_{11}^2 + s_{11}s_{12} - 2s_{12}^2}; \quad c_{12} = \frac{-s_{12}}{s_{11}^2 + s_{11}s_{12} - 2s_{12}^2} \tag{4.28}$$

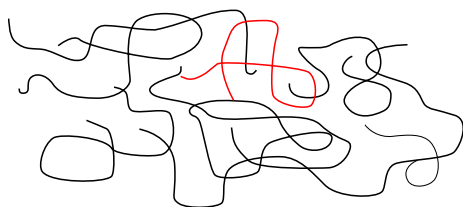


Figure 5.1: A diagram of an amorphous polymer.

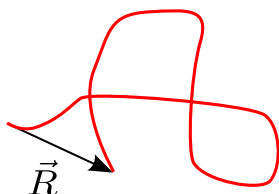


Figure 5.2: The end-to-end vector,  $\vec{R}$ , for a polymer molecule.

## 5 Structure of Amorphous Polymers

Materials science is the study and application of the relationships between the properties of a material, the structure required to obtain these properties, and the processing methods which can be used to obtain these properties. Our discussion of polymer synthesis was motivated primarily by a need to understand processing methods for polymer materials. We also introduced the structure of different polymers at the atomic level, corresponding to the arrangements of individual atoms in the polymeric repeat units. Our discussion now moves to the structure of polymers on a molecular scale. We begin with amorphous polymers, and follow with a discussion of semicrystalline polymers. Ultimately, we will find that our understanding of many of the important properties of polymers can be related to these structural features by simple, yet remarkably accurate theories. In particular, the theory of rubber elasticity relates the elastic properties of an elastomer to the molecular structure described here.

The squiggly lines in Figure 5.1 represent the backbones of individual molecules in an amorphous polymer. (One molecule is highlighted in red) Our goal is to relate the properties of an amorphous polymer to the distribution of shapes of these molecules. Ultimately, we will show that many of the mechanical properties of amorphous polymers at temperatures above the glass transition are related to this distribution of polymer shapes.

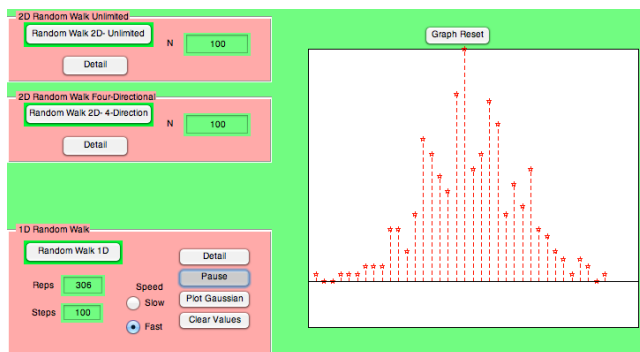


Figure 5.3: Random walk animation

## 5.1 End-to-end Vector for Polymer Molecules

The shape of this particular molecule can only be completely specified by describing the path taken by the molecule from one end to the other. Fortunately, the most important quantity is much simpler. This quantity **end-to-end vector**,  $\vec{R}$  which is simply the vector spanning the two ends of a given polymer molecule. This vector will in general be different for different polymer molecules in a sample, but the distribution of vectors can be accurately predicted. The shapes of amorphous polymer molecules are random, and random walk statistics can be used to describe the distributions of end-to-end vectors that are obtained.

## 5.2 Random Walk in One Dimension

We can understand much of what we need to understand by considering the simplest case of a random walk in 1 dimension. In this case our 'walker' takes  $N_x$  steps, each of which is a randomly chosen move to either the left or right. At the end of these  $N_x$  steps we write down how many steps removed from the starting point our walker is. We refer to this number as  $i$ . For example, if the walker ends up 4 steps to the right of where he ended up, then  $i = 4$ . Where our walker ended up after one particular trip is not very important though. We need to have him take lots of trips, and collect statistics to see where he ended up after taking a large number of trips. We'll let him take a total of  $M$  trips, and write down the number of times,  $n$ , that the walker has ended up  $i$  steps from where we started. If the walk is really random, then the relationship between  $n$  and  $i$  will be approximated by Eq. 5.1

$$n(i) = 2M \left( \frac{1}{2\pi N_x} \right)^{1/2} \exp \left( \frac{-i^2}{2N_x} \right) \quad (5.1)$$

We can check that the summation is appropriately normalized. In other words, is the following expression valid?

$$\sum_i n_i = M \quad (5.2)$$

The summation here is over all possible values of  $i$ . Note that for a random walk with an even number of steps, only even values of  $i$  are possible. Similarly, for a walk with an odd number of steps, only odd values of  $i$  are possible. We can get the summation we want by summing over all integer values of  $i$  and then dividing by two:

$$\sum_i n(i) = \frac{M}{\sqrt{2\pi N_x}} \sum_{i=-\infty}^{\infty} \exp\left(\frac{-i^2}{2N_x}\right) \approx \frac{M}{\sqrt{2\pi N_x}} \int_{-\infty}^{\infty} \exp\left(\frac{-i^2}{2N_x}\right) di \quad (5.3)$$

Functions of the form  $f(x) \propto \exp - (x/A)^2$  (where  $A$  is a constant) are called Gaussian functions, and generally describe random processes. The following integrals of a Gaussian function will be very useful for us:

$$\begin{aligned} \int_{-\infty}^{\infty} \exp - (x/A)^2 dx &= A\sqrt{\pi} \quad (\text{a}) \\ \int_{-\infty}^{\infty} x \exp - (x/A)^2 dx &= 0 \quad (\text{b}) \\ \int_{-\infty}^{\infty} x^2 \exp - (x/A)^2 dx &= A^3\sqrt{\pi}/2 \quad (\text{c}) \end{aligned} \quad (5.4)$$

In our case,  $A = \sqrt{2N_x}$ , so  $\sum_i n(i) = M$  and our expression for the Gaussian distribution of random walks is indeed normalized.

### 5.3 Average of a Function

The entire distribution represented by the Gaussian function will be useful to us, but it is still useful to have some averages. We encountered averages already in our discussion of the number and weight average distribution. In general, if  $P_x(x)$  is the probability that a discrete variable has a value of  $x$ , then the average value of  $x$  (referred to as  $\langle x \rangle$ ) is obtained from the following expression:

$$\langle x \rangle = \sum_x x P_x(x) \quad (5.5)$$



where the sum is over all possible values of  $x$ . Similarly, the average of  $x^2$  is given by:

$$\langle x^2 \rangle = \sum_x x^2 P_x(x) dx \quad (5.6)$$

The procedure can be generalized to calculate the average of any function of  $x$ :

$$\langle f(x) \rangle = \sum_x f(x) P_x(x) \quad (5.7)$$

**Exercise:** Suppose I put the following 10 numbers into a drawer: 1, 4, 8, 12, 19, 25, 28, 33, 37, 45. I randomly pick a number from the drawer and then return it. What is the average value of all the numbers that I pick if I continue with this exercise?

**Solution:** We just use Eq. 5.5. Since there are 10 numbers and I am equally likely to be picked, they each have a value of 0.1 for  $P_r$ . So in this case we have:

$$= 0.1 (1 + 4 + 8 + 12 + 19 + 25 + 28 + 33 + 37 + 45) = 21.2$$

In this case the answer is just the average of all the numbers, which is about as simple it gets.

In general for a function of  $i$ , where  $i$  is only able to take on discrete values, we have:

$$\langle f(i) \rangle = \sum_i f(i) P_r(i)$$

What if we have a function of a continuous variable,  $x$ ? In this case, we must replace  $P(i)$ , with  $P_r(x) dx$ , where  $P_r(x) dx$  is the probability that the continuous variable has a value between  $x$  and  $x + dx$ . We must also replace the summation with the appropriate integral to obtain the following result:

$$\langle f(x) \rangle = \int f(x) P_r(x) dx \quad (5.8)$$

**Exercise:** Suppose I put the following 10 numbers into a drawer: 1, 4, 8, 12, 19, 25, 28, 33, 37, 45. I randomly pick a number from the drawer and then return it. What is the average value of all the numbers that I pick if I continue with this exercise?

**Solution:** Calculate the average value of  $x^2$ , assuming that  $x$  is equally likely to take on all values between 1 and 10, and that no values outside this range are possible. We know that  $P_r$  has some constant value between 1 and 10. In order for our procedure to work, we need to make sure that the probability distribution is normalized, with  $\int_{x_{min}}^{x_{max}} P_r(x) dx = 1$ . In our case this gives  $P_r = 1/9$  and we get:

$$\langle x^2 \rangle = \frac{1}{9} \int_1^{10} x^2 dx = \frac{1}{27} x^3 \Big|_1^9 = \frac{10^3 - 1}{27} = \frac{999}{27} = 37$$

## 5.4 Averages for Random Walks

If the length of each step taken by the random walker is  $a$ , then the distance between the beginning and the end of the walk is simply  $i$  times this step length:

$$R_x = ia$$

We can substitute  $R_x/a$  for  $i$  and  $dR_x/a$  for  $di$  in Eq. 5.3 to get an expression for the total number of walks  $M$ . We'll generalize a bit further and replace the limits of  $-\infty$  and  $\infty$  for  $i$  to limits of  $R_{min}$  and  $R_{max}$  for  $R_x$ . We obtain the following for  $M(R_{min}, R_{max})$ , the total number of walks with values of  $R_x$  between  $R_{min}$  and  $R_{max}$ :

$$M(R_{min}, R_{max}) = M \int_{R_{min}}^{R_{max}} P_x dR_x \quad (5.9)$$

with the probability density function,  $P_x$  given as follows:

$$P_x = \frac{1}{\sqrt{2\pi N_x a^2}} \exp\left(\frac{-R_x^2}{2N_x a^2}\right) \quad (5.10)$$

To calculate the average values of  $R_x$  and  $R_x^2$ , referred to as  $\langle R_x \rangle$  and  $\langle R_x^2 \rangle$ , respectively, we use Eq. 5.8 to calculate the averages:

$$\langle R_x \rangle = \int_{-\infty}^{\infty} R_x P_x dR_x = \frac{1}{\sqrt{2\pi N_x a^2}} \int_{-\infty}^{\infty} R_x \exp\left(-\frac{R_x^2}{2N_x a^2}\right) dR_x = 0 \quad (5.11)$$

$$\langle R_x^2 \rangle = \int_{-\infty}^{\infty} R_x^2 P_x dR_x = \frac{1}{\sqrt{2\pi N_x a^2}} \int_{-\infty}^{\infty} R_x^2 \exp\left(-\frac{R_x^2}{2N_x a^2}\right) dR_x = N_x a^2 \quad (5.12)$$

We know intuitively that Eq. 5.11 must be true because the Gaussian distribution function is symmetric: positive and negative values of  $R_x$  with equal magnitudes are equally likely. This means that any contribution to  $\langle R_x \rangle$  will be exactly offset by a contribution with the opposite sign. For this reason, the root mean square end-to-end distance,  $\sqrt{\langle R_x^2 \rangle} = \sqrt{N_x} a$ , is typically used to describe the spatial extent of a random walk.

## 5.5 Random Walks in 3 Dimensions

Now we can extend some of these results to describe the shapes of real polymer molecules. We begin with a discussion of two dimensional random walks. The simplest extension is to give our random walker 4 choices for his movements. In addition to moving to the left and right, he can now move up and down, as illustrated in Figure 5.4a. If we move the constraint that there are only 2 directions in which the walker can move, we get the example shown in Figure 5.4b. These trajectories are now beginning to look like the shapes of actual polymer molecules, which is why this whole exercise is relevant.

Much of our understanding of amorphous polymers is based on our treatment of individual molecules as random walks in three dimensions. We assume that we can treat a polymer of degree of polymerization  $N$  as a random walk of  $N$  steps, each with an effective length of  $a$ , which we refer to as the **Statistical segment length**. The statistical segment length does not correspond to a real polymer dimension that we can get directly by looking at the structure of the polymer molecule. We need more detailed models of chain dimensions for that. For now, you just need to know that it is a length that gives the right overall molecular size. To simplify our treatment and make the connection back to the statistics that we already developed for one-dimensional random walks, we make the following simplifying assumptions:

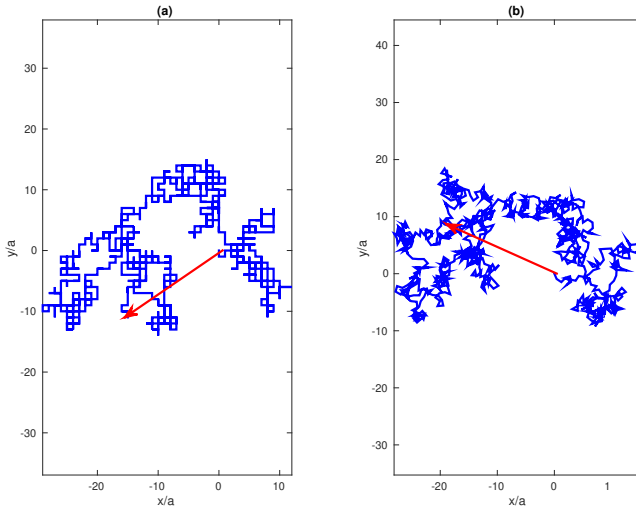


**Figure 5.4:** 2-D Random Walk of 1000 steps on a square lattice (a) and with random bond angles (b). The end-to-end vector,  $\vec{R}$ , is shown in each case.

- We will get the overall statistics right by assuming a simple lattice model (as in Figure 5.4), where the a chain is able to move in any of the x, y or z directions.
- Of the  $N$  steps made by the chain,  $N/3$  of them move in each of the x, y and z directions.

The value of  $R_x$  that we studied in the one dimensional random walk case is just the x component of the end-to-end vector, which also has y and z components:

$$\vec{R} = R_x \hat{x} + R_y \hat{y} + R_z \hat{z} \quad (5.13)$$

where  $\hat{x}$ ,  $\hat{y}$  and  $\hat{z}$  are unit vectors in the x, y and z directions, respectively. The probability,  $P_{xyz}$  that a given random walk of  $N$  steps in three dimensions has an end-to end vector of with x, y and z components of  $R_x$ ,  $R_y$  and  $R_z$  is given by multiplying the probabilities for the individual components:

$$P_{xyz} = P_x P_y P_z = R_0^3 \left( \frac{3}{2\pi} \right)^{3/2} \exp \left( \frac{-3R^2}{2R_0^2} \right) \quad (5.14)$$

Here we have assumed that  $P_y$  and  $P_z$  have the same form as  $P_x$  from Eq. 5.10, with y or z substituting for x as appropriate. We have also used the following relationships:

$$R^2 = R_x^2 + R_y^2 + R_z^2, \quad (5.15)$$

$$N_x = N_y = N_z = N/3, \quad (5.16)$$

along with the following definition of  $R_0$ :

$$R_0 = \sqrt{Na} \quad (5.17)$$

Recall that  $P_{xyz}(R_x, R_y, R_z)dR_x dR_y dR_z$  is the probability that x component of the end-to-end vector is between  $R_x$  and  $R_x + dx$ , the y component is between  $R_y$  and  $R_y + dy$ , and the z component is between  $R_z$  and  $R_z + dz$ . We can also define a probability density  $P_R$ , where  $P_R dR$  is the probability that the magnitude of the end-to-end vector lies between  $R$  and  $R + dR$ . Because the probability only depends on  $R$  for an isotropic system (as must be the case for a truly random walk), we can substitute  $4\pi R^2 dR$  for  $dR_x dR_y dR_z$  to obtain:

$$P_R = 4\pi R^2 P_{xyz} = \frac{4.15R^2}{R_0^3} \exp\left(\frac{-3R^2}{2R_0^2}\right) \quad (5.18)$$

Note that  $R_0^2$  is the average of  $R^2$ , obtained from the following version of Eq. 5.8:

$$\langle R^2 \rangle = \int_0^\infty R^2 P_R dR = \frac{4.15}{R_0^3} \int_0^\infty R^4 \exp\left(\frac{-3R^2}{2R_0^2}\right) = R_0^2 \quad (5.19)$$

Note that the distribution is normalized:  $\int_0^\infty P_R d\bar{R} = 1$ .

**Exercise:** What fraction of molecules in an amorphous polymer have end to end vectors that are within 10% of  $R_0$ ?

**Solution:** We define a new variable,  $\bar{R}$ , such that  $\bar{R} = R/R_0$ . With this definition of  $\bar{R}$ , rewrite Eq. 5.18 in the following way:

$$P_{\bar{R}} = 4.15\bar{R}^2 \exp\left(-1.5\bar{R}^2\right)$$

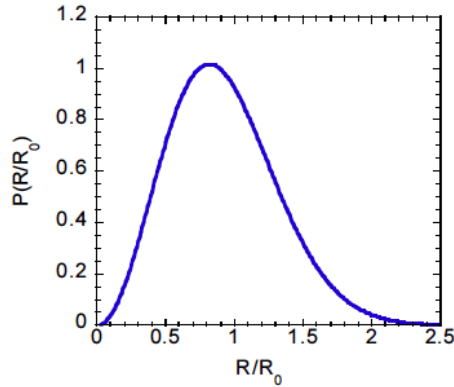
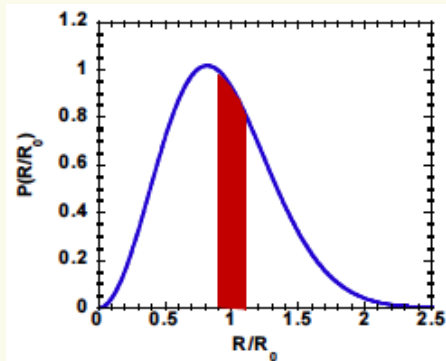


Figure 5.5: Probability density.

Note that this expression for  $P_{\bar{R}}$  is normalized, with  $\int_0^\infty P_{\bar{R}} d\bar{R} = 1$ . We need to integrate the probability density from  $\bar{R}=0.9$  to  $\bar{R} = 1.1$ :

$$P_r^{tot} = 4.15 \int_{0.9}^{1.1} \bar{R}^2 \exp(-1.5\bar{R}^2) d\bar{R}$$

This corresponds to the shaded area in the following figure:



Numerical integration of the equation above gives  $P_r^{tot} = 0.18$ , which corresponds to the red shaded area. This is the total fraction of molecules with  $R$  between  $0.9 R_0$  and  $1.1 R_0$ .

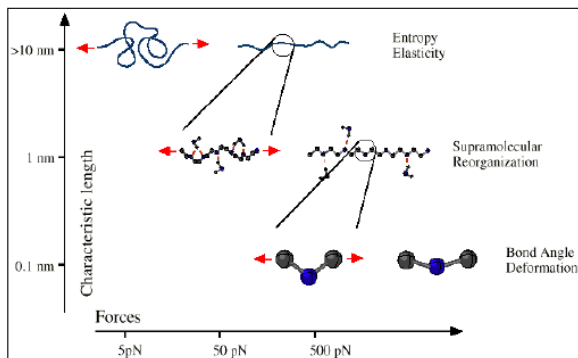


**Figure 6.1:** Molecular deformation occurring at different force and length scales (from From Osterhelt et al.: <http://www.iop.org/EJ/abstract/1367-2630/1/1/006/>).

## 6 Rubber Elasticity

Crosslinked rubbers are unique in that thermodynamic arguments can be used to predict their elastic moduli with remarkable accuracy. Our starting point will be a description of the free energy of an elastomer as a function of its deformation. This free energy is dominated by entropic contributions arising from restrictions on the number of different conformations (or shapes) that polymer strands are able to adopt. The detailed descriptions of polymer chain statistics given earlier were developed so that we would be in a position to describe the mechanical properties of rubbery materials. The description of rubber elasticity given here is proof that statistics and thermodynamics are actually useful!!

### 6.1 Molecular Deformation

Different types of molecular deformations, and the characteristic lengths and forces, are illustrated in Figure 6.1. In rubber elasticity we are interested in deformations due to changes in the overall shapes of the molecules, with typical molecular forces in the range of 10 pN and deformations in the range of 10 nm. In this force regime we don't need to worry about the specific chemistry of the polymer backbone. All that matters is the distance between the two ends of the molecule. Figure 6.2 shows the situation in this regime of 'entropic elasticity' in more detail.

The origins of entropic elasticity can be understood in terms of the probability density,  $P_{xyz}$ , that describes the relative probability that the end-to-end vector has a specific set of  $x$ ,  $y$  and  $z$  components. This probability depends on the

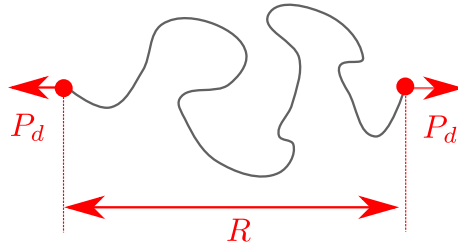


**Figure 6.2:** Illustration of force,  $P_d$ , that must be applied to a single molecule to maintain an end-to-end separation of  $R$ .

magnitude of the end-to-end vector normalized by  $R_0$ , the root-mean-squared value of the end-to-end vector. For our purposes here we'll see that we don't actually need the normalization for  $P_{xyz}$  - we just need to understand how it depends on  $|\vec{R}|$ . For simplicity we refer to  $|\vec{R}|$  simply as  $R$  in our discussion, with  $P_{xyz}$  given as follows:

$$P_{xyz} \propto \exp\left(\frac{-3R^2}{2R_0^2}\right) \quad (6.1)$$

The value of  $P_{xyz}$  is proportional to the number of molecular configurations,  $\Omega$ , that are consistent with this particular value of  $R$ , so we can write:

$$\Omega(\vec{R}) = C \exp\left(\frac{-3R^2}{2R_0^2}\right) \quad (6.2)$$

where  $C$  is some constant that we don't know.

The entropy is obtained from the number of possible molecular shapes:

$$S_d(\vec{R}) = k_B \ln \Omega(\vec{R}) = k_B \ln C - \frac{3k_B R^2}{2Na^2} \quad (6.3)$$

The free energy is assumed to be entirely dominated by this entropic contribution:

$$F_d(\vec{R}) = -TS_d(\vec{R}) = -k_B T \ln C + \frac{3k_B T R^2}{2Na^2} \quad (6.4)$$



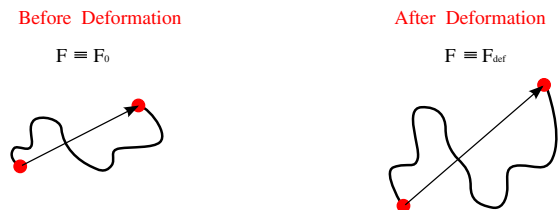


**Figure 6.3:** Contrasting free energies before and after deformation

In reality, there is a small enthalpic contribution to the stretching free energy as well, because stretching the chain increases the relative proportion of higher energy gauche bonds, but we're not going to worry about that correction here. Because we are only every interested in changes in the free energy, constant terms that don't depend on  $R$  are going to drop out when we compare free energies, so the detailed value of this constant is not going to matter.

This expression for the elastic free energy of an individual molecule in terms of its end-to-end distance is remarkably simple. It is one of the most important and widely used results in polymer science. In the following section, we will see how it is used to obtain estimates for the elastic modulus of a crosslinked elastomer.

## 6.2 Free energy of a stretched rubber

When a rubber is stretched, the free energy increases. In general the free energy increase has enthalpic and entropic contributions ( $F_d = H_d - TS_d$ ). The basic assumption of rubber elasticity theory is that the free energy increase due to deformation is dominated by the decrease in the entropy. In other words  $|T\Delta S_d| \gg |\Delta H_d|$ . The second assumption we will make is that the deformation at a microscopic level mimics the deformation at a macroscopic level. In other words, relative changes in the spacings between crosslink points are identical to relative changes in the overall sample demonstrations. This assumption is referred to as the affine deformation assumption.

## 6.3 Free energy change due to deformation

What really matters when determining the mechanical properties of a material is the change in free energy resulting from a deformation, which we express in terms of the molecular extension ratios in the  $x$ ,  $y$  and  $z$  directions. Prior to deformation, we have  $\vec{R} = R_x\hat{x} + R_y\hat{y} + R_z\hat{z}$ , so that  $R^2 = R_x^2 + R_y^2 + R_z^2$ . The undeformed free energy,  $F_0$ , is given by using this expression for  $R^2$  in Eq. 6.4:

$$F_0 = -k_B T \ln C + \frac{3k_B T}{2Na^2} \{R_x^2 + R_y^2 + R_z^2\} \quad (6.5)$$

For an isotropic system the orientation of the coordinate axis do not matter. Here assume that  $x$ ,  $y$  and  $z$  axes correspond to principal axes, with principal axis 1 directed along  $\hat{x}$ , principal axis 2 directed along  $\hat{y}$  and principal axis 3 directed along  $\hat{z}$ . After deformation, the values of  $R_x$ ,  $R_y$  and  $R_z$  are each multiplied by the appropriate extension ratio ( $\vec{R} = \lambda_1 R_x \hat{x} + \lambda_2 R_y \hat{y} + \lambda_3 R_z \hat{z}$ ), so that  $R^2 = \lambda_1^2 R_x^2 + \lambda_2^2 R_y^2 + \lambda_3^2 R_z^2$ . The deformed free energy,  $F_{def}$  is:

$$F_{def} = -k_B T \ln C + \frac{3k_B T}{2Na^2} \{ \lambda_1^2 R_x^2 + \lambda_2^2 R_y^2 + \lambda_3^2 R_z^2 \} \quad (6.6)$$

The free energy change due to deformation of the molecule is given as follows:

$$\Delta F_d = F_{def} - F_0 = \frac{3k_B T \{ (\lambda_1^2 - 1)R_x^2 + (\lambda_2^2 - 1)R_y^2 + (\lambda_3^2 - 1)R_z^2 \}}{2Na^2} \quad (6.7)$$

This result is for the deformation of a single polymer molecule, which for a crosslinked elastomer corresponds to a segment that connects crosslink points. There are a huge number of these segments in a macroscopic chunk of rubber. To get the free energy change for the material as a whole, we need to replace  $R_x^2$  by  $n_{el} \langle R_x^2 \rangle$ , where  $n_{el}$  is the total number of network strands and  $\langle R_x^2 \rangle$  is the average value of  $R_x^2$  for these segments. We need to make similar substitutions for  $R_y^2$  and  $R_z^2$  to obtain the following:

$$\Delta F_d = \frac{3k_B T n_{el} \{ (\lambda_1^2 - 1) \langle R_x^2 \rangle + (\lambda_2^2 - 1) \langle R_y^2 \rangle + (\lambda_3^2 - 1) \langle R_z^2 \rangle \}}{2Na^2} \quad (6.8)$$

Now we assume that the material was isotropic when it was crosslinked, so that  $\langle R_x^2 \rangle = \langle R_y^2 \rangle = \langle R_z^2 \rangle = \langle R^2 \rangle / 3$ . With this assumption, and with  $R_0^2 = Na^2$ , we obtain the following result:

$$\Delta F_d = \frac{k_B T n_{el} \langle R^2 \rangle \{ \lambda_1^2 + \lambda_2^2 + \lambda_3^2 - 3 \}}{2R_0^2} \quad (6.9)$$

Note that  $\langle R^2 \rangle$  is the mean square end-to-end distance of the polymer strands that span the crosslinks, and that  $R_0^2$  is the value of  $\langle R^2 \rangle$  when the polymer strands obey random walk statistics. The relationship between these two quantities depends on the conditions of the crosslinking reaction.

It is often useful to work in terms of intensive free energy changes (free energy per unit volume). The free energy of deformation per unit volume  $\Delta f_d$  is obtained very simply from  $\Delta F_d$  by dividing by  $V$ , the volume of a sample. We retain the same expression as shown above, but with the strand concentration,  $\nu_{el}$  substituted for the number of strands,  $n_{el}$ :

$$\Delta f_d = \frac{\Delta F_d}{V} = \frac{k_B T \nu_s \beta \{ \lambda_1^2 + \lambda_2^2 + \lambda_3^2 - 3 \}}{2} \quad (6.10)$$

where  $\nu_{el}$  and  $\beta$  are defined as follows:

$$\nu_{el} = \frac{n_{el}}{V}; \quad \beta = \frac{\langle R^2 \rangle}{R_0^2} \quad (6.11)$$

Like the intensive free energy, the strand concentration,  $\nu_s$  is useful because it does not depend on the overall size and shape of the elastomer. The assumptions used to develop the free energy expression given above correspond to the simplest model of rubber elasticity, which is often referred to as the Neo-hookean model. In our discussion of the specific cases of shear and uniaxial deformation that we discuss below, we make the additional assumption that the material is incompressible, in which case the product of the three principal extension ratios is one:

$$\lambda_1 \lambda_2 \lambda_3 = 1 \quad (6.12)$$

## 6.4 Shear deformation of an elastomer

For pure shear we need to relate the shear strain,  $\gamma$ , to the extension ratios,  $\lambda_1$ ,  $\lambda_2$  and  $\lambda_3$ . Pure shear is a two dimensional stress state, with  $\lambda_3 = 1$  so the Neo-hookean strain energy function (Eq. 6.10) reduces to the following:

$$\Delta f_d = \frac{k_B T \nu_s \beta \{ \lambda_1^2 + \lambda_2^2 - 2 \}}{2} = \frac{k_B T \nu_s \beta (\lambda_1 - \lambda_2)^2}{2} = \frac{k_B T \nu_s \beta \gamma^2}{2} \quad (6.13)$$

The shear stress is obtained by differentiation of the strain energy function with respect to  $\gamma$  (Eq. ??):

$$\sigma_{12} = \frac{d}{d\gamma}(\Delta f_d) = G\gamma \quad (6.14)$$

where  $G$  is the shear modulus, given as follows:

$$G = k_B T v_s \beta \quad (6.15)$$

Note that the shear stress is proportional to the shear strain, even for large values of the strain.

## 6.5 Uniaxial deformation of an elastomer

For uniaxial extension or compression the deformation is applied along one axis, which we define as the  $z$  axis. We assume that our material is isotropic, so that the extensions in the 1 and 2 directions are identical to one another, i.e.  $\lambda_1 = \lambda_2$ . In addition, the material is assumed to be incompressible, so  $\lambda_1 \lambda_2 \lambda_3 = 1$ . We therefore have  $\lambda_1 = \lambda_2 = \lambda_3^{-1/2}$ . We can therefore write the free energy of a deformed elastomer as a function of the single extension ratio,  $\lambda_3$ :

$$\Delta f_d = \frac{G}{2} \left\{ \lambda_3^2 + \frac{2}{\lambda_3} - 3 \right\} \quad (6.16)$$

The engineering stress is obtained by differentiating with respect to  $\lambda_z$  (Eq. ??):

$$\sigma_{eng} = \frac{d}{d\lambda} (\Delta f_d) = G \left\{ \lambda_3 - \frac{1}{\lambda_3^2} \right\} \quad (6.17)$$

Young's modulus ( $E$ ) is defined as the derivative of the stress with respect to strain, evaluated at low strain ( $\lambda_z = 1$ ):

$$E \equiv \left. \frac{\partial \sigma_{eng}}{\partial \lambda_z} \right|_{\lambda_z=1} = G \left. \left\{ 1 + \frac{2}{\lambda_3^3} \right\} \right|_{\lambda_3=1} = 3G = 3v_s \beta k_B T, \quad (6.18)$$

The concentration of network strands ( $v_s$ ) is the inverse of the volume per strand. This can be calculated from the molecular weight and density. Defining  $M_s$  as the number average molecular weight of a network strand (molecular weight between crosslinks) gives:

$$v_s \left( \frac{\text{strands}}{\text{volume}} \right) = \frac{\rho \text{ (mass/volume)}}{M_s \text{ (mass/mole)}} \cdot N_{av} \text{ (strands/mole)} \quad (6.19)$$

where  $N_{av}$  is Avogadro's number ( $6.02 \times 10^{23}$ ). With  $R = k_B N_{av} = 8.314 \text{ J/mole} \cdot \text{K}$  the expression

$$E = \frac{3\rho\beta RT}{M_s}$$

Finally, note that  $1 \text{ J/m}^3 = 1 \text{ Pa}$ . Stresses and elastic moduli have units of force/area or energy/volume.

**Exercise:** Calculate the expected value of Young's modulus for a crosslinked polyisoprene that has a number average molecular between crosslinks of 4000 g/mole. The density of polyisoprene is  $0.9 \text{ g/cm}^3$ . Assume that the polymer was crosslinked under equilibrium conditions in the melt state.

**Solution:** Because the polymer was crosslinked under equilibrium conditions, the network strands obey random walk statistics, with  $\beta = 1$ . To keep everything in SI units, we need the density in units of  $\text{kg/m}^3$  ( $1 \text{ g/cm}^3 = 1000 \text{ kg/m}^3$ ), and  $M_s$  in  $\text{kg/mol}$ . In our example,  $\rho = 900 \text{ kg/m}^3$  and  $M_s = 4 \text{ kg/mol}$ . We'll also assume that we are interested in the elastic modulus near room temperature ( $T \approx 300 \text{ K}$ ).

$$E = \frac{3(900 \text{ kg/m}^3)(8.314 \frac{\text{J}}{\text{mol}\cdot\text{K}})(300\text{K})}{4\text{kg/mol}} = 1.6 \times 10^6 \text{ J/m}^3 = 1.6 \times 10^6 \text{ Pa.}$$

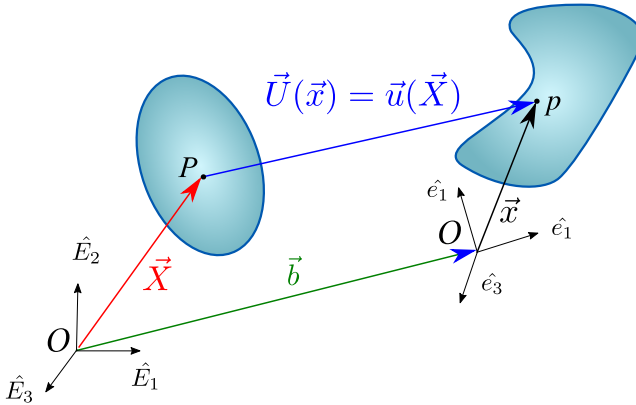


**Figure 7.1:** Location of two points,  $P_1$  and  $P_2$ , before and after an applied deformation.

## 7 Finite (Large) Strain

As we know from the previous section on rubber elasticity, with soft materials we are often interested in large strains, where it is not always sufficient to expand the displacement in a Taylor series and keep only the first derivative term, as was done in Section 3. In cases like this we need a more generalizable formulation. The description here is based largely on the Wikipedia article on finite strain theory[5] that was mentioned briefly in the previous section. We need to introduce some additional notation, and define various matrix quantities that simplify things considerably. Our starting point is to redraw Figure 3.11, in a way that allows to more explicit account for the fact strains that we encounter are going to be quite large. We begin with the following two important changes:

- Since we are generally interested in how the separation between two different points ( $P_1$  and  $P_2$  in Figure 3.11), changes, we will point the coordinate axis at  $P_1$  and label point 2 simply as  $P$ .

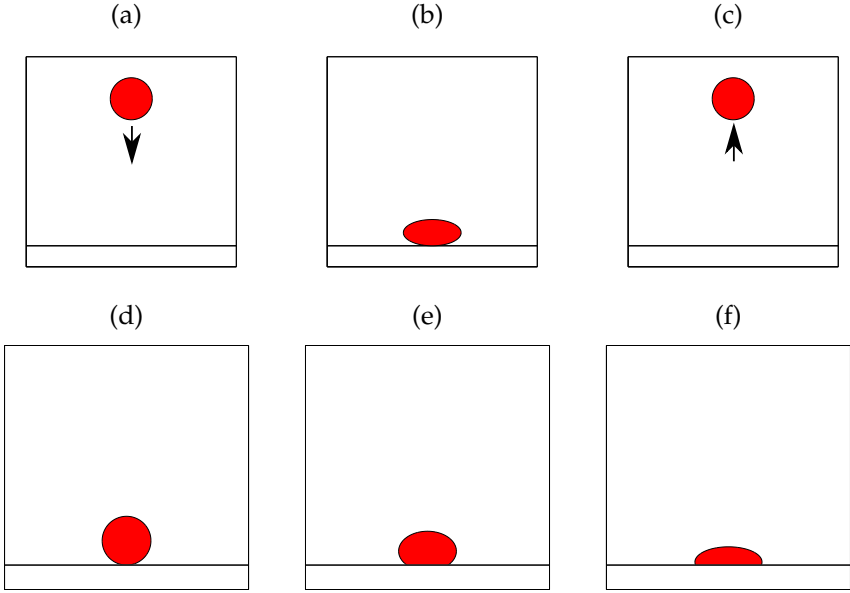


**Figure 8.1:** Illustration of viscoelastic behavior. Images of a viscoelastic material behaving elastically as it bounces from a surface (a-c) and the same material spreading over a surface at long times (d-f).

## 8 Linear Viscoelasticity

### 8.1 Intro to Time-Dependent Behavior

Many of the concepts of rubber elasticity still apply under certain situations to materials that are not actually crosslinked. Consider, for example, the behavior of Silly-Putty. Silly-putty is based on silicones that are uncrosslinked. Nevertheless, this material still bounces like an ordinary crosslinked rubber ball. This is because over very short times it behaves elastically. The deformation energy stored in the material as it comes into contact with the surface and deforms is available to propel the material back into the air as the deformation relaxes and this strain energy is converted to kinetic energy. If we let the sample sit on a surface for a long period of time, however, it eventually flows and behaves as a liquid.

Before we discuss the way that the properties of viscoelastic materials are characterized, it is useful to discuss the limiting behaviors of purely elastic solids and perfectly viscous liquids. We illustrate this by showing how different materials respond to a shear strain,  $\gamma$  that begins to increase at some constant rate to some final value, and is then fixed at this final value as illustrated in the top panel of Figure 8.3. The response for solids, liquids and viscoelastic materials

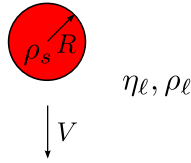


**Figure 8.2:** Terminal velocity of a sphere descending in a viscous fluid.

is as described below.

**Solids:** In this case the stress is proportional to the strain, and the rate at which the strain is applied does not matter. As a result the time dependence of the stress looks just like the time dependence of the strain. The slopes of the time-dependent stress and strain curves (the top two curves in Figure 8.3) are related to one another by the shear modulus of the material.

**Liquids:** In liquids the stress is proportional to the rate at which the strain is applied, and is independent of the current strain. Liquids do not store any strain energy, and as soon as the strain stops changing, the stress drops back to zero. The stress for the time dependent strain shown in Figure 8.3 is constant while the stress is increasing and is zero otherwise. The stress is given by the shear viscosity,  $\eta$ , as follows:

$$\sigma_{xy} = \eta \frac{d\gamma}{dt} = \eta \dot{\gamma} \quad (8.1)$$

As a simple illustration of the significance of the viscosity, we can calculate the time it takes for a small sphere of metal to drop to the bottom of pool of water. Suppose we use an iron particle with a radius of  $1\mu\text{m}$ . The situation is as shown in Figure 8.2. The gravitational force,  $F$ , causing the ball to sink is proportional to the volume of the sphere, and the difference in densities between the solid and liquid:

$$F = g \frac{4}{3} \pi R^3 (\rho_s - \rho_l) \quad (8.2)$$

Here  $\rho_s$  is the density of the solid sphere,  $\rho_l$  is the density of the surrounding liquid,  $R$  is the radius of the sphere and  $g$  is the gravitational acceleration ( $9.8 \text{ m/s}^2$ ). This force is balanced by the viscous force exerted by the water on the sphere as the sphere moves the liquid with a velocity,  $v$ . For a viscous liquid this force is proportional to the velocity. It is also proportional to the viscosity of the liquid and to the radius of the sphere. The specific relationship is as follows:



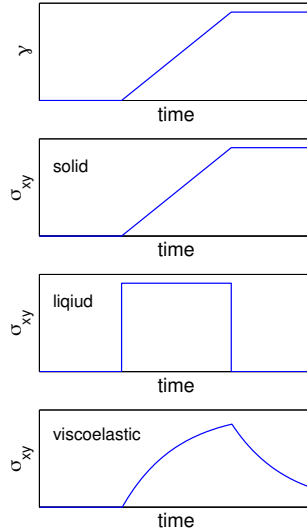


**Figure 8.3:** Interactive contrast of elastic, viscous, and viscoelastic response.

$$F = 6\pi V\eta R \quad (8.3)$$

At steady state, the velocity reaches a value that is obtained by equating the forces in Eqs.8.2 and 8.3. In this way we obtain:

$$V = \frac{2}{9} \frac{gR^2}{\eta} (\rho_s - \rho_\ell) \quad (8.4)$$

Iron has a density of  $7.87 \text{ g/cm}^3$  ( $7870 \text{ kg/m}^3$ ) and water has a density of  $1000 \text{ kg/m}^3$  and a viscosity of  $10^{-3} \text{ Pa}\cdot\text{sec}$ . From this we get a velocity of  $16 \text{ }\mu\text{m/s}$ .

**Viscoelastic Materials:** Viscoelastic materials have characteristics of both solids and liquids. The shear stress depends on both the shear stress and the strain rate, and is not a simple function of either one. The shear stress actually depends on the details of the previous strain history, as described in more detail below.

While the shear geometry is most commonly used to characterize liquid-like materials, solid-like materials are more commonly investigated in a uniaxial tensile geometry, as illustrated in Figure 8.4. Viscoelastic solids will have a value for Young's modulus,  $E$ , that depends on the time scale of the measurement. Imagine a tensile experiment where a strain of  $e_0$  is instantaneously applied to the sample. In a viscoelastic material, the resulting stress will decay

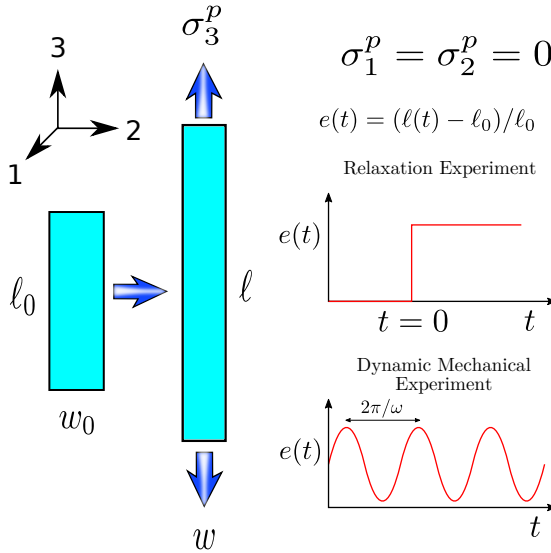


**Figure 8.4:** Tensile geometry for defining the tensile relaxation modulus,  $E(t)$ , and the frequency-dependent complex tensile modulus,  $E^*$ .

with time while we maintain the strain at this fixed value. The time dependence of the resulting tensile stress,  $\sigma$ , enables us to define a time-dependent relaxation modulus,  $E(t)$ :

$$E(t) = \frac{\sigma(t)}{e_0} \quad (8.5)$$

We are often interested in the application of an oscillatory strain to a material. Examples include the propagation of sound waves, where wave propagation is determined by the response of the material at the relevant frequency of the acoustic wave that is propagating through the material. In an oscillatory experiment, referred to as a dynamic mechanical experiment in Figure 8.4, the applied shear strain is an oscillatory function with an angular frequency,  $\omega$ , and an amplitude,  $e_0$ :

$$e(t) = e_0 \sin(\omega t) \quad (8.6)$$

Note that the strain rate,  $\frac{de}{dt}$ , is also an oscillatory function, with the same angular frequency, but shifted with respect to the strain by  $90^\circ$ :

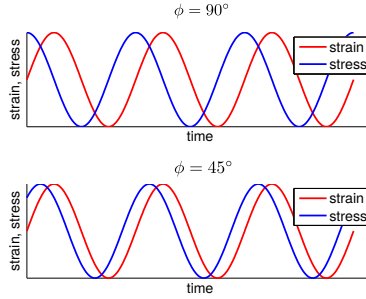


**Figure 8.5:** Time dependent stress and strain in a dynamic mechanical experiment.

$$\frac{de}{dt} = e_0 \omega \cos(\omega t) = \gamma_0 \omega \sin(\omega t + \pi/2) \quad (8.7)$$

The resulting stress is also an oscillatory function with an angular frequency of  $\omega$ , and is described by its amplitude and by the phase shift of the relative to the applied strain:

$$\sigma(t) = \sigma_0 \sin(\omega t + \phi) \quad (8.8)$$

Now we can define a complex modulus with real and imaginary components as follows:

$$E^* = E' + iE'' = |E^*| e^{i\phi} \quad (8.9)$$

There are a couple different ways to think about the complex modulus,  $E^*$ . As a complex number we can express it either in terms of its real and imaginary components ( $E'$  and  $E''$ , respectively), or in terms of its magnitude,  $|E^*|$  and phase,  $\phi$ . The magnitude of the complex modulus is simply the stress amplitude normalized by the strain amplitude:

$$|E^*| = \sigma_0 / e_0 \quad (8.10)$$

The phase angle,  $\phi$ , describes the lag between the stress and strain in the sample. Examples for  $\phi = 90^\circ$  (the maximum value, characteristic of a liquid) and  $\phi = 45^\circ$  are shown in Figure 8.5.

In order to understand the significance of the real and imaginary components of  $E^*$  we begin with the Euler formula for the exponential of an imaginary number:

$$e^{i\phi} = \cos \phi + i \sin \phi, \quad (8.11)$$

where  $i$  is the imaginary unit (*i.e.*  $i = \sqrt{-1}$ ). Use of this expression in Eq. 8.9, we see that the **storage modulus**,  $E'$  gives the stress that is in phase with the strain (the solid-like part), and is given by the following expression:

$$E' = |E^*| \cos \phi \quad (8.12)$$

Similarly, the **loss modulus**,  $E''$ , gives the response of the material that is in phase with the strain rate (the liquid-like part):

$$E'' = |E^*| \sin \phi \quad (8.13)$$

We can combine Eqs. 8.12 and 8.13 to get the following expression for  $\tan \phi$ , commonly referred to simply as the **loss tangent**:

$$\tan \phi = \frac{E''}{E'} \quad (8.14)$$

The loss tangent gives the ratio of the energy dissipated in one cycle of an oscillation to the maximum stored elastic energy during this cycle. We can define the complex shear modulus,  $G^*$  in a similar way, with  $G', G'', \phi$  and  $|G^*|$  related to one another in a way that corresponds to the relationship of the components of  $E^*$ . Because the shear geometry is more amenable to the testing of both liquids and solids, we'll use this geometry to illustrate other time dependent quantities in our discussion below.

## 8.2 Shear Relaxation Modulus

In a shear geometry (Fig. 8.6) we can also conduct relaxation experiments or oscillatory experiments. The shear relaxation modulus is defined as the ratio of the resulting time dependent stress to this initial strain:

$$G(t) \equiv \frac{\sigma_{xy}(t)}{\gamma_0} \quad (8.15)$$

As with  $E(t)$ , the shear modulus is independent of  $\gamma_0$ , provided that  $\gamma_0$  is sufficiently small. This low strain regime defines the regime of linear viscoelasticity. In the remainder of this section we confine ourselves to this linear regime, assuming a shear geometry so that the relevant time and frequency-dependent property is the shear modulus,  $G$ .

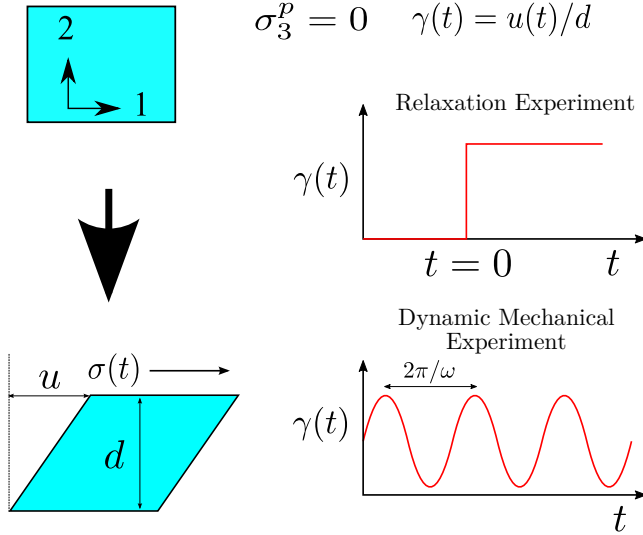


**Figure 8.6:** Shear geometry for defining the shear relaxation modulus,  $G(t)$  and the frequency- dependent complex shear modulus  $G^*$ .

### 8.3 Boltzmann Superposition Principle

In the linear viscoelastic regime the effects of strains applied at different times are additive, a concept known as the **Boltzmann superposition principle**. A simple example is illustrated in Figure 8.7, where the following step strains are applied to the sample:

- A strain of  $\Delta\gamma_1$  applied at time  $t_1$
- A strain of  $\Delta\gamma_2$  applied at time  $t_2$
- A strain of  $\Delta\gamma_3$  applied at time  $t_3$

The stress contribution from these different strains is obtained by multiplying by the shear relaxation modulus, evaluated at the time that has passed since the strain was applied. If strain was applied at  $t_1$ , for example, the stress at some later time,  $t$ , is obtained by multiplying by  $G(t - t_1)$ . Adding up the contributions from the three different step strains in our example leads to the following:

$$\sigma_{xy} = \Delta\gamma_1 G(t - t_1) + \Delta\gamma_2 G(t - t_2) + \Delta\gamma_3 G(t - t_3) \tag{8.16}$$

This expression can easily be extended to include an arbitrary number of step strains:

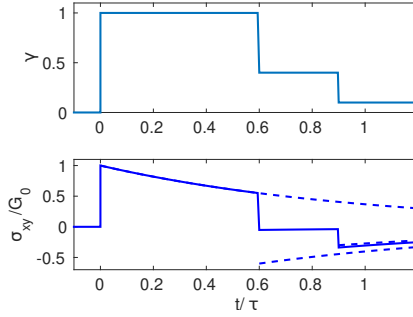


**Figure 8.7:** Material response to a series of step strains.

$$\sigma_{xy} = \sum_i \Delta\gamma_i G(t - t_i) \quad (8.17)$$

By taking a sum of very small strain increments, we can generalize this expression to account for a continuously changing strain. We begin by writing  $\Delta\gamma_i$  in the following way:

$$\Delta\gamma_i = \frac{d\gamma}{dt}(t_i)\Delta t_i = \dot{\gamma}(t_i)\Delta t_i \quad (8.18)$$

This substitution leads to the following expression for the stress:

$$\sigma_{xy} = \sum_i \dot{\gamma}(t_i)G(t - t_i)\Delta t_i \quad (8.19)$$

We can write this in integral form by taking  $\Delta t_i \rightarrow 0$  and replacing the summation by an integral over all times less than the current time:

$$\sigma_{xy}(t) = \int_{-\infty}^t \dot{\gamma}(t_i)G(t - t_i)dt_i \quad (8.20)$$

This expression gives the current stress that remains as a result of all of the strains introduced at different times in the past. It is often convenient to change variables so that  $s = t - t_i$ ,  $dt_i = -ds$ . Note that  $s = \infty$  when  $t_i = -\infty$ , and  $s = 0$  when  $t_i = t$ . The integral can therefore be rewritten as follows:

$$\sigma_{xy}(t) = \int_0^{\infty} \dot{\gamma}(t-s)G(s)ds \quad (8.21)$$

Note that because  $s$  represents time,  $G(s)$  and  $G(t)$  represent the same time-dependent relaxation modulus. We are just using different variables ( $s$  and  $t$ ) to represent time.

The simplest application of Eq. is 'steady shear', where a constant strain rate is applied. Because  $\dot{\gamma}$  is independent of time in this case, it can be brought outside the integral, giving the following:

$$\sigma_{xy} = \dot{\gamma} \int_0^{\infty} G(t)dt \quad (8.22)$$

The following expression is obtained for the viscosity:

$$\eta_0 = \frac{\sigma_{xy}}{\dot{\gamma}} = \int_0^{\infty} G(t)dt \quad (8.23)$$

We refer to this viscosity as the **zero shear viscosity**, because it assumes that the material is in the linear viscoelastic regime, where the applied stress is low enough so that the stress is proportional to the magnitude of the applied strain. The subscript '0' is a reminder to us that the zero shear viscosity corresponds to a limiting value of the viscosity that is obtained at a very low strain rate.

## 8.4 Idealized Relaxation Curves

One thing to keep in mind when looking at the viscoelastic properties of materials is that processes occur over a very large range of time scales. To capture all of these time scales we typically plot the time on a logarithmic scale. The same is true for the frequency-domain experiments discussed below. The relaxation modulus can often vary of several orders of magnitude, so that we also plot the relaxation modulus itself on a logarithmic scale.

Three different idealized forms of the relaxation modulus are shown in Figure 8.8. The simplest behavior corresponds to a **Maxwell model**, where a single

relaxation time,  $\tau_g$ , describes the decay in the modulus from the glassy value of  $G_g$ :

$$G(t) = G_g \exp(-t/\tau_g) \quad (8.24)$$

This relaxation time could, for example, describe the decay in the modulus from a glassy value of  $\approx 10^9$  Pa. This relaxation time can be viewed as a 'glass transition time', and its existence is a clue that some equivalence between time and temperature must exist. The relaxation time characterizing the glass transition depends very strongly on the temperature, but is independent of the polymer molecular weight. If the polymer molecular weight is very high, however, the polymers become entangled with one another, and behave elastically for times that are too short for these entanglements (shown schematically in Figure 8.9) to relax by molecular diffusion. In addition to  $\tau_g$ , there is a second transition time,  $\tau_e$ , determined by the lifetime of these molecular entanglements. Addition of this second relaxation results in the following expression for the relaxation modulus:

$$G(t) = G_g \exp(-t/\tau_g) + G_e \exp(-t/\tau_e) \quad (8.25)$$

Here  $G_e$  is the plateau modulus (often referred to as  $G_N^0$  in the literature). Entanglements behave like crosslinks, but they have finite lifetimes as the molecules diffuse and the entanglements are eliminated and reformed elsewhere. The plateau modulus is given by the concentration of entanglements,  $v_e$ , or equivalently, by the number average molecular weight between entanglements,  $M_e$  (referred to as the entanglement molecular weight):

$$G_e = v_e k_B T = \frac{\rho R T}{M_e} \quad (8.26)$$

The actual relaxation behavior of polymeric materials is complex, and can generally not be described in detail by including only one or two relaxation times. The actual relaxation behavior can always be described with sufficient accuracy by a **generalized Maxwell model**, where we include a large number of individual exponential relaxation processes:

$$G(t) = \sum_{i=1}^{N_r} G_i \exp(-t/\tau_i) \quad (8.27)$$

Inclusion of a sufficiently large number of relaxation processes (large  $N_r$ ) enables very complicated relaxation behavior to be modeled accurately.



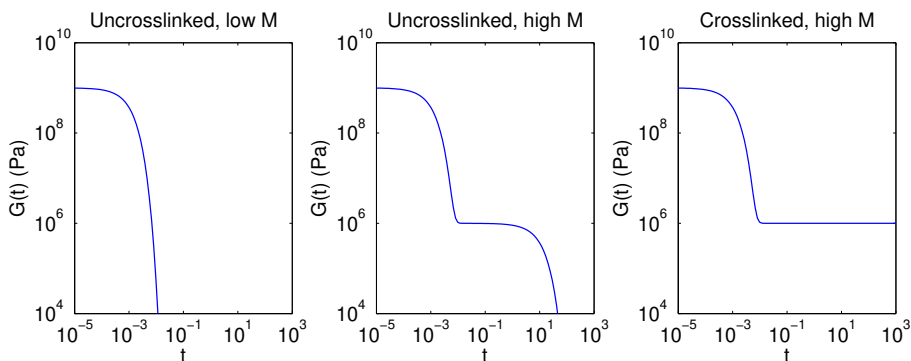


Figure 8.8: Characteristic relaxation curves.

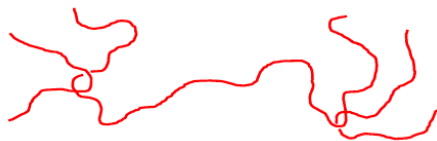


Figure 8.9: Schematic representation of a molecular entanglement.

## 8.5 Temperature Dependence

A characteristic of single-component polymeric materials is that the temperature dependence of all of the different relaxation times is the same. The concept is illustrated in Figure 8.10, which shows the relaxation modulus at two different temperatures for an idealized material with two different relaxation times. The relaxation times scale with temperature according to the same temperature dependent shift factor,  $a_T$ . The shift factor is equal to one at a reference temperature,  $T_{ref}$ , and increases as the temperature is decreased. Because both relaxation times are multiplied by the same factor, the curve is shifted linearly along the logarithmic x axis.

Because all of the relaxation times are multiplied by  $a_T$  when the temperature is changed, data obtained at different temperatures superpose when plotted as a function of  $t/a_T$ . As a result the relaxation behavior over a large range of times can be obtained by measuring the relaxation spectrum at different times, and shifting the data to the reference temperature.

The **Vogel equation** is an empirical equation that is often used to describe the temperature dependence of the shift factor,  $a_T$ :

$$\log(a_T) = A + \frac{B}{T - T_\infty} \quad (8.28)$$

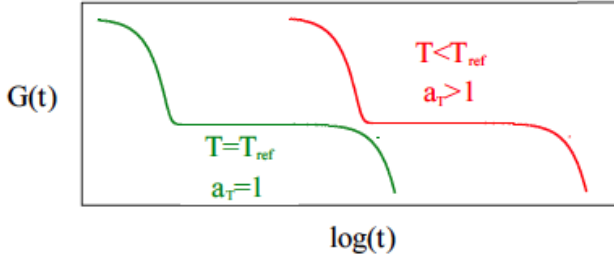


**Figure 8.10:** Temperature dependence of a material with two relaxation times.

The factor  $A$  is determined from the requirement that  $a_T = 1$  at  $T = T_{ref}$ :

$$A = -\frac{B}{T_{ref} - T_{\infty}} \quad (8.29)$$

The relaxation times diverge to  $\infty$  at  $T = T_{\infty}$ , which in free volume theory is the temperature at which the free volume of the equilibrium liquid goes to zero.

## 8.6 Relationship between Frequency-Dependent and Time-Dependent Dynamic Moduli

Experimentally, a wide variation in time scales is accessed by oscillating or vibrating the sample and measuring the frequency response of the material. Consider, for example, an oscillatory shear strain:

$$\gamma = \gamma_0 \sin(\omega t) \quad (8.30)$$

The strain rate is also sinusoidal:

$$\dot{\gamma}(t) = \frac{d\gamma(t)}{dt} = \omega\gamma_0 \cos(\omega t) = \omega\gamma_0 \sin(\omega t + \pi/2) \quad (8.31)$$

Note that the strain and the strain rate are out of phase by  $\pi/2$  ( $90^\circ$ ). This concept of a phase difference is very important in understanding the frequency dependent dynamic moduli. In this case we use Boltzmann superposition to obtain an expression for the stress:

$$\sigma_{xy}(t) = \int_0^{\infty} \dot{\gamma}(t-s)G(s)ds = -\omega\gamma_0 \int_0^{\infty} \cos\{\omega(t-s)\} G(s)ds \quad (8.32)$$

Now we make use of the following trigonometric identity:

$$\cos(a-b) = \sin(a)\sin(b) + \cos(a)\cos(b) \quad (8.33)$$

We can therefore write the time dependent stress in the following way.

$$\sigma_{xy}(t) = \gamma_0\omega \left[ \int_0^{\infty} G(s)\sin(\omega s)ds \right] \sin(\omega t) + \gamma_0\omega \left[ \int_0^{\infty} G(s)\cos(\omega s)ds \right] \cos(\omega t) \quad (8.34)$$

We define  $G'$  (storage modulus) and  $G''$  (loss modulus) such that  $G'$  describes the component of the stress that is in phase with the strain (the elastic component) and  $G''$  describes the component of the stress that is in phase with the strain rate (the viscous component).

$$\frac{\sigma_{xy}(t)}{\gamma_0} = G'(\omega)\sin(\omega t) + G''(\omega)\cos(\omega t) \quad (8.35)$$

By comparing Equations 8.34 and 8.35, we obtain the following for  $G'$  and  $G''$ :

$$\begin{aligned} G'(\omega) &= \omega \int_0^{\infty} G(t)\sin(\omega t)dt \\ G''(\omega) &= \omega \int_0^{\infty} G(t)\cos(\omega t)dt \end{aligned} \quad (8.36)$$

It is useful to consider the behavior of  $G'$  and  $G''$  in limiting cases where the system is a perfectly elastic solid with no viscous character, and where the material is a Newtonian liquid with no elastic character:

**Perfectly Elastic System:** In this case the shear modulus is independent of both time and frequency. For  $\gamma(t) = \gamma_0 \sin(\omega t)$  we have:

$$\sigma_{xy}(t) = G\gamma(t) = G\gamma_0 \sin(\omega t) \quad (8.37)$$

Comparing to Eq. 8.35 gives:

$$\begin{aligned} G' &= G \\ G'' &= 0 \end{aligned} \quad (8.38)$$

**Perfectly Viscous System:** We again have  $\gamma(t) = \gamma_0 \sin(\omega t)$ , but this time the shear stress depends only on the strain rate:

$$\sigma_{xy}(t) = \eta \frac{d\gamma(t)}{dt} = \eta\omega\gamma_0 \cos(\omega t) \quad (8.39)$$

Comparing to Eq. 8.35 gives:

$$\begin{aligned} G' &= 0 \\ G''(\omega) &= \omega\eta \end{aligned} \quad (8.40)$$

The **loss tangent**,  $\tan(\phi)$ , gives the ratio of dissipated and stored elastic energy during a given cycle of deformation. This quantity is maximized when the inverse of the frequency corresponds to a characteristic relaxation time of the material. For a material with two characteristic relaxation times,  $\tau_1$  and  $\tau_2$ ,  $\tan(\phi)$  will be maximized at  $\omega = 2\pi/\tau_1$  and  $\omega = 2\pi/\tau_2$ .

## 8.7 Torsional Resonator

We can now consider the specific example of a **torsional resonator**, shown below in Figure 8.11. The equation of motion for the spring as it is being twisted is[6]:

$$T = K_t\theta + I\frac{d^2\theta}{dt^2} \quad (8.41)$$

where  $\theta$  is the rotation angle,  $T$  is the torque on the resonator,  $K_t$  is the torsional stiffness and  $I$  is the moment of inertia of the system, which depends on the

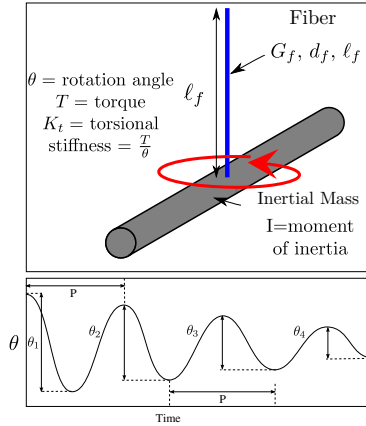


**Figure 8.11:** Torsional resonator.

details of the inertial bar used in the experiment. For a cylindrical fiber  $K_t$  is given by the following expression:

$$K_t \equiv \frac{T}{\theta} = \frac{\pi G d^4}{32 \ell} \tag{8.42}$$

The resonant angular frequency of the oscillator,  $\omega_n$  is given by the following expression:

$$\omega_n = \sqrt{\frac{K_t}{I}} \tag{8.43}$$

The solution to Eq. 8.41 for the case where  $T = 0$  and we just let the fiber move (by twisting to a certain angle and letting it go, for example) is as follows:

$$\theta = \theta_0 \cos(\omega_n t) \tag{8.44}$$

This analysis assumes that the system is entirely elastic. What if the spring has some viscoelastic character to it? We begin by using Euler's formula (Eq. 8.11) to rewrite Eq. 8.44 in the following way:

$$\theta = \theta_0 \text{Real}(\exp(i\omega_n t)) \tag{8.45}$$

Now all we need to do is to replace the modulus,  $G$ , with the complex modulus,  $G^*$ , and everything works out fine. Here's what happens:

- The torsional stiffness,  $K_t$  gets transformed to a complex torsional stiffness  $K_t^*$

- The resonant frequency,  $\omega_n$  gets transformed to a complex resonant frequency,  $\omega_n^*$
- The imaginary part of the complex resonant frequency becomes an exponential damping function

To understand this last point, suppose write  $\omega_n^*$  in the following way:

$$\omega_n^* = \omega_n' + i\omega_n'' \quad (8.46)$$

Putting this back into Eq. 8.45 gives:

$$\theta = \theta_0 \text{Real}(\exp(i\omega_n' t)) \exp(-\omega_n'' t) \quad (8.47)$$

Using the Euler formula (Eq. 8.11) to expand  $\exp(i\omega_n' t)$  and taking the real part gives:

$$\theta = \theta_0 \cos(\omega_n' t) \exp(-\omega_n'' t) \quad (8.48)$$

So the imaginary part of the complex frequency describes the decay of oscillation with time.

## 8.8 Viscoelastic Models

Models of viscoelasticity can be represented visually by connecting solid-like and liquid-like elements together. In materials science we're used to the solid-like elements. They are simply elastic springs where the force is proportional to the extension of the spring. In terms of stress and strain, the stress,  $\sigma$  is proportional to the strain,  $e$ . There is no time-dependence to the behavior of an ideal spring. The stress is proportional to the strain, regardless of how fast or slow the strain is applied. In many real materials the rate at which the strain is applied matters as well, and this is where the dashpots come in. A **dashpot** is a liquid-like element where the stress is proportional to the rate at which the strain is changing, with the viscosity being the ratio between the stress and the strain rate. Schematic representations of springs and dashpots are shown in Figure 8.12. We assume a tensile geometry in our discussion of the viscoelastic models, so the relevant modulus is  $E$  as opposed to  $G$ , although this same formalism is generally applied to the shear moduli as well.

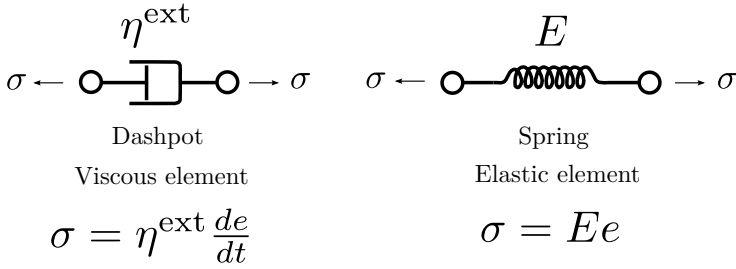


**Figure 8.12:** Schematic representations of springs and dashpots used to represent the time-dependent response of viscoelastic materials. Because the geometry here is assumed to be an extensional geometry, we refer to the viscosity as  $\eta^{\text{ext}}$ .

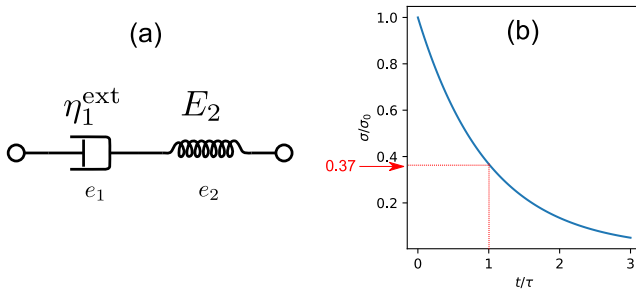


**Figure 8.13:** a) Maxwell model and b) the exponential stress relaxation function that it represents. Note that for an exponential relaxation,  $\tau$  is the time at which the stress decays to 37% of its initial value.

### 8.8.1 Maxwell model

The simplest viscoelastic model that contains both liquid-like and solid-like elements is the **Maxwell model** consisting of a linear dashpot with viscosity  $\eta_1$  in series with a linear spring with a modulus,  $E_2$  (see Figure 8.13). Because the elements are in series the stress is the same in each one of them. This stress can be related to the strain  $e_1$  in the dashpot and the strain  $e_2$  in the spring through the following expressions:

$$\sigma = \eta_1 \frac{de_1}{dt} \tag{8.49}$$

$$\sigma = E_2 e_2 \tag{8.50}$$

The total strain,  $e$  is  $e_1 + e_2$ , so the time derivative of the total strain is:

$$\frac{de}{dt} = \frac{de_1}{dt} + \frac{de_2}{dt} = \frac{\sigma}{\eta_1^{\text{ext}}} + \frac{1}{E_2} \frac{d\sigma}{dt} \tag{8.51}$$

In a stress relaxation experiment the strain instantaneous increased to an initial value of  $e_0$  and we follow the relaxation of the stress at this fixed strain. Because the dashpot cannot respond instantaneously, all of the initial strain is in the spring, *i.e.*,  $e_0 = e_2$  and the initial stress,  $\sigma_0$  is equal to  $E_0 e_0$ . The solution to Eq. 8.51 for this initial condition and for  $de/dt = 0$  is:

$$\sigma(t) = E e_0 \exp(-t/\tau) \quad (8.52)$$

with the relaxation time,  $\tau$ , given by the following expression:

$$\tau = \eta_0^{\text{ext}}/E_0 \quad (8.53)$$

We divide by  $e_0$  to obtain the relaxation modulus:

$$E(t) \equiv \sigma(t)/e_0 = E_0 \exp(-t/\tau) \quad (8.54)$$

We can also obtain the solution for the stress in the case where we apply an oscillatory strain. To get the response of a single Maxwell element in an oscillatory experiment we need to substitute Eq. 8.54 for  $E(t)$  into Eq. 8.36 for  $E'$  and  $E''$  (replacing  $G^*$  with  $E^*$ , since we are assuming a tensile geometry in this example):

$$\begin{aligned} E'(\omega) &= \omega \int_0^{\infty} \exp\left(-\frac{t}{\tau}\right) \sin(\omega t) dt \\ E''(\omega) &= \omega \int_0^{\infty} \exp\left(-\frac{t}{\tau}\right) \cos(\omega t) dt \end{aligned} \quad (8.55)$$

We get a bit of help here because these equations now involve **Laplace transforms**, which we can either look up or evaluate with a symbolic math solver (in our case the sympy module of Python). The Laplace transform,  $\mathcal{L}\{f(t)\}(s)$ , of a function,  $f(t)$  is defined in the following way:[7]

$$\mathcal{L}\{f(t)\}(s) = \int_0^{\infty} f(t) \exp(-st) dt \quad (8.56)$$

By comparison to Eq. 8.55 we see that  $E'$  involves the Laplace transform of the sine function and  $E''$  involves the Laplace transform of the cosine function:

$$\begin{aligned} E'(\omega) &= \omega \mathcal{L}\{\sin(\omega t)\}(s) \\ E''(\omega) &= \omega \mathcal{L}\{\cos(\omega t)\}(s) \end{aligned} \quad (8.57)$$

with  $s = 1/\tau$ . Use of symbolic Python (code at [msecore.northwestern.edu/331/python/maxwell\\_Estar.py](https://msecore.northwestern.edu/331/python/maxwell_Estar.py)) results in the following:



$$E^*(\omega) = E'(\omega) + iE''(\omega) = \frac{E_0\omega\tau}{\omega\tau - i} \quad (8.58)$$

The Python code generates  $E'$  and  $E''$  directly, but the expression for  $E^*$  contains all the information we need. Once we have this value we can extract  $E'$  and  $E''$  by multiplying the top and bottom of Eq. 8.58 by  $\omega\tau + i$ , remembering that  $i^2 = -1$ . Taking the real and imaginary components of  $E^*$  then gives the following for  $E'$  and  $E''$ :

$$E'(\omega) = \frac{E(\omega\tau)^2}{1 + (\omega\tau)^2} \quad (8.59)$$

$$E''(\omega) = \frac{E\omega\tau}{1 + (\omega\tau)^2} \quad (8.60)$$

These expressions are plotted in Figure 8.14, along with  $[E^*]$  and  $\phi$ . Note the following:

**For  $\omega = 1/\tau$  ( $\omega\tau = 1$ ):**

- $E' = E''$
- $\phi = 45^\circ$
- $E''$  is equal to its maximum value

**For  $\omega \gg 1/\tau$  ( $\omega\tau \gg 1$ , high frequency regime):**

- $E' \approx E_0, E'' \ll E_0$
- $\phi \approx 0$

**For  $\omega \ll 1/\tau$  ( $\omega\tau \ll 1$ , low frequency regime):**

- $E'' \gg E'$
- $E'' \approx \omega\eta_0^{\text{ext}}$
- $E' \propto \omega^2$
- $\phi \approx 90^\circ$

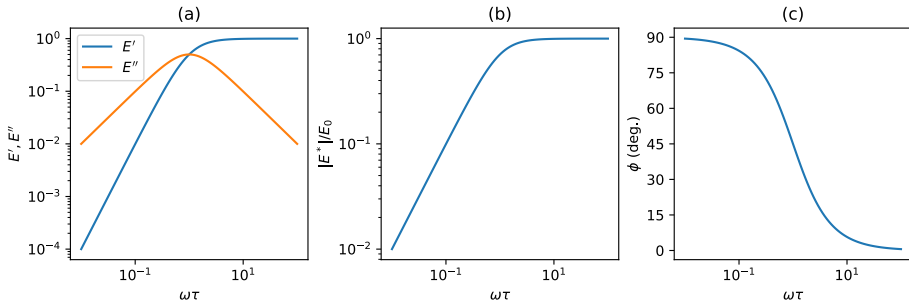


**Figure 8.14:** Frequency dependence of the rheological properties for the Maxwell model (plot generated with [msecore.northwestern.edu/331/python/maxwell\\_plot.py](https://msecore.northwestern.edu/331/python/maxwell_plot.py)).

The fact that  $E'' \approx \omega\eta_0^{\text{ext}}$  is generally true for liquid-like materials, even if the behavior at higher frequencies is more complicated. Provided that the viscoelastic phase angle approaches  $90^\circ$  at sufficiently low frequencies, we can define  $\eta_0$  more generally as a **zero extension rate viscosity** in the following way:

$$\eta_0^{\text{ext}} = \lim_{\omega \rightarrow 0} \frac{E''}{\omega} \quad (8.61)$$

The 'ext' superscript is a reminder to us that we are dealing with an extensional geometry. An analogous equation can be used to define a **zero shear rate viscosity**, which we refer to simply as  $\eta_0$ :

$$\eta_0 = \lim_{\omega \rightarrow 0} \frac{G''}{\omega} \quad (8.62)$$

We also note that while the loss modulus,  $E''$ , is maximized at an intermediate frequency, the storage modulus,  $E'$ , and the magnitude of the complex modulus,  $|E^*|$ , both increase as a function of the frequency (or remain constant with increasing frequency). This increase or constancy in  $E'$  and  $|E^*|$  with increasing frequency must **always** be true, because any general relaxation for a material can be written as the summation of individual exponential relaxations (the generalized Maxwell model described below).

### 8.8.2 Standard Linear Solid

For a single Maxwell element the relaxation modulus decays to zero at long times ( $t \gg \tau$ ). In many real systems we are interested in describing the decay of the relaxation modulus from a large value at short times to a much smaller

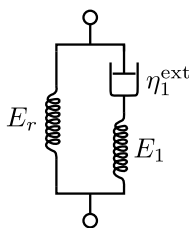


Figure 8.15: Standard linear solid.

value at larger times. The **standard linear solid** accounts for this by putting an elastic element with a modulus of  $E_r$  (the 'relaxed' modulus) in parallel with a single Maxwell element as shown in Figure 8.15. The extra spring adds directly to stress response, so all we have to do is add  $E_r$  to the expressions for  $E(t)$  and  $E^*(\omega)$  that were obtained from the Maxwell model:

$$E(t) = E_r + E_1 \exp(-t/\tau_1) \quad (8.63)$$

$$E^*(\omega) = E_r + \frac{E_1 \omega \tau_1}{\omega \tau_1 - i} \quad (8.64)$$

So we see that the standard linear solid describes the relaxation of the modulus from an initial value of  $E_1 + E_r$  at very short times to a relaxed value of  $E_r$  at long times. The standard linear solid is the simplest model for describing the transition of an amorphous, crosslinked polymer from glassy polymer behavior to rubbery behavior with typical values of  $E_1$  and  $E_r$  being  $10^9$  Pa and  $10^6$  Pa, respectively.

### 8.8.3 Generalized Maxwell Model

For real systems, the behaviors of  $E(t)$  and  $E^*(\omega)$  are usually much more complicated than given by the predictions of the Maxwell model or standard linear solid. To describe the behavior for real materials, we can add an arbitrary number of Maxwell elements in parallel, resulting in the **generalized Maxwell model** shown in Figure 8.16. The stresses for each of the parallel elements are additive, so  $E(t)$  and  $E^*(\omega)$  are given by the following expressions:

$$E(t) = E_r + \sum_j E_j \exp(-t/\tau_j) \quad (8.65)$$

$$E^*(\omega) = E_r + \sum_j \frac{E_j \omega \tau_j}{\omega \tau_j - i} \quad (8.66)$$

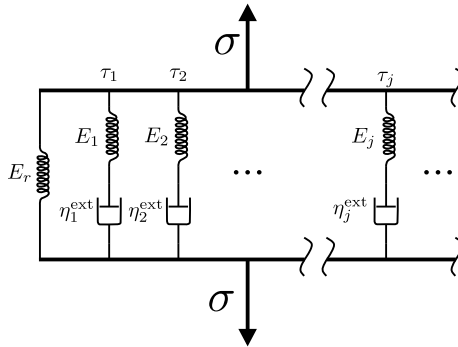


Figure 8.16: Generalized Maxwell model.

with  $\tau_j = \eta_j^{\text{ext}}/E_j$ . Any linearly viscoelastic material response can be described by a generalized Maxwell model, provided that we include a sufficient number of Maxwell elements.

#### 8.8.4 Kelvin-Voigt Model

The **Kelvin-Voigt model** consists of a spring and dashpot in parallel, as shown in Figure 8.17. In this case the stresses in two elements are additive and the strains in the two elements are the same:

$$\sigma = \eta_1^{\text{ext}} \frac{de}{dt} + E_1 e \quad (8.67)$$

The Kelvin-Voigt model is the simplest model for the description of a creep experiment, where the stress jumps instantaneously from 0 to  $\sigma = \sigma_0$  and we track the strain as a function of time. We have:

$$e(t) = \frac{\sigma_0}{E_1} (1 - \exp(-t/\tau)); \quad \tau = \eta_1^{\text{ext}}/E_1 \quad (8.68)$$

The dynamic modulus for the Kelvin-Voigt element is given by the following expression:

$$E^* = E_0 + i\omega\eta_0 \quad (8.69)$$

So that  $E'$  is simply equal to  $E$ , and  $E''$  is equal to  $\omega\eta_0$ .

#### 8.8.5 Viscoelastic Models for Shear Deformation

It is easier to visualize springs and dashpots in an extensional geometry, which is why we used this geometry to illustrate their use in describing the time-

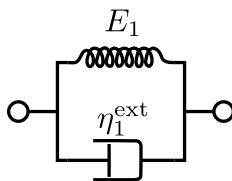


Figure 8.17: Kelvin-Voigt Model.

and frequency-dependent behavior of viscoelastic materials. The exact same formalism can be used to describe the properties in a shear geometry as well. We just need to replace  $E^*$ ,  $E'$  and  $E''$  with  $G^*$ ,  $G'$  and  $G''$ . We also drop the 'ext' superscript from the viscosities, since the viscosity is generally assumed to refer to the shear viscosity. For an incompressible liquid,  $\eta^{\text{ext}} = 3\eta$ , just as  $E = 3G$  for a compressible solid (with Poisson's ratio = 0.5).

## 8.9 Time-Temperature Superposition of Dynamic Mechanical Data

For many materials we are interested in the dynamic mechanical properties over a very wide range of frequencies, including those for which direct measurements are not possible. Fortunately, in many cases we can use the concept of **time-temperature equivalence** to obtain the response at a very wide range of frequencies by measuring over a much more limited frequency range, but over a range of temperatures. We can do this because for many materials all of the relevant relaxation times have the same temperature dependence. Materials for which this is the case are said to be 'thermorheologically simple', meaning that the temperature-dependence of their linear viscoelastic properties is 'simple'.

As an example of a thermorheologically simple material, we consider here the behavior of poly(t-butyl acrylate) and amorphous polymer with a glass transition temperature near 45 °C. In Figure 8.18 we plot the frequency dependence of  $[G^*]$  and  $\phi$  for 5 different temperatures. (The Python code used to generate Figures 8.18 - 8.21 is available at [msecore.northwestern.edu/331/python/ptba\\_master\\_curve.py](https://msecore.northwestern.edu/331/python/ptba_master_curve.py), with the raw data available at [msecore.northwestern.edu/331/data/ptbadata.xlsx](https://msecore.northwestern.edu/331/data/ptbadata.xlsx).) The range of angular frequencies extends from 0.1 s<sup>-1</sup> to 100 s<sup>-1</sup>. If time temperature equivalence holds, then changing the temperature will change all of the relaxation times by the same temperature-dependent multiplicative factor,  $a_T$ . We see from Eq. 8.66 that the response of the material is always determined by the product of  $\omega$  and a relaxation time. Since all of the relaxation times are proportional to  $a_T$ , we would expect the values of  $E^*$  to overlap with one another if we plot them as a function of  $\omega a_T$ . When the scale of the frequency axis is

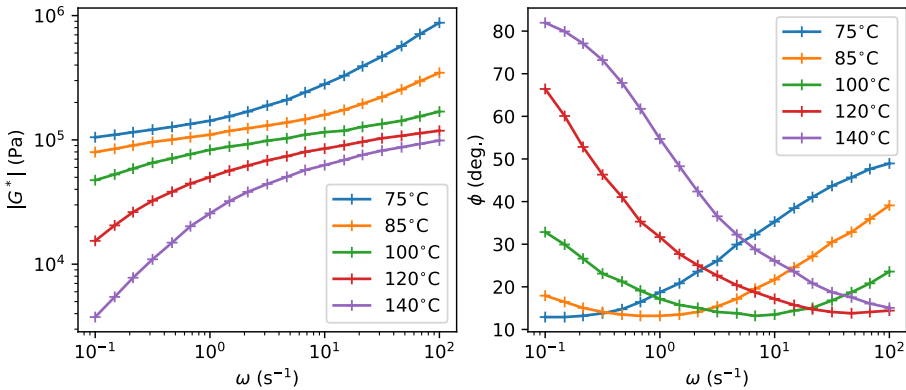


**Figure 8.18:** Frequency dependence of  $|G^*|$  and  $\phi$  for a poly(*t*-butyl acrylate) polymer at 4 different temperatures.

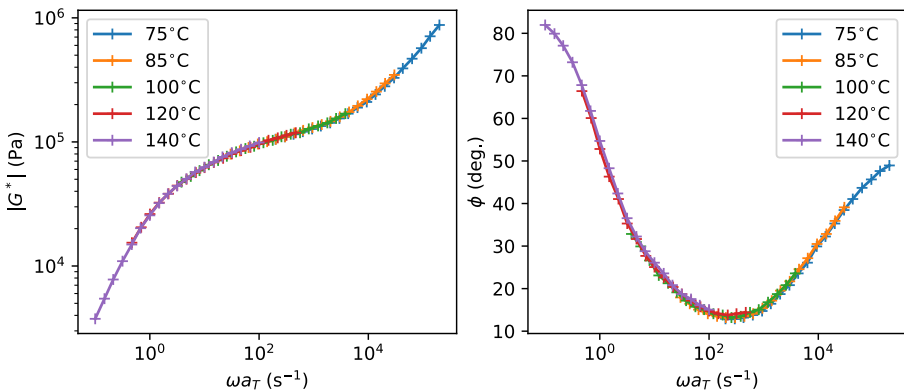


**Figure 8.19:** Frequency dependence of  $|G^*|$  and  $\phi$  for a poly(*t*-butyl acrylate) polymer at 4 different temperatures.

logarithmic, as is generally the case for these sorts of plots, changing the temperature shifts the curves right or left. Increasing the temperature decreases the relaxation times, and shifts the curves to the left, whereas decreasing the temperature shifts to the curves to the right. The actual shift factors are chosen empirically by seeing what values get the data to actually superpose. When the data from Figure 8.18 is shifted in this way we get the curves shown in Figure 8.19, using the shift factors plotted in Figure 8.20. The reference temperature was chosen as 140 °C.

The Vogel-Fulcher-Tamman equation is often used to describe the shift factors:

$$\ln(a_T) = \frac{-B}{T_{ref} - T_\infty} + \frac{B}{T - T_\infty} \quad (8.70)$$

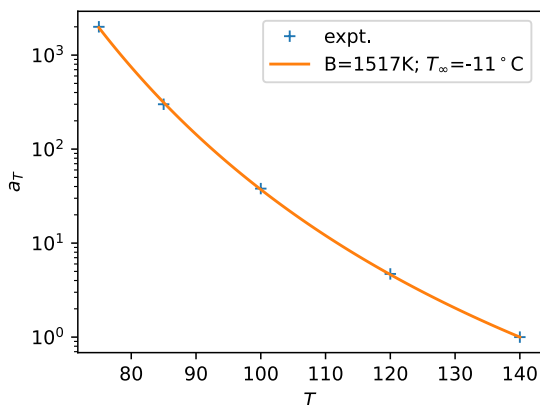


**Figure 8.20:** Shift factors used to generate the temperature-shifted master curves shown in Figure 8.19. The solid line is the VFT equation (Eq. 8.70), using a reference temperature,  $T_{ref}$ , of 140 °C and the values of  $B$  and  $T_\infty$  shown on the plot.

Most polymers have  $B$  in the range of 2000K and  $T_\infty$  around 50K below the glass transition temperature. Master curves for the storage and loss moduli,  $G'$  and  $G''$ , respectively, are shown in Figure 8.21.

### Measurement of the Entanglement Molecular Weight

It was mentioned above that amorphous polymers with a sufficiently large molecular weight are entangled, with these entanglements acting as temporary crosslinks in the material. These temporary crosslinks produce a 'plateau' in  $G'$  at intermediate frequencies, and a corresponding minimum in the phase angle,  $\phi$ , indicating that the behavior of the material has a substantial elastic character in this frequency regime. The modulus in this region is called the plateau modulus,  $G_N^0$ . The specific value of  $G_N^0$  is generally taken as the inflection point in  $G'$ , or as the value of  $G'$  at the frequency at which  $\phi$  is minimized. Once  $G_N^0$  is known, the entanglement molecular weight,  $M_e$  can be determined from the relevant expression from rubber elasticity theory:

$$G_N^0 = \frac{\rho RT}{M_e} \quad (8.71)$$

### Viscosity from Rheological Data

The zero shear viscosity,  $\eta_0$ , at the temperature where  $a_T = 1$  is determined from the low frequency data, in the regime where  $G''$  is proportional to  $\omega$  and where  $\phi \approx 90^\circ$  (Eq. 8.62). The full temperature dependence of  $\eta_0$  is then given

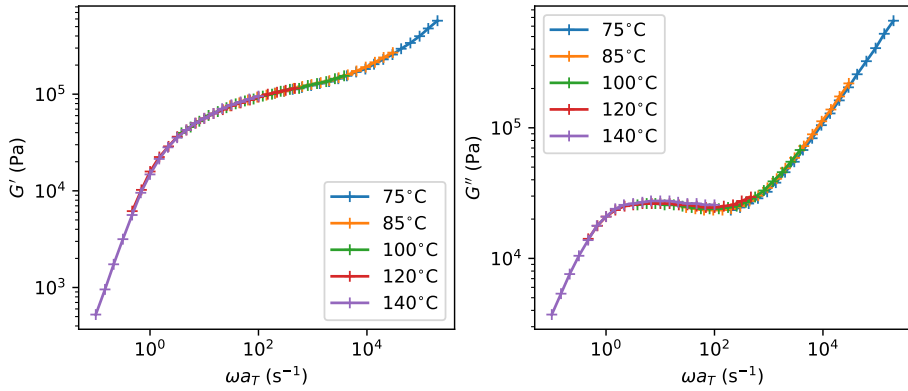


**Figure 8.21:** Temperature-shifted master curves for dependence of  $|G^*|$  and  $\phi$  for a poly(t-butyl acrylate) polymer at 4 different temperatures.

by the measured temperature dependence a dependence of  $a_T$ , since  $a_T$  has the same temperature dependence as the viscosity.



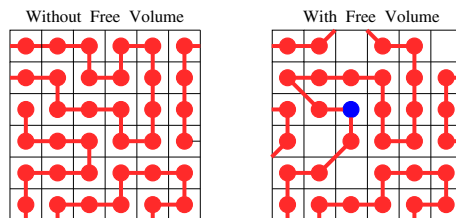


Figure 9.1: Conceptual representations of polymers with and without free volume.

## 9 The Glass Transition

The information presented so far about the structure of amorphous polymers applies both to elastomers like natural rubber, in addition to engineering thermoplastics like polystyrene. The properties of rigid plastics and rubber are obviously quite different, in spite of these similarities. The difference is that below a certain temperature, molecular motion is no longer possible, and the material becomes a relatively hard solid. This transition between “soft” and “hard” behavior occurs at the **glass transition temperature**,  $T_g$ .

### 9.1 Free volume

A very useful way to think about the glass transition involves the concept of unoccupied space, or ‘free volume’ in a polymer. This concept is illustrated conceptually in Figure 9.1. The red dots connected together by lines represent polymer molecules. In this lattice model of polymers, the red dots are constrained to fit on a lattice. (The lattice is completely artificial, and does not exist in reality). These dots represent the ‘**occupied volume**’. Empty lattice sites represent **free volume**. The lattice on the left has no free volume, so there is no way for the molecules to move by the ‘hopping’ of segments into a small region of unoccupied space. The lattice on the right does have free volume, however, so that molecular motion is relatively easy.

The conceptual free volume model of the glass transition makes the assumption that **volume thermal expansion coefficient**,  $\alpha$  is defined in the following manner:

$$\alpha = \frac{1}{V} \frac{dV}{dT} \quad (9.1)$$

Note that the linear thermal expansion coefficient, defined in terms of the linear dimensions of the sample rather than the volume, is equal to  $\alpha/3$ . If the

fractional change in free volume is small ( $\Delta V/V \ll 1$ ) then  $\alpha$  describes the linear relationship between the change in volume in the change in temperature:

$$\frac{\Delta V}{V} = \alpha \Delta T \quad (9.2)$$

In the glassy phase ( $T < T_g$ ), the free volume is assumed to remain constant, so that increases in the volume are governed entirely by increases in the occupied volume:

$$\frac{\Delta V_{occ}}{V} = \alpha \Delta T \quad (9.3)$$

In the liquid phase ( $T > T_g$ ), the free volume and occupied volumes both increase with temperature, and we have:

$$\frac{\Delta V}{V} = \frac{\Delta V_f}{V} + \frac{\Delta V_{occ}}{V} = \alpha_\ell \Delta T \quad (9.4)$$

Combining 9.3 and gives the following expression for the free volume in the liquid state:

$$\frac{\Delta V_f}{V} = (\alpha_\ell - \alpha_g) \Delta T \quad (9.5)$$

Now we define a new temperature,  $T_\infty$  which is the theoretical temperature at which the free volume would go to zero, if the material were to continue to follow the liquid behavior below  $T_g$ . It is illustrated schematically in Figure 9.2. To determine the fractional free volume at the glass transition, we use Eq. 9.5 with  $\Delta T = T_g - T_\infty$ , recognizing that  $V_f/V = 0$  at  $T = T_\infty$ :

Typically,  $T_\infty$  is about 50K below the measured glass transition temperature, and the fractional free volume at  $T_g$  is in the range of a couple percent.

The concept of free volume can be helpful in sorting out how the glass transition depends on the structure of the polymer, based on the following two guidelines:

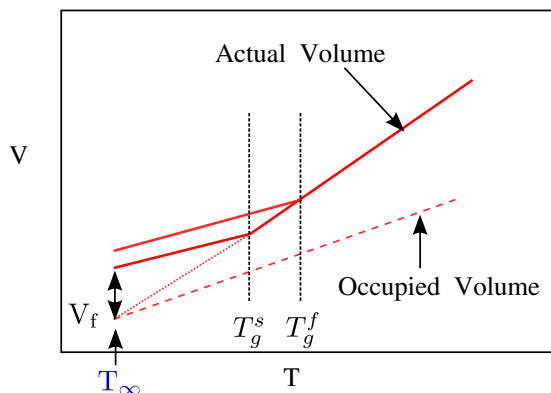


Figure 9.2: The glass transition and the free volume concept.

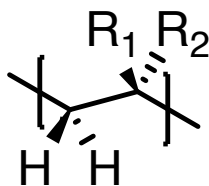
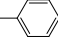
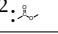
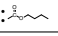


Figure 9.3: Structure of the repeat units for the materials listed in Table 9.1.

1. Changes to the polymer structure that increase the free volume needed in and  $r$  for the backbone of the polymer to move will increase  $T_g$ . Making the backbone very stiff (by the incorporation of phenyl groups, as in PET) increase  $T_g$ . Also, bulky, 'fat' substituents (like methyl or phenyl groups) tend to increase  $T_g$  when added to the backbone.
2. Changes to the polymer structure that introduce extra free volume will decrease  $T_g$ . This is the case for long, thin additions to the backbone, such as alkyl chains ( $-(\text{CH}_2)_n-$ ).

Without experience it's difficult to know which of these effects is greater. If I add something to the backbone for example, does it create more free volume that it needs to move? The best way to get a handle on this is to take a look at the glass transition temperatures of atactic polymers with the general chemical structure shown in Figure 9.3. The glass transition temperatures for these different polymers are listed in Table 9.1.

**Exercise:** Polystyrene has a volume thermal expansion coefficient of  $6 \times 10^{-4} \text{ K}^{-1}$  for temperatures above  $T_g$ , and a thermal expansion coefficient of

	R <sup>1</sup> =H	R <sup>1</sup> =CH <sub>3</sub>
R <sup>2</sup> : H	-125	-13
R <sup>2</sup> : CH <sub>3</sub>	-13	-75
R <sup>2</sup> : 	100	180
R <sup>2</sup> : 	10	105
R <sup>2</sup> : 	-54	20

**Table 9.1:** Glass transition temperatures (in °C) for polymers with the general structure shown in Figure 9.3 (From ref.[8]).

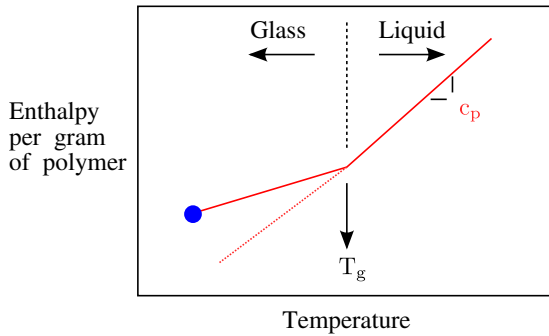


**Figure 9.4:** A graph of enthalpy vs temperature

$2 \times 10^{-4} \text{ K}^{-1}$  for temperatures below  $T_g$ . Estimate the ratio of the free volume to the total volume of sample in the glassy state. Assume that  $T_\infty$  is 50K below  $T_g$ .

**Solution:** Since the fractional free volume is assumed to be fixed below  $T_g$ , we are looking for the fractional free volume at the glass transition, as given by Eq. 9.5. With  $\alpha_\ell = 6 \times 10^{-4} \text{ K}^{-1}$ ,  $a_g = 2 \times 10^{-4} \text{ K}^{-1}$  and  $T_g - T_\infty = 50 \text{ K}$ , we obtain:

$$\frac{V_f}{V} = (4 \times 10^{-4} \text{ K}^{-1}) (50 \text{ K}) = 0.02$$

This value of 0.02 is a typical value for the fractional free volume in a glassy polymer.

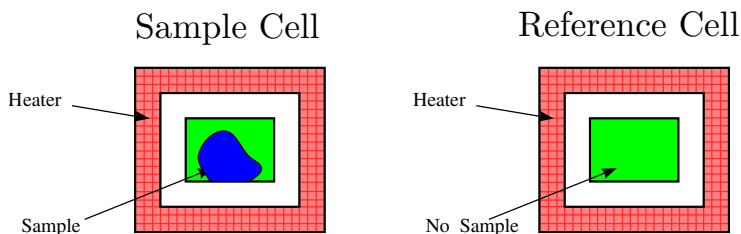


Figure 9.5: Simple schematic representation of a calorimeter.

## 9.2 Enthalpy and Heat Capacity

The heat capacity ( $c_p$ ) of the liquid is larger than the heat capacity of the glass. Note that the enthalpy itself is continuous at  $T = T_g$ . The glass transition is therefore a second order transition - thermodynamic quantities like volume, enthalpy and entropy are continuous at the transition but the derivatives of these quantities with respect to temperature are discontinuous.

## 9.3 Differential Scanning Calorimetry (DSC)

Glass transition temperatures are most commonly measured by differential scanning calorimetry. The technique can be used to measure the glass transition temperature of a polymer, in addition to the temperature at which a polymer melts or crystallizes. The heat of fusion (heat required to melt a semicrystalline polymer) can also be obtained. Heat flowing into the sample is endothermic, and heat flowing out of the sample is exothermic. We have plotted endothermic heat flow in the positive direction, and exothermic heat flow in the negative direction. Unfortunately, there is no universally followed sign convention for displaying DSC data. Sometimes endothermic heats are plotted in the negative direction. In order to avoid confusion, the endothermic direction is commonly indicated on the DSC plot, as we have done in the curve shown in Figure 9.6. Students are encouraged to look at the Macrogalleria web sites on the glass transition[?] and differential scanning calorimetry[9] for discussions at the appropriate level for this class.

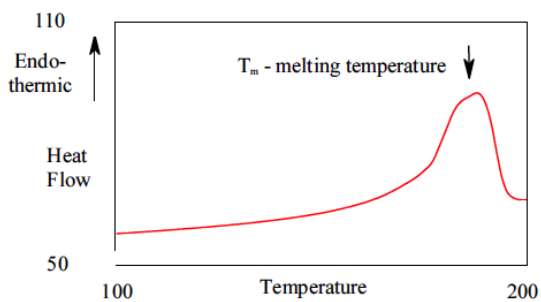
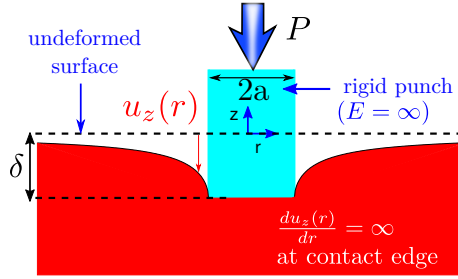


Figure 9.6: Graph of heat flow vs temperature.



**Figure 10.1:** Indentation of a soft surface with a rigid, flat-ended cylindrical punch of radius  $a_0$ .

## 10 Contact Mechanics

In a simple tensile test involving a sample with a uniform cross section, the stresses and strains are both uniform throughout the entire sample. In almost any real application where we care about mechanical properties, this is not the case however. A simple example of this is the case where we press a rigid, cylinder into a soft, compliant material as shown in Figure 10.1.

### 10.1 Sign conventions

Sign conventions have a tendency to lead to confusion. This issue is particularly problematic in contact mechanics because compressive loads are considered to be positive, but a compressive stress is negative. Here's a summary of the sign conventions relevant to our treatment of contact mechanics:

- $P$  (force): a positive force is compressive
- $\delta$  (displacement): a positive displacement is compressive
- $\sigma$  (stress): a positive stress is tensile
- $\epsilon$  (strain): a positive strain is tensile

In order not to get too hung up in issues related to the sign, we define  $P_t$  and  $\delta_t$  as the tensile loads and displacements:

$$\begin{aligned} P_t &= -P \\ \delta_t &= -\delta \end{aligned} \tag{10.1}$$

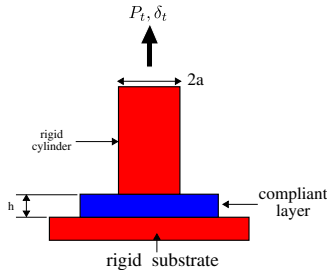


Figure 10.2: Flat punch contact geometry. For an elastic half space,  $h \rightarrow \infty$ .

## 10.2 Flat Punch Indentation

(Note: Many of issues presented here are discussed in more detail in a published review article: see ref.[10]).

Consider a flat-ended cylindrical punch with a radius of  $a$  in contact with another material of thickness,  $h$ , as shown schematically in Figure 10.2. The material being indented by a punch rests on a rigid substrate. We are interested in the compressive force,  $P$ , that accompanies a compressive displacement,  $\delta$ , applied to the indenter.

### 10.2.1 Flat Punch: Approximate Result for an elastic half space.

For an elastic half space ( $h \rightarrow \infty$ ), the strain field under the indenter is nonuniform. The largest strains are confined to a region with characteristic dimensions defined by the punch radius,  $a$ . We can get a very approximate expression for the relationship between the compressive load,  $P$ , and the compressive displacement,  $\delta$  from the following approximate concepts:

- The average strain in the highly deformed region of the sample must increase linearly with  $\delta$ . Because strain is dimensionless we need to divide  $\delta$  by some length scale in the problem to get a strain. For an elastic half space with  $h = \infty$  the only length scale in the problem is the punch radius,  $a$ . So the strain fields must depend on  $\delta/a$ . We'll take this one step further and assume that  $\delta/a$  is an average in a region of volume  $\approx a^3$  under the punch:

$$e_{avg} = -\delta/a \quad (10.2)$$

- The average contact stress,  $\sigma_{avg}$  under the punch can be quantitatively defined by dividing the compressive load by the stress:

$$\sigma_{avg} = -P/\pi a^2 \quad (10.3)$$



- An approximate relationship between  $P$  and  $\delta$  is obtained by assuming that the stress and strain are related through the elastic modulus, *i.e.*  $\sigma_{avg} = Ee_{avg}$ . Using the equations above for the compliance,  $C_0$ :

$$C_0 \equiv \frac{\delta}{P} \approx \frac{1}{\pi E a} \quad (10.4)$$

### 10.2.2 Flat punch - Detailed Result

In a more general situation both of the contacting materials (the indenter and the substrate) may deform to some extent, so the compliance depends on the properties of both materials. If the materials have Young's moduli of  $E_1$  and  $E_2$  and Poisson's ratios of  $\nu_1$  and  $\nu_2$ , then the expression for  $C_0$  is:

$$C_0 \equiv \frac{\delta}{P} = \frac{\delta_t}{P_t} = \frac{1}{2E_r a} \quad (10.5)$$

where  $E_r$  is the following **reduced modulus**:

$$\frac{1}{E_r} = \frac{1 - \nu_1^2}{E_1} + \frac{1 - \nu_2^2}{E_2} \quad (10.6)$$

Note that for a stiff indenter, ( $E_2 \gg E_1$ ) we have  $E_r = \frac{E_1}{1 - \nu_1^2}$ . This is the plane strain modulus that appears in a variety of situations, which we derive below.

### 10.2.3 Plane strain modulus.

The plane strain modulus,  $E_r$ , describes the response of a material when it cannot contract in one of the directions that is perpendicular to an applied tensile stress. It's easy to derive this by using the compliance matrix for an amorphous material, which must look like this;

$$\begin{bmatrix} e_1 \\ e_2 \\ e_3 \\ e_4 \\ e_5 \\ e_6 \end{bmatrix} = \frac{1}{E} \begin{bmatrix} 1 & -\nu & -\nu & 0 & 0 & 0 \\ -\nu & 1 & -\nu & 0 & 0 & 0 \\ -\nu & -\nu & 1 & 0 & 0 & 0 \\ 0 & 0 & 0 & 2(1+\nu) & 0 & 0 \\ 0 & 0 & 0 & 0 & 2(1+\nu) & 0 \\ 0 & 0 & 0 & 0 & 0 & 2(1+\nu) \end{bmatrix} \begin{bmatrix} \sigma_1 \\ \sigma_2 \\ \sigma_3 \\ \sigma_4 \\ \sigma_5 \\ \sigma_6 \end{bmatrix} \quad (10.7)$$

In writing the compliance matrix this way, we have used the fact that Young's modulus is  $1/s_{11}$  and the Poisson's ratio is  $-s_{12}/s_{11}$ , so we have  $s_{11} = 1/E$

and  $s_{12} = -\nu/E$ . Suppose we apply a stress in the 1 direction, and require that the strain in the 2 direction is 0. This requires that a non-zero stress develop in the 2 direction. If we assume that  $\sigma_3 = 0$ , we have:

$$e_2 = \frac{-\nu}{E}\sigma_1 + \frac{\sigma_2}{E} \quad (10.8)$$

If  $e_2$  is constrained to be zero, we have:

$$\sigma_2 = \nu\sigma_1 \quad (10.9)$$

Now we can put this value back into Eq. 10.7 and solve for  $e_1$ :

$$e_1 = \frac{1}{E} \left( \sigma_1 - \nu^2\sigma_1 \right) \quad (10.10)$$

The plane strain modulus relates  $\sigma_1$  to  $e_1$ , which for the case assumed above ( $e_2 = 0$ ) gives:

$$E_r = \frac{\sigma_1}{e_1} = \frac{E}{1 - \nu^2} \quad (10.11)$$

### 10.3 Flat Punch Detachment and the Energy Release Rate

If adhesive forces cause the punch to stick to the substrate, we can use fracture mechanics to understand the force required for detachment to occur. The situation is as shown in Figure 10.3 for a flat-ended cylindrical punch with a radius of  $a_0$ . The surface profile of the substrate (assumed in this case to be an elastic half space, *i.e.*,  $h = \infty$ ) is given by the following expression[11]:

$$u_z = (2\delta_t/\pi) \arcsin(a/r) \quad (10.12)$$

where  $\delta_t$  is the applied tensile displacement and  $a$  is the actual radius of the contact area between the punch and the substrate. In Figure 10.3 we compare the shapes of the surface for the following two cases:

- $a = a_0$ : this is the initial contact condition, where the substrate is in contact with the full surface of the indenter.
- $a = a_0/2$ : the contact radius has been reduced to half its initial value.

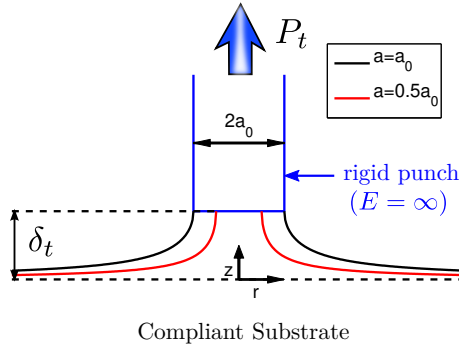


Figure 10.3: Surface profile under a flat punch, from Eq. 10.12.

The decrease in  $a$  from  $a_0$  to  $a_0/2$  is accompanied by a decrease in the stored elastic strain energy, and this strain energy is what drives the decrease in the contact area. While it may not be immediately obvious from Figure 10.3, the detachment problem is actually a fracture mechanics problem. This is because the edge of the contact can be viewed as a crack, which grows as the contact area shrinks. In the following section we describe a generalized energy based approach to for quantifying the driving force for the contact area to decrease before applying this approach to the specific problem of a flat cylindrical punch.

### 10.3.1 Energy Release Rate for a Linearly Elastic Material

Specifying the stress field is the same as specifying the stored elastic energy. Fracture occurs when available energy is sufficient to drive a crack forward, or equivalently in our punch problem, to reduce the contact area between the punch and the substrate. To begin we define the following variables:

- $W$  = work done on system by external stresses
- $U_{el}$  = elastically stored energy
- $W - U_{el}$  = energy available to drive crack forward.

The **energy release rate**,  $\mathcal{G}$ , describes the amount of energy that is used to move a crack forward by some incremental distance. Formally it is described in the following way:

$$\mathcal{G} = \frac{d}{dA_c} (W - U_{el}) \quad (10.13)$$

where  $A_c$  is the crack area. Fracture occurs when the applied energy release rate exceeds a critical value characteristic of the material, defined as the critical energy release rate,  $\mathcal{G}_c$ . The fracture condition is therefore:

$$\mathcal{G} = \mathcal{G}_c \quad (10.14)$$

The lowest possible value of  $\mathcal{G}_c$  is  $2\gamma$  where  $\gamma$  is surface energy of the material. That's because the minimal energy to break a material into two pieces is the thermodynamic energy associated with the two surfaces. Some typical values for the surface energy of different materials are listed below (note that  $1 \text{ mJ/m}^2 = 1 \text{ erg/cm}^2 = 1 \text{ dyne/cm}$ ).

- Polymers: 20-50 mJ/m<sup>2</sup> Van der Waals bonding between molecules
- Water: 72 mJ/m<sup>2</sup> Hydrogen bonding between molecules
- Metals:  $\approx 1000 \text{ mJ/m}^2$  Metallic bonding

We can derive a simple expression for the energy release rate if we assume that the material has a linear elastic response. Consider, for example, an experiment where we apply a tensile force,  $P_t$ , to a sample, resulting in a tensile displacement,  $\delta_t$ , as illustrated in Figure 10.4a. If the material has a linear elastic response, the behavior is as illustrated in Figure 10.4. Suppose that the crack area remains constant as the material is loaded to a tensile force  $P_t$ . The sample compliance,  $C$ , is given by the slope of the displacement-force curve:

$$C = \left. \frac{d\delta_t}{dP_t} \right|_{A_c} \quad (10.15)$$

Now suppose that the crack area is increased by an amount  $dA_c$  while the load remains fixed at  $P_t$ , *i.e.* the system moves from point 1 to point two on Figure 10.4b. This increases the compliance by an amount  $dC$ , resulting in corresponding increase in the displacement of  $P_t \delta C$ . If we now unload the sample from point 2 back to the origin, the slope of this unloading curve is given by the enhanced compliance,  $C + \delta C$ . At the end of this loading cycle we have put energy into the sample equal to the shaded area in Figure 10.4b. This is the total work done on the system by the external stresses ( $W$  in Eq. 10.13), and given by the following expression:

$$\delta W = \frac{1}{2} P_t^2 \delta C \quad (10.16)$$

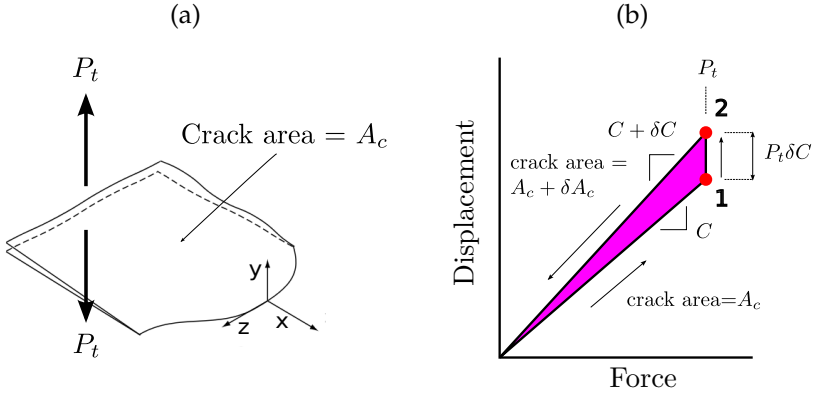


Figure 10.4: Derivation of the compliance expression for  $\mathcal{G}$ .

Because the sample at the beginning and end of this process is unstrained, we have  $U_{el} = 0$ . We can now take the limit where  $\delta A_c$  becomes very small to replace  $\delta W / \delta C$  with the derivative,  $dW / dC$  to obtain:

$$\mathcal{G} = \lim_{\delta A_c \rightarrow 0} \frac{\delta W}{\delta A_c} = \frac{P_t^2}{2} \frac{dC}{dA_c} \tag{10.17}$$

### 10.3.2 Stable and Unstable Contact

Two different behaviors are obtained as two contacting materials are separated, depending on the relationship between  $\mathcal{G}$  and the contact area  $A$ . These behaviors are referred to as stable contact ( $d\mathcal{G}/dA > 0$ ) and unstable contact ( $d\mathcal{G}/dA < 0$ ). The difference between these behaviors is illustrated in Figure 10.5, and can be understood by considering two surfaces that are initially brought into contact to establish a contact area,  $A_0$ . We then increase the tensile load,  $P_t$ , thereby increasing the applied energy release rate. As the tensile load and the corresponding tensile displacement are increased,  $\mathcal{G}$  increases until it reaches the critical value,  $\mathcal{G}_c$ . The tensile load at this point is defined as the critical load  $P_c$ , and is the load at which  $A$  begins to decrease. We fix the tensile load at  $P_c$  and observe one of two possible behaviors:

**Unstable Detachment:** If  $d\mathcal{G}/da < 0$ , a decrease in  $A$  gives rise to an increase in  $\mathcal{G}$ , and the contact is unstable, so that the indenter rapidly detaches from the indenter once  $a$  starts to decrease.

**Stable Detachment:** If  $d\mathcal{G}/dA > 0$ , a decrease in  $a$  corresponds to a decrease in  $\mathcal{G}$ . In this case the contact is stable, and the load (or displacement) must be

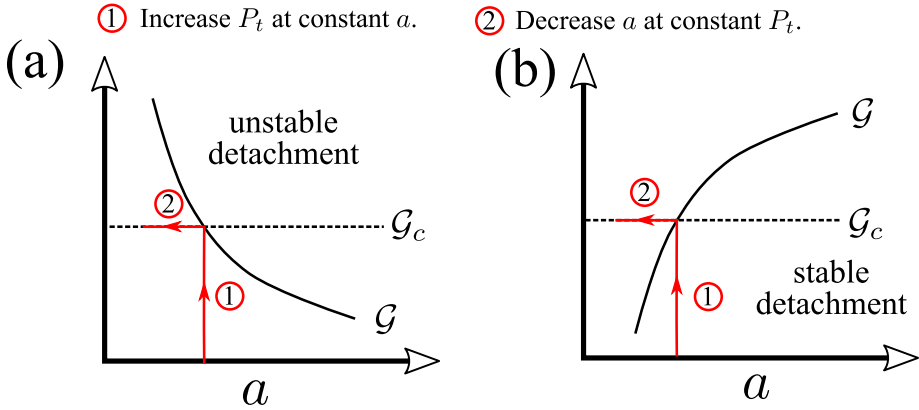


**Figure 10.5:** Illustration of stable contact, where  $P_t$  must increase continuously in order for the contact area to continue to decrease, and unstable contact, where the contact area reduces rapidly to zero as soon as a critical tensile load is attained.

increased further to continue to decrease the contact area. Detachment in this case occurs gradually as the load continues to increase.

### 10.3.3 Application of the Griffith Approach to the Flat Punch Problem

The edge of the contact is a crack, which advances as  $a$  decreases. We can use Eq. 10.17 for the energy release rate to obtain the following:

$$\mathcal{G} = -\frac{P_t^2}{2} \frac{dC}{dA} = -\frac{P_t^2}{4\pi a} \frac{dC}{da} \tag{10.18}$$

where we have assumed that the contact area remains circular, with  $A = \pi a^2$ . Not that  $A$  in this expression is the contact area between the indenter and the substrate, and NOT the crack area. The negative sign in Eq. 10.18 emerges from the fact an decrease in contact area corresponds to an equivalent increase in the crack area, so we have:

$$\frac{dC}{dA} = -\frac{dC}{dA_c} \tag{10.19}$$

With  $C = C_0 = 1/2E_r a$  (Eq. 10.5) we obtain the following expression for  $\mathcal{G}$ :

$$\mathcal{G} = \frac{P_t^2}{8\pi E_r a^3} \tag{10.20}$$

In some situations it is more convenient to express the energy release rate in terms of the tensile displacement,  $\delta_t$ . The most general expression is used by using  $C = \delta_t/P_t$  to substitute  $P_t$  with  $\delta_t/C$  in Eq. 10.17:

$$\mathcal{G} = -\frac{\delta_t^2}{2C^2} \frac{dC}{dA} = -\frac{\delta_t^2}{4\pi a C^2} \frac{dC}{dA} \quad (10.21)$$

If the compliance is the value for an elastic half space (Eq. 10.5), then we obtain the following expression for the energy release rate in terms of the displacement:

$$\mathcal{G} = \frac{E_r \delta_t^2}{2\pi a} \quad (10.22)$$

It is useful at this point to make the following general observations:

- In fracture mechanic terms the contact edge is an interfacial crack. An advancing crack corresponds to a reduction in  $a$ , and a receding crack corresponds to an increase in  $a$ .
- In general,  $\mathcal{G}$  is determined by the applied load and the geometry.
- $\mathcal{G}_c$  is a property of the interface. The crack moves forward ( $a$  decreases) when the value of  $\mathcal{G}$  determined by the loading conditions exceeds  $\mathcal{G}_c$ . The detachment criterion is that the energy release rate,  $\mathcal{G}$ , is equal to the critical energy release rate,  $G_c$ , when the applied tensile force is equal to the critical pull-off force,  $P_c$ :

$$G_c = \frac{P_c^2}{8\pi E_r a^3} \quad (10.23)$$

This equation can be rearranged to give the following for the pull-off force:

$$P_c = \left(8\pi E_r a^3 G_c\right)^{1/2} \quad (10.24)$$

- Detachment from of a flat punch from an elastic half space ( $a/h = 0$ ) is unstable for load controlled (constant  $P_t$ ) OR displacement controlled (constant  $\delta_t$ ) conditions. In each of these cases the contact radius,  $a$ , is equal to the punch radius,  $a_0$ , at the beginning of an experiment.

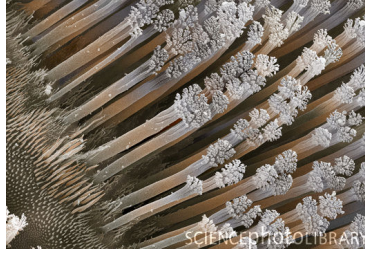


Figure 10.6: Electron micrograph of Gecko setae.

### 10.3.4 Detachment: Size Scaling

An interesting aspect of Eq. 10.24 is that the pull-off force scales with  $a^{3/2}$ , whereas the punch cross sectional area scales more strongly with  $a$  ( $A = \pi a^2$ ). This behavior has some interesting consequences, which we can obtain by dividing  $P_c$  by the punch cross sectional area to obtain a critical pull-off stress,  $\sigma_c$ :

$$\sigma_c = \frac{P_c}{\pi a^2} = \left( \frac{8E_r \mathcal{G}_c}{\pi a} \right)^{1/2} \quad (10.25)$$

Note that the detachment stress increases with decreasing punch size.

Let's put in some typical numbers to see what sort of average stresses we end up with:

- $E_r \approx 10^9$  Pa (typical of glassy polymer)
- $\mathcal{G}_c \approx 0.1$  J/m<sup>2</sup> (twice the surface energy of a typical organic material)
- $a \approx 100$  nm (smallest reasonably possible value)
- $\sigma_c \approx 50$  MPa

In order for stresses to be obtained, the pillars must be separated so that the stress fields in substrate don't overlap. This decreases the maximum detachment stress from the previous calculation by about a factor of 10, so that the largest stress we could reasonably expect is  $\approx 5$  MPa. That's still a pretty enormous stress, corresponding to 500 N (49 Kg) over a 1 cm<sup>2</sup> area. This is still difficult to achieve, however, because it requires that the pillar array be extremely well aligned with the surface of interest, a requirement that is very difficult to meet in practice. Nevertheless, improvements in the pull-off forces



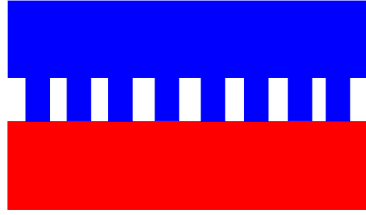


**Figure 10.7:** Schematic representation of an array of pillars in contact with a flat surface.

can be realized by structuring the adhesive layer, and this effect is largely responsible for the adhesive behavior of geckos and other creatures with highly structured surfaces.

### 10.3.5 Thickness Effects

When the thickness,  $h$ , of the compliant layer between a rigid cylindrical punch and a rigid, flat substrate decreases, the mechanics change in a way that makes it more difficult to pull the indenter out of contact with the compliant layer. For the geometry shown in Figure 10.8 we can write the compliance of the material in the following way:

$$C = \frac{1}{2E_r a} f_C \quad (10.26)$$

For an elastic half space ( $h \rightarrow \infty$ )  $f_C = 1$ . The factor  $f_C$  accounts for changes in the compliance due to the decreased thickness of the layer. In general it depends on Poisson's ratio for the compliant layer and the confinement ratio,  $a/h$  (the ratio of the punch radius to the thickness of the layer). For an incompressible compliant layer with  $\nu = 0.5$  the following expression for  $f_C$  provides an excellent approximation to the behavior of the compliance on the aspect ratio,  $a/h$ : [10]

$$f_C = \left[ 1 + 1.33 (a/h) + 1.33 (a/h)^3 \right]^{-1} \quad (10.27)$$

The behavior of  $f_C$  as a function of  $a/h$  is plotted in Figure 10.9. A series of geometric correction factors can be derived from this expression for  $f_C$ . The

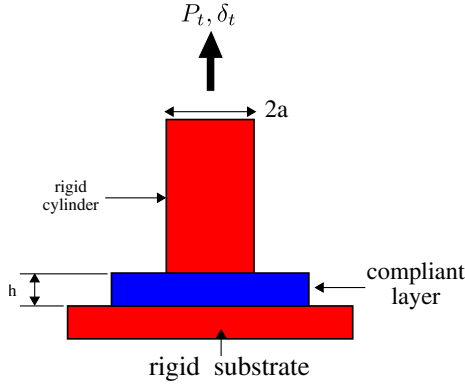


**Figure 10.8:** A thin, compliant layer being indented with a rigid, cylindrical punch.

first of these is a correction factor for the compliance of the energy release rate expression with the tensile load,  $P_t$ , as the independent variable. In this case we use Eq. 10.18 to get write the expression for the energy release rate in the following form:

$$\mathcal{G} = -\frac{P_t^2}{4\pi a} \frac{dC}{da} = \frac{P_t^2}{8\pi E_r a^3} f_{\mathcal{G}p} \tag{10.28}$$

Here  $f_{\mathcal{G}p}$  accounts for deviations in the compliance derivative due to the confinement effects, in this case determined by the ratio between the actual value of  $dC/da$  and the value of this quantity for  $a/h = 0$ :

$$f_{\mathcal{G}p} = \frac{dC}{da} / \frac{dC}{da} \Big|_{a/h=0} \tag{10.29}$$

Finally, we can use the the fact that  $P_t = \delta_t/C$  to get a similar expression for  $\mathcal{G}$  in terms of the tensile displacement,  $\delta_t$ :

$$\mathcal{G} = \frac{E_r \delta_t^2}{2\pi a} f_{\mathcal{G}\delta} \tag{10.30}$$

In this case  $f_{\mathcal{G}\delta}$  includes the dependence on  $a/h$  of both the compliance and it's derivative with respect to  $a$ . This dependence is evident from Eq. 10.21, where  $\mathcal{G}(\delta_t)$  is seen to be proportional to  $dC/da$  and is inversely proportional to  $C^2$ . The  $a/h$  dependence of  $dC/da$  is accounted for by  $f_{\mathcal{G}p}$ , and the  $a/h$  dependence of  $C$  is accounted for by  $f_C$ , so we obtain the following for  $f_{\mathcal{G}\delta}$ :

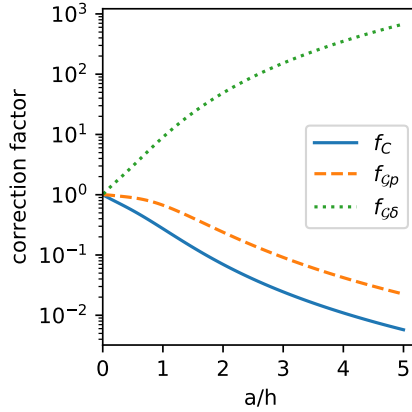


**Figure 10.9:** Geometric correction factors for the flat punch geometry (generated with python code given as example ?? in the appendix).

$$f_{G\delta} = \frac{f_{Gp}}{f_c^2}$$

The confinement functions  $f_{Gp}$  and  $f_{G\delta}$  are both equal to one for  $a/h = 0$  and are plotted as a function of  $a/h$  for  $\nu = 0.5$  in Figure 10.9. A practical consequence of the decrease in  $f_{Gp}$  with decreased  $h$  is that a larger tensile force is required in order to remove the cylinder from its contact with the compliant layer. With a small value of  $f_{Gp}$ , a larger tensile load needs to be applied in order for  $\mathcal{G}$  to exceed the critical energy release rate,  $\mathcal{G}_c$ .

## 10.4 Contact of Paraboloids

### 10.4.1 Non-Adhesive Case

Suppose that the indenter is not flat, but has a parabolic profile that can be described by the following expression:

$$z = A_p r^2 \tag{10.31}$$

Here  $z$  is the vertical distance from the apex of the parabola,  $r$  is the radial distance from symmetry axis for the paraboloid and  $A_p$  is a constant that defines the shape of the paraboloid. A sphere has a parabolic shape near the apex, which can be seen by considering the equation for a sphere of Radius  $R$  that has its center at  $r = 0, z = R$  (see Figure 10.10):

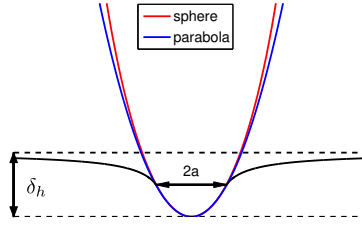


**Figure 10.10:** Non-adhesive contact of a rigid, parabolic indenter into an elastic material.

$$r^2 + (z - R)^2 = R^2 \quad (10.32)$$

Solving Eq. 10.32 for  $z$  gives:

$$z = R \left( 1 \pm \sqrt{1 - (r/R)^2} \right) \quad (10.33)$$

For small  $x$ ,  $\sqrt{1 - x} \approx 1 - x/2$ , so for  $r \ll R$  we have:

$$z = \frac{r^2}{2R} \quad (10.34)$$

where we have taken the solution with the smaller value of  $z$ , corresponding to the bottom of the sphere. From a comparison of Eqs. 10.32 and 10.34, we see the paraboloid is a good approximation for the shape of a sphere, with the sphere radius given by  $1/2A_p$ . For this reason we use  $R$  instead of  $A$  to characterize the parabolic shape, since the results can be applied to contact of spheres, provided that the contact dimensions are much smaller than  $R$ . Generally everything works well as long as  $r/R < 4$ .

The compressive force  $P_h$  required to push a rigid parabolic indenter into the surface of the material ( $\delta_h$  in Figure 10.10) is given by the following expression:

$$\delta_h = a^2/R \quad (10.35)$$

Note that this is a completely geometric relationship that does not depend on the modulus of the material that is being indented. The compressive force required to establish a contact radius of  $a$  is referred to as  $P_h$ , and is given by the following expression:

$$P_h = \frac{4E_r a^3}{3R} \quad (10.36)$$

We can use Eq. 10.35 to substitute for  $a$  and obtain a relationship between  $P_h$  and  $\delta_h$ :

$$P_h = \frac{4E_r}{3} R^{1/2} \delta_h^{3/2} \quad (10.37)$$

The assumption here is that there is no adhesion between the indenter and the substrate, *i.e.*,  $\mathcal{G} = K_I = 0$ . The fact that there is no stress concentration at the interface is consistent with the fact that the slope of the surface profile of the compliant material is continuous at  $r = a$ . This surface profile is plotted in Figure 10.10 and is given by the following expression:[11]

$$u_z = \frac{\delta}{\pi} \left\{ \left( 2 - (r/a)^2 \right) \arcsin(a/r) + (r/a) \left( 1 - (a/r)^2 \right)^{1/2} \right\} \quad (10.38)$$

#### 10.4.2 Effects of Adhesion on Contact

The easiest way to understand the effect of adhesion on the contact between a parabolic is to consider a hypothetical situation where we turn off the adhesion and bring the indenter into contact with the surface, resulting in the deformation illustrated in Figure 10.10. Now we turn on the adhesion, and begin retracting the indenter from the surface, maintaining a fixed projected contact radius  $a$ . The situation for the case where we have retracted the tip to the point where the tip apex is level with the undeformed surface ( $\delta_t = 0$ ) is illustrated in Figure 10.11. The applied compressive load required to reach a given contact radius is less than the value of  $P_h$  given by Eq. 10.36 ( $P < P_h$ ). Similarly, the compressive displacement required to reach a given contact radius is less than the value given by Eq. 10.35 ( $\delta < \delta_h$ ). These deviations from  $\delta_h$  and  $P_h$  are related by the system compliance, which for this geometry is  $C_0$  as given by Eq. 10.5:

$$\frac{\delta - \delta_h}{P - P_h} = C_0 = \frac{1}{2E_r a} \quad (10.39)$$

Combination of Eqs. 10.5 and 10.39 gives the following relationship between  $\delta$ ,  $P$  and  $E_r$ :

$$\delta = \frac{a^2}{3R} + \frac{P}{2E_r a} \quad (10.40)$$

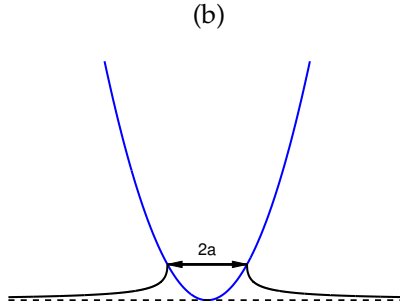


**Figure 10.11:** An example of the surface profile for adhesive contact for the case where  $\delta_t = 0$ .

This expression is the one that needs to be used in order to obtain the reduced modulus in situations where adhesive forces between the indenter and the substrate modify the contact radius. It use requires that the contact radius be measured independently. This is easy to do when the contact area is big enough to visualize directly, but is a very difficulty problem for very small contacts (as in atomic force microscopy) where the contact is too small to visualize optically.

Once we know the reduced modulus of the system, we can obtain the energy release rate. The expression for the energy release rate for curved object in contact with surface in a way that is very similar to what we did for the flat punch in Section 10.3. The only difference is that in the absence of adhesion we need to apply a compressive load,  $P_h$  (given by Eq. 10.36):

$$\mathcal{G} = -\frac{(P_t + P_h)^2}{2} \frac{dC}{dA} = \frac{(P_t + P_h)^2}{8\pi E_r a^3} \quad (10.41)$$

This equation can be rearranged to give  $a^3$  as a function of the compressive load,  $P$  ( $P = -P_t$ ), to give an expression that was derived in 1971 by Johnson, Kendall and Roberts [12] and commonly referred to as the **JKR equation**:

$$a^3 = \frac{3R}{4E_r} \left( P + 3\pi\mathcal{G}R + \left( 6\pi\mathcal{G}RP + (3\pi\mathcal{G}R)^2 \right)^{1/2} \right) \quad (10.42)$$

## 10.5 Indentation with Berkovich Trips

Parabolic tips are often used in measurements of adhesion or of the elastic properties of materials. For Hardness measurements tips with sharp corners are more commonly used. One example is the **Berkovich tip** shown in Figure 10.12.

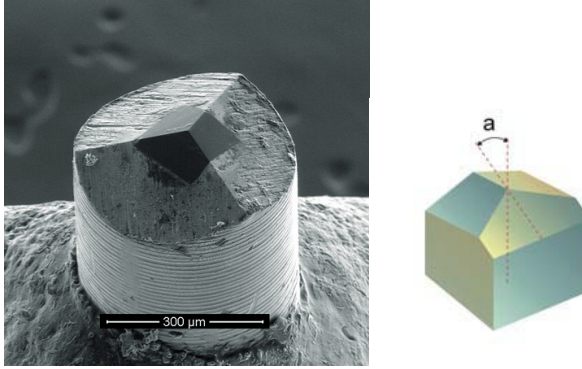


**Figure 10.12:** Geometry of a Berkovich tip commonly used in indentation experiments. The angle,  $a$ , is  $65.35^\circ$  for a standard Berkovich tip.

The hardness,  $H$ , of a material is given by the ratio of the load to the projected contact area of the non-recoverable indent made in the material by the indenter. In our case we obtain the hardness from the maximum load,  $P_{max}$  (illustrated in Figure 10.13), and from the corresponding projected area,  $A$ , of the hardness impression:

$$H = \frac{P_{max}}{A} \quad (10.43)$$

The projected area is related to the contact depth,  $\delta_c$ , by a relationship that depends on the shape of the indenter[13]. For a Berkovich tip the appropriate relationship is:

$$A = 24.5\delta_c^2 \quad (10.44)$$

The procedure for determining the contact depth was developed by Oliver and Pharr, where the following expression is used to estimate the contact depth:

$$\delta_c = \delta_{max} - 0.75\frac{P_{max}}{S} \quad (10.45)$$

where  $\delta_{max}$  is the maximum penetration depth of the indenter tip and  $S$  is the contact stiffness, determined experimentally as the initial slope of the linear portion of unloading curve (see Figure 10.13). From the measured values of  $S$ ,  $P_{max}$  and  $\delta_{max}$ , we use Equations 10.44 and 10.45 to determine  $A$ . The reduced modulus is then obtained from the following expression for the contact stiffness, assuming a value for the contact stiffness that is the same for a circular contact of the same area:

$$S = \frac{2}{\sqrt{\pi}}E_r\sqrt{A} \quad (10.46)$$

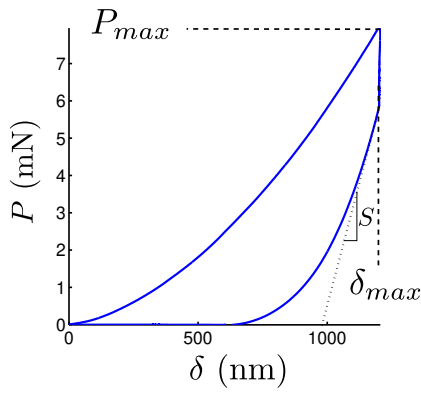


**Figure 10.13:** Typical load-displacement curve for indentation of the polyester resin used to embed the paint samples, labeled to illustrate the values of  $P_{max}$ ,  $\delta_{max}$  and  $S$ .



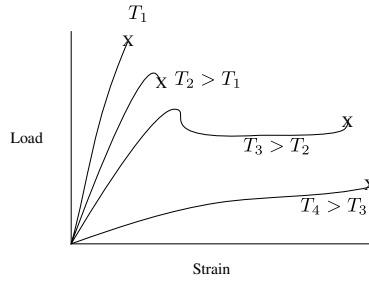


Figure 11.1: Typical generic temperature behavior at different temperatures.

## 11 Fracture

The stress-strain behavior for a many material can exhibit a range of phenomena, depending on the temperature. This is particularly true of many polymers, which can show the range of behaviors in a uniaxial tensile test shown in Figure 11.1. While not all of these behaviors are necessarily observed in the same material, the following general regimes can often be identified, based on 4 different temperature regimes ( $T_1$ ,  $T_2$ ,  $T_3$  and  $T_4$ ).

- $T_1$ : Brittle behavior. This is generally observed at sufficiently low temperatures.
- $T_2$ : Ductile behavior (yield before fracture)
- $T_3$ : cold drawing (stable neck)
- $T_4$ : uniform deformation

Here we are concerned with brittle behavior( $T_1$ ), or in some cases situations where there is a small degree of ductility in the sample ( $T_2$ ).. There are two equivalent approaches for describing the fracture behavior. The first of these is the energy based approach described in the previous section, where an existing crack in a material grows when the applied energy release rate is larger than some critical value. In this section we explore the second approach, where characteristic stress field in the vicinity of a crack exceeds some critical value.

### 11.1 Fracture Modes

Different fracture modes are defined by the relationship between the applied stress and the crack geometry. These are illustrated schematically in Figure

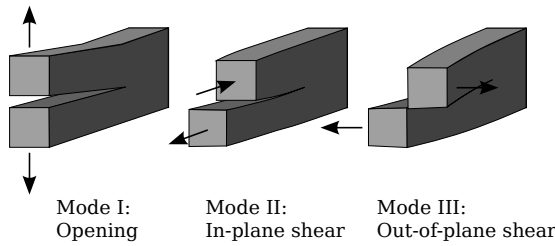


Figure 11.2: Fracture Modes .

11.2 Fracture of a homogeneous material fracture generally occurs under Mode I conditions, and this is the most important condition. Mode II conditions, where a shear stress is applied in the direction perpendicular to the crack front, is often important for interfacial fracture, including the adhesive bonding of materials with different properties. Mode III is generally not important for our purposes.

## 11.2 Stress Concentrations

In the previous section on contact mechanics we introduced the concept of the energy release rate,  $\mathcal{G}$ , which can be viewed as the driving force for crack propagation. Failure occurs when  $\mathcal{G}$  exceeds a critical value,  $\mathcal{G}_c$ . This energy-based approach was originally formulated by Griffith, and is referred to as the **Griffith model** for this reason. We can also describe the driving force for crack propagation in terms of the detailed stress field in the vicinity of the tip of a propagating crack. This approach was developed by Irwin, and is referred to here as the **Irwin model**. The key concept here is that stresses are enhanced, or 'concentrated' in the vicinity of a defect like a crack. The easiest way to start thinking about this is to look at the nature of the stress distribution around a circular hole in a two-dimensional plate (Figure 11.3). A stress is a force per unit area, so we can imagine dividing up the stress into individual force lines, which are equidistant when the stress is uniform. Near a defect the lines of force are closer to one another, indicating that the stress is higher in this area. The maximum tensile stress at the sides of the hole is three times the average applied stress.

For an ellipse of with axis  $a_c$  perpendicular to the applied stress and axis  $b_c$  parallel to the applied stress (see Figure 11.4), the maximum stress in this case is given by the following expression:

$$\sigma_{max} = \sigma_0 \left( 1 + 2 \frac{a_c}{b_c} \right) \quad (11.1)$$

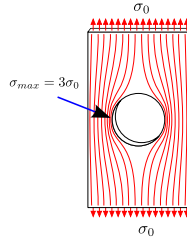


**Figure 11.3:** Force lines around a circular defect.

Note that we recover the behavior described above for a circular whole, where  $a_c = b_c$  and  $\sigma_{max}/\sigma_0=3$ . We can also write this in terms of the radius of curvature of the ellipse,  $\rho_c$ , at the point of maximum stress:

$$\rho_c = \frac{b_c^2}{a_c} \quad (11.2)$$

Combination of Eqs. 11.1 and 11.2 gives:

$$\sigma_{max} = \sigma_0 \left( 1 + 2\sqrt{a_c/\rho_c} \right) \quad (11.3)$$

We are usually interested in very sharp cracks, where  $a_c/\rho_c \gg 1$ . In this case we can ignore the factor of 1 in Eq. 11.3 and we get the following proportionality:

$$\sigma_{max} \propto \sigma_0 \sqrt{a_c} \quad (11.4)$$

This combination of parameters, with the applied stress multiplied by the square root of the crack length, plays a very important role in fracture mechanics, as we describe in more detail below.

### 11.3 Stress Intensity Factor

Consider a planar crack in the  $x$ - $z$  plane, as shown conceptually Figure 11.5. The stress in the vicinity of the crack tip can be expressed in the following form:

$$\sigma = \frac{K}{\sqrt{2\pi d}} f(\theta) \quad (11.5)$$

where  $K$  is the stress intensity factor,  $d$  is the distance from the crack tip and  $f(\theta)$  is some function of the angle  $\theta$  that reduces to 1 for the direction directly

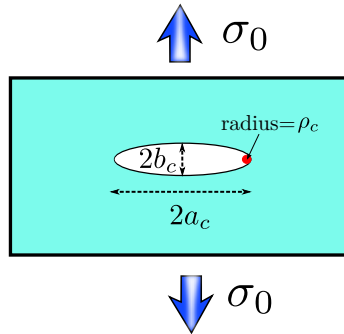


**Figure 11.4:** Elliptical crack with a crack tip radius of curvature,  $\rho_c$ .



**Figure 11.5:** Cartesian (a) and polar (b) coordinate axes use  $d$  to define stresses in the vicinity of a crack tip.

in front of a crack ( $\theta = 0$ ). Different functional forms exist for  $f(\theta)$  for the different stress components  $\sigma_{xx}$ ,  $\sigma_{yy}$ , etc. The detailed stress fields depend on the loading mode (Mode I, II or III, or some combination of these), and the corresponding stress fields are specified by the appropriate value of  $K$  ( $K_I$  for mode I,  $K_{II}$  for mode II or  $K_{III}$  for mode III).

**Mode I loading**

The stresses in the vicinity of a mode I crack are given by the following[14]:

$$\begin{pmatrix} \sigma_{11} \\ \sigma_{22} \\ \sigma_{12} \end{pmatrix} = \frac{K_I}{\sqrt{2\pi d}} \cos \frac{\theta}{2} \begin{pmatrix} 1 - \sin \frac{\theta}{2} \sin \frac{3\theta}{2} \\ 1 + \sin \frac{\theta}{2} \sin \frac{3\theta}{2} \\ \cos \frac{3\theta}{2} \sin \frac{\theta}{2} \end{pmatrix} \tag{11.6}$$

This compact notation is used to specify the three relevant values of  $f(\theta)$ . For example, for  $\sigma_{11}$  we have the following:

$$\sigma_{11} = \left( K_I / \sqrt{2\pi d} \right) \cos(\theta/2) \left( 1 - \sin \frac{\theta}{2} \sin \frac{3\theta}{2} \right) \tag{11.7}$$

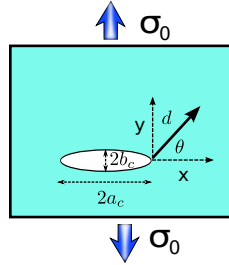


**Figure 11.6:** An internal crack in a homogeneous solid.

These expressions assume that the crack tip is very sharp, with a very small radius of curvature,  $\rho_c$ . If  $d$  is comparable to  $\rho_c$ , these equations no longer apply. Consider for example, the presence of an internal crack of length  $a_c$  and radius of curvature  $\rho_c$  in a thin sheet of material, shown schematically in Figure 11.6. In this case the stress at the crack edge is  $\sigma_{max}$  as given by Eq. 11.3. An assumption in the use of Eq. 11.6 is that the stresses are substantially less than  $\sigma_{max}$ . In other words,  $K$  describes the stress field close to the crack tip, but still at distances away from the crack tip that are larger than the crack tip radius of curvature,  $\rho_c$ .

The mode I stress intensity factor for this geometry is given by the applied stress,  $\sigma_0$  and the crack length  $a_c$ :

$$K_I = \sigma_0 \sqrt{\pi a_c} \tag{11.8}$$

For values of  $d$  that are substantially larger than  $\rho_c$  but smaller than  $a_c$ , we can determine the stresses from Eq. 11.6, with  $K_I$  as given by Eq. 11.8.

**Mode II loading**

For mode II loading the crack tip stress fields are given by the following set of expressions[14]:

$$\begin{pmatrix} \sigma_{11} \\ \sigma_{22} \\ \sigma_{12} \end{pmatrix} = \frac{K_{II}}{\sqrt{2\pi d}} \begin{pmatrix} -\sin \frac{\theta}{2} \left( 2 + \cos \frac{\theta}{2} \cos \frac{3\theta}{2} \right) \\ \sin \frac{\theta}{2} \cos \frac{\theta}{2} \cos \frac{3\theta}{2} \\ \cos \frac{\theta}{2} \left( 1 - \sin \frac{\theta}{2} \sin \frac{3\theta}{2} \right) \end{pmatrix} \tag{11.9}$$

It is generally difficult to determine  $K_{II}$  in a straightforward way, and finite element methods must often be used to determine it for a given loading condition and experimental geometry. Once  $K_{II}$  is known, the crack tip stress fields can be obtained from Eq. 11.9.

### Mode III loading

While mode III loading is often encountered in practical applications, it is generally avoided in experiments aimed at assessing the fracture behavior of materials, and is not considered further in this text.

## 11.4 Fracture condition

In the stress-based theory of fracture, the material fails when the stress intensity factor reaches a critical value that depends on the material. For mode I loading, we refer to this critical stress intensity factor as  $K_{IC}$ . Setting  $\sigma_0$  to the fracture stress,  $\sigma_f$ , and setting  $K_I$  to  $K_{IC}$  in Eq. 11.8 gives:

$$K_{IC} = \sigma_f \sqrt{\pi a_c} \quad (11.10)$$

Rearranging gives:

$$\sigma_f = K_{IC} / \sqrt{\pi a_c} \quad (11.11)$$

So the fracture stress decreases as the flaw size,  $a_c$ , increases. This is why a material can appear to be fine, even though small cracks are present in the material. The cracks grow very slowly, but when they reach a critical size for which Eq. 11.11 is satisfied, the material fails catastrophically.

The fracture toughness,  $K_{IC}$  has strange units - a stress multiplied by the square root of a length. In order to understand where this characteristic stress and the characteristic length actually come from, we need to consider the actual shape of the crack tip. Using Eq. 11.3 we see that the maximum stress in front of the crack tip,  $\sigma_{max}^f$ , at the point of fracture is:

$$\sigma_{max}^f \approx 2\sigma_f \sqrt{a_c / \rho_c} \quad (11.12)$$

where we have assumed that  $\sqrt{a_c / \rho_c} \gg 1$ , so that we can ignore the extra factor of 1 in Eq. 11.3. Now we can use Eq. 11.10 to substitute  $K_{IC}$  for  $\sigma_f$ . After rearranging we get:

$$K_{IC} \approx \sigma_{max}^f \frac{\sqrt{\pi}}{2} \sqrt{\rho_c} \approx \sigma_{max}^f \sqrt{\rho_c} \quad (11.13)$$

This expression is really only valid for a crack tip with a well-defined radius of curvature, which is often not the case. Models that aim to predict and understand the fracture toughness of materials are all based on understanding the details of the yielding processes very close to the crack tip, and the resulting crack shape. We'll return to this issue later. For now we can summarize the stress-based approach fracture mechanics as follows:

- With the exception of a very small region near the crack tip, all of the strains are elastic.
- There is a very small plastic zone in the vicinity of a crack tip, with a characteristic dimension,  $\rho$  that is determined by the details of the way the material plastically deforms.
- Fracture occurs when the stress field defined by  $K_I$  reaches a critical value.

## 11.5 General relationship between $K$ and $\mathcal{G}$

The stress intensity factor and the energy release rate are related to one another through the following expression:

$$\mathcal{G} = \frac{K_I^2 + K_{II}^2 + K_{III}^2}{E_r} \quad (11.14)$$

Here  $E_r$  is the reduced modulus that is slightly different for plane stress and plane strain conditions:

$$\begin{aligned} E_r &= E \quad (\text{Plane stress conditions}) \\ E_r &= \frac{E}{1-\nu^2} \quad (\text{Plane strain conditions}) \end{aligned} \quad (11.15)$$

Plane stress conditions generally apply for very thin samples, whereas plane strain conditions apply for thick samples, and also for the axisymmetric punch problems that we have discussed earlier in this text.

The fact that  $\mathcal{G} \propto K_I^2$  for a mode I fracture experiment is illustrated in Figure 11.7, which we use to show the relationship between stress and stored elastic energy for an elastically deformed sample. The energy input to the sample up to the point of fracture, which we refer to as  $U_f$ , is the area under the stress strain curve:

$$U_f = \frac{1}{2} \sigma_f \epsilon_f = \frac{1}{2} \frac{\sigma_f^2}{E_r} \quad (11.16)$$

The stress intensity factor,  $K_I$  at the fracture point is proportional to the stress,  $\sigma_f$ , and the strain energy release rate,  $\mathcal{G}$ , at the point of failure is proportional to the total stored elastic energy,  $U_f$ . This means that the following proportionality must hold:

$$\mathcal{G} \propto \frac{K_I^2}{E_r} \quad (11.17)$$

This is consistent with Eq. 11.14, but we need to do a more detailed analysis to get the prefactor exactly right.

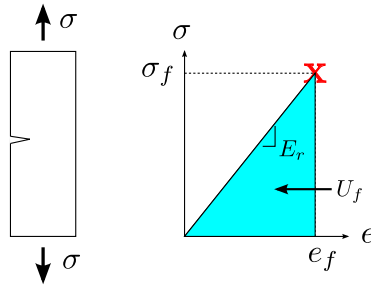


Figure 11.7: Schematic stress/strain curve for a brittle material in the presence of a crack.

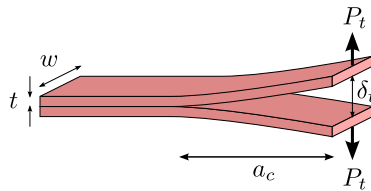


Figure 11.8: Double cantilever beam geometry.

## 11.6 Some Specific Geometries

### 11.6.1 Double cantilever beam geometry

The double cantilever beam geometry illustrated in Figure 11.8 is a common test used to measure crack propagation in materials. It is commonly used to measure the adhesion between two materials that have been glued together. It consists of two beams, each with width,  $w$ , and thickness,  $t$ . The crack length,  $a_c$  in this geometry is the distance between the parts of the beam where the force is applied and the beginning of the region of the sample where the two beams are in contact with one another.

For the double cantilever beam geometry the compliance is given by the following expression:

$$C \equiv \frac{\delta_t}{P_t} = \frac{8a_c^3}{Ewt^3} \tag{11.18}$$

The crack area,  $A_c$  is obtained by the crack length,  $a_c$  by the width of the sample:



$$A_c = wa_c \quad (11.19)$$

So we have:

$$\frac{dC}{dA_c} = \frac{1}{w} \frac{dC}{da_c} \quad (11.20)$$

We now combine Eqs. 11.18 and 11.20 to obtain the following for the energy release rate:

$$\mathcal{G} = \frac{P_t^2}{2w} \frac{dC}{da_c} = \frac{12a_c^2 P_t^2}{Ew^2 t^3} \quad (11.21)$$

At fixed load,  $\mathcal{G}$  increases as the crack length increases - unstable geometry!

can use We Eq. 11.18 to substituted  $\delta_t$  for  $P_t$  and write the compliance in the following way.

$$\mathcal{G} = \frac{3\delta_t^2 t^3 E}{16a_c^4} \quad (11.22)$$

At a fixed displacement, crack will grow until  $\mathcal{G} = \mathcal{G}_c$  and then stop. This is a better way to do the experiment.

### 11.6.2 Flat Punch Geometry: Thick Compliant Layer

For the flat punch case, the following analytic expression exists for the shape of the normal stress distribution directly under the punch (the plane with  $z = \delta_t$  in Figure 10.3):

$$\frac{\sigma_{zz}}{\sigma_{avg}} = 0.5 \left(1 - (r/a)^2\right)^{-1/2} \quad (11.23)$$

Here the average stress,  $\sigma_{avg}$  is defined as follows:

$$\sigma_{avg} \equiv \frac{P}{\pi a^2} \quad (11.24)$$

Note that  $\sigma_{zz}$  diverges at the edge of the punch ( $r = a$ ). We know that this must be the case because of the stress concentration that exists at the edge of the punch. To get an expression for stress concentration,  $K_I$  at this edge, we first defined  $d$  as the distance from the punch edge:

$$d \equiv a - r \quad (11.25)$$

Substituting  $d$  for  $r$  in Eq. 11.23 gives:

$$\frac{\sigma_{zz}}{\sigma_{avg}} = \frac{1}{2} \left[ 2d/a - (d/a)^2 \right]^{-1/2} \quad (11.26)$$

The stress intensity factor describes the stress field near the contact edge, where  $a/d$  is small. We can ignore the term involving the square of  $a/d$  to obtain the following expression  $\sigma_{zz}$  that is valid near the contact edge:

$$\frac{\sigma_{zz}}{\sigma_{avg}} \approx \frac{1}{2^{3/2}} \left( \frac{d}{a} \right)^{-1/2} \quad (11.27)$$

by comparing to Eq. 11.6 for  $K_I$  we obtain the following:

$$K_I = \frac{1}{2} \sigma_{avg} (\pi a)^{1/2} \quad (11.28)$$

Now we can use the following equation to obtain the following expression for  $\mathcal{G}$  (assuming  $K_{II} = K_{III} = 0$ ):

$$\mathcal{G} = \frac{K_I^2}{2E_r} = \frac{\pi a \sigma_{avg}^2}{8E_r} = \frac{P_f^2}{8\pi E_r a^3} \quad (11.29)$$

This is the same result that we got above (see Eq. 10.20), so everything checks out okay. Note that the extra factor of two in the relationship between  $\mathcal{G}$  and  $K_I$  in Eq. 11.29 comes from the fact the punch is rigid, so it has no stored elastic energy. Because elastic energy is stored only on one side of the interface, the value of  $\mathcal{G}$  for crack propagation at the interface with the rigid indenter (Figure 10.3) is half the value of  $\mathcal{G}$  for a crack propagating through an elastic material (Figure 11.5, for example).

### 11.6.3 Flat Punch Geometry: Thin Compliant Layer

Decreasing the thickness of the compliant layer also changes the distribution of normal stresses in contact with the layer. These normal stresses are plotted for different values of  $a/h$  in Figure 11.10.

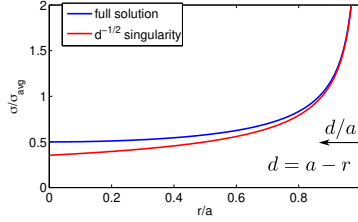


**Figure 11.9:** Comparison of the full solution for the flat punch contact stresses (Eq. 11.23) with the  $d^{-1/2}$  singularity obtained from  $K_I$  (Eq. 11.28).

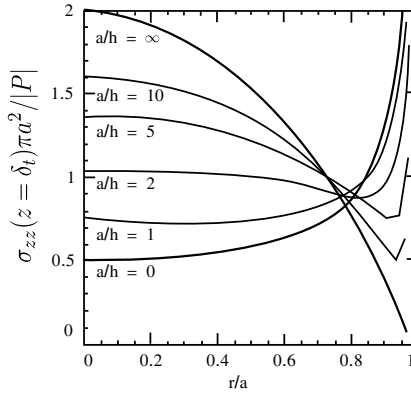


**Figure 11.10:** Dependence of the stress distribution under a flat punch for different values of the confinement ration,  $a/h$ .

- Max. stress in center for thin, incompressible layers ( $\nu = 0.5$ ).
- Decrease in edge stress singularity (decrease  $K_I$ ) for thin layers.

Since for very thin layers failure does not initiate from the edge because the driving force for this 'edge crack' vanishes as  $h$  becomes very thin. Instead, failure initiates from small defects within the central part of the contact zone where  $\sigma_{zz}$  is the highest. The mode I stress intensity factor for a circular, internal crack of radius  $a_c$  is given by the following expression:

$$K_I = \frac{2}{\sqrt{\pi}} \sigma_{zz} \sqrt{a_c} \quad (11.30)$$

Note that the prefactor in this expression is slightly different than what is given in Eq. 11.8 because of the different crack geometries. Eq. 11.8 is for a rectangular crack and Eq. 11.30 is for a circular crack. The energy release rate for the circular crack is given by using the relationship between  $K_I$  and  $\mathcal{G}$  valid for a mode I crack at the interface between compliant and rigid materials (Eq. 11.29):

$$\mathcal{G} = \frac{K_I^2}{2E_r} = \frac{2a_c \sigma_{zz}^2}{\pi E_r} \quad (11.31)$$

## 11.7 Fracture Toughness of Materials

In the Griffith (energy-based) model of fracture, material fracture occurs when the applied energy release rate,  $\mathcal{G}$ , exceeds a threshold value,  $\mathcal{G}_C$ , which is characteristic of the material. This value is called the critical strain energy release rate, and is a measure of the fracture toughness of the material, just as the critical stress intensity factor is a measure of the fracture toughness. The critical values of  $K$  and  $\mathcal{G}$  are related to one another through Eq. 11.14. For mode I fracture,  $K_{II} = K_{III} = 0$ , and this equation reduced to the following:

$$\mathcal{G}_{IC} = \frac{K_{IC}^2}{E_r} \quad (11.32)$$

Note that we have added the subscript 'I' to  $\mathcal{G}$  to remind ourselves that this number corresponds to mode I fracture condition.

Values of  $\mathcal{G}_C$  are a bit easier to understand conceptually than values of  $K_{IC}$ , since  $\mathcal{G}_C$  is simply the energy required to break a sample. We can obtain some estimates of  $\mathcal{G}_C$  by making some assumptions about where energy goes. Typical values of  $\mathcal{G}_C$  are as follows:

**Table 11.1:** Typical fracture toughness values (plane strain) for different material.

Material	$E$ (GPa)	$K_{IC}$ (MPa $\sqrt{m}$ )	$G_{IC}$ J/m <sup>2</sup>
Steel	200	50	12,000
Glass	70	0.7	7
High M polystyrene or PMMA	3	1.5	750
High Impact Polystyrene	2.1	5.8	16,000
Epoxy Resin	2.8	0.5	100
Rubber Toughened Epoxy	2.4	2.2	2,000
Glass Filled Epoxy Resin	7.5	1.4	300

- $\mathcal{G}_C = 2\gamma$  ( $\approx 0.1$  J/m<sup>2</sup>) if only work during fracture is to break Van der Waals bonds
- $\mathcal{G}_C \approx 1 - 2$  J/m<sup>2</sup> if only work during fracture is to break covalent or metallic bonds across interface
- $\mathcal{G}_C \gg 1$  J/m<sup>2</sup> if fracture is accompanied by significant plastic deformation of the sample. For the whole fracture mechanics formulation we are using to be valid, the zone of plastic deformation where this energy dissipation is occurring should be small compared to the overall sample size.

Actual values of  $\mathcal{G}_C$  are much larger than these values (see Table 11.1) because a significant amount of plastic deformation occurs near the crack tip.

We can use numbers from Table 11.1 to say something about the size of the plastically deformed zone in front of a crack tip. We know that in the elastic region directly in front of a propagating crack, the stress scales as  $K_I/\sqrt{2\pi d}$ , where  $d$  is the distance in front of the crack tip. If the maximum stress is equal to the yield stress,  $\sigma_y$ , then this the material must be yielded for values of  $r$  that give a stress exceeding  $\sigma_y$ . A propagating crack has  $K_I = K_{IC}$ , so if the size of the plastic zone is  $h_p$ , we have:

$$\sigma_y \approx \frac{K_{IC}}{\sqrt{2\pi h_p}} \quad (11.33)$$

Rearranging gives:

$$h_p \approx \frac{K_I^2}{2\pi\sigma_y^2} \approx \frac{\mathcal{G}_{IC}}{\sigma_y} \frac{E}{2\pi\sigma_y} \quad (11.34)$$

This formula is approximate because it neglects the fact that yielding of the material actually changes the stress distribution. The details of what is going on

in the plastic zone depend on the materials system of interest. Below we give a case study for what happens for some common amorphous, glassy polymers (non-crystalline polymers deformed at temperatures below their glass transition temperature).

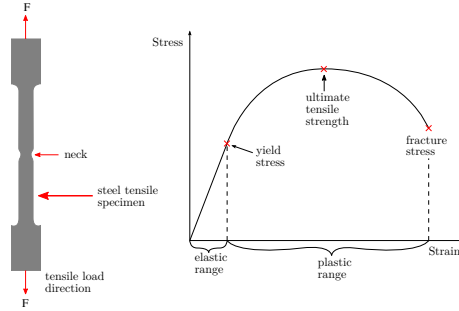


Figure 12.1: Tensile testing sample and representative data for a ductile sample.

## 12 Yield Behavior

The yield point of a material corresponds to the onset of permanent deformation, originating for example from the movement of dislocations. The stress/ $s$ -strain curve for a simple tensile test is shown in Figure 12.1, with the tensile yield stress,  $\sigma_y$ , corresponding to the onset of permanent, irreversible deformation in the material. For most materials this corresponds to the onset of non-linearity in the stress-strain curve (rubber is the exception, and that case is discussed in more detail in 331). What we need is a generalized criterion that can be used to determine the onset of yield for any stress state. These yield criteria all focus on the importance of the shear stress.

### 12.1 Yield Surfaces

The full stress state of a material is defined by the 3 principal stresses,  $\sigma_1^p$ ,  $\sigma_2^p$  and  $\sigma_3^p$ . The stress state of a material can therefore be specified on a 3-dimensional space where the values of these 3 principal stresses are plotted on three orthogonal axes. The yield surface is the surface in this space that separates the stress states where yielding will occur from those where it will not occur. Here we describe two of the most common yield surfaces, those defined by the Tresca and Von Mises yield criteria.

#### 12.1.1 Tresca Yield Criterion

The **Tresca yield criterion** is the simplest one in that we just assume that shear occurs whenever the maximum shear stress in the sample exceeds some critical value value  $\tau_c$ . In mathematical terms, yield occurs under the following conditions:

$$\frac{|\sigma_i^p - \sigma_j^p|_{max}}{2} > \tau_c \quad (12.1)$$

where the 'max' subscript indicates that we take the principal stress difference ( $\sigma_1^p - \sigma_2^p$ ,  $\sigma_2^p - \sigma_3^p$  or  $\sigma_1^p - \sigma_3^p$ ) with the largest magnitude. The yield stress,  $\sigma_y$ , is typically measured in a uniaxial tensile experiment, where  $\sigma_2^p = \sigma_3^p = 0$ , and plastic yielding of the material occurs when  $\sigma_1^p > \sigma_y$ . In a uniaxial tensile experiment, the maximum shear stress is half the applied tensile stress, so  $\tau_{crit} = \sigma_y/2$ .

### 12.1.2 Von Mises Yield Criterion

A more complicated yield criterion is that yield occurs when the **Von Mises stress**,  $\sigma_e$ , exceeds some critical value. The Von Mises stress is given as follows:

$$\sigma_e = \frac{\sqrt{2}}{2} \sqrt{(\sigma_2^p - \sigma_1^p)^2 + (\sigma_3^p - \sigma_1^p)^2 + (\sigma_3^p - \sigma_2^p)^2} \quad (12.2)$$

For uniaxial deformation, as in a simple compression or tensile test, yielding occurs when  $\sigma_e > \sigma_y$ . The Tresca and Von Mises yield surfaces for a two dimensional stress state ( $\sigma_3^p=0$ ) are shown in Figure 12.2a. Yielding does not occur inside the surface, but does occur outside the surface. Figure 12.2a is one particular cross section through a 3d yield surface. Another representation is shown in Figure 12.2b, which shows the yield surface viewed along the hydrostatic axis ( $\sigma_1^p = \sigma_2^p = \sigma_3^p$ ).

**Exercise:** The tensile yield stress of a materials is measured as 45 MPa by a uniaxial tensile test.

1. What will the shear stress of the material be if the material yields at a critical value of the Tresca stress?
2. How does your answer change if the material yields at a specified value of the Von Mises stress?

**Solution:**

1. The shear yield strength prediction, according to the Tresca criterion, is simply given by the maximum shear stress, at the yield point, which for a uniaxial tensile test is  $\sigma_y/2 = 22.5$  MPa.



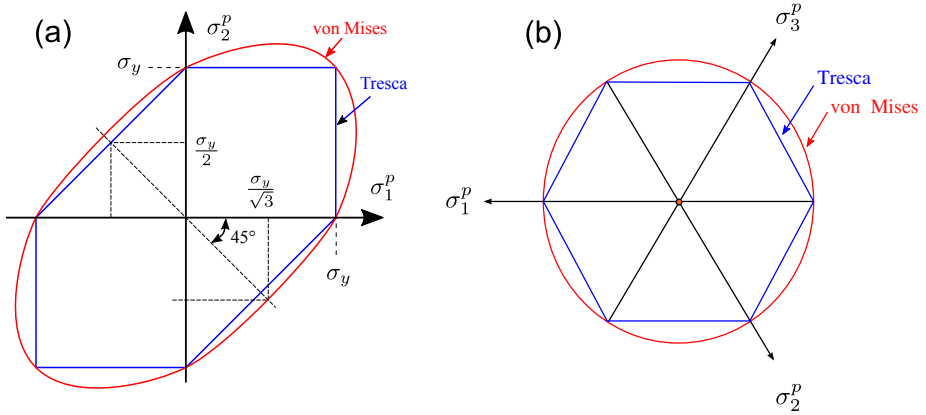


**Figure 12.2:** Cross sections of the Tresca and Von Mises yield surfaces at the  $\sigma_3^p = 0$  plane, and viewed down the hydrostatic line ( $\sigma_1^p = \sigma_2^p = \sigma_3^p$ ).

- Suppose the stress for the tensile experiment is oriented in the 3 direction, so at the yield point,  $\sigma_3^p = \sigma_y$  and  $\sigma_1^p = \sigma_2^p = 0$ . Substitution of these values into Eq. 12.2 gives  $\sigma_e = \sigma_y$ , as it should (the prefactor of  $\sqrt{2}/2$  was chosen to force this to be the case). Now suppose that we apply a shear stress in the 1-2 plane, so we have  $\sigma_1^p = \tau$ ,  $\sigma_2^p = -\tau$  and  $\sigma_3^p = 0$ . Putting these values into Eq. 12.2 gives  $\sigma_e = \sqrt{3}\tau$ . Rearranging to give an expression for  $\tau$ , and taking  $\sigma_e = \sigma_y$  gives  $\tau = \sigma_y / \sqrt{3} = 26 \text{ MPa}$ .

### 12.1.3 Coulomb Yield Criterion

The Coulomb yield criterion is a modification of the Coulomb criterion that takes into account that the critical shear stress will be modified by the normal stress acting on the shear plane. We would expect a compressive normal stress to increase the shear stress, whereas a tensile normal stress will decrease the critical shear stress. If the critical shear stress varies linearly with the normal shear stress we have the following:

$$\tau_c = \tau_c^0 - \mu\sigma_N \tag{12.3}$$

Consider a sample that is subjected to a uniaxial compressive stress with a magnitude of  $\sigma_1$  shown in Figure 12.3. According to the Coulomb yield criterion (Eq. 12.3) yield will occur on the plane for which  $\tau + \mu\sigma_N$  is maximized, which means we need to maximize  $\sin(2\theta) - \mu \cos(2\theta)$  to determine the plane on which yielding will occur. We have:

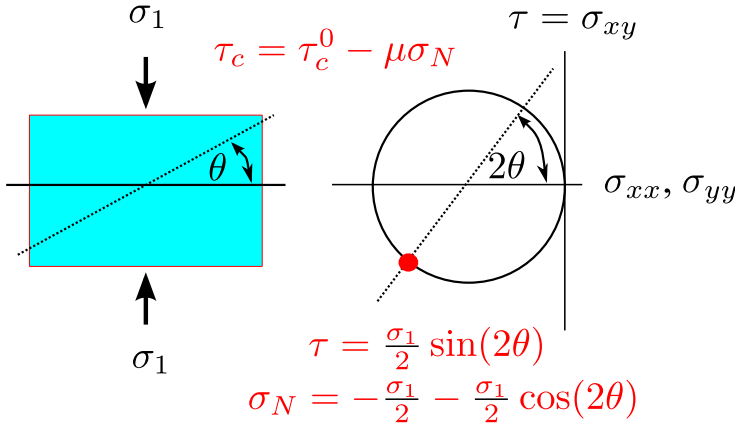


**Figure 12.3:** Normal stress and shear stress on a plane inclined by an angle  $\theta$  with respect to horizontal.

$$\frac{d}{d\theta} (\sin(2\theta)) = \mu \frac{d}{d\theta} (\cos(2\theta))$$

Solution of this equation gives  $\tan(2\theta) = -1/\mu$ . After a bit more trigonometry, we get find that the yield condition is first met for  $\theta = 45^\circ + \phi$  (and the corresponding mirror plane about the  $y$  axis), with  $\mu = \tan(2\phi)$ .

## 12.2 Localized Deformation

A material that obeys the strain hardening law of Eq. ?? will fail when a portion of the sample becomes thinner than the remainder of the sample. The overall behavior of the sample is a balance between the fact that the strain is larger in this region, and can therefore support a larger true stress, but the cross section is larger, so that a larger true stress is needed just to maintain a constant force along the length of the sample. To understand how to think about this we need to consider the relationship between the true stress and the engineering stress.

Consider a sample that is being deformed in uniaxial extension, as illustrated in Figure 12.4. A sample with an undeformed cross sectional area of  $A_0$  and undeformed length of  $\ell_0$  is stretched with a force,  $P$ . The engineering tensile stress,  $\sigma_{eng}$ , is obtained by dividing the load by the undeformed cross section, and the true tensile stress,  $\sigma_t$  is obtained by dividing the load by the actual cross sectional area of the deformed sample:

$$\sigma_{eng} = P/A_0 \tag{12.4}$$

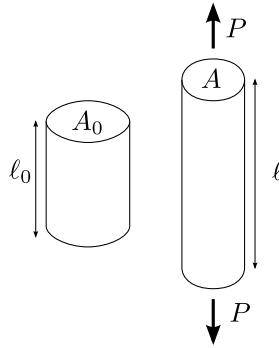


Figure 12.4: Uniaxial tensile test.

$$\sigma_{true} = P/A \quad (12.5)$$

In general, the bulk modulus of a material is much larger than its yield stress, so the applied stresses associated with yield phenomena are not large enough to significantly change the volume. As a result, the sample deforms at constant volume, so we have:

$$Al = A_0l_0 \quad (12.6)$$

The relationship between the true stress and the engineering stress is therefore as follows:

$$\sigma_t = \sigma_{eng}l/l_0 = \sigma_{eng}\lambda \quad (12.7)$$

### 12.2.1 Considère Construction

The **Considère construction** is a simple construction that can be used to determine the stability of regions in a sample at large tensile deformations. It can be used to distinguish between unstable and stable necking of a sample, illustrated schematically in Figure 12.5. We begin by considering a region of the sample that has a slightly thinner cross section than the rest of the sample. The true stress in this region of the sample will be higher than the rest of the sample because we are dividing the applied load by a lower cross section. Two things can happen at this point, the first possibility is that the larger stress in this region of the sample leads to greater deformation, and the sample breaks as the necked region begins to thin down. This is the unstable necking condition illustrated on the left side of Figure 12.5. In this case the maximum force,  $P$ , applied to the sample is the force where the neck begins to form.

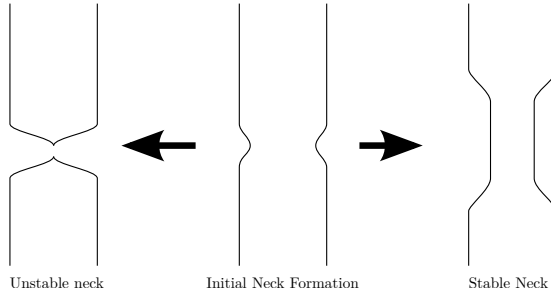


**Figure 12.5:** Schematic representation of stable and unstable necking of a sample under tensile loading conditions.

The second possibility is that the increased strain in the necked region leads to substantial strain hardening, so that this region of the sample is able to support the larger true stress in that region. Under the appropriate conditions the cross section of the necked region will stabilize at a value that is determined by the stress/strain relationship for the material. The sample deforms by ‘drawing’ new material into this necked region, as illustrated on the right side of Figure 12.5.

To understand when stable or unstable necking occur, we begin by recognizing that the onset of neck formation corresponds to a maximum tensile force that the material is able to sustain. In mathematical terms:

$$\frac{dP}{d\lambda} = 0 \quad (12.8)$$

Since the engineering stress is the load divided by the undeformed cross sectional area, which is a constant, we can write Eq. 12.8 as follows:

$$\frac{d\sigma_{eng}}{d\lambda} = 0 \quad (12.9)$$

We can rewrite this expression in terms of the true stress by recognizing that  $\sigma_{eng} = \sigma_t / \lambda$  (see Eq. 12.7), from which we obtain:

$$\lambda \frac{d\sigma_t}{d\lambda} - \sigma_t = 0 \quad (12.10)$$

which we rearrange to the following:

$$\frac{d\sigma_t}{d\lambda} = \frac{\sigma_t}{\lambda} \quad (12.11)$$

This condition is met when a line drawn from the origin of a plot of  $\sigma_t$  vs.  $\lambda$  is tangent to the curve.

### 12.2.2 Stable and Unstable Necking

Use of the Considère construction is illustrated in Figure 12.6, where we show curves of the true stress vs. extension ratio for a material that does not form a stable neck (part a) and one that does form a stable neck (part b). In part a it is only possible to draw one line originating from the origin that is tangent to the stress-strain curve (point A in Figure 12.6). A necking instability forms when the true stress reaches this value, resulting in a thinned-down region of the sample. This region continues to thin down until the sample breaks. The maximum engineering stress that the sample sees prior to failure is given by the slope of the tangent line in Figure 12.6a.

In Figure 12.6b, it is possible to draw two lines from the origin that are tangent to the curve, with tangent points labeled as A and B. The tangent at point B represents a maximum in the applied force (the stress-strain curve lies below the tangent line) and the tangent at point A represents a minimum in the applied force (the stress-strain curve lies above the tangent line). At point B the neck stabilizes. Additional material is drawn into the necked region with a characteristic draw ratio that given by the value of  $\lambda$  at point B. The engineering stress at which this drawing occurs is less than the engineering stress required to form the neck in the first place. This means that the load during the drawing process to form the stable neck is lower than the stress required to form the neck in the first place. This phenomenon is generally observed in glassy polymeric materials ( $T < T_g$ ) or semicrystalline polymers for which stable neck formation is observed.

$$\frac{d\sigma_t}{d\lambda} = \frac{\sigma_t}{\lambda} \quad (12.12)$$

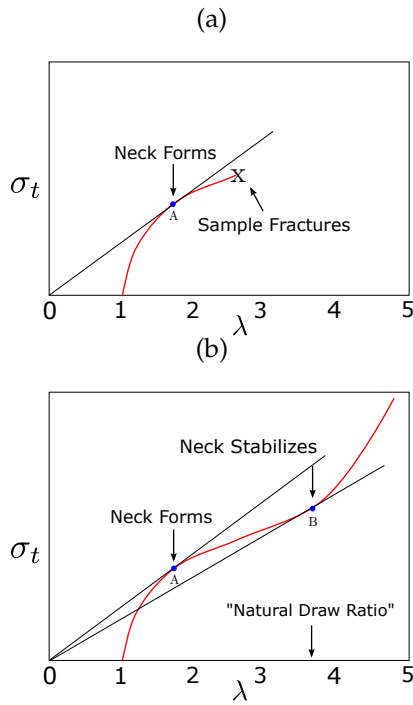


**Figure 12.6:** Considère construction for a material that does not form a stable neck (a) and a material that does form a stable neck (b).

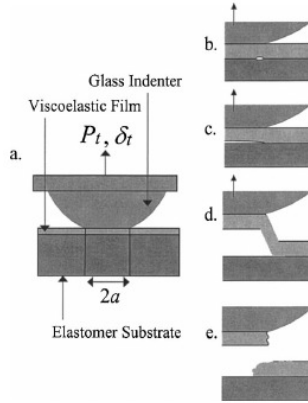


Figure 13.1: Adhesive transfer of a thin, viscoelastic film.

## 13 Weibull Analysis of Failure

Failure of brittle materials is determined by the largest flaw size, since the largest flaw size will have the largest value of  $K$  for a given applied stress. As an example of the use of Weibull statistics, consider the adhesive transfer of a thin layer of a material from a flat, flexible substrate to a rigid, curved indenter as illustrated in Figure 13.1. The basic geometry of the experiment is illustrated in Figure 13.1a, and consists of a thin, viscoelastic film that is coated on an elastomeric substrate. A hemispherical glass indenter is brought into contact with the film and is then pulled away from the surface. The system is designed so that the adhesion of the film to the glass indenter is stronger than the adhesion to the elastomeric substrate, the film will be transferred from the substrate to the indenter. The process occurs by the sequence of steps illustrated in parts b-e of Figure 13.1:

- b) A crack is nucleated at a defect site at the interface between the film and the substrate at a region where the hydrostatic pressure is maximized.
- c) This crack propagates under the indenter as the material is the indenter is pulled away from the substrate.
- d) Eventually the entire film in has detached from the substrate over the region where it is contact with the indenter. The remainder of the film begins to peel away from the substrate surface.
- e) The film breaks at the edge of the area of contact with the indenter.

Details of this experiment can be found in reference[15]. The most important thing to keep in mind is that the whole transfer process is controlled by the

initial appearance of a cavity at the indenter/substrate interface (Figure 13.1b). This happens when  $p_{max}$ , the maximum hydrostatic tension at the film/substrate interface, reaches a critical value that we refer to as  $p_{cav}$ . Qualitatively we find that  $p_{cav}$  is close to  $E_{sub}$ , the elastic modulus of the substrate, but cavitation occurs for different values of  $p_{cav}$ . The **Weibull distribution** for the survival probability,  $P_s$  (the probability that cavitation has NOT occurred) is as follows:

$$P_s = \exp \left[ - \left( \frac{p_{max}}{p_{cav}} \right)^M \right] \quad (13.1)$$

Here  $M$  is the Weibull modulus, which is a measure of the distribution of failure probabilities. We generally want  $M$  to be large, so that the distribution stresses is very narrow. For example, if  $M \rightarrow \infty$ ,  $P_s = 0$  for  $p_{max} > p_{cav}$  and  $P_s = 1$  for  $p_{max} < p_{cav}$ .

We can take natural logs of both sides a couple of times to convert Eq. 13.1 to the following:

$$\ln [\ln (1/P_s)] = M \ln p_{max} - M \ln p_{cav} \quad (13.2)$$

This means that we can obtain the Weibull modulus as the slope of a plot of  $\ln [\ln (1/P_s)]$  vs.  $p_{max}$ . The procedure for obtaining  $P_s$  as a function of  $p_{max}$  is as follows:

1. Start with a data set that includes the measured values of the critical stress at which the sample failed. In our example this would be a list of values of  $p_{max}$  at the point where the sample failed.
2. Organize this list from the lowest value of  $p_{max}$  to the highest value.
3. Use the list to obtain the survival probability,  $P_s$ , for each value of  $p_{max}$ . The survival probability is the fraction of samples that did NOT fail for the given value of  $p_{max}$ . For example, if our data set has 50 samples in it then the survival probability for the lowest measured value of  $p_{max}$  is 49/50. The survival probability for the next highest value of  $p_{max}$  is 48/50, etc. We do this for all of the samples except for the one with the highest value of  $p_{max}$ , since a value of 0 for  $P_s$  would cause problems in the analysis.

In our example the stress is expressed as local maximum in the hydrostatic tension,  $p_{max}$ , and  $p_{cav}$  is a characteristic value of  $p_{max}$  for which a substantial fraction of samples have failed. From Eq. 13.1 we see that the survival probability is  $1/e=1/2.72=0.37$ . A Weibull analysis can be applied in a range of situations, including tensile failure of brittle glass rods. In this case the Weibull



analysis applies, with the tensile stress  $\sigma$  as the dependent variable, and with a characteristic tensile stress,  $\sigma_{avg}$  for which the survival probability is 37%:

$$P_s = \exp \left[ - \left( \frac{\sigma}{\sigma_{avg}} \right)^M \right] \quad (13.3)$$

The point of the Weibull analysis is to obtain an expression that can be sensibly extrapolated to survival probabilities that are very close to 1. With  $\exp(-x) \approx 1 - x$  for small  $x$ , and with  $P_f = 1 - P_s$ , we have the following expression for failure probability, assuming  $P_f$  is low:

$$P_f \approx \left( \frac{\sigma}{\sigma_{avg}} \right)^M \quad (13.4)$$

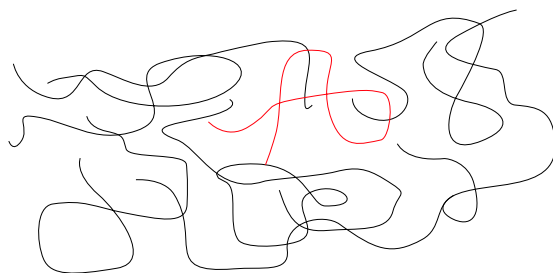


Figure 14.1: Structure of an amorphous polymer.

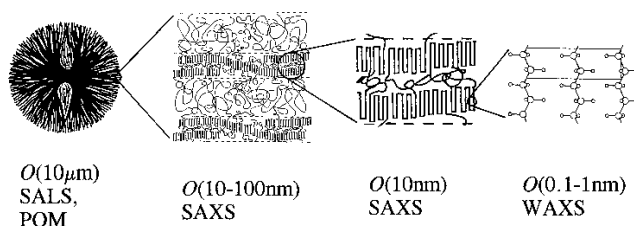


Figure 14.2: Structure at different length scales for a semicrystalline polymer.

## 14 Deformation of Polymers

The deformation mechanisms in polymeric materials are completely different from those in metals and ceramics, and (almost) never have anything to do with the motion of dislocations. To begin with, we can separate into the polymers that are partially crystalline and those that are not. As one would expect, the structures of these non-crystalline (amorphous) and semicrystalline polymers are very different, as shown schematically in Figure Crystallization and glass formation are the two most important concepts underlying the physical properties of polymers. The ways in which the molecules are organized in non-crystalline (amorphous) polymers and semicrystalline polymers are very different, as illustrated in Figures 14.1 and 14.3. Polymers crystallize at temperatures below  $T_m$  (melting temperature) and form glasses at temperatures below  $T_g$  (glass transition temperature). All polymers will form glasses under the appropriate conditions, but not all polymers are able to crystallize. The classification scheme shown in Figure [Polymers classification scheme](#) divides polymeric materials based on the locations of  $T_g$  and  $T_m$  (relative to the use temperature,  $T$ ) and is a good place to start when understanding different types of polymers.

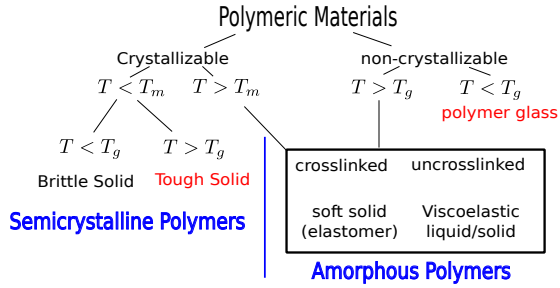


Figure 14.3: Polymers classification scheme.

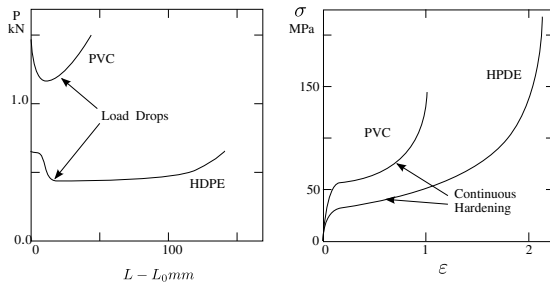


Figure 14.4: Load-Displacement and true stress-true strain curves for PVC (polyvinyl chloride) and HDPE (high density polyethylene).

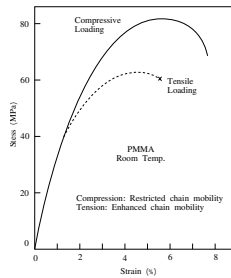
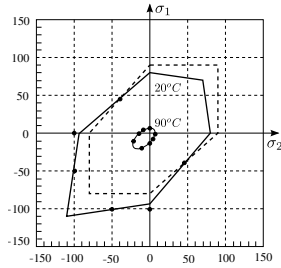
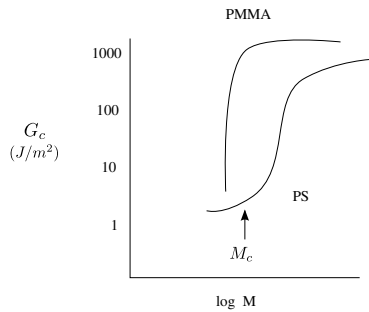


Figure 14.5: Stress-strain curves for PMMA (polymethylmethacrylate) under tensile and compressive loading conditions.



**Figure 14.6:** Yield surface for PMMA at 20°C and at 90°C. For comparison a map of the Tresca yield criterion (where normal forces do not matter) shown as the dashed line.



**Figure 14.7:** Molecular weight dependence of fracture toughness for polystyrene (PS) and poly(methyl methacrylate) (PMMA).



Figure 14.8

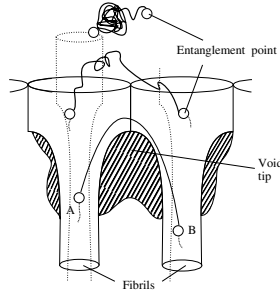


Figure 14.9: Conceptual drawing of fibrils at the interface between the crazed and uncrazed material (from ref.[16])

14.0.1 Case Study: Fracture toughness of glassy polymers

Deformation is significant, but  $G_{Ic}$  is still small compared to other engineering materials.

**Deformation Mechanisms** Suppose we do a simple stress strain experiment on polystyrene. Polystyrene deforms by one of two different mechanisms:

1. Shear bands due to strain softening (decrease in true stress after yield in shear).
2. **Crazing** - requires net dilation of sample (fracture mechanism for PS and PMMA).

Crazes are load bearing - but they break down to form cracks - failure of specimen.

**Crazing** Fibrils are cold drawn polymer. Extension ratio remains constant as craze widens

Crack propagation:

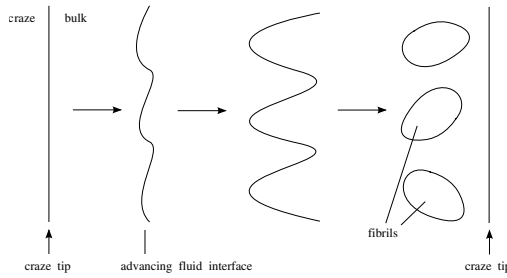


**Figure 14.10:** Meniscus instability mechanism for the formation of craze fibrils.

1. 1) new fibrils are created at the craze tip
2. 2) fibrils break to form a true crack at the crack tip
3. Crazeing requires a stress field with a tensile hydrostatic component  $\sigma_1 + \sigma_2 + \sigma_3 > 0$  (crazes have voids between fibrils)
4. Crazeing occurs first for PMMA in uniaxial extension ( $\sigma_2 = 0$ )
5.  $G_{Ic}$  is determined by energy required to form a craze ( $\approx 1000 \text{ J/m}^2$ )
6. Crazeing requires strain hardening of fibrils - material must be entangled ( $M > M_c$ ),  $M_c$  typically  $\approx 30,000 \text{ g/mol}$ .
7. In general, shear yielding competes with crazeing at the crack tip

### Meniscus instability mechanism (fibril formation at craze tip)

Material near the craze tip is strain softened, and can flow like a fluid between two plates.

<http://n-e-r-v-o-u-s.com/blog/?p=1556>

**Competition between Shear Deformation and Crazeing** Shear deformation is preferable to crazeing for producing high toughness.

Plane stress - shear yielding and crazeing criteria (for PMMA)

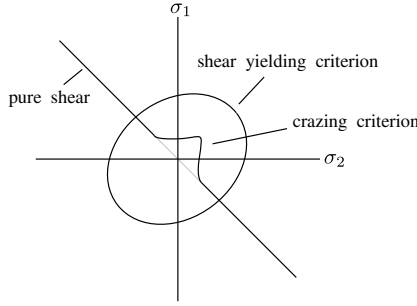


**Figure 14.11:** Deformation map for the shear yielding and crazing for plane stress conditions ( $\sigma_3^p = 0$ )

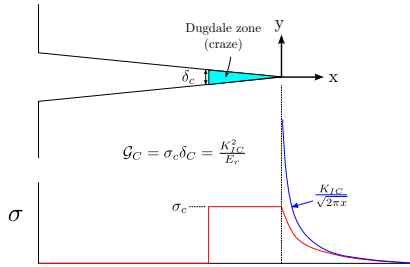


**Figure 14.12:** Crack tip stresses in the Dugdale model.

**Dugdale model** Earlier we considered the maximum stress in front of an elliptical craze

Assumptions:

- 1) Tensile stress throughout plastic zone is constant value,  $\sigma_c$
- 2) This stress acts to produce a crack opening displacement  $\delta_c$

$$G_{IC} = \delta_c \sigma_c \tag{14.1}$$

The Dugdale zone (the craze in our polystyrene example) modifies the stress field so that it doesn't actually diverge to infinity, since infinite stresses are not really possible.

**High Impact Polystyrene:** Polystyrene (PS) is a big business - how do we make it tougher? High impact polystyrene (HIPS) is a toughened version of polystyrene produced by incorporating small, micron-sized rubber particles in the material. The morphology is shown in Figure 14.13, and consists small PS inclusions embedded in rubber particles that are in turn embedded in the PS matrix materials. The rubber particles act as stress concentrators that act as nucleation points for crazes.

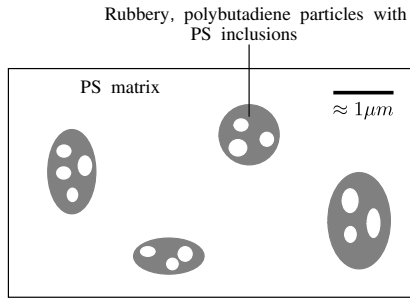


**Figure 14.13:** Morphology of high impact polystyrene.

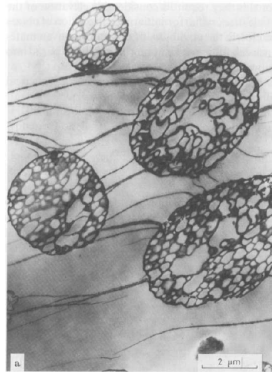


**Figure 14.14:** Multiple crazes in high impact polystyrene.

**Tensile Behavior:** In Figure 14.15 we compare the tensile behavior of normal polystyrene (PS) and high impact polystyrene (HIPS). The rubber content in the material reduces the modulus but substantially increases the integrated area under the stress/strain curve up to the point of failure, which is a measure of the toughness of the material. We can summarize the differences between PS and HIPS as follows:

- PS is brittle, with  $E = 3\text{GPa}$  and relatively low fracture toughness
- HIPS is ductile, with a lower modulus, ( $E = 2.1\text{ GPa}$ ) and a much larger energy to fracture.

This area under the stress/strain curve is not a very quantitative measure of toughness because we don't have any information about the flaw size responsible for the eventual failure of the material.



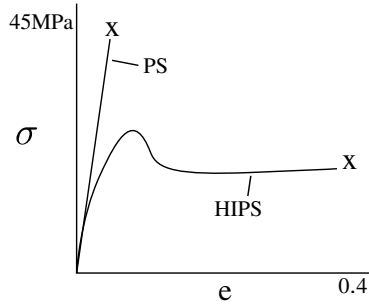


**Figure 14.15:** Schematic stress-strain curves for polystyrene (PS) and high impact polystyrene (HIPS) in the absence of a crack.

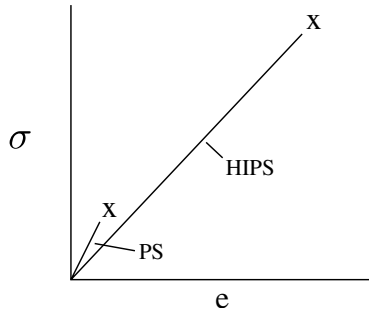


**Figure 14.16:** Schematic stress-strain curves for polystyrene (PS) and high impact polystyrene (HIPS) in the presence of a crack.

deformation via crazing in vicinity of rubber particles (stress concentrators) throughout sample

**Samples with Pre-crack:**

(measurement of  $K_{IC}$  or  $G_{IC}$ )

- Deformation limited to region around crack tip
- Much more deformation for HIPS - higher toughness

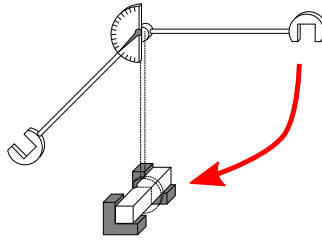


Figure 14.17: Charpy impact test.

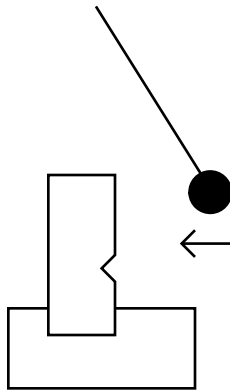


Figure 14.18: Izod impact geometry.

**Impact Tests** Impact tests are designed to investigate the failure of materials at high rates. Two common standardized are the **Izod impact test** and the **Charpy impact test**. They both involve measuring the loss in kinetic energy of a swinging pendulum as it fractures a sample. The geometry of a Charpy impact test is illustrated in Figure 14.17. Decrease in pendulum velocity after breaking sample gives impact toughness. For a useful discussion of a Charpy impact test, see <https://www.youtube.com/watch?v=tpGhqQvftAo>.

For most materials the fracture toughness is rate dependent, but some general features for toughening materials often apply at both high and low fracture rates. For example, high impact polystyrene is much tougher than polystyrene at high strain rates, for the same general reasons outlined in Section 14.0.1.

## 15 Case Study: Thermoreversible Gels from Triblock Copolymer Solutions

### 15.1 Introduction

Many of the principles of this course are illustrated by the behavior solutions of acrylic triblock copolymers in higher alcohols. The specific molecular structures of the polymer and the solvent are shown in Figure 15.1 and consist of a midblock of poly(*n*-butyl acrylate) (PnBA) between two blocks of poly(methyl methacrylate) (PMMA). The value of  $\chi$  for the PnBA/solvent system is less than 0.5 for all temperatures of interest, but the  $\chi$  for the PMMA/solvent system has the following temperature dependence:

$$\chi = 1.45 - 0.0115T \quad (15.1)$$

with  $T$  in °C.

The following points are illustrated by this example:

1. Polymers are soluble in solvents when  $\chi < 0.5$ .
2. For  $\chi > 0.5$ , the solvent content within the polymer can be obtained from the chemical potential expression.
3. To understand the temperature dependence of the solubility you need to know the temperature dependence of  $\chi$ .
4. Polymer liquids have higher heat capacities than the corresponding polymer glasses.
5. Calorimetry can be used to detect the enthalpy recovery peak from an aged polymer glass.
6. Gelation occurs when the average functionality is  $\approx 2$ .
7. Time-temperature superposition works when the structure does not change appreciably with Temperature.
8. The viscosity is obtained by integrating  $G(t)$  or from the response at very low frequencies.

From Eq. 15.1 we see that the value of  $\chi$  characterizing the PMMA/solvent interaction is greater than 0.5 for  $T < 83$  °C. At temperatures above 83 °C the PMMA and PnBA blocks are both in good solvent conditions, and the polymer behaves as a normal polymer solution. At lower temperatures, however, the PnBA midblock remains in good solvent conditions, but the PMMA endblocks

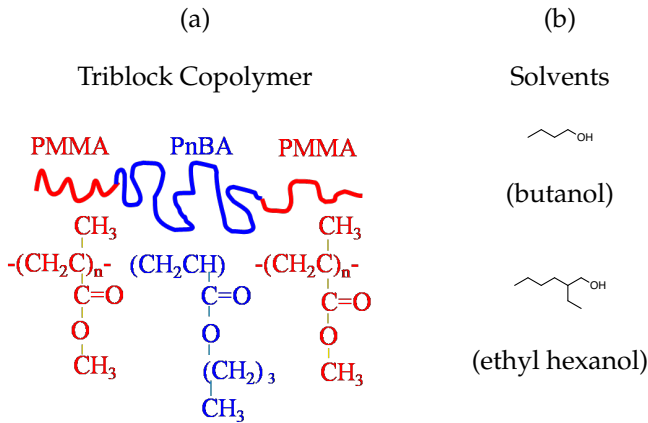


**Figure 15.1:** Chemical structure of gel-forming triblock copolymer gels (a), and the alcohols used as the solvents (b).

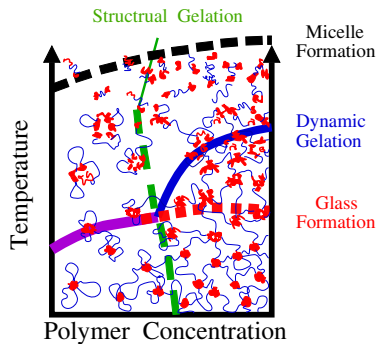


**Figure 15.2:** Schematic representation of the temperature and concentration dependence of the structure of the triblock copolymer solutions.

are no longer soluble. As a result these endblocks aggregate to form the micellar structures illustrated schematically in Figure 15.2. As a solution is cooled,  $\chi$  increases and solvent is expelled from these aggregates. When sufficient solvent has been expelled from the PMMA aggregates, they become glassy, and the system behaves as a solid.

## 15.2 Thermoreversible Gelcasting of Ceramics

The transition from 'liquid-like' to 'solid-like' behavior as the temperature is changes enable these materials to be used in a variety of applications, including the ceramics processing application illustrated in Figures 15.3 and 15.4. In

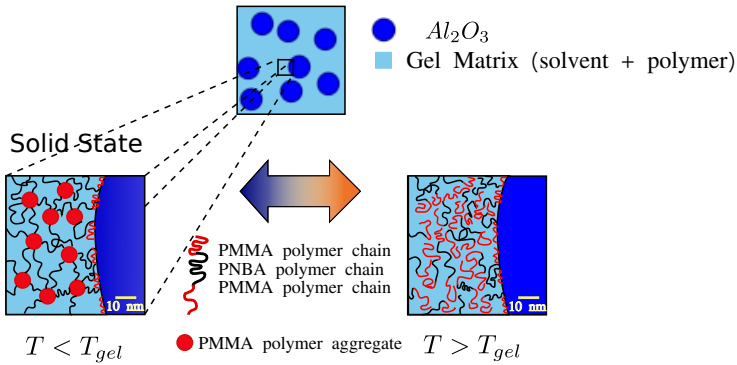


**Figure 15.3:** Schematic representation of the alumina particles dispersed within a thermoreversible triblock copolymer gel.

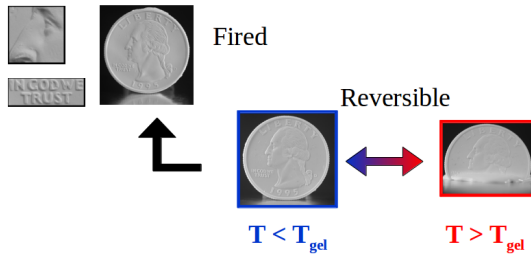


**Figure 15.4:** Illustration of the thermoreversible gelcasting process.

this application ceramic particles are added to the triblock copolymer at a relatively high volume fraction (around 50% by volume). The thermoreversible nature of the triblock copolymer solution allows the suspension to be poured into a silicone mold at high temperatures (typically  $\approx 80^\circ\text{C}$ ). When the system is cooled to room temperature, the triblock copolymer forms a solid gel and the material can be removed from the mold. A ceramic material with the shape of the mold is obtained by letting the solvent evaporate from the suspension, and firing the object at elevated temperature to burn off the polymer and sinter the ceramic particles together.

### 15.3 Quantifying the Solid/Liquid Transition

The temperature dependence of the mechanical properties of the triblock copolymer solutions are quantified by the frequency dependence of the storage and loss moduli,  $G'(\omega)$  and  $G''(\omega)$ . It is conceptually simpler to think in terms of the time-dependence of the relaxation modulus,  $G(t)$ , which can be written as a sum of exponential relaxations:

$$G(t) = \sum_i G_i \exp(-t/\tau_i) \quad (15.2)$$

In the frequency domain, the values storage and loss moduli are given by the following expressions:

$$G'(\omega) = \sum_i \frac{G_i \tau_i^2 \omega^2}{1 + \tau_i^2 \omega^2} \quad (15.3)$$

$$G''(\omega) = \sum_i \frac{G_i \tau_i \omega}{1 + \tau_i^2 \omega^2} \quad (15.4)$$

The most important thing for us is the viscosity, which we can obtain in terms of the values of  $G_i$  and  $\tau_i$ , or in terms of the loss modulus at very low frequencies:

$$\eta = \sum_i G_i \tau_i = \lim_{\omega \rightarrow 0} \frac{G''}{\omega} \quad (15.5)$$

We generally obtain data as a master plot (where the frequency is multiplied by the temperature shift factor,  $a_T$ ). In this case we obtain the temperature dependence of the viscosity by multiplying by  $a_T$ :

$$\eta = a_T \lim_{a_T \omega \rightarrow 0} \frac{G''}{a_T \omega} \quad (15.6)$$

We can also obtain an expression for the limiting modulus at high frequency (or low temperature):

$$G_0 = \sum_i G_i \quad (15.7)$$

Finally, we define an average relaxation time,  $\tau_{av}$  in the following way:

$$\tau_{av} = \frac{\eta}{G_0} = \frac{\sum G_i \tau_i}{\sum G_i} \quad (15.8)$$

Values of the storage and loss moduli for the triblock copolymer solutions are shown in Figure 15.5, along with the values of  $G_i$  and  $\tau_i$  used to fit the data. The temperature dependent viscosity for a solution with  $\phi_p = 0.15$  is shown in Figure 15.6, and the temperature dependent relaxation times for a variety of solution concentrations are shown in Figure 15.7.

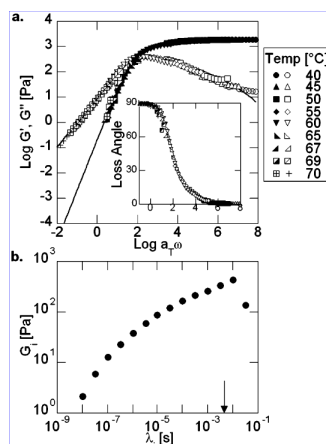


**Figure 15.5:** a) Master curves for  $G'$  and  $G''$  (symbols) with fits to Eqs.15.3 and 15.4. b) Values of  $G_i$  and  $\tau_i$  used to fit the data from part a (the relaxation times,  $\tau_i$  are referred to by  $\lambda_i$  in the figure). The reference temperature (defined as the temperature where  $a_T = 1$ ) is 65 °C for these data.

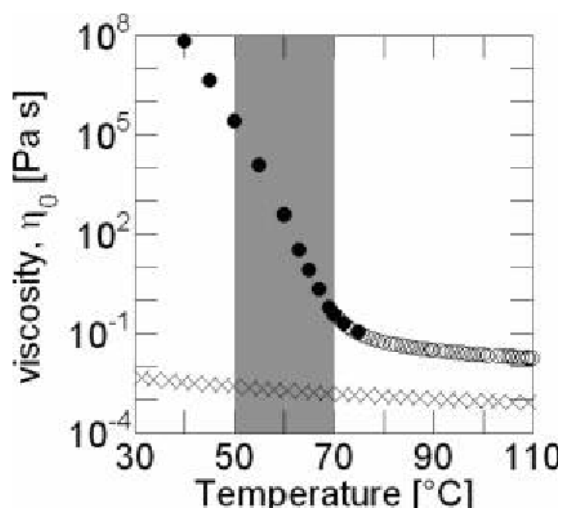


**Figure 15.6:** Temperature dependence of the viscosity for a triblock copolymer solution with  $\phi_p = 0.15$ . in 2-ethyl hexanol. The x's represent the solvent viscosity.

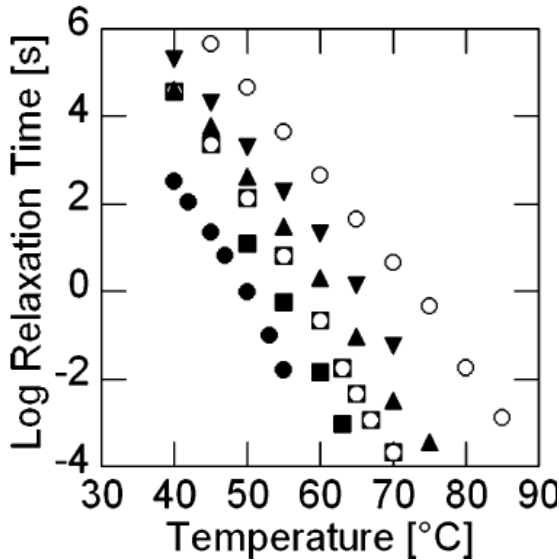


**Figure 15.7:** Values of the average relaxation time,  $\tau_{av}$  as a function of temperature. Data are included for  $\phi_p = 0.05$  ( $\bullet$ )  $\phi_p = 0.10$  ( $\blacksquare$ )  $\phi_p = 0.15$  ( $\square$ )  $\phi_p = 0.20$  ( $\blacktriangle$ )  $\phi_p = 0.25$  ( $\blacktriangledown$ )  $\phi_p = 0.30$  ( $\circ$ ).

## 15.4 Characterizing the Glass Transition in PMMA domains

The glass transition is typically observed as step change in heat flow as a sample is cooled through the glass transition. In our case the PMMA domains go through a glass transition during cooling, but the PMMA concentration is so low that the glass transition is not clearly observed during cooling or when the sample is immediately reheated after cooling (see Figure 15.8). However, a large enthalpy peak is observed after the sample has been left to ‘age’ at room temperature for a long time before reheating the sample. As shown in Figure 15.9, the enthalpy peak gets larger and moves to higher temperature as the aging time at room temperature is increased. This peak has the appearance of a melting peak associated with crystallization, but in this case it arises from the glassy PMMA domains.

The origins of the enthalpy peak observed during the aging experiments can be understood by realizing that the glass transition separates an equilibrium, liquid regime at temperatures above  $T_g$  from a non-equilibrium, glassy regime at temperatures below  $T_g$ . At temperatures below the glass transition, the enthalpy content of the sample is higher than the equilibrium enthalpy content defined by the extrapolation of the liquid behavior (the dashed line in Figure 15.10). As a result, the enthalpy slowly decreases toward this equilibrium line as the sample is aged below the glass transition. The decrease in enthalpy during this aging process is labeled as  $\Delta H_a$  in Figure 15.10. When the sample



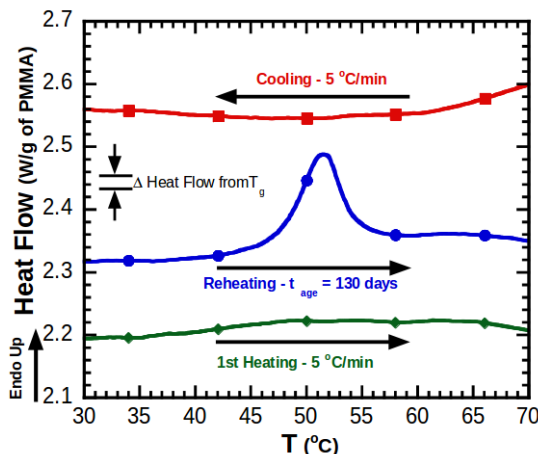


**Figure 15.8:** Measured heat flow during cooling, immediate reheating, and reheating after room temperature storage for 130 days.

is reheated, the enthalpy increases with temperature according to the glassy heat capacity,  $C_p^g$ . As a result the enthalpy content eventually crosses the equilibrium line and becomes less than the equilibrium enthalpy content. At a temperature somewhere just above  $T_g$ , the sample is able to equilibrate, and the enthalpy increases by an amount  $\Delta H_r$  in order to catch up to the equilibrium value. This is the enthalpy corresponding to the peaks in Figure 15.9. As the aging time decreases,  $\Delta H_a$  and  $\Delta H_r$  both decrease, and the temperature at which the enthalpy is recovered moves closer to  $T_g$ . The actual value of the  $T_g$  can be estimated by measuring the area of the enthalpy recovery peak and plotting against the location of this peak. Doing this for the data shown in Figure 15.9 results in an estimate for  $T_g$  of the PMMA domains of 35 °C.

As a final check on all of this, we can see if it makes sense that the glass transition of the PMMA domains should be around 35 °C. The glass transition of PMMA is about 125 °C, which is certainly a lot higher than the value of 35 °C that we are claiming here. However, we need to remember that the PMMA domains contain a lot of solvent, and this solvent will depress  $T_g$  significantly. How much solvent do we expect there to be in the PMMA domains? From Eq. 15.1 we obtain  $\chi=1.05$  at  $T = 35$  °C. The relationship between  $\chi$  and  $\phi_s$ , the solvent volume fraction in the PMMA cores of the micelles is obtained by setting  $N_p$  to  $\infty$  and setting the solvent chemical potential (from EqH.43) to 0:

$$\begin{aligned} \ln(\phi_s) + 1 - \phi_s + \chi(1 - \phi_s)^2 &= 0 \\ \ln(1 - \phi_p) + \phi_p + \chi\phi_p^2 &= 0 \end{aligned} \quad (15.9)$$

This equation needs to be solved numerically to obtain  $\phi_s$  (or  $\phi_p$ ) from a speci-

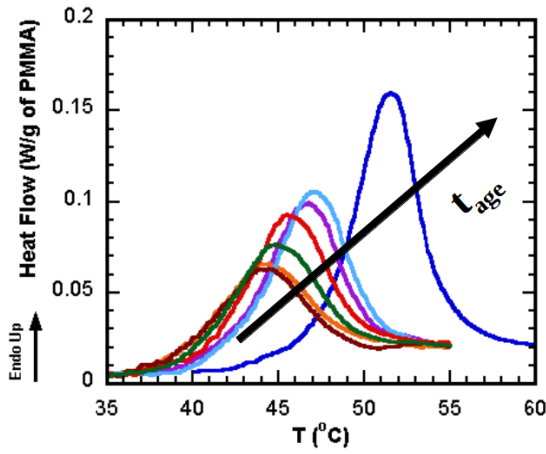


Figure 15.9: Dependence on the enthalpy recovery peak on the aging time.

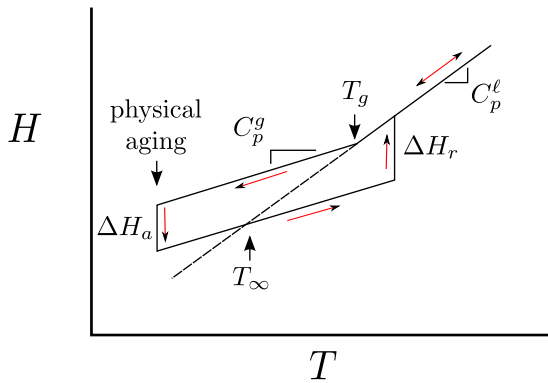
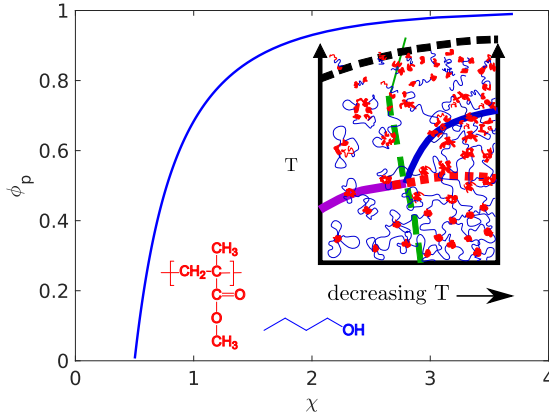


Figure 15.10: Origins of the enthalpy recovery peak.



**Figure 15.11:** Relationship between  $\phi_p$  and  $\chi$  obtained from Eq. 15.9.

fied value of  $\chi$ . A simple MATLAB script used to do this is given in Section???. A value of 1.05 for  $\chi$  gives  $\phi_s=0.289$ . Independent measures of the glass transition temperature of bulk PMMA samples with solvent loadings comparable to this do in fact show measured glass transition temperatures close to 35 °C. The relationship between  $\chi$  and  $\phi_p$  given by Eq. 15.9 is plotted in Figure 15.11.

## 15.5 Concentration Dependence of the Gel Modulus

Elasticity of the triblock copolymer solutions at low temperatures arises from the fact that the middle, PnBA blocks of the copolymer can span different PMMA aggregates, thereby linking the whole structure together. The PMMA aggregates behave as physical crosslinks with a functionality given by the number of midblocks that that bridge different aggregates. This functionality is obtained by multiplying the aggregation number, *i.e.* the number of PMMA endblocks in a single aggregate, by the probability  $f$  that a PnBA midblock spans two different PMMA aggregates (we also have to divide by two to account for the fact that there are two PMMA blocks on each triblock copolymer molecule). Aggregation numbers depend on the polymer concentration, and are typically very large, as illustrated in Figure 15.12. For high molecular weight polymers the percolation threshold, where the average functionality of a micelle is 2, is quite low, corresponding to  $\phi_p \approx 0.035$ . Above this percolation threshold, the shear modulus is given by the following expression:

$$G_0 = \nu k_B T \frac{D^2}{R_0^2} \quad (15.10)$$

Here  $D$  is the average distance between micelle cores, which can be measured experimentally by x-ray scattering. We also have  $R_0 = N^{1/2}a$ , where  $N$  is

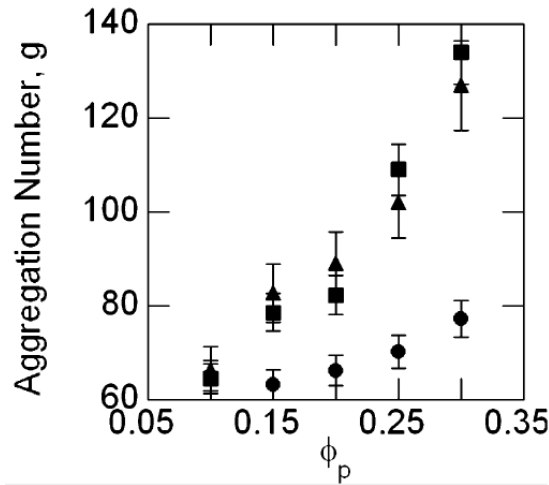


**Figure 15.12:** Concentration dependence of aggregation number for three different PMMA-PnBA-PMMA block copolymer solutions. The three data sets correspond to three different triblock copolymers, with different molecular weights for the PMMA and PnBA blocks.

the midblock degree of polymerization and  $a$  is the statistical segment length for the midblock. The quantity  $\nu$  is the concentration of 'load bearing strands', which in this case is the concentration of triblock copolymer chains with bridging midblocks:

$$\nu = \frac{f\phi_p\rho N_{av}}{M}$$

where  $M$  is the molecular weight of the triblock copolymer molecule and  $\rho$  is the polymer density. The modulus is strongly concentration dependent because of the concentration dependence of the bridging fraction,  $f$ , which is shown in Figure 15.13. Measured and calculated values of  $G_0$  are shown in Figure 15.14.

## 15.6 Hydrogels: Water as the Solvent

As a final illustration of what can be done with these sorts of triblock copolymer gels, we consider materials where the midblock is replaced with poly(acrylic acid), a polymer that is water soluble at neutral pH. The structure of these polymer is shown in Figure 15.15. This figure also shows a scheme for forming gels from these materials. Instead of adjusting  $\chi$  between the solvent and the PMMA endblocks by changing temperature, we do this by adding a small amount of water to the solvent (which is initially dimethyl sulfoxide).

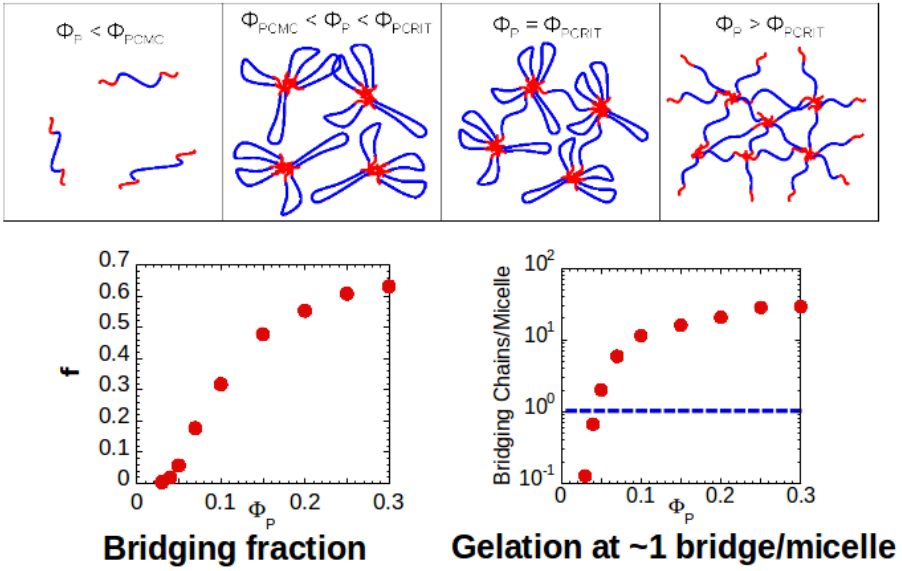


Figure 15.13: Concentration dependence of the network functionality.

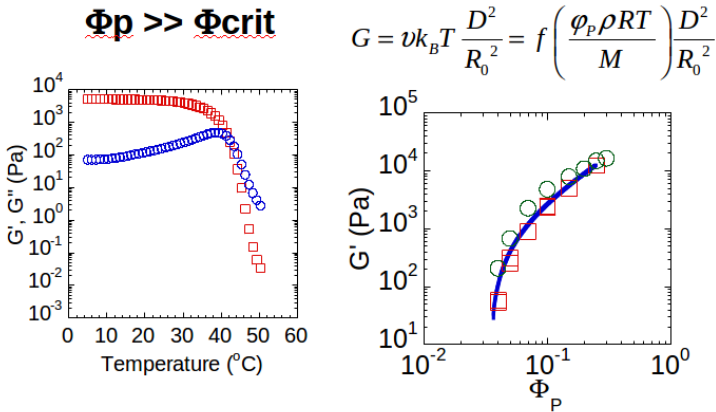
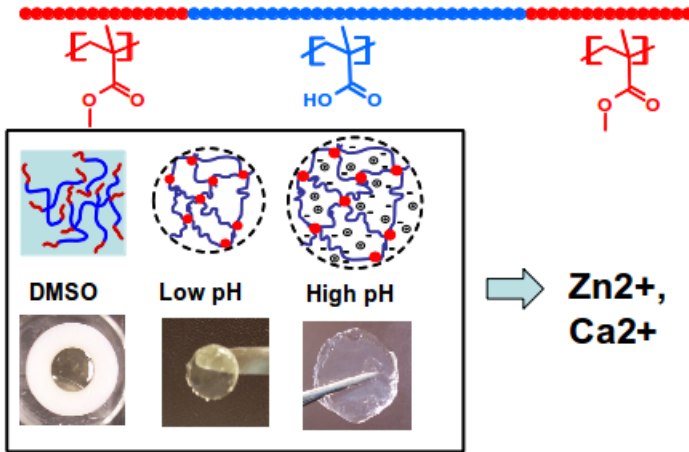
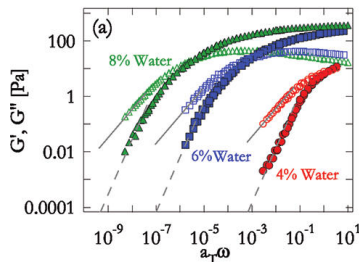


Figure 15.14: Calculated and experimental concentration dependence of the network functionality.



**Figure 15.15:** Formation and ionic crosslinking of PMMA-PMAA-PMMA triblock copolymer hydrogels (PMAA = poly(methacrylic acid)).



**Figure 15.16:** Master plots of storage and loss moduli for PMMA-PMAA-PMMA triblock copolymer gels in DMSO/water mixtures, for water contents within the solvent of 4, 6 and 8 wt. %.

Addition of just a small amount of water increases the effective value of  $\chi$  characterizing the solvent/PMMA interaction. The result is that the relaxation times for the triblock copolymer solution increase dramatically, as illustrated by the rheological data in Figure 15.16. The effects of solvent composition can be illustrated by introducing a shift factor,  $a_s$  that depends on the composition of the solvent. Its use is illustrated in Figure 15.17. The viscosity at a given temperature is proportional to  $a_s$ , so we see that small increases in the water content of the solvent result in an increase in the solution viscosity by several orders of magnitude. This occurs because water induces the aggregation of PMMA blocks into discrete domains, just as reducing temperature did for the case where alcohol was used as the solvent.

A useful feature of the hydrogels formed from the triblock copolymers with

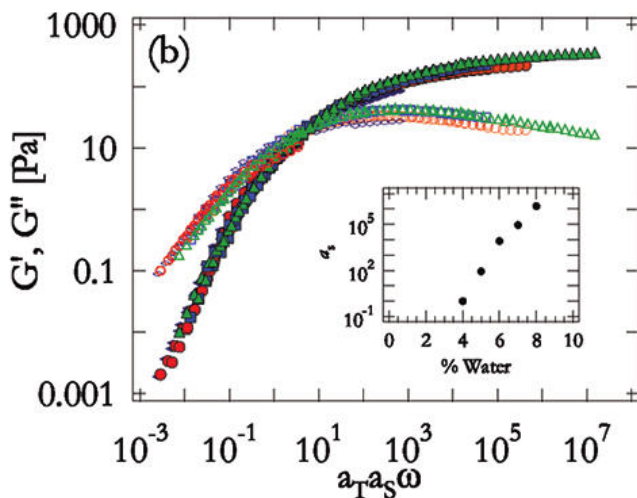


Figure 15.17: 'Super Master' plot of the data from Figure.

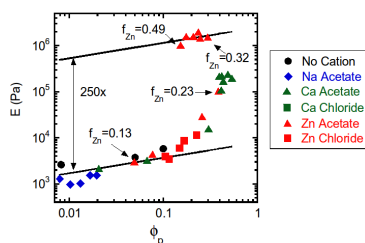
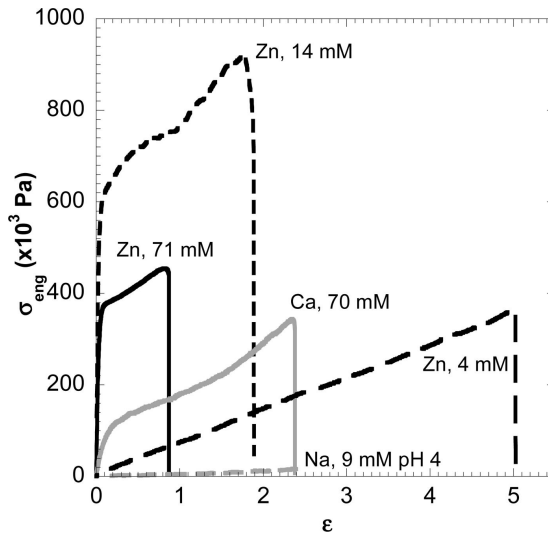


Figure 15.18: Elastic modulus for triblock copolymer gels that have been ionically crosslinked to varying degrees.

the poly(acrylic acid midblocks) is that the properties can be changed dramatically by immersing the gels in solutions containing divalent cations like  $\text{Ca}^{2+}$  or  $\text{Zn}^{2+}$ . These ions add additional crosslinks to the material, increasing the modulus by a factor of 100 or more (Figure 15.18). The materials also have high toughness, and can be extended to several times their original length prior to failure (Figure 15.19).



**Figure 15.19:** Tensile stress/strain curves for ionically crosslinked triblock copolymer gels.



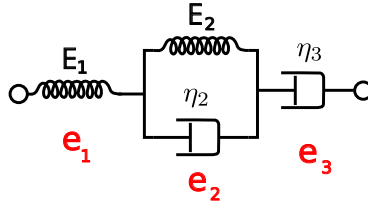


Figure 16.1: Linear creep model.

## 16 Creep Behavior

In a creep experiment we apply a fixed stress to a material and monitor the strain as a function of time at this fixed stress. This strain is generally a function of both the applied stress,  $\sigma$  and the time,  $t$ , since the load was applied.

### 16.1 Creep in the Linear Viscoelastic Regime

In the linear viscoelastic regime the strain is linearly dependent on the applied stress,  $\sigma$ , allowing us to define the **creep compliance function**,  $J(t)$ , in the following way:

$$J(t) \equiv \frac{e(\sigma, t)}{\sigma} \quad (16.1)$$

An example of the sort of spring/dashpot model used to describe creep behavior of a linear viscoelastic material is shown in Figure 16.1. The model consists of a single Kelvin-Voigt element in series with a spring and a dashpot. In this example the strain obtained in response to a jump in the stress from 0 to  $\sigma$  at  $t = 0$  can be represented as the sum of three contributions:  $e_1$ ,  $e_2$ , and  $e_3$ :

$$e(\sigma, t) = e_1(\sigma) + e_2(\sigma, t) + e_3(\sigma, t) \quad (16.2)$$

In this equation  $e_1$  corresponds to an instantaneous elastic strain,  $e_2$  is the recoverable viscoelastic strain and  $e_3$  is the plastic strain, with the three different components illustrated in Figure 16.2, and given by the following expressions:

$$\begin{aligned} e_1 &= \frac{\sigma}{E_1} \\ e_2 &= \frac{\sigma}{E_2} [1 - \exp(-t/\tau_2)] \\ e_3 &= \frac{\sigma}{\eta_3} t \end{aligned} \quad (16.3)$$

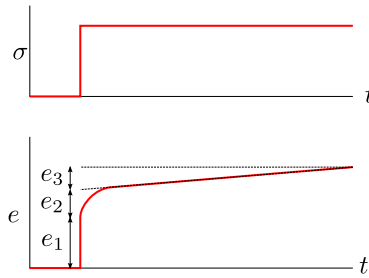


Figure 16.2: Strain contributions in a nonlinear creep model.

In many cases we are interested in situations where the strain does not increase linearly with the applied stress. The yield point is one obvious example of nonlinear behavior. In ideally plastic system, we only have elastic strains for stresses below the yield stress, but above the yield stress the strains are much larger.

## 16.2 Nonlinear Creep: Potential Separability of Stress and Time Behaviors

The situation becomes much more complicated in the nonlinear regime, where it is no-longer possible to define a stress-independent creep compliance function. In general the strain in the nonlinear regime is a complex function of both the time and the applied stress. In some cases, however, we can separate the stress dependence from the time dependence and write the stress in the following way:

$$e(\sigma, t) = f(\sigma) J(t) \quad (16.4)$$

If this sort of separability holds, then it is possible to make predictions of creep based on limited experimental data. The procedure is illustrated in Figure 16.3 and involves the following steps:

1. Measure  $e(t)$  at different different stresses ( $\sigma_1$  and  $\sigma_2$ ) in Figure 16.3. If the ratio  $e(\sigma_1, t) / e(\sigma_2, t)$  is constant for all value of  $t$ , then the separability into stress dependent and time-dependent functions works (at least for these two stress levels). These experiment enable us to obtain the time dependent function  $J(t)$ .
2. To get the stress-dependent function,  $f(\sigma)$ , it is sufficient to make a series of measurements at a single, experimentally convenient time.

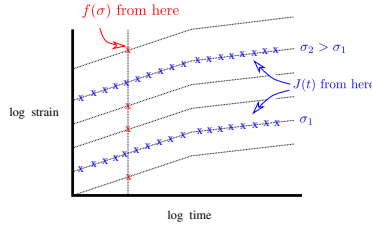


**Figure 16.3:** Creep response of a material with separable dependencies on stress and time.

### 16.3 Use of empirical, analytic expressions

The procedure outlined in the previous Section only works if the ratio  $e(\sigma_1, t) / e(\sigma_2, t)$  is independent of the time. This is not always the case. However, it is often possible to fit the data to relatively simple models. These models are similar to the spring and dashpot models of Section??, but a linear stress response is not necessarily assumed. One example corresponds to a nonlinear version of the linear model shown in Figure 16.1. As with the linear model, the strain components are assumed to consist of an elastic strain,  $e_1$ , a recoverable viscoelastic strain,  $e_2$  and a plastic strain,  $e_3$ . However, we now use nonlinear elements to describe  $e_2$  and  $e_3$ , with these two strain components given by the following expressions:

$$\begin{aligned}
 e_1 &= \frac{\sigma}{E_1} \\
 e_2 &= C_1 \sigma^n [1 - \exp(-C_2 t)] \\
 e_3 &= C_3 \sigma^n t
 \end{aligned}
 \tag{16.5}$$

Not that the material behavior is specified by 5 constants,  $E, C_1, C_2, C_3, n$ , that we need to obtain by fitting to actual experimental data. For a linear response ( $n = 1$ ) we can make a connection to the spring and dashpot models described earlier. In this case the behavior of the material is represented by the model of linear viscoelastic elements shown in Figure 16.4, and the constants appearing in Eq. 16.5 correspond to the following linear viscoelastic elements from Figure 16.1:

$$\begin{aligned}
 E &= E_1 \\
 C_1 &= 1/\eta_2 \\
 C_2 &= E_2/\eta_2 \\
 C_3 &= 1/\eta_3
 \end{aligned}
 \tag{16.6}$$

This is just one possible nonlinear model that can be used. An additional nonlinear element is obtained from Eyring rate theory, and is described in the following Section.

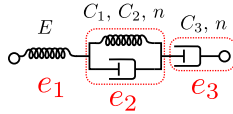


Figure 16.4: Nonlinear creep model.

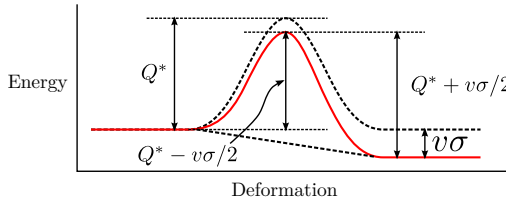


Figure 16.5: Effect of an applied stress on a thermally activated creep process.

## 16.4 Eyring Model of Steady State Creep

The **Eyring rate model** of creep is a very general model aimed at understanding the effect of the stress on the flow properties of a material. It can be used to describe a very wide range of materials, and is based on the modification of the activation energy for material for flow by the applied stress.

### 16.4.1 Material Deformation as a Thermally Activated Process

Our starting point is to realize that material deformation is a thermally activated process, meaning that there is some energy barrier that needs to be overcome in order for deformation to occur. The general idea is illustrated in Figure 16.5. The stress does an amount of work on the system equal to  $v\sigma$ , where  $\sigma$  is the applied stress and  $v$  is the volume of the element that moves in response to this applied stress. The quantity  $v$  is typically referred to as an **activation volume**. The net result of the application of the stress is to reduce the activation barrier for motion in the stress direction by an amount equal to  $v\sigma/2$  and to increase the activation barrier in the opposite direction by this same amount.

**Eyring Rate Law** We can develop an expression for the strain rate by recognizing that the net strain rate is given by the net frequency of hops in the forward direction. The frequency of hops in the forward and reverse directions, which we refer to as  $f_1$  and  $f_2$ , respectively, are given as follows:

$$f_1 = f_0 \exp\left(-\frac{Q^* - v\sigma/2}{k_B T}\right) = \exp\left(-\frac{Q^*}{k_B T}\right) \exp\left(\frac{v\sigma}{2k_B T}\right) \quad (16.7)$$

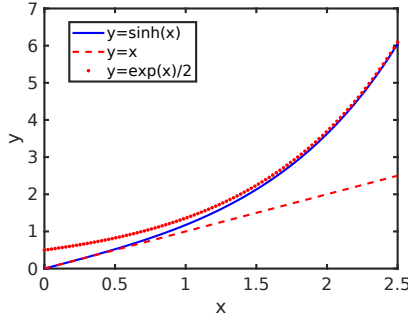


Figure 16.6: Behavior of the hyperbolic sine function.

$$f_2 = f_0 \exp\left(-\frac{Q^* + v\sigma/2}{k_B T}\right) = \exp\left(-\frac{Q^*}{k_B T}\right) \exp\left(\frac{-v\sigma}{2k_B T}\right) \quad (16.8)$$

The net rate of strain is proportional to  $f_1 - f_2$ , the net frequency of hops in the forward direction:

$$\frac{de}{dt} = A(f_1 - f_2) = Af_0 \exp\left(-\frac{Q^*}{k_B T}\right) \left[ \exp\left(\frac{v\sigma}{2k_B T}\right) - \exp\left(\frac{-v\sigma}{2k_B T}\right) \right] \quad (16.9)$$

Where  $A$  is a dimensionless constant. Using the following definition of the **hyperbolic sine** function ( $\sinh$ ):

$$\sinh(x) = (e^x - e^{-x}) / 2 \quad (16.10)$$

we obtain the following expression for the strain rate:

$$\frac{de}{dt} = 2Af_0 \exp\left(-\frac{Q^*}{k_B T}\right) \sinh\left(\frac{v\sigma}{2k_B T}\right) \quad (16.11)$$

Before considering the behavior of the Eyring rate equation for high and low stresses, it is useful to consider the overall behavior of the  $\sinh$  function, which is illustrated in Figure 16.6. Note that for small  $x$ ,  $\sinh x \approx x$ , and for large  $x$ ,  $\sinh(x) \approx 0.5 \exp(x)$ .

**Low Stress Regime** In the low-stress regime we can use the approximation  $\sinh(x) \approx x$  to get the following expression, valid for  $v\sigma \ll k_B T$ .

$$\frac{de}{dt} = \frac{Af_0v\sigma}{k_B T} \exp\left(-\frac{Q^*}{k_B T}\right) \quad (16.12)$$

In this regime the strain rate is linear in stress, which means that we can define a stress-independent viscosity from the following expression:

$$\frac{de}{dt} = \frac{\sigma}{\eta} \quad (16.13)$$

Comparing Eqs.16.12 and16.13 gives the following for the viscosity:

$$\eta = \frac{k_B T}{Af_0 v} \exp\left(\frac{Q^*}{k_B T}\right) \quad (16.14)$$

So the Eyring theory reduces to an Arrhenius viscosity behavior in the linear, low-stress regime.

**High Stress Regime** In the high-stress regime, we use the fact that  $\sinh(x) \approx \frac{\exp(x)}{2}$  for large  $x$  to obtain the following expression for  $v\sigma \gg k_B T$ :

$$\frac{de}{dt} = Af_0 \exp\left(-\frac{Q^*}{k_B T}\right) \exp\left(\frac{v\sigma}{2k_B T}\right) \quad (16.15)$$

Equivalently, we can write the following:

$$\frac{de}{dt} = Af_0 \exp\left(-\frac{Q^* - v\sigma/2}{k_B T}\right) \quad (16.16)$$

The effective activation energy decreases linearly with increasing stress, giving a very nonlinear response. In practical terms the activation volume is obtained by plotting  $\ln(de/dt)$  vs.  $\sigma$ , with the slope being equal to  $v/2k_B T$ .

**Physical significance of  $v$**  Eyring rate models are most often used for polymeric systems. In this case the activation volume can be viewed as the volume swept out by the portions of a polymer molecule which move during a fundamental creep event, as illustrated schematically in Figure 16.7. A large activation volume means that cooperative deformation of a large region of the material is required in order for the material to flow. Low values of the activation volume indicate that the deformation is controlled by a very localized event, corresponding, for example, to the rupture of a single covalent bond.

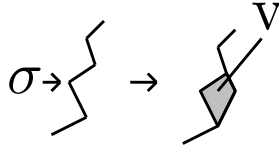


Figure 16.7: Illustration of the activation volume.

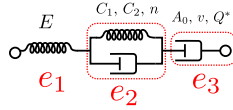


Figure 16.8: Nonlinear creep model, including an Eyring rate element for the steady-state creep component.

### 16.4.2 Additional Nonlinear Dashpot Elements

Nonlinear elements based on the Eyring rate model can also be included in our spring and dashpot models of viscoelastic behavior. For example, we can use an Eyring rate model to describe the stress dependence of the steady state creep of a nonlinear model, in which case Figure 16.4 gets modified to Figure 16.8. The steady state component is specified by the prefactor  $Af_0$  the activation energy  $Q^*$ , and the activation volume,  $v$ .

## 17 495 Problems

Notes:

- If you use MATLAB or Python to solve any of these problems, include the code that you used.

### 17.1 Course Organization

1) Send an email to Prof. Shull ([k-shull@northwestern.edu](mailto:k-shull@northwestern.edu)) and Qihua ([r6p5t6@u.northwestern.edu](mailto:r6p5t6@u.northwestern.edu)) with any thoughts that you have about topics for your journal club presentation at the end of the quarter. Also, make a suggestion for a 'soft material of the day' for Prof. Shull to mention at the beginning of lecture.

### 17.2 The Stress Tensor

2) Consider the following stress tensor:

$$\sigma_{ij} = \begin{bmatrix} 4 & 3 & 0 \\ 3 & 1 & 2 \\ 0 & 2 & 6 \end{bmatrix} \times 10^6 \text{ Pa}$$

- Calculate the stress tensor for coordinate axes rotated by  $30^\circ$  about the z axis (the 3 axis).
- Repeat the calculation for a  $30^\circ$  rotation around the x axis (the 1 axis).
- Calculate the three principal stresses.
- Calculate the maximum shear stress in the sample.

3) Consider the following stress tensor:

$$\sigma_{ij} = \begin{bmatrix} -2 & 1.4 & 0 \\ 1.4 & 6 & 0 \\ 0 & 0 & 2 \end{bmatrix} \times 10^6 \text{ Pa}$$

- Draw a Mohr circle representation of the stress contributions in the xy plane
- What are the three principal stresses?
- Show that the the sum of the diagonal components from original stress tensor is equal to the sum of the three principal stresses. What is the hydrostatic pressure for this stress state?



### 17.3 Strains

4) An engineering shear strain of 1 (100%) is applied to a rubber cube with dimensions of  $1\text{cm} \times 1\text{cm} \times 1\text{cm}$ . Young's modulus for the rubber sample is  $10^6$  Pa, and you can assume it is incompressible.

- Sketch the shape of the object after the strain is applied, indicating the dimensions quantitatively.
- On your sketch, indicate the magnitude and directions of the forces that are applied to the object in order to reach the desired strain.
- Calculate the 3 principal extension ratios characterizing the final strain state.

### 17.4 Typical Moduli

5) Calculate the sound velocities for shear and longitudinal waves traveling through the materials listed in the 'Representative Moduli' table from the course text.

### 17.5 Matrix Representation of Stress and Strains

6) For an isotropic system there are only two independent elastic constants,  $s_{12}$  and  $s_{11}$ . This is because if properties are isotropic in the 1-2 plane, the compliance coefficient describing shear in this plane,  $s_{44}$ , is equal to  $2(s_{11} - s_{12})$ . We can use the Mohr's circle construction to figure out why this equality must exist.

- Start with the following pure shear stress and strain states:

$$\sigma = \begin{bmatrix} 0 & \sigma_{12} & 0 \\ \sigma_{12} & 0 & 0 \\ 0 & 0 & 0 \end{bmatrix}; \quad e = \begin{bmatrix} 0 & e_{12} & 0 \\ e_{12} & 0 & 0 \\ 0 & 0 & 0 \end{bmatrix}$$

Use the matrix formulation to obtain a relationship between  $\sigma_{12}$  and  $e_{12}$  in this coordinate system.

- (b) Rotate the coordinate system by  $45^\circ$  so that the stress state looks like this:

$$\sigma = \begin{bmatrix} \sigma_1^p & 0 & 0 \\ 0 & \sigma_2^p & 0 \\ 0 & 0 & 0 \end{bmatrix}; \quad e = \begin{bmatrix} e_1^p & 0 & 0 \\ 0 & e_2^p & 0 \\ 0 & 0 & 0 \end{bmatrix}$$

Use the Mohr's circle construction to write these principal stresses and strains in terms of  $\sigma_{12}$  and  $e_{12}$ . Then use the matrix formulation to obtain an expression between  $\sigma_{12}$  and  $e_{12}$  in this rotated coordinate system.

- (c) For an isotropic system, the relationship between  $\sigma_{12}$  and  $e_{12}$  should not depend on the orientation of the coordinate axes. Show that the only way to reconcile the results from parts a and b is for  $s_{44}$  to be equal to  $2(s_{11} - s_{12})$ .

7) Consider a material with orthorhombic symmetry, with different properties along the 1, 2 and 3 directions. Young's moduli are measured along the 3 different directions, and we obtain the following results:

$$E_1 = 5.5 \text{ GPa}; E_2 = 2.0 \text{ GPa}; E_3 = 3 \text{ GPa}$$

- (a) Is this material a metal, a ceramic or a polymer? How do you know?  
 (b) The compliance matrix,  $s$ , is a symmetric 6x6 matrix as shown below. For this material, cross out all of the elements that must be zero.

$$\begin{bmatrix} s_{11} & s_{12} & s_{13} & s_{14} & s_{15} & s_{16} \\ s_{12} & s_{22} & s_{23} & s_{24} & s_{25} & s_{26} \\ s_{13} & s_{23} & s_{33} & s_{34} & s_{35} & s_{36} \\ s_{14} & s_{24} & s_{34} & s_{44} & s_{45} & s_{46} \\ s_{15} & s_{25} & s_{35} & s_{45} & s_{55} & s_{56} \\ s_{16} & s_{26} & s_{36} & s_{46} & s_{56} & s_{66} \end{bmatrix}$$

- (c) What are the values of  $s_{11}$ ,  $s_{22}$  and  $s_{33}$  for this material?  
 (d) A value of 0.38 is obtained for Poisson's ratio is measured in the 1-2 plane by applying a tensile stress in the 1 direction and measuring the strains in the 2 direction. What is the value of  $s_{12}$  for this material?

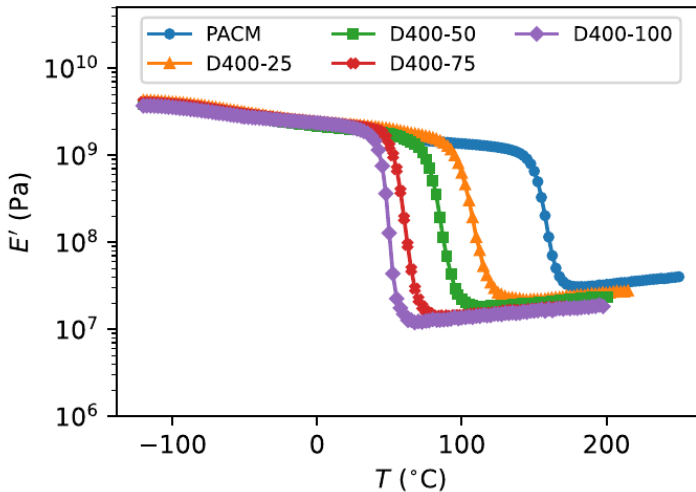
8) Consider a material with elastic constants given by the following compliance matrix:

$$s_{ij} = \begin{bmatrix} 14.5 & -4.78 & -0.019 & 0 & 0 & 0 \\ -4.78 & 11.7 & -0.062 & 0 & 0 & 0 \\ -0.019 & -0.062 & 0.317 & 0 & 0 & 0 \\ 0 & 0 & 0 & 31.4 & 0 & 0 \\ 0 & 0 & 0 & 0 & 61.7 & 0 \\ 0 & 0 & 0 & 0 & 0 & 27.6 \end{bmatrix} \text{ GPa}^{-1}$$

- (a) Describe the symmetry of this material, and explain your reasoning.
- (a) What is the highest value for Young's modulus that you would expect for this material? What direction does it correspond to?
- (b) Calculate the value of Poisson's ratio obtained from an experiment where the materials is pulled in the 3 direction and change in sample width in the 2 direction is measured.
- 9) In developing an expression for  $E_\ell$  it is actually easiest to use the stiffness matrix, since the only nonzero strain is the normal strain in the direction of compression. If this is compression is in the 1 direction, then  $E_\ell = \sigma_{11}/e_{11}$ . Use this information, and the information provided in the text about the relationship between  $[s]$  and  $[c]$  to get an expression for  $E_\ell$  in terms of  $s_{11}$  and  $s_{12}$ , and show that  $E_\ell = K_b + 4G/3$

## 17.6 Rubber Elasticity

- 10) Consider the data below for the temperature dependence of the elastic modulus for an epoxy system (data from Polymer, 221, 123560 (2021)). (For our purposes you can assume that the value plotted for  $E'$  is Young's modulus, and that Poisson's ratio for the materials is 0.5).



- (a) Use the value where  $E'$  is a minimum to estimate the number average molecular weight between crosslinks for the material labeled PACM (blue circles) and D400-100 (purple diamonds).

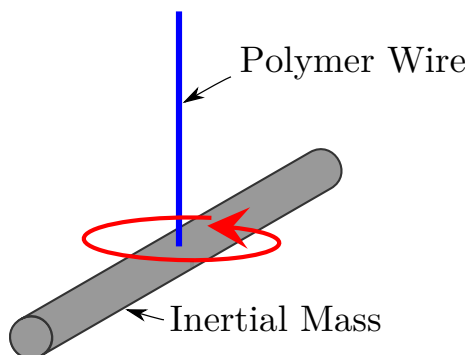
- (b) The two materials from the previous section represent the reaction of a stoichiometrically balanced mixture of epoxy with a diamine crosslinker. From the paper cited above, compare the molecular weights of these different components and comment on the values that you calculated from part 1. Do your numbers make sense?
- (c) Is the increase in modulus at the higher temperatures consistent with the theory of rubber elasticity? To answer this question, calculate the fractional change in modulus that you would expect between 80 °C and 200 °C. Compare this to the actual modulus ratio for the D400-100 sample.

## 17.7 Viscoelasticity

11) The following questions relate to the DGEBA-PACM/Jeffamine system that was introduced in class.

- (a) For the D230-based system, make a plot comparing the temperatures where the slope in  $\log(E')$  vs. temperature is maximized, and also the temperature where  $\tan(\delta)$  is maximized. Comment on the relationship between these two temperatures.
- (b) How many moles of D230 need to be combined with one mole of DGEBA to make a stoichiometric mixture? (no PACM added)
- (c) How many grams of D230 need to be combined with one mole of DGEBA to make a stoichiometric mixture? (again assume that no PACM is added. Note that 230 in this case is the molecular weight of the Jeffamine in g/-mole. You'll need to calculate or look up the molecular weight of DGEBA to do this DGEBA stands for diglycidyl ether of bisphenol A, but DGEBA is pretty standard abbreviation for it).
- (d) What happens to the amount of jeffamine you need to add to get a stoichiometric ratio as the molecular weight of the jeffamine is increased as you move from D230 to D400 to D2000 to D4000? (a qualitative answer is okay - you don't need to be quantitative for this. Continue to assume that no PACM is added).
- (e) What happens to the glass transition temperature for samples without any PACM as the molecular weight of the Jeffamine increases from 230g/mole to 400 g/mole? Describe how you obtained  $T_g$  from the data shown in the lecture. Also describe why the trend in  $T_g$  is as you describe.
- (f) Mixtures with DGEBA and an equal amount of jeffamine and PACM become cloudy as the molecular weight of the jeffamine increases. Why is this?

12) Consider a cylindrical metal bar with a density of  $7.6 \text{ g/cm}^3$ , a diameter of 1 cm and a length of 10 cm. It is suspended from a polymer fiber with a length,  $\ell$ , of 30 cm and a diameter of 1 mm.

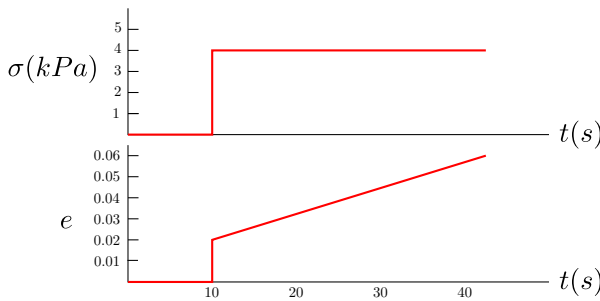


- (a) Suppose the fiber is perfectly elastic, with a shear modulus  $10^9 \text{ Pa}$ . Calculate the natural frequency of the system if the bar is rotating back and forth, causing the fiber to twist.
- (b) Suppose the fiber is viscoelastic, with  $G'$  at the frequency calculated from part a equal to  $10^9 \text{ Pa}$ , and with  $G'' = 10^7 \text{ Pa}$ . How many periods of the oscillation will take place before the magnitude of the oscillation decays by a factor of  $e$  (2.72)? Note: the rotational moment of inertia for the suspended metal bar in this geometry is  $m\ell^2/12$ , where  $m$  is the total mass of the bar and  $\ell$  is its length.
- 13) As mentioned in class, the Maxwell model, with a viscous element and an elastic element in series with one another, is the simplest possible model for a material that transitions from solid-like behavior at short times, to liquid-like behavior at long times. For a shear geometry we refer to the elastic element as  $G_0$  and the viscous element as  $\eta$ .
- (a) For what angular frequency are the storage and loss moduli equal to one another for a material that conforms to the Maxwell model? Express your answer in terms of the relaxation time,  $\tau$ .
- (b) Suppose the material is oscillated at a frequency that is ten times the frequency you calculated from part a. Does the material act more like a liquid or a solid at this frequency? Describe your reasoning.
- (c) Calculate the values of  $G'$  and  $G''$  at the frequency from part b, and calculate the phase angle,  $\phi$  describing the phase lag between stress and strain in an oscillatory experiment. Note that the following expression relates  $\phi$ ,  $G'$  and  $G''$ :

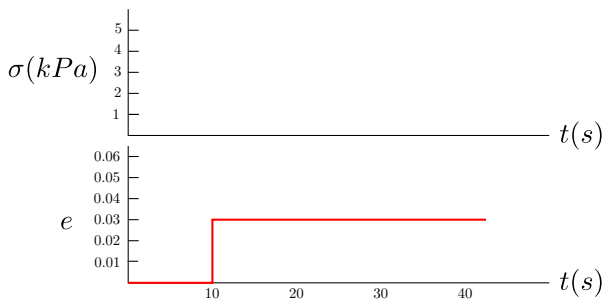
$$\tan \phi = \frac{G''}{G'}$$

Does this phase angle make sense, given your answer to part b? Compare your value of  $\phi$  to the values you expect for a perfectly elastic solid and a perfect liquid.

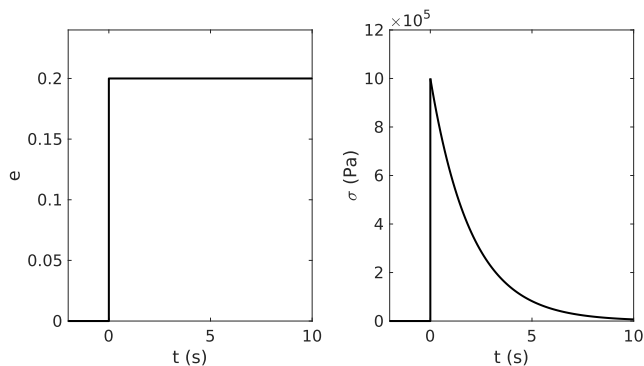
14) The following stress and strain response are observed for a material during the initial stages of a creep experiment.



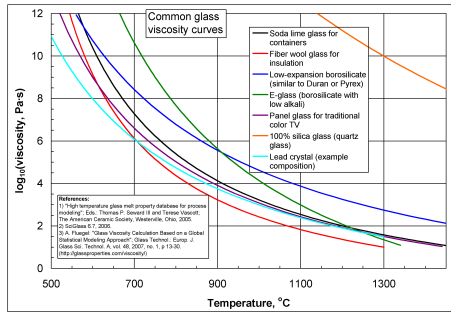
- (a) Draw a spring/dashpot model that describes this behavior. Label moduli and viscosities as quantitatively as possible.
- (b) A stress relaxation test (strain shown below) is performed on the same material. On the stress axis below, draw the stress response that you expect for the model you have drawn from part a.



15) A tensile experiment is performed on a viscoelastic material, with the tensile strain ( $e$ ) and tensile stress ( $\sigma$ ) exhibiting the time dependence shown in the following figure:



- (a) Draw a spring and dashpot model that would give this response. Give values (modulus or viscosity) for each element in your model (the values of these quantities are not expected to be exact).
- (b) Suppose the sample were vibrated in tension at a frequency of 1000 Hz (cycles per second). Estimate the value of  $|E^*|$  (magnitude of the complex shear modulus) that you would expect to obtain.
- (c) For what range of frequencies do you expect the loss modulus ( $E''$ ) to exceed the storage modulus ( $E'$ ) for this material?
- 16)** Can creep of a glass window by viscous flow give measurable changes in sample dimensions over a very long period of time? To sort this out, do the following:
- (a) Estimate the stress at the bottom of a very tall pane of window glass, due to the weight of the window itself. Look up the density of silica glass, and a height of the window that makes sense (choose a big one).
- (b) Estimate the viscosity that would be needed to give a measurable change in sample dimensions after 400 years.
- (c) Using the data below, does it make sense to you that observable flow could noticeably change the dimensions of the window? (You'll need to make some assumptions about how the viscosity will extrapolate to room temperature.)



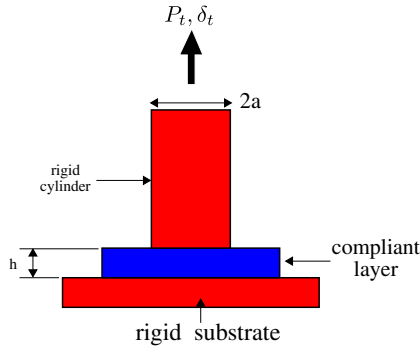
17) In the text we use data from the poly(*t*-butyl acrylate) (PTBA) system to illustrate the concept of time-temperature superposition. This problem steps through this exact same process but with a different data set. You can use any software that you want for this, but the best procedure is to adapt the Python code for the PTBA system, which you can down load from [msecore.northwestern.edu/331/python/ptba\\_master\\_curve.py](http://msecore.northwestern.edu/331/python/ptba_master_curve.py). The PTBA data can be found at [msecore.northwestern.edu/331/data/ptbadata.xlsx](http://msecore.northwestern.edu/331/data/ptbadata.xlsx), but we want to repeat the same procedure for poly(2-vinyl pyridine) (PVP), using the data found at [msecore.northwestern.edu/331/data/pvpdata.xlsx](http://msecore.northwestern.edu/331/data/pvpdata.xlsx).

- Plot the frequency dependence of  $|G^*|$  and  $\phi$  for the each of the 5 temperatures provided in the data set.
- Find shift factors that give well-superposed master curves for  $|G^*|$  and  $\phi$  when plotted against  $\omega a_T$ . Plot the master curves for both quantities, and show your plot of  $a_T$  vs. Temperature. Use 200 °C as the reference temperature for which  $a_T = 1$ .
- Fit the  $a_T$  data to the Vogel-Fulcher-Tamman equation. What values do you get for  $T_\infty$  and  $B$ . Compare  $T_\infty$  to the glass transition temperature of 100 °C, and compare the value of  $B$  to the value of  $B$  obtained from the PTBA sample.
- Describe how your plot of  $a_T$  vs. temperature would look if you used 130 °C as the reference temperature (you do not need to make a separate plot).
- Plot  $\eta_0$ , the zero-shear viscosity for the PVP sample as a function of temperature.

## 17.8 Contact Mechanics

18) Consider the contact of a flat rigid punch with a thin elastic layer, as shown schematically below:



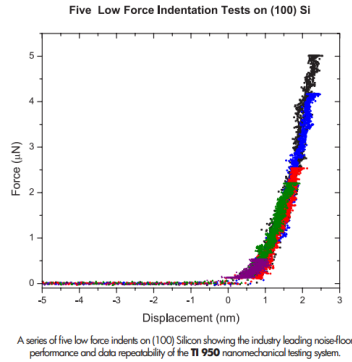


Suppose the compliant layer is incompressible gel ( $\nu = 0.5$ ), with a Young's modulus,  $E$ , of  $10^4$  Pa. The critical energy release rate for failure at the gel/punch interface is  $0.1 \text{ J/m}^2$ . The punch radius,  $a$ , is 3 mm.

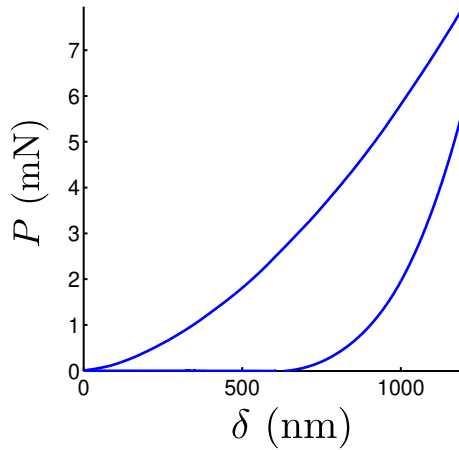
- (a) What is the tensile force required to separate the punch from the layer if the layer is infinitely thick?
  - (b) What is the stress intensity factor,  $K_I$ , just prior to detachment of the punch from the surface?
  - (c) How close to the punch edge do you need to be for the tensile stress at the punch/layer interface to be equal to the modulus of the layer?
- 19)** Describe in qualitative terms what happens to the following quantities as the thickness,  $h$ , of the compliant layer from the previous problem decreases:
- (a) The overall compliance of the system.
  - (b) The load required to detach the indenter from the substrate.
  - (c) The displacement at which the indenter detaches from the substrate.
  - (d) The shape of the tensile stress distribution at the punch/substrate interface.

## 17.9 Nanoindentation

**20)** Commercial nanoindenters are generally not suitable for the characterization of soft materials. To understand why this is the case, consider the following indentation data from the Hysitron web site (this is for the same instrument that Northwestern has in the NUANCE facility):

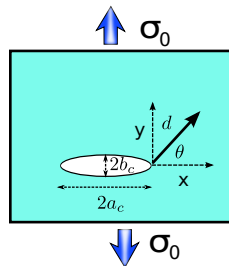


- (a) If the data in this figure are obtained with a rigid spherical indenter of radius  $R$ , use the data from this figure to estimate the value of  $R$ . Assume that the material is being indented elastically and that adhesion can be neglected. (You'll need to look up mechanical property data for silicon).
- (b) Suppose that the material is replaced by an elastomer with a modulus of  $10^6$  Pa. What value of  $R$  would need to be used to obtain the same Force displacement curve for this much softer material? (Assume that the effects of adhesion can be eliminated by performing the indentation in a suitable liquid).
- 21) Suppose an elastomeric sphere with a radius of 1 mm and a reduced modulus,  $E^*$ , of  $10^6$  Pa is placed on a flat, rigid substrate. Suppose also that the adhesion between the sphere and the substrate is characterized by a critical energy release rate of  $0.05$  J/m<sup>2</sup>, independent of the crack velocity or direction of crack motion. Calculate the radius of the circular contact area that develops between the elastomer and the surface, assuming that there is no external load applied to the sphere (apart from its weight).
- 22) Obtain the hardness and elastic modulus from the following nanoindentation curve, obtained from a Berkovich indenter:



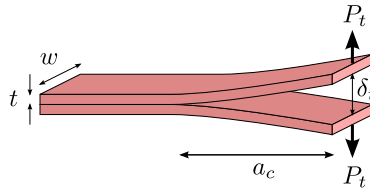
### 17.10 Fracture Mechanics

23) The stress fields in the vicinity of a crack tip in a material are determined by the distance,  $d$ , from the crack, and the polar angle  $\theta$ , defined in the following diagram.



- For a fixed value of  $d$ , plot the behavior of  $\sigma_{xx}$ ,  $\sigma_{yy}$  and  $\sigma_{xy}$  for a mode I crack as a function of  $\theta$ .
  - What happens to the stresses for  $\theta = 180^\circ$ ? Why does this make sense?
  - A mode I crack will travel in the direction for which the normal stress acting across the crack surfaces is maximized. What direction is this?
- 24) As a crack advances, what happens to the stiffness of the cracked body? What happens to the compliance?

25) A set of double cantilever beam adhesion test specimens was fabricated from a set of aluminum alloy samples. The geometry as shown below:



Suppose each of the two beams has a thickness ( $t$ ) of 10 mm, a width ( $w$ ) of 20 mm and a length of 80 mm. The double cantilever beam sample was produced by using an adhesive to glue the two beams together. Assume the precrack with a length,  $a_c$ , of 10 mm. The critical energy release rate for the adhesive is  $65\text{J/m}^2$ .

- Calculate the values of the tensile load,  $P$ , and the displacement,  $\Delta$ , where the crack starts to propagate.
  - In a load-controlled experiment,  $P_t$  is held constant once the crack starts to propagate, and in a displacement controlled test  $\Delta$  is held constant once the crack starts to propagate. From the relationship between  $\mathcal{G}$  and  $P_t$ ,  $\Delta$  and  $a$ , describe why the load controlled experiment results in unstable crack growth, but the displacement controlled experiment results in stable crack growth.
  - From your answer to part b, describe how you would design an experiment where you measured the energy release rate required to propagate the crack at a specified velocity.
- 26) Describe the difference between a crack and a craze? How is the maximum width of a craze related to  $\mathcal{G}_c$  and  $K_{IC}$ ?
- 27) What is a Charpy impact test conducted, and what does it measure?
- 28) Silicones containing resin fillers are used as an encapsulant materials in light emitting diodes (LEDs) in order to protect the electronics from harsh environments and to aid in heat dissipation. Near the surface of the electronic components, temperatures can go as high as  $200^\circ\text{C}$  for extended time periods.

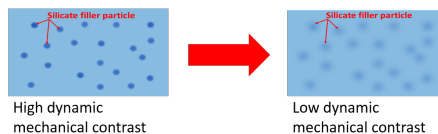


**Figure 17.1:** High dynamic mechanical contrast is important

- Given that a high dynamic mechanical contrast is desirable in creating a soft material with high fracture toughness, what would you suggest as a design criteria in order to maintain high dynamic mechanical contrast at high temperatures? (Hint: think about the role of the  $T_g$  of the matrix and filler content.)
- Thermal mismatch at the interface between the encapsulant and electronic can lead to residual stresses that promote crack propagation. In assessing the performance of the encapsulant at the interface, should a failure stress or a failure strain criteria be used? Why?
- From a thermal management and mechanics perspective, why do you think a soft encapsulant (e.g. silicone) will be more preferable over a hard encapsulant (e.g. glass)?

## 17.11 Weibull Statistics

**29)** A set of glass rods with a Weibull modulus of 30 are fractured in a uniaxial tensile test. The stress at which 63% of the samples fracture is 100 MPa.

- What is the maximum stress if you want to make sure that less than one in 100 rods fail? (Note that  $1/e$  is 0.37).
- What is the maximum stress if you want to make sure that less than one in  $10^6$  rods fail?
- What does the stress need to be to get less than 1 failure in  $10^6$  if the Weibull modulus is 10 instead of 30?

**30)** What determines the value of the Weibull modulus in a brittle material?

**31)** A brittle material with a specified geometry fails with a 50% probability at a tensile stress of 100 MPa. From the failure statistics, it is determined that the Weibull modulus for this material is 40. What fraction of these materials will fail at a tensile stress of 70 MPa?

## 17.12 Yield Criteria

32) A cube of material is loaded triaxially resulting in the following principal stresses at the point

of plastic yielding:  $\sigma_1^p = 140$  MPa,  $\sigma_2^p = 20$  MPa, and  $\sigma_3^p = 35$  MPa.

- What is the shear strength of the material according to the Tresca yield criterion?
- If the the value of  $\sigma_3^p$  were increased to 70 MPa, how does this change your result? Explain.

33) The tensile yield stress of a materials is measured as 45 MPa by a uniaxial tensile test.

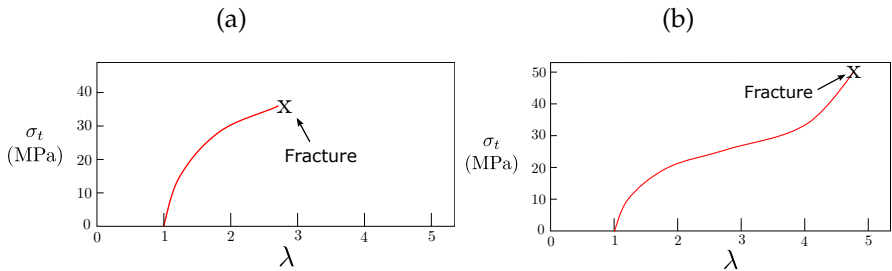
- What will the shear stress of the material by if the materials yields at a specified value of the Tresca stress?
- Now calculate the same quantity (shear yield stress) if the material yields at a specified value of the Von Mises stress.
- Suppose the material is a glassy polymer like Plexiglas, and Tresca yield stress is obtained from a uniaxial compression experiment and from a uniaxial tensile experiment. Which of these experiments to you expect to give the largest Tresca yield stress?

34) What is the effect of the resolved normal stress on the yield behavior of crystalline metals and ceramics? What about polymers? Describe any differences between the two cases.

35) A sample of pure iron has a uniaxial tensile yield strength of 100 MPa. Assume that the yield behavior is described by the Von Mises yield criterion.

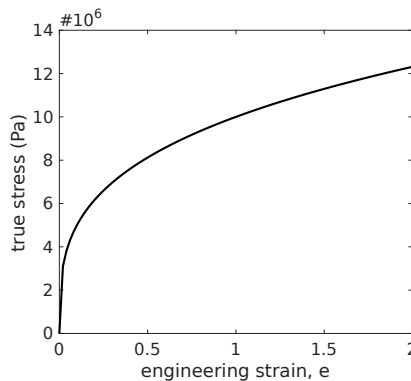
- What do you expect for the yield strength of the material in a state of uniaxial compression?
- What will the yield strength be under a stress state of pure hydrostatic pressure?
- What is the shear yield strength of the material.

36) Consider the following two stress-strain curves obtained from a glassy polymer material. In these plots  $\sigma_t$  is the true stress and  $\lambda$  is the extension ratio ( $1+e$ , where  $e$  is the tensile strain).



- Sketch the behavior of the engineering stress vs extension ratio that you expect for each of these samples in a uniaxial tensile test. Be as quantitative as possible. Briefly describe why you drew the curves the way you did.
- Which of these samples can be cold drawn? What value do you expect for the draw ratio? (The plastic strain in the drawn region of the sample)?
- Suppose the cross sectional area of each sample is  $1 \text{ cm}^2$ . What is the maximum load that the sample will be able to support prior to failure for each of the two samples?

37) Consider a material with the following true stress vs. engineering strain behavior, measured in uniaxial extension:



- Suppose the cross sectional area of this material is  $1 \text{ cm}^2$ . Calculate the maximum force that this material would be able to support prior to failure.
- Will this material form a stable neck? If so, what is the characteristic strain in the necked region?

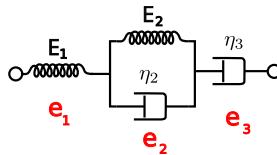
38) The following stress tensor describes the state of stress of a material at its yield point:

$$\sigma = \begin{bmatrix} 0 & 3 & 0 \\ 3 & 0 & 0 \\ 0 & 0 & -5 \end{bmatrix} \text{ MPa}$$

Suppose the same material is subjected to stress state of simple shear. At what value of the applied shear stress do you expect yielding to occur, assuming that the material obeys a Tresca yield criterion.

### 17.13 Nonlinear Viscoelasticity and Creep

39) A step stress ( $0$  for  $t < 0$ ,  $\sigma$  for  $t > 0$ ) is applied to a solid which can be modeled by the following combination of linear springs and dashpots:



- (a) This model is useful because it includes a non-recoverable creep component, a recoverable time dependent creep component, and an instantaneous, recoverable strain.
- Identify the element (or combination of elements) in the above model which is associated with each of these three contributions to the strain.
  - Write down the expression for the total strain,  $e(t)$ , after the imposition of the step increase in stress.
  - Suppose the stress is applied for a long time, so that the strain is increasing linearly with time. At some time,  $t'$ , the stress is removed. Derive an expression for the change in strain after the stress is removed.
- (b) This model has been applied to creep data for oriented polyethylene at room temperature. Model predictions were compared to data obtained from samples of high molecular weight (High M) and low molecular weight (Low M). Both samples were drawn to the same draw ratio. The following values of  $E_1$ ,  $E_2$ ,  $\eta_2$  and  $\eta_3$  were obtained from experimental data:

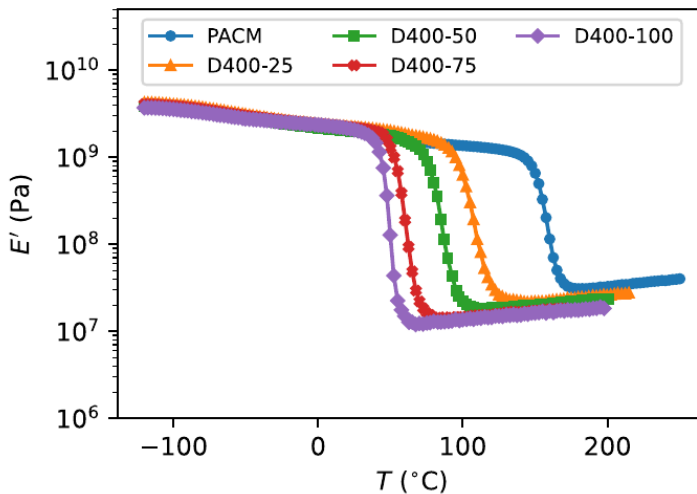


Sample	$\sigma$ (GPa)	$E_1$ (GPa)	$E_2$ (GPa)	$\eta_3$ (GPa-s)	$\eta_2$ (GPa-s)
Low M	0.025	17.4	33.5	$1.8 \times 10^5$	4300
Low M	0.05	13.6	35.6	$6.3 \times 10^4$	5000
Low M	0.1	17.7	26.4	$3.1 \times 10^4$	2200
Low M	0.15	17.7	26.5	$2.6 \times 10^4$	2300
Low M	0.2	16.4	26.8	$1.2 \times 10^4$	2000
High M	0.1	18.3	31.9	$3.1 \times 10^6$	$8.7 \times 10^4$
High M	0.15	16.6	21.3	$1.7 \times 10^6$	$7.3 \times 10^4$
High M	0.2	15.8	32.7	$7.7 \times 10^5$	$3 \times 10^4$
High M	0.3	25.4	39.1	$4.8 \times 10^4$	2800
High M	0.4	25.0	43	$3 \times 10^4$	3000
High M	0.5	21.7	46	$2.5 \times 10^4$	5000

From the values of  $\eta_3$  given in this table, determine the stress dependence of the steady state creep rate. From this stress dependence, calculate the activation volume for non-recoverable creep in the high and low molecular weight samples, and compare these values to one another.

## 17.14 Polymer Swelling

40) Rheological data is obtained for some polymers and we obtain the following:



We know that we can obtain the average molecular weight between crosslinks from these data. We can also obtain this information from swelling experiments (at least approximately). To see if this is feasible in this case, calculate

the amount of swelling you would expect for the PACM and D400-100 polymers if they are immersed in toluene. Assume  $\chi=0.4$  and a density of  $1 \text{ g/cm}^3$  for the polymer. Note that the swelling theory uses a degree of polymerization between crosslinks, which you can take as the volume of a network strand divided by the solvent volume (you'll need to look up the density for toluene somewhere).

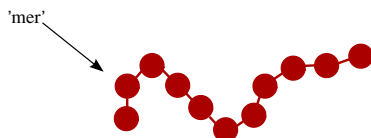


Figure A.1: Schematic representation of a polymer

## A Synthetic Polymers

Most of this book is devoted to synthetic polymers because of their widespread use and importance, and because they illustrate many of the key concepts that are relevant to natural polymers and other soft materials. We begin with a basic introduction to the synthesis of polymeric materials, and the  $z$  component is between properties of these materials. We conclude with some examples of soft materials made up of building blocks that are held together by relative weak forces.

### A.1 What is a Polymer

A polymer is a large molecule made from many small **repeat units** or 'mers'. There is an inherent anisotropy at the molecular level because both strong and weak bonding interactions are important:

- Strong covalent bonds are formed within a molecule (between 'mers').
- Weak Van der Waals or hydrogen bonding are formed between molecules, and cause the materials to condense into a solid or liquid phase.

### A.2 Classification Scheme

Crystallization and glass formation are the two most important concepts underlying the physical properties of polymers. Polymers crystallize at temperatures below  $T_m$  (melting temperature) and form glasses at temperatures below  $T_g$  (glass transition temperature). All polymers will form glasses under the appropriate conditions, but not all polymers are able to crystallize. The **classification scheme** shown in Figure A.2 divides polymeric materials based on the locations of  $T_g$  and  $T_m$  (relative to the use temperature,  $T$ ) and is a good place to start when understanding different types of polymers.

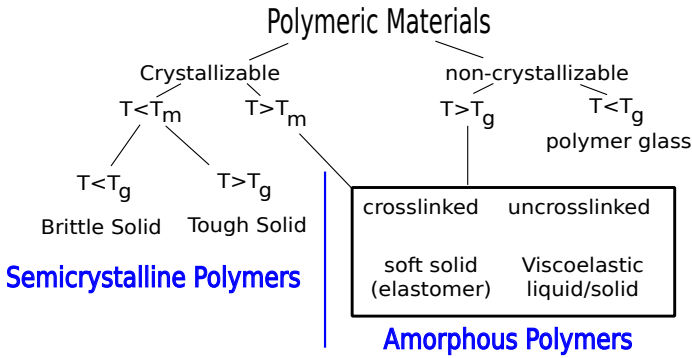
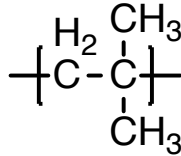


Figure A.2: Classification scheme for polymeric materials.



Polychloroprene  
(Neoprene)



Polyisobutylene



Silicone

Figure A.3: Examples of elastomeric materials.

## Elastomers

Traditional elastomers are amorphous materials with a glass transition temperature less than the use temperature so that they remain flexible. They are generally crosslinked so that they do not flow over long periods of time. Common examples are shown in Figure A.3.

## Glassy Polymers

Glassy polymers are amorphous like elastomers, but their glass transition temperature is above the use temperature. Because of this they behave as rigid solids, with elastic moduli in the range of  $10^9$  Pa. Glassy polymers do not need to be crosslinked, because below  $T_g$  the molecules and flow of the material is suppressed. Also, because the materials are homogenous over length scales comparable to the wavelength of light, they are transparent. Common examples are illustrated in Figure A.4.



Poly(methyl methacrylate)  
(PlexiGlas)



Polycarbonate



Poly(phenylene oxide)

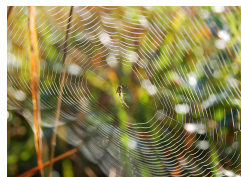
**Figure A.4:** Examples of glassy polymers.



Polyethylene terephthalate.



Poly(tetrafluoroethylene)  
(Teflon)



Spider Web

**Figure A.5:** Examples of semicrystalline polymers.

## Semicrystalline Polymers

Semicrystalline polymers must have molecular structures that are compatible with the formation of an ordered lattice. Most atactic polymers are amorphous (non-crystalline) for this reason (with the exception being examples like poly(vinyl alcohol) where the side group is very small). Another requirement is that  $T_g$  be less than  $T_m$ . If the glass transition temperature is higher than  $T_m$  the material will form a glass before crystallization can occur. In the glassy polymer the material is kinetically trapped in the glassy state, even though the crystalline state has a lower free energy below  $T_m$ . Examples of some semicrystalline polymers are shown in Figure A.5.

## A.3 Understanding Polymer Chemistry

Crystallization and glass formation processes are central to our understanding of polymeric materials, we must eventually address the following question:

- How is a polymer's tendency to crystallize or form a glass determined by its molecular structure?

Before we answer this question, however, we must answer the following question:

- What determines this molecular structure, and how are our choices limited?

In order to answer this question properly, we need to study the processes by which polymeric materials are made. Polymer synthesis involves organic chemistry. After familiarizing ourselves with some of the relevant polymer chemistry, we will be in a position to study the physical properties of polymers. For this reason, our discussion of molecular structure in polymers will include some chemistry.

### A.3.1 Covalent Bonding

Polymer molecules consist of atoms (primarily carbon, nitrogen, oxygen and hydrogen) which are covalently bound to one another. The fraction of the periodic table that can form strong covalent bonds is relatively small, corresponding to the ten atoms shown in yellow in Figure A.6 (H, C, N, O, F, Si, P, S, Cl, Br). It is useful at this point to recall some of the basic principles governing the bonding between these atoms:

- Nitrogen, oxygen, carbon and the other covalent bond forming atoms with  $M > 6$  (F, Si, P, S, Cl, Br) are surrounded by 8 electrons, included shared electrons.
- Hydrogen atoms are surrounded by 2 electrons, included shared electrons.
- A single bond involves two shared electrons, a double bond involves 4 shared electrons, and a triple bond involves 6 shared electrons.

### A.3.2 Lewis Diagrams

Lewis diagrams ([Wikipedia link](#)) provide a convenient way of keeping track of the valence electrons in covalently bonded compounds. Several examples are given here. Note how the rules given on the previous page are followed in each case.

### A.3.3 Bonding

The following principles of covalent bonding in organic materials are very helpful:

Group Period	1	2	3	4	5	6	7	8	9	10	11	12	13	14	15	16	17	18	
1	1 H																		2 He
2	3 Li	4 Be	Polymer-Forming Elements										5 B	6 C	7 N	8 O	9 F	10 Ne	
3	11 Na	12 Mg											13 Al	14 Si	15 P	16 S	17 Cl	18 Ar	
4	19 K	20 Ca	21 Sc	22 Ti	23 V	24 Cr	25 Mn	26 Fe	27 Co	28 Ni	29 Cu	30 Zn	31 Ga	32 Ge	33 As	34 Se	35 Br	36 Kr	
5	37 Rb	38 Sr	39 Y	40 Zr	41 Nb	42 Mo	43 Tc	44 Ru	45 Rh	46 Pd	47 Ag	48 Cd	49 In	50 Sn	51 Sb	52 Te	53 I	54 Xe	
6	55 Cs	56 Ba	57 La	72 Hf	73 Ta	74 W	75 Re	76 Os	77 Ir	78 Pt	79 Au	80 Hg	81 Tl	82 Pb	83 Bi	84 Po	85 At	86 Rn	
7	87 Fr	88 Ra	89 Ac	104 Rf	105 Db	106 Sg	107 Bh	108 Hs	109 Mt	110 Ds	111 Rg	112 Cn	113 Nh	114 Fl	115 Mc	116 Lv	117 Ts	118 Og	
				58 Ce	59 Pr	60 Nd	61 Pm	62 Sm	63 Eu	64 Gd	65 Tb	66 Dy	67 Ho	68 Er	69 Tm	70 Yb	71 Lu		
				90 Th	91 Pa	92 U	93 Np	94 Pu	95 Am	96 Cm	97 Bk	98 Cf	99 Es	100 Fm	101 Md	102 No	103 Lr		

**Figure A.6:** Periodic table, illustrating the ten atoms that make up the covalently-bonded portion of polymeric materials.

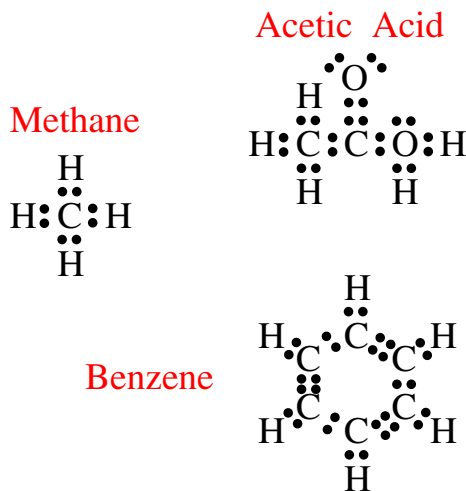


**Figure A.7:** Examples of Lewis Diagrams

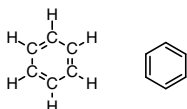


Figure A.8: Examples of Shorthand Notation when drawing chemical structures

- Carbon, Silicon: group 14 (4 valence electrons) - 4 more needed to complete shell -C, Si form 4 bonds with neighboring atoms.
- Nitrogen, Phosphorous: group 15 (5 valence electrons) - 3 more needed to complete shell -N, P form 3 bonds with neighboring atoms.
- Oxygen, Sulfur: group 16 (6 valence electrons) - 2 more needed to complete shell -O, S form 2 bonds with neighboring atoms.
- Hydrogen (group 1) or Fluorine, Chlorine, Bromine (Group 17): F, Cl, Br form 1 bond with neighboring atoms.

(The situation for P and S is actually a bit more complicated when either of these atoms are bonded to oxygen, but these general rules serve our purpose for now.) The chemical structures throughout this book can be seen to obey these rules.

### A.3.4 Shorthand Chemical Notation

Most of the chemical structures illustrated in this text are relatively simple, consisting of single and double bonds between atoms. We generally don't bother to write all of the carbons and hydrogens into the structure. We use the following common conventions.

- If no element is included, element at junctions between different bonds are assumed to be carbon.
- If atoms are missing, so that the rules given above for the number of bonds attached to each atom type are not satisfied, the missing atoms are hydrogens.

An example of this convention is shown below in the structure for **benzene**:

Note the resonance between the two possible ways of drawing the double bonds in the drawing on the left. Molecules with these types of alternating **aromatic compounds**.



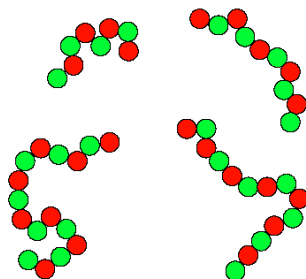


**Figure B.1:** Polymers produced by step growth polymerization. The red and green circles correspond to 'A' and 'B' monomers that react with one another to form the polymer.

## B Polymerization Reactions

Polymerization is the process by which small molecules react with one another to form large polymer molecules. Polymerization reactions can be broken up into the following two general categories:

- 1) Step Growth Polymerizations:** Collections of A and B species react with one another. In linear step growth polymerizations, the ends of molecules react with one another to form longer molecules. A variety of reactions are possible, so you need to know at least a little organic chemistry. We'll focus on just a few of the most common cases.
- 2) Chain Growth Polymerizations:** Each polymer chain has one reactive site to which additional monomers are added.
- 3) Additional Resource:** The Macrogalleria web site has some excellent, simple descriptions of polymerization reactions. Specific examples are referenced at different points throughout this book.

[Click here for Macrogalleria polymerization overview.](#)

### B.1 Step-Growth Polymerizations

In this example green and red monomers can only react with each other. Because there are 5 more red monomers than green monomers, there are 5 molecules remaining at the end of the reaction, with each of these molecules

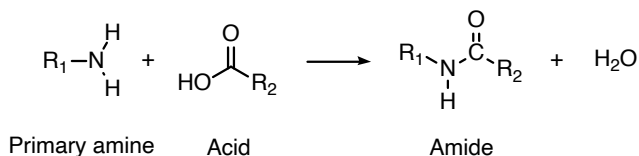


**Figure B.2:** Formation of an amide from an amine and a carboxylic acid

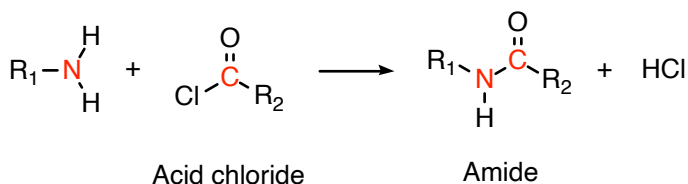


**Figure B.3:** Formation of an amide from a primary amine and an acid chloride

possessing two red end groups. The extent of reaction,  $p$  is defined as the fraction of available reactive groups which have actually undergone a reaction. Values close to one are needed in order to obtain useful, high molecular weight polymer. A delicate stoichiometric balance generally needs to be maintained (same amount of red and green monomers) in order to obtain high molecular weight.

The following pages illustrate some of the specific reactions which take place during the polymerization process. To illustrate the concepts involved, we consider the following polymer types, all of which are produced by step-growth polymerization:

- (a) Polyamides
- (b) Polyesters
- (c) Polyurethanes
- (d) Epoxies

### B.1.1 Polyamides

In this example, a primary amine reacts with a carboxylic acid to form an amide linkage. Water is liberated during the condensation reaction to form the amide. Primary amines and acid chlorides undergo a similar reaction:

Acid chlorides react very rapidly with amines at room temperature, which is very useful for demonstration purposes. Acid chlorides can also react with water to form carboxylic acids, however, and commercial polyamides are generally produced by reaction with carboxylic acids.

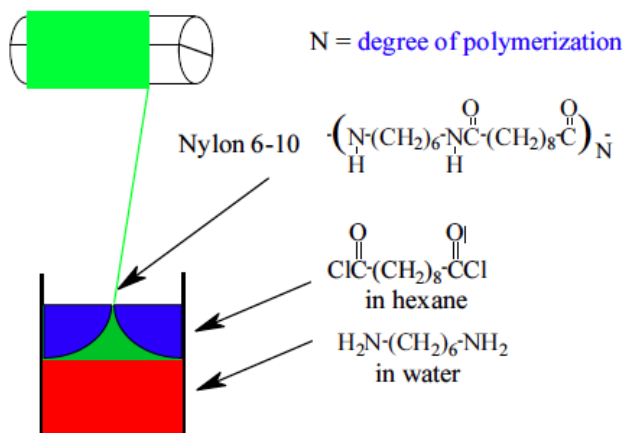


Figure B.4: Schematic representation of the interfacial polymerization of nylon.

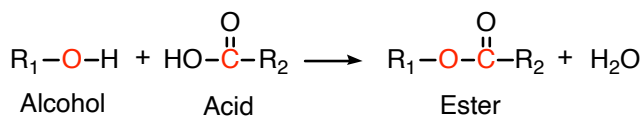


Figure B.5: Formation of an ester from an alcohol and a carboxylic acid.

## B.2 Interfacial Polymerizations

### B.2.1 Polyesters

Polyesters can be formed by condensation reactions of alcohols with carboxylic acids:

Polyethylene terephthalate (Mylar, Dacron, 2L soda bottles) is a common example. Note that under appropriate conditions, the reverse reaction (**hydrolysis**) reaction can also take place, where the addition of water to an ester bond forms the acid and the alcohol. This reaction is important in a variety of polymers used in biomedical applications, which degrade in the body via hydrolysis of the polymer. Polycaprolactone is one example.

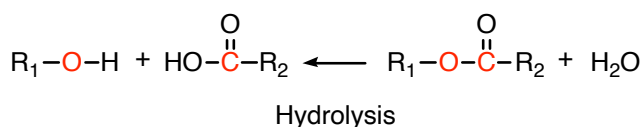


Figure B.6: Ester hydrolysis: The reverse of the esterification reaction.

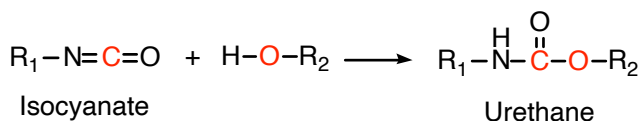


Figure B.7: Urethane Formation

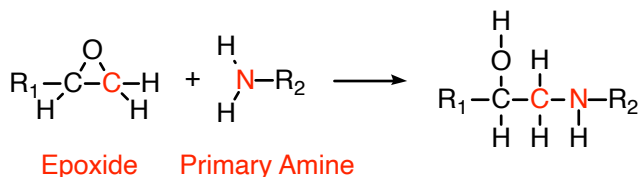


Figure B.8: Reaction of an epoxide with a primary amine.

### B.2.2 Polyurethanes

Polyurethanes are formed by the reaction of isocyanates with alcohols, as shown below:

Note that this is NOT a condensation reaction, since no byproducts are formed during the reaction. Also note that the urethane linkage contains an oxygen atom in the backbone, whereas the amide linkage does not. (The  $R^1$  and  $R^2$  substituents can have different structures, but are always attached to the illustrated linkages by carbon atoms.)

### B.2.3 Epoxies

All epoxies involve reactions of epoxide groups (3-membered rings containing an oxygen atom) with curing agents. Amine curing agents are very common, as illustrated Figure , which shows a primary amine reactant with an epoxide group).

The secondary amines which remain can react with additional epoxide groups to form a branched structure as shown in Figure B.9. The reactive functionality of a primary diamine is 4 when the reaction is with an epoxide (as opposed to its functionality of 2 in the case where the diamine reacts with an acid or acid chloride).

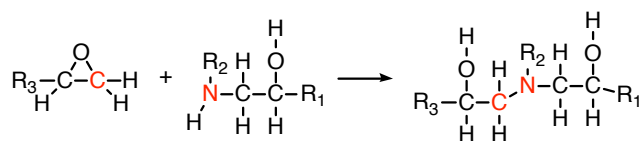


**Figure B.9:** Reaction of an epoxide with a secondary amine.

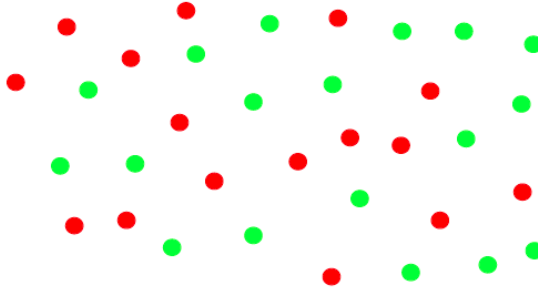


Figure C.1: Nonlinear Step Growth Polymerization

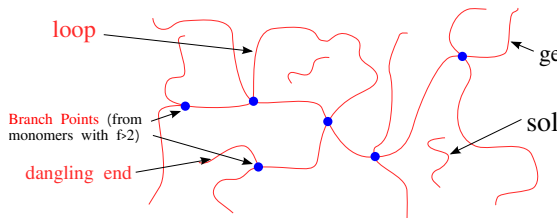


Figure C.2: Molecular schematic of gel network.

## C Non-Linear Step Growth Polymerizations

Nonlinear step-growth polymerizations involve the use of monomers that have a reactive functionality,  $f$ , which is greater than 2.

### C.1 Gelation

A network (or gel) is formed when the molecular weight of the largest molecule in the system reaches infinity. Everything which is covalently attached to this single very large molecule is part of the gel fraction.

Unattached molecules which are not part of the **gel fraction** make up the **sol fraction**. The **gel point** refers to the point in the polymerization reaction at which point a gel fraction first appears, and the overall process is referred to as **gelation**.

### C.2 Prepolymers

In many cases, the length of the polymer between branch points is determined by the molecular weight of a **prepolymer**. Prepolymers generally have a reactive functionality of 2.



Figure C.3: Example of a Prepolymer

The following factors determine the property of the network:

- (a) Molecular weight of prepolymer
- (b) Composition of prepolymer
- (c) Functionality of curing agent (4 for diamine curing of epoxies)
- (d) Extent of reaction (number of dangling ends)
- (e) Network structure (loops, entanglements, etc.)

### C.3 Corothers Theory of Gelation

We begin with  $n_a$  molecules with a reactive functionality of  $f_a$  that are able to react with  $n_b$  molecules with a reactive functionality of  $f_b$ . For illustrative purposes, consider the perfectly stoichiometric case where the total functionality of all the A monomers is equal to the total functionality of all the B monomers:

$$n_a f_a = n_b f_b \quad (\text{C.1})$$

We define an average reactive functionality,  $f_{av}$ , so that  $(n_a + n_b) f_{av}$  is equal to the total number of functional groups:

$$(n_a + n_b) f_{av} = n_a f_a + n_b f_b \quad (\text{C.2})$$

The number of initial molecules corresponding to a given number of functional groups is inversely proportional to  $f_{av}$ . For large values of  $f_{av}$ ,  $p$  does not have to reach unity in order for the total number of molecules to be reduced to one. An expression for  $N_n$  can be obtained substituting  $p f_{av}/2$  for  $p$  in Eq. , describing the evolution of  $M_n$  with  $p$  for linear step growth polymerization:

$$N_n = \frac{1}{2 - p f_{av}} \quad (\text{C.3})$$

The quantity  $p f_{av}$  describes the average number of times that any given molecule has reacted. The number average molecular weight is predicted to diverge to infinity when this average number of reactions per molecule is 2.

This occurs when  $p = p_{gel}$ , where  $p_{gel}$  Standard extent of reaction at the end-point. Setting  $p_{gel} f_{av} = 2$  gives:

$$p_{gel} = \frac{2}{f_{av}} \quad (\text{C.4})$$

This simple equation for the gel point is very useful, although it is important to remember that this derivation suffers from the following deficiencies:

- (a) Gelation actually occurs for finite  $N_n$ , since  $N = \infty$  only for the largest molecule.
- (b) The theory neglects loop formation (reactions between two portions of the same molecule). These reactions change the shape of a given molecule, but do not decrease the overall number of molecules.

The first assumption tends to overestimate  $p_{gel}$ , and the second assumption tends to underestimate  $p_{gel}$ . A more accurate description of gelation requires a much more detailed theory than the one presented here.

When one molecule which spans the entire sample, it can no longer flow like a liquid. One the characteristics of non-linear step growth polymerizations is that the viscosity (resistance to flow) of the reaction mixture increases as the extent of reaction increases, and eventually diverges at the gel point. Also, the reaction rate generally decreases as the reaction proceeds and the reactive molecules become larger and larger. These features are illustrated conceptually in Figure C.4. Here we show schematic representations of the time-dependent extent of reaction, along with the time dependence of the number average degree of polymerization,  $N_n$ , and of two physical properties of the material:  $\eta_0$  and  $E_\infty$ . Here  $\eta_0$  is the limiting viscosity measured at very low shear rates, and  $E_\infty$  is the elastic modulus measured at very long times. The viscosity is a characteristic of a liquid material, and characterizes the material for values of the extent of reaction,  $p$ , that are less than the extent of reaction corresponding to the gel point,  $p_{gel}$ . For values of  $p$  that exceed  $p_{gel}$ , the material behaves as a solid, and has a finite elastic modulus,  $E_\infty$ . At the gel point, the viscosity diverges to infinity, since it is no longer possible for the material to flow. Instead, the material becomes an elastic solid, with a value of  $E_\infty$  that increases from 0 at the gel point.

Note that that materials near the gel point are viscoelastic, and can no longer be described by a single value of the viscosity or modulus. Instead, these properties depend on the timescale of the measurement, as described in more detail on the section on viscoelasticity.



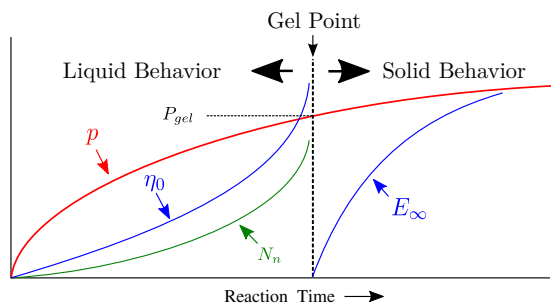
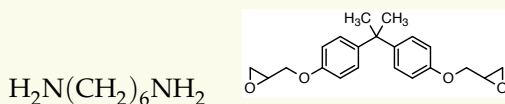


**Figure C.4:** Time-dependence of property development in a nonlinear step growth polymerization.

**1) Exercise:** A very simple epoxy formulation has bisphenol A diglycidyl ether as the epoxide component and hexamethylene diamine as the crosslinker:



A) Hexamethylenedi-  
amine

B) Bisphenol A  
diglycidyl ether

- How many grams of hexamethylene diamine should be added to 1g of Bisphenol A diglycidyl ether in order to optimize the polymerization reaction in a homogeneous solution?
- Estimate the fraction of amine groups that need to react in order to reach the gel point.

**2) Solution:** In this case monomer A (the hexamethylenediamine) has a molecular formula of  $\text{C}_6\text{H}_{16}\text{N}_2$ , corresponding to a molecular weight,  $M_a$ , of 116 g/mole. The functionality of monomer A,  $f_a$ , is 4 in this case, since each primary amine is able to react with 2 epoxide groups. Monomer B has a molecular formula of  $\text{C}_{21}\text{H}_{24}\text{O}_4$ , giving  $M_b = 340$  g/mole, and a reactive functionality,  $f_b$  of 2. We want the total functionality of the A monomers to be equal to the total functionality of the B monomers in this case, which means that the molar quantities of A and B monomers should be related by Eq. C.1, from which we obtain the following for  $n_a$ :

$$n_a = \frac{n_b f_b}{n_a} = \frac{n_b}{2}$$

We have 1g of B, which we divide by it's molecular weight to get the number of moles:

So we know we need about  $1.45 \times 10^{-3}$  moles of the hexamethylenediamine. Multiplying by its molecular weight of 116 g/mole gives a total mass of 0.17g. Note that we need a lot less of A than B in this case. If we want our two component epoxy to consist of two parts that we combine in nearly equal volumes, we'll have to add some extra stuff to part A (the diamine part) that doesn't take part in the curing reaction.

To figure out the average functionality, we arrange Eq. C.2 to give the following for  $f_{av}$ :

$$f_{av} = \frac{n_a f_a + n_b f_b}{n_a + n_b}$$

Combining this with Eq. C.4 for the gel point gives:

$$p_{gel} = \frac{2(n_a + n_b)}{n_a f_a + n_b f_b}$$

Substituting our stoichiometric condition that  $n_a = n_b/2$  gives  $p_{gel} = 0.75$ .

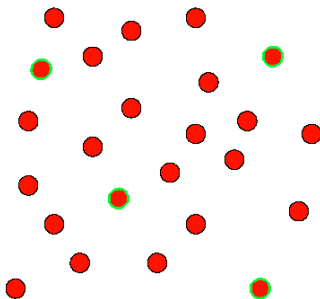


Figure D.1: Chain growth polymerization.

## D Chain-Growth Polymerizations

In chain growth polymerization monomers are added one at a time to a reactive site at that typically remains at the end of the monomer that has been most recently added. There are three phases of the reaction that need to be considered in general:

- Initiation: In this step the a reactive species is formed that is able to form covalent bond with a monomer, reforming the active species at the end of the growing polymer chain.
- Propagation: Monomers are added one at a time to the growing chain.
- Termination: The reactive undergoes a reaction of some sort that causes it to lose its reactivity toward other monomers. The polymer chain is 'dead' at this point, and no longer grows in length.

### D.1 Chain Growth Polymerization Mechanisms

Chain growth polymerizations generally occur either by addition to a double bond, or by opening a ring. In both cases the overall number of bonds is conserved, and there are no condensation products. If the cases where chain growth occurs by addition to double bond between two carbon atoms, the following takes place:

- A new bond is formed between the active sight and one if the doubly bonded carbons
- The double bond is shifted to a single bond.

In a ring opening polymerization, the following takes place:

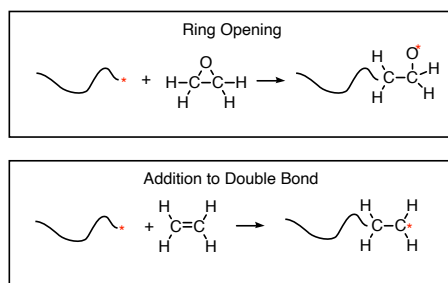


**Figure D.2:** The two basic types of chain growth polymerizations.

- A new bond is formed between the active species and one of the atoms in a cyclic monomer.
- An adjacent bond in the monomer is broken.
- The active site moves to the end of the linear molecule.

## D.2 Reactive Species for Chain Growth Polymerization

Three of the most common active sites are a free radical, negatively charged anion, and a positively charged cation, illustrated in Figure D.3 for the addition to the double bond of vinyl polymers. Vinyl polymers have the general structure  $\text{CH}_2\text{CHR}$ , where R is something other than hydrogen. In each of these cases, a single monomer repeat unit is added to the end of the chain, and the reactive site moves to the end of the chain, on the repeat unit that has just been added. Reactions in organic chemistry are all about keeping track of what the bonding electrons are doing, and Lewis diagrams are very helpful in this sense. In the figures designed to illustrate different propagation and termination reactions, we just show the Lewis structures for some of the bonds, to make it simpler to keep track of the situation before and after the reaction has taken place. For our purpose we are not as interested in the detailed reaction mechanism, which would require that we provide a bit more information about the structure of some of the short-lived reaction intermediate.

## D.3 Initiation

The previous section outlines the chemistry of some different propagation reactions, where monomers are added to an active site. Initiation is the step by which the active site is produced at the beginning. Here we give two simple examples, one for initiation of a radical polymerization, and the second being the initiation of an anionic polymerization.

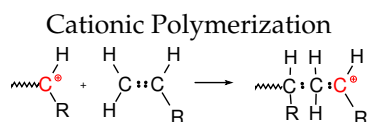
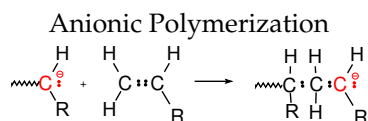
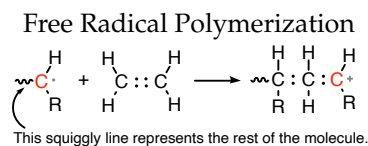


**Figure D.3:** Propagation mechanisms for three common chain growth polymerization mechanisms.

### D.3.1 Initiation of a free radical polymerization

In this example, illustrated in Figure D.4, a peroxide bond between two oxygen atoms splits to form two free radicals. These radicals are able to add to the double bond in a vinyl monomer like styrene to initiate the polymerization reaction.

### D.3.2 Initiation of an anionic polymerization

In the example shown in Figure D.5 is very simple conceptually. The reaction is done in solution, and a small amount of secondary butyl lithium is simply added to a solution of styrene molecule in an appropriate organic solvent. The carbon-lithium bond is very reactive, and has a lot of ionic character. It can really be viewed as an existing anion that is ready to react directly with the styrene monomer.

## D.4 Termination Mechanisms

Termination is the process by which reactive chain ends become unreactive. Termination reactions can be avoided in 'living polymerizations' like anionic and cationic polymerizations.

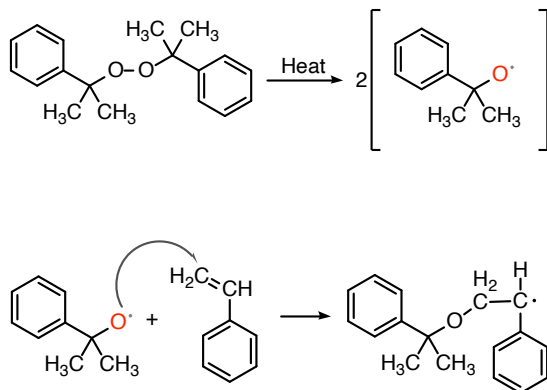


**Figure D.4:** Initiation off a radical polymerization reaction with an epoxide that decomposes into two radical species at elevated temperature.

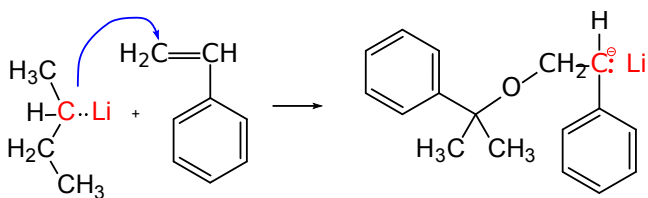


**Figure D.5:** Initiation off a radical polymerization reaction with an epoxide that decomposes into two radical species at elevated temperature.

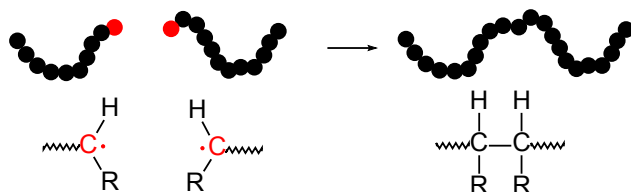


Figure D.6: Termination by radical recombination.

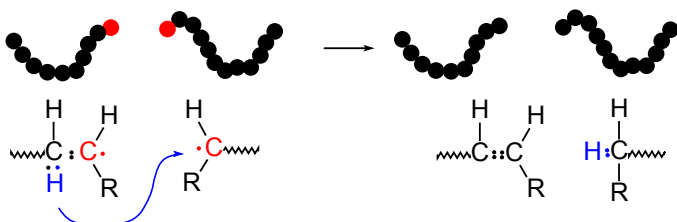


Figure D.7: Termination by disproportionation. The circled proton, along with an electron, moves from the molecule on the right, terminating the free radical on the left. The remaining electrons on the molecule on the left rearrange themselves into a double bond.

#### D.4.1 Radical Recombination

Termination reactions cannot be eliminated in free radical polymerizations, since two free radicals can always combine directly to form a single bond, as illustrated below in Figure D.6.

As unpaired electrons, free radicals are very reactive towards one another. As illustrated in this example, two free radicals can readily combine with one another to form a covalent bond. Combination is therefore one type of termination reaction which is very prominent with free radical polymerizations. Note that the number of molecules decreases by one during the combination reaction.

#### D.4.2 Disproportionation

Plain Laytionation reactions can be viewed as the transfer of a proton andEntanglementsfrom one active molecule to another. The animation here illustrates how the transfer results in the termination of both molecules, with the formation of a double bond. In the final state, the carbon atoms all have eight electrons (including shared electrons) in the valence shell. The molecular

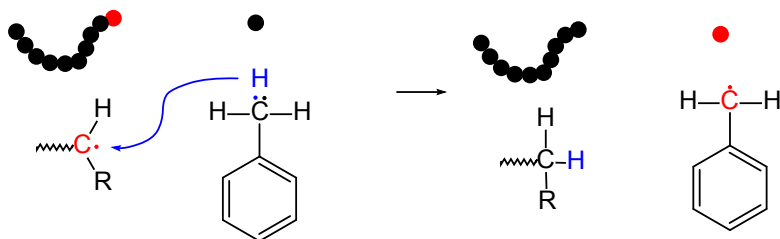


Figure D.8: Chain transfer to toluene.

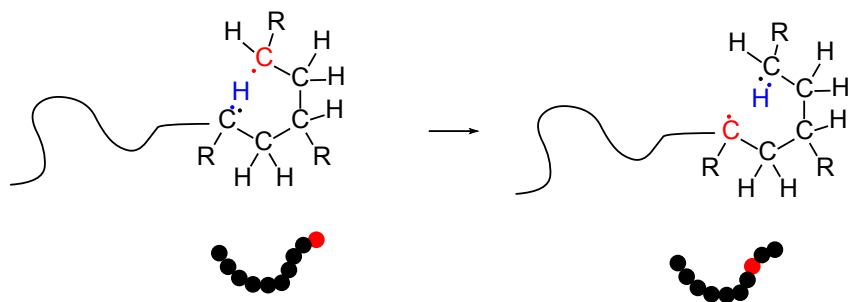


Figure D.9: An Animation of Intramolecular Chain Transfer

weights of the two polymer molecules remain essentially unchanged (with the exception of the transfer of a single proton).

### D.4.3 Chain Transfer

Chain transfer refers to the migration of the active free radical from one molecule to the other. In this example, the active radical from the growing polymer chain is terminated by the addition of a proton and an electron from the toluene molecule on the right. The net result is that the free radical is transferred from the polymer molecule to the solvent molecule (toluene), which can then initiate the polymerization of additional monomer. Note that the process is very similar to disproportionation, except that the species which donates the proton and electron does not already have a free radical.

## D.5 Intramolecular Chain Transfer

In this example, the active radical moves from the end of the polymer chain to a different portion on the same polymer chain. Polymerization continues from this radical, resulting in the formation of a short branch, in this case consisting



of four carbons. Because the branches are randomly placed along the polymer backbone, they interfere with the polymer's ability to crystallize.

**1) Exercise:**

- (a) Chain transfer agents, like toluene in the previous example, can be intentionally added to give some control over the molecular weights of polymers synthesized by free radical polymerizations. In a qualitative sense, how will the addition of chain transfer agents change the number average molecular weight of the polymer?
- (b) How does your answer to this question change if the chain transfer is always to other sites within the same polymer molecule?
- (c) Termination reactions involving free radical polymerizations involve the elimination of two radicals to form a new bond. Where does this new bond appear for combination and disproportionation reactions?

## D.6 Polymerization of Dienes

Dienes are monomers with two double bonds, with a single bond between them. Examples include butadiene, isoprene and chloroprene. The situation for isoprene is illustrated in Figure D.10. The monomer has 4 carbon atoms in a line, which we number 1 through 4. Double bonds connect carbons 1 to 2 and 3 to 4, and a single bond connects carbon 2 to 3. Carbons 2 and 3 are distinguishable from one another because carbon 2 is bonded to a methyl group that is not present on carbon 3. When a propagating polymer chain interacts with the isoprene monomer, addition can occur in any of 4 different ways, which are illustrated in Figure D.10:

- 1,2 addition: The active chain end adds across the bond between carbons 1 and 2, just as it would in a normal polymerization.
- 3,4 addition: Like 1,2 addition, but the reaction occurs across the bond between carbons 3 and 4.
- 1,4 addition: Here the reactive site attaches to carbon 1 and the active site moves to carbon 4, with a double bond being formed between carbons 2 and 3. This double bond can exist in a 'cis' conformation or 'trans' configurations. These cis and trans configurations represent chemically different structures, resulting in polymers with different properties.

Natural rubber is a naturally occurring version of polyisoprene that is harvested from certain tropical trees. The excellent elastomeric properties of this

material arise from the pure *cis* 1-4 microstructure that is produced during the natural polymerization of this polymer. Because of the zigzag nature of the polymer backbone, it does not readily crystallize. A segment of the backbone of the polymer is shown in Figure D.11. This schematic shows a portion of the molecule in a fully extended form. Because of the easy rotation about single bonds, the molecules actually exist in a collection of random configurations.

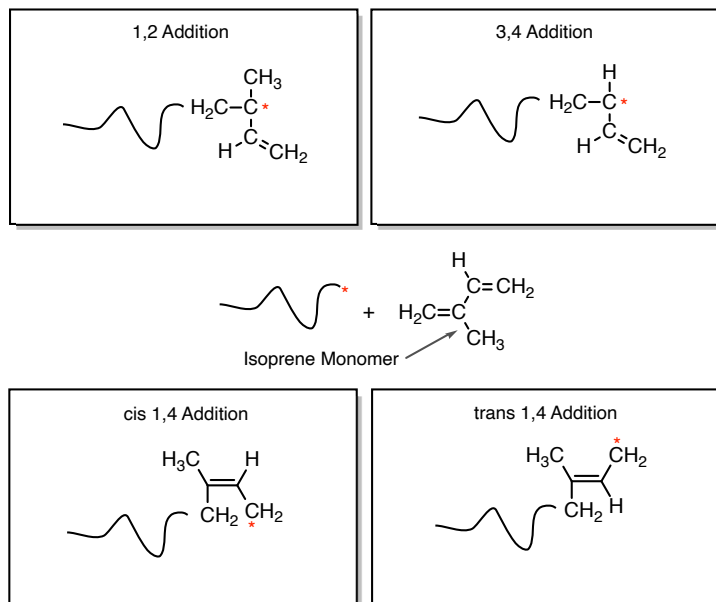


Figure D.10: Polymerization of Isoprene

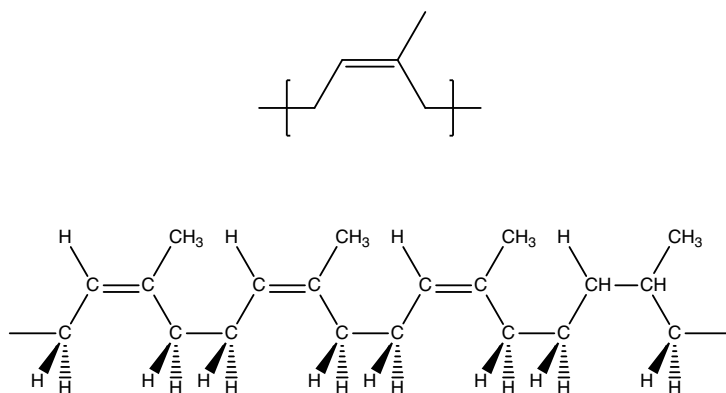


Figure D.11: The chemical structure of natural rubber (*cis* 1-4 polyisoprene)..

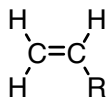


Figure D.12: Chemical structure of a vinyl monomer.

## D.7 Living Polymerizations

Living polymerizations are chain growth polymerizations that proceed without termination or chain transfer reactions. Relatively monodisperse polymers ( $M_w/M_N < 1.1$ ) can typically be obtained when the initiation rate is faster than the propagation rate. Block copolymers are formed by the sequential addition of two (or more) different monomer types in a living polymerization.

## D.8 Vinyl Polymers and Tacticity

**Vinyl polymers** are an important class of polymers produced by chain growth polymerizations. They are produced from vinyl monomers with the following general structure:

When a vinyl monomer is polymerized and we stretch the resulting polymer chain out so that the backbone C-C bonds all lie on the same plane, the 'R' groups end up on different sides of the molecule. The distribution of these R groups determines the **tacticity**, according to the following definitions:

- Isotactic: All R groups on same side of the molecule.
- Syndiotactic: R groups on alternate sides of the molecule.
- Atactic R groups randomly placed.

These different tacticities are illustrated in Figure D.13.

Tacticity is significant because it determines the ability of a polymer to crystallize. The disordered structure of an atactic polymer is inconsistent with the ordered structure of a crystalline polymer. As a result, atactic polymers generally cannot crystallize. Standard exceptions to this rule include polymers where the 'R' group is very small, so that this group can be incorporated into an ordered crystalline array, even if it is randomly placed along the polymer chain. For this reason polyvinyl chloride can be partially crystalline even if the polymer is atactic. Atactic polystyrene and atactic polypropylene, however, are always amorphous.

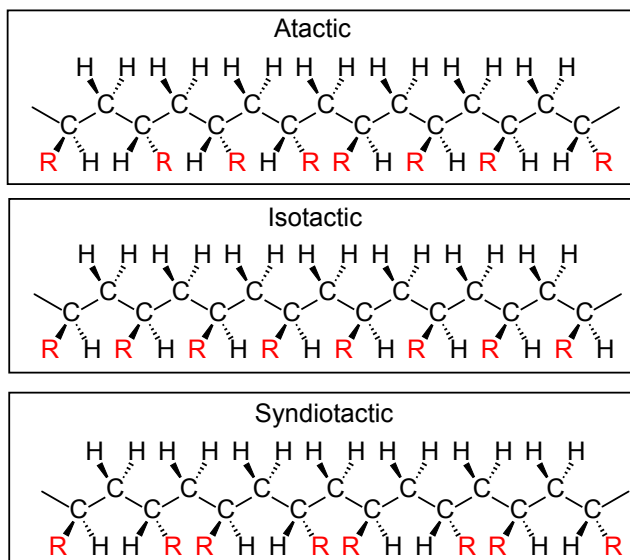


Figure D.13: Illustration of different polymer tacticities.

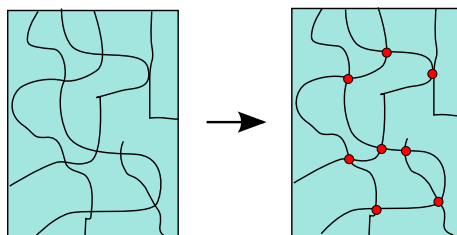


Figure D.14: Diagram representation of crosslinking.

## D.9 Crosslinking

Crosslinking is the process by which separate molecules in an amorphous polymer are chemically attached to one another, as shown schematically in Figure D.14. The black lines indicate individual molecules, and the red dots represent crosslink points where these molecules are 'tied' together.

A representative and commercially important crosslinking system, known by the commercial name of Sylgard 184, consists of the two different parts shown in Figure D.15. Part 1 consists of poly(dimethyl siloxane) polymer with vinyl groups (double bonds) at each end of the polymer molecules. Part 2 contains a silicone crosslinker with several silane groups (Si-H) that are able to react with the vinyl groups as shown in Figure D.16. The reaction can be viewed as a step growth reaction involving a component with a reactive functionality of 2 (part

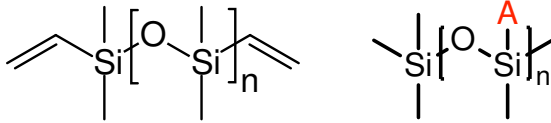
Part 1:  $n \approx 60$ Part 2:  $n \approx 10$ 

Figure D.15: A diagram of silicone crosslinking.

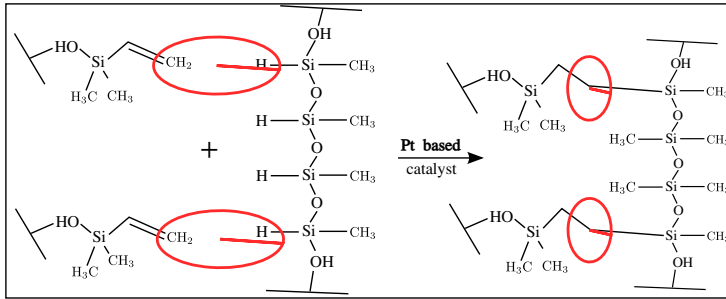


Figure D.16: Reaction diagram of silicone crosslinking.

1) and a second component with a reactive functionality that is much larger than 2 (part 2).

## E Common Polymers

Here we list some common polymer produced by the different synthesis methods introduced in the previous sections.

### E.1 Chain Growth: Addition to a Double Bond

#### E.1.1 Polyethylene

The simplest polymer from a structural standpoint is polyethylene, with the structure shown below in Figure E.1. Tacticity is not relevant in this case, since there are no substituents other than hydrogen on the carbon backbone.

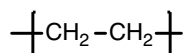


Figure E.1: Chemical structure of polyethylene.

**1) High Density Polyethylene:** High density polyethylene refers to version with very little chain branching, thus resulting in a high degree of crystallinity. Completely linear polyethylene has a melting point of 138 °C, and a glass transition temperature near -100 °C.

$$T_g \approx -120 \text{ }^\circ\text{C}, T_m = 138 \text{ }^\circ\text{C (perfectly linear)}$$

**2) Low Density Polyethylene:** Low density polyethylenes (LDPE's) and high density polyethylenes (HDPE's) are identical in their chemical structure at the atomic level. They are actually structural isomers of one another. Chain branching within low density polyethylene inhibits crystallization, resulting in a material with a melting point lower than 138 degrees C. The decreased crystallinity of LDPE results in a material which is more flexible (lower elastic modulus) than HDPE.

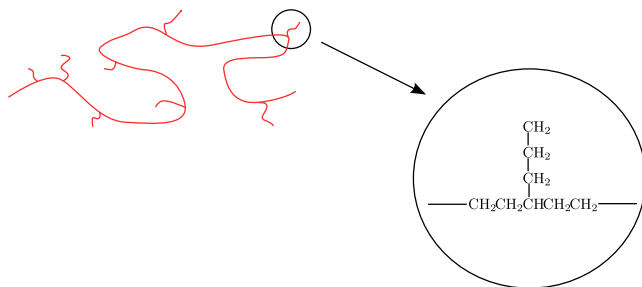


Figure E.2: Structure of low density polyethylene

The chain branches responsible for inhibiting crystallization in low density polyethylene are typically short. This illustration shows a 3-carbon (propyl) branch, potentially resulting from intramolecular chain transfer during the polymerization reaction.

$$T_g \approx -120^\circ\text{C}, T_m < 138^\circ\text{C} \text{ (depending on branching)}$$

**3) The Importance of Molecular Weight:** Polymeric materials generally have favorable mechanical properties only when the molecular weight is very large - typically hundreds of thousands of g/mol. The point is illustrated with polyethylene:

- $M = 16$  g/mol: ethylene gas
- $M \cong 200$  g/mol: candle wax
- $M \cong 2 \times 10^5 - 5 \times 10^5$  g/mol: milk jugs, etc.
- $M \cong 3 \times 10^6 - 5 \times 10^6$  g/mol: ultrahigh molecular weight polyethylene. This materials as excellent toughness and wear resistance, and is often used as one of the contact surfaces in joint implants.

### E.1.2 Polypropylene

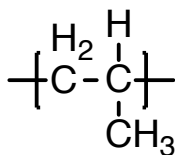


**Figure E.3:** Structure of polypropylene

The most widely used form of polypropylene is isotactic, with a melting point of  $171^\circ\text{C}$  (for the perfectly isotactic version - a few degrees lower for the actual commercial versions), and a glass transition temperature which is well below room temperature ( $\approx 5^\circ\text{C}$ ). Single crystals of polypropylene have lower moduli than single crystals of polyethylene along the chain direction, because of the helical structure of propylene. The modulus of isotropic semicrystalline polypropylene is often larger than that of high density polyethylene, however, because of the details of the semicrystalline structure that is formed. The uses of polypropylene and high density polypropylene are similar.

### E.1.3 Polybutene-1

This polymer included to illustrate the evolution of the polymer properties when we continue to make the side chain longer.

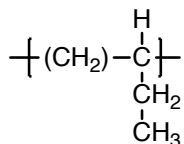


Figure E.4: Polybutene-1

### E.1.4 Poly(methyl methacrylate):

Poly(methyl methacrylate) (PMMA) is one of the most common materials used to make polymer glass. It is commonly known by the DuPont tradename Plexiglas,<sup>TM</sup> and has a glass transition temperature between 100 °C and 125 °C, depending on the tacticity. It also forms the basis for many biomaterials, including dental adhesives.

$$T_g = 100 - 125 \text{ }^\circ\text{C}, \text{ no } T_m \text{ (atactic)}$$

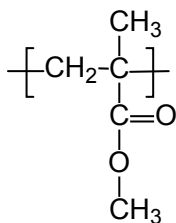


Figure E.5: Poly(methyl methacrylate)

### E.1.5 Poly(methyl acrylate)

Poly(methyl acrylate) is not a widely used polymer, primarily because its glass transition temperature is too low ( $\approx 5 \text{ }^\circ\text{C}$  for the atactic polymer) to be useful as a rigid polymer glass, and too high to be useful as an elastomer. It is included here to illustrate the effect that removing the extra methyl group from the polymer backbone has on the glass transition of the polymer.

$$T_g = 5 \text{ }^\circ\text{C}, \text{ no } T_m \text{ (atactic)}$$



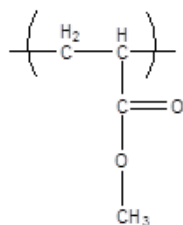


Figure E.6: Poly(methyl acrylate).

### E.1.6 Neoprene

Neoprene, also called polychloroprene, is a material commonly used in wetsuits. Like polyisoprene, it can be polymerized in different forms, corresponding to 1-2, 3-4, cis 1-4 and trans 1-4 addition of the monomer (trans 1-4 addition shown below). This pictured wetsuit has a 0.5mm layer of neoprene sandwiched between layers of nylon and another synthetic material.

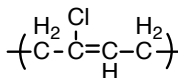


Figure E.7: Neoprene (polychloroprene).

### E.1.7 Polyisobutylene

Polyisobutylene is a common material used to make elastomers, referred to more simply as 'butyl' rubber. It is generally copolymerized by with a small amount of isoprene, so that the resulting double bonds can be used to form a crosslinked material. It is more resistant to solvent penetration than most elastomers, and is often used in applications (like the gloves above) where barrier resistance is needed.

$$T_g = -75^\circ\text{C}, T_m = 2^\circ\text{C}$$

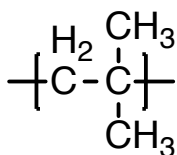


Figure E.8: Polyisobutylene.

### E.1.8 Polystyrene

Polystyrene is almost always atactic, and therefore amorphous. It has a glass transition temperature of 100 °C, and is therefore a glassy polymer at room temperature. Its uses are typically in packing material "Styrofoam", and for making cheap plastic objects, like the vials shown above. When suitably modified by the addition of other types of polymers, it is the basis for relatively high performance plastics such as high impact polystyrene (HIPS) and acrylonitrile-butadiene-styrene (ABS).

$$T_g = 100^\circ\text{C}, \text{ no } T_m \text{ (atactic)}$$

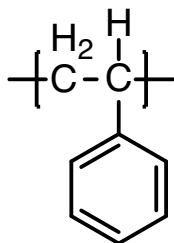


Figure E.9: Structure of polystyrene.

### E.1.9 Poly(tetrafluoroethylene) (PTFE)Poly(tetrafluoroethylene) (PTFE)

Poly(tetrafluoroethylene) is more commonly known by its DuPont trade name, **Teflon**. Its most outstanding properties are its low surface energy and its low friction against a variety of other materials. It has very poor mechanical properties, however, and is difficult to process by its melting temperature exceeds the temperature at which it begins to degrade.

$$T_g = 130^\circ\text{C} \text{ (by one report[17]); } T_m \approx 330^\circ\text{C}.$$

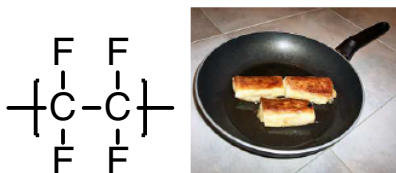


Figure E.10: Monomer unit of poly(tetrafluoroethylene) (Image from[18]).

**E.1.10 Poly(vinyl acetate)**

Poly(vinyl acetate) is often used as base for chewing gum. It is glassy at room temperature but becomes softer at body temperature, which is just above  $T_g$ .

$$T_g = 30^\circ\text{C}, \text{ no } T_m \text{ (atactic)}$$

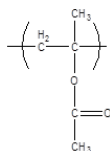


Figure E.11: Monomer unit of poly(vinyl acetate)

**E.1.11 Poly(vinyl chloride) (PVC)**

Poly(vinyl chloride) can be partially crystalline even if the material is atactic, because the "R" group in this case is a chlorine atom, which is relatively small. The glass transition temperature of the material is  $85^\circ\text{C}$ , although the addition of small molecules as "plasticizers" can reduce  $T_g$  to below room temperature. When a material is referred to as "vinyl", it is probably PVC. Record albums (before the age of compact disks) and water pipes are commonly made out of poly(vinyl chloride).

$$T_g = 85^\circ\text{C}, \text{ no } T_m \text{ (atactic)}$$

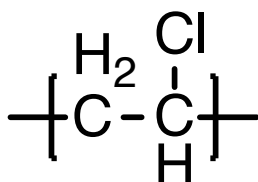


Figure E.12: Structure of poly(vinyl chloride)

**E.1.12 Poly(vinyl pyridine)**

Poly(vinyl pyridine) is very similar to polystyrene, and its physical properties (entanglement molecular weight, *etc.*) are quite similar to the properties of polystyrene. It exists in one of two forms, poly(2-vinyl pyridine) (P2VP

and poly(4-vinyl pyridine) (P4VP), based on the location of the nitrogen in the phenyl ring. Both types interact strongly with metals. The polymers are not used in wide quantities, but have been useful in a range of model studies of polymer behavior, often when incorporated with another material as part of a block copolymer.

$$T_g = 100\text{ }^\circ\text{C, no } T_m \text{ (atactic)}$$

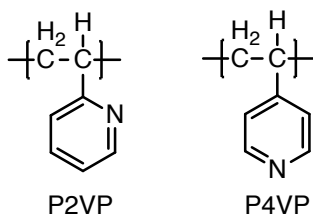


Figure E.13: Structure of two types of poly(vinyl pyridine)

## E.2 Chain Growth: Ring Opening

### E.2.1 Poly(ethylene oxide)

Poly(ethylene oxide) (PEO) is generally formed by the ring opening polymerization of ethylene oxide. It is also referred to as polyethylene glycol, although this generally refers to lower molecular weight versions with hydroxyl end groups. PEO is water soluble, and is used in a wide range of biomedical applications, often in a gel form. Lithium salts are also soluble in PEO, and PEO/Li complexes are often used as an electrolyte in battery and fuel cell applications.

$$T_g = -65\text{ }^\circ\text{C}; T_m \approx 65\text{ }^\circ\text{C}$$

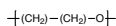


Figure E.14: Monomer unit of poly(ethylene oxide)

### E.2.2 Polycaprolactam:

Polycaprolactam is the polyamide equivalent of polycaprolactone, and is synthesized by the ring opening polymerization of the corresponding cyclic amide. It is often referred to as Nylon 6, since there are 6 carbon atoms in the repeating unit of the polymer. Note that this is different than Nylon 6,6 produced by condensation polymerization, where the repeat unit has 6 carbons originating from each of the two monomers used in the polymerization reaction.

$$T_g \approx 50^\circ\text{C}; T_m \approx 220^\circ\text{C}$$

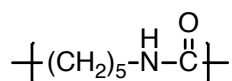


Figure E.15: Polycaprolactam.

### E.2.3 Polycaprolactone:

Polycaprolactone somewhat unique in that is a polyester that is synthesized by ring opening polymerization of a cyclic ester. It can be viewed as a polyester version of the polyamide, polycaprolactam. Contrary to step growth polymerization of polyesters, the ester linkage is not formed during the polymerization reaction, but is already present in the monomer. Polycaprolactone is biodegradable because the polymer slowly degrades by ester hydrolysis over time.

$$T_g \approx -50^\circ\text{C}; T_m = 60^\circ\text{C}$$

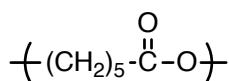


Figure E.16: Polycaprolactone.

## E.3 Step Growth Polymers

A variety of common polymers are discussed briefly in the pages below.

### E.3.1 Kevlar™

Kevlar™ is a trademark of DuPont, Inc. The name actually is used to refer to a variety of aromatic polyamides, or aramids. As the name suggests, the polymers have phenyl groups in the backbone of the chain, and the repeat units are joined by amide linkages. The simplest possible aramid has the structure shown in Figure E.17.

$T_m$ : above degradation temperature for the polymer.

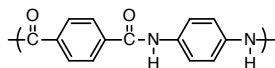


Figure E.17: Monomer unit of one version of Kevlar

### E.3.2 Polycarbonate

A variety of polycarbonates exist. The most common one, (with the GE trademark of Lexan) has a glass transition temperature of 150 °C. It is used for compact disks, eyeglass lenses, and shatterproof glass. See <http://www.pslc.ws/macrog/pcsyn.htm> for a good description of the synthesis of polycarbonate via a step growth, condensation reaction involving a phenolic di-alcohol and phosgene ( $\text{COCl}_2$ ).

$$T_g \approx 150^\circ\text{C}$$

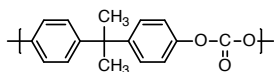


Figure E.18: Polycarbonate.

### E.3.3 Polyethylene Terephthalate (PET)

Polyethylene terephthalate (trade names include Mylar and Dacron) is produced in fiber form for textiles, and in film form for recyclable bottles, etc. Its degree of crystallinity is highly dependent on the processing conditions, since it can easily be quenched to a glassy state before crystallization is able to occur.

$$T_g = 80^\circ\text{C}$$

$$T_m = 260^\circ\text{C}$$

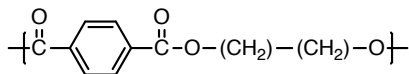


Figure E.19: Polyethylene Terephthalate

### E.3.4 Poly(phenylene oxide)

Polyphenylene oxide is a high performance polymer has many varied uses, largely because of its excellent performance at high temperatures.

$$T_g \approx 190^\circ\text{C}$$

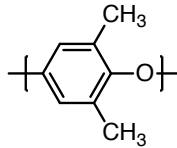


Figure E.20: Poly(phenylene oxide). <http://plastiquarian.com/ppo.htm>

### E.3.5 Ultem Polyetherimide

Ultem (a trademark of GE) is a form of polyetherimide. It is a high performance polymer that combines high strength and rigidity at elevated temperatures with long term heat resistance ( $T_g = 215^\circ\text{C}$ ). The repeat unit is illustrative of the complex chemical structure of many modern, high performance polymers.

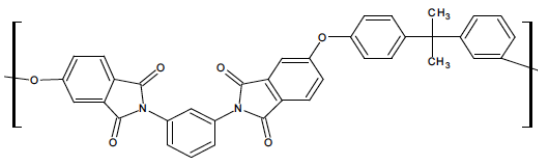


Figure E.21: Structure of Ultem polyetherimide, with some materials that have been made from it. [http://www.alcanair.com/products/e/100/120p01\\_e.htm](http://www.alcanair.com/products/e/100/120p01_e.htm)

### E.3.6 Silicones

Silicones are an important class of synthetic polymers which do not have carbon in the backbone. Instead, the backbone consists of alternating silicon and oxygen atoms. Different classes of silicones are specified by the substituents on the silicon atoms. Poly(dimethyl siloxane) (PDMS), with methyl substituents, is the most important silicone. Its glass transition and melting temperatures



Figure E.22: Poly(dimethyl siloxane).

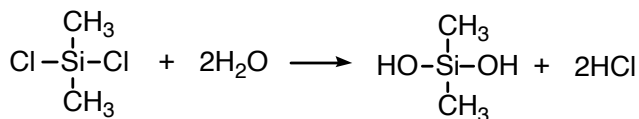


Figure E.23: Hydrolysis of chlorosilane bonds.

are very low, so that it remains flexible at very low temperatures. It also has a very low surface energy, and forms a hydrophobic surface that is very water resistant.

$$T_g = \sim -130^\circ\text{C}; T_m = -45^\circ\text{C}$$

We list PDMS here as a step growth polymer because it can be produced from a self-condensation of silanol (SiOH) groups. The starting point is actually dimethyl-dichlorosilane. In the presence of water the SiCl bonds hydrolyze to SiOH:

The resultant silanol groups can then condense by the elimination of water:

One of the interesting features of silicones is that they can also be synthesized by anionic, ring opening polymerization of cyclic, oligomeric forms of PDMS. Here's one example:

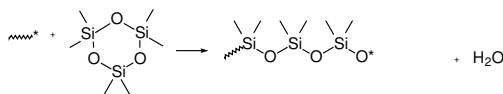
## E.4 Copolymers

The polymers considered so far are homopolymers, which means they consist of a single chemical repeat unit. Copolymers consist of more than one repeat

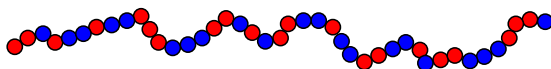


Figure E.24: Condensation of silanol groups.





**Figure E.25:** Anionic ring opening polymerization of a cyclic silicone oligomer.



**Figure E.26:** Schematic representation of a statistical copolymer.

unit. Examples include **statistical copolymers**, where the different repeating units are distributed throughout a molecule, as shown schematically in Figure E.26.

In **block copolymers**, the different repeating units appear as distinct 'blocks'. A diblock copolymer for example, can be viewed as two different homopolymer molecules that have been covalently joined to one another as shown in Figure E.27. A wide variety of interesting block copolymer morphologies have been observed. Diblock copolymers are most often synthesized by living, chain growth polymerizations.

**4) Exercise:** Describe a procedure for making a diblock copolymer of polystyrene and poly(methyl methacrylate).

**5) Solution:** The details of how to do this go a bit beyond the scope of this text, but conceptually we know we need to do the following in sequence: Add an appropriate initiator for a living chain growth polymerization, add monomer 'A' until all of it reacts, add monomer B until all of it reacts, terminate the reaction. Here are the details that can work for this system.

- (a) Add an appropriate initiator. We don't want to use a radical initiator, because we need to avoid the inevitable termination reactions. From the information given in this text, either anionic or cationic polymerization. It turns out that the only anionic polymerization works in this case. We'll choose tetrahydrofuran as a solvent, clean it up very well to get rid of any impurities, and add some secondary butyllithium (see

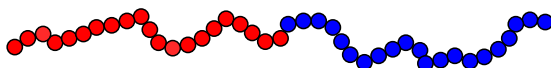


**Figure E.27:** Schematic representation of a block copolymer.

Fig. D.5) as the initiator. The molar quantity of initiator will be equal to the number of moles of polymer we get at the end of the reaction.

- (b) Add the first monomer to the initiator solution. The order matters in this case. We need to add the styrene first, and choose reaction conditions so that the initiation is much faster than the subsequent polymerization. This ensures that the polymers all have roughly the same length, since they all started polymerizing at the same time.
- (c) Once all the styrene reacts, we add the methyl methacrylate monomer to the solution. Because the polymerization is 'living', the active chain ends from the polystyrene part of the polymerization are still available to react with the methyl methacrylate.
- (d) Terminate the reaction. This is very easy to do, and can be done by adding a small amount of methanol to the reaction, to produce lithium methoxide and a 'dead' chain after the proton from alcohol trades places with the lithium that is associated with the negatively charged carbon at the end of the polymer chain.

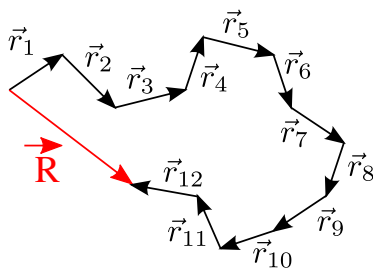


Figure F.1: Vector diagram of a polymer.

## F Models of Chain Dimensions

Our discussion of random walk statistics tells us what the shapes of the molecules look like when we know the statistical segment length, but it doesn't tell us what the statistical segment length actually is for a particular polymer. Clearly the statistical segment length must be related to the detailed chemical structure of the repeat unit itself. For example, we wouldn't expect that polyvinyl chloride and polyethylene terephthalate would have the same statistical segment length, based on the very different chemical structures of these polymers. To obtain a prediction for the statistical segment length we need to zoom in and consider the actual backbone bonds that are connecting the polymer together. In general every bond is vector,  $\vec{r}$  with a length and an orientation. As illustrated in Figure F.1, the end-to-end vector is obtained by adding up all  $N_b$  bond vectors ( $N_b=12$  in this example):

$$\vec{R} = \sum_{i=1}^{N_b} \vec{r}_i = \vec{r}_1 + \vec{r}_2 + \vec{r}_3 + \dots + \vec{r}_{N_b} \quad (\text{F.1})$$

### F.1 General Considerations

We are interested in the average magnitude of the end-to-end vector. As discussed in the previous section, the average of  $\vec{R}$  itself is not useful, since it just averages to zero. We are interested in the average value of the square of the magnitude of the end-to end vector. This quantity is equal to the dot product of the end-to-end vector with itself:

$$R^2 = \vec{R} \cdot \vec{R} = (\vec{r}_1 + \vec{r}_2 + \vec{r}_3 + \dots + \vec{r}_{N_b}) \cdot (\vec{r}_1 + \vec{r}_2 + \vec{r}_3 + \dots + \vec{r}_{N_b}) \quad (\text{F.2})$$

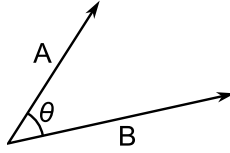


Figure F.2: Definition of the angle between two vectors.

The dot product has  $N_b^2$  terms, which can be represented in the following matrix form:

$$R^2 = \begin{Bmatrix} \vec{r}_1 \cdot \vec{r}_1 & +\vec{r}_1 \cdot \vec{r}_2 & +\vec{r}_1 \cdot \vec{r}_3 & +\dots & +\vec{r}_1 \cdot \vec{r}_{N_b} \\ +\vec{r}_2 \cdot \vec{r}_1 & +\vec{r}_2 \cdot \vec{r}_2 & +\vec{r}_2 \cdot \vec{r}_3 & +\dots & +\vec{r}_2 \cdot \vec{r}_{N_b} \\ +\vec{r}_3 \cdot \vec{r}_1 & +\vec{r}_3 \cdot \vec{r}_2 & +\vec{r}_3 \cdot \vec{r}_3 & +\dots & +\vec{r}_3 \cdot \vec{r}_{N_b} \\ +\dots & +\dots & +\dots & +\dots & +\dots \\ +\vec{r}_{N_b} \cdot \vec{r}_1 & +\vec{r}_{N_b} \cdot \vec{r}_2 & +\vec{r}_{N_b} \cdot \vec{r}_3 & +\dots & +\vec{r}_{N_b} \cdot \vec{r}_{N_b} \end{Bmatrix} \quad (F.3)$$

The dot product between two vectors,  $\vec{A}$  and  $\vec{B}$  is given in general by  $|\vec{A}||\vec{B}|\cos\theta$  where  $\theta$  is the angle between the two vectors, illustrated below in Figure F.2. At this point we will make our first simplifying assumption, which is that the lengths of all bonds along the backbone are identical. This assumption is certainly valid for vinyl polymers, and other polymers which have only C-C single bonds along the backbone.

If this bond length is  $\ell$ , then  $R^2$  can be represented as follows, where  $\theta_{ij}$  is the angle between bond  $i$  and bond  $j$ :

$$R^2 = \ell^2 \begin{Bmatrix} \cos\theta_{11} & +\cos\theta_{12} & +\cos\theta_{13} & +\dots & +\cos\theta_{1N_b} \\ +\cos\theta_{21} & +\cos\theta_{22} & +\cos\theta_{23} & +\dots & +\cos\theta_{2N_b} \\ +\cos\theta_{31} & +\cos\theta_{32} & +\cos\theta_{33} & +\dots & +\cos\theta_{3N_b} \\ +\dots & +\dots & +\dots & +\dots & +\dots \\ +\cos\theta_{N_b1} & +\cos\theta_{N_b2} & +\cos\theta_{N_b3} & +\dots & +\cos\theta_{N_bN_b} \end{Bmatrix} \quad (F.4)$$

The average value of  $R$ , will be determined by the average values of  $\theta_{ij}$ . In mathematical terms, we have the following expression:

$$\langle R^2 \rangle = \ell^2 \begin{Bmatrix} \langle \cos\theta_{11} \rangle & +\langle \cos\theta_{12} \rangle & +\langle \cos\theta_{13} \rangle & +\dots & +\langle \cos\theta_{1N_b} \rangle \\ +\langle \cos\theta_{21} \rangle & +\langle \cos\theta_{22} \rangle & +\langle \cos\theta_{23} \rangle & +\dots & +\langle \cos\theta_{2N_b} \rangle \\ +\langle \cos\theta_{31} \rangle & +\langle \cos\theta_{32} \rangle & +\langle \cos\theta_{33} \rangle & +\dots & +\langle \cos\theta_{3N_b} \rangle \\ +\dots & +\dots & +\dots & +\dots & +\dots \\ +\langle \cos\theta_{N_b1} \rangle & +\langle \cos\theta_{N_b2} \rangle & +\langle \cos\theta_{N_b3} \rangle & +\dots & +\langle \cos\theta_{N_bN_b} \rangle \end{Bmatrix} \quad (F.5)$$

In more compact notation we can write:

$$\langle R^2 \rangle = \ell^2 \sum_{i,j=1}^{N_b} \langle \cos \theta_{ij} \rangle \quad (\text{F.6})$$

So we have reduced the problem to figuring out what the values of  $\langle \cos \theta_{ij} \rangle$  are in the system. This requires a specific model of how the bonds are joined to one another. In the following sections we consider two specific models (the freely jointed and freely rotating models), and a general model where the bond rotation angles are constrained.

## F.2 Freely Jointed Chain Model

The simplest (and most unrealistic) model of chain dimensions is the freely jointed chain model, where all bond orientations are equally likely. In the freely jointed chain model  $\langle \cos \theta_{ij} \rangle = 0$  for  $i \neq j$ , because orientations giving positive and negative values of  $\cos \theta_{ij}$  are equally likely. The only exception is for the  $N_b$  diagonal terms for which  $i = j$ . These represent the projection of a vector onto itself, and all have  $\theta = 0$  and  $\cos \theta = 1$ .

$$\langle R^2 \rangle = N_b \ell^2 \quad (\text{F.7})$$

## F.3 Freely Rotating Chain Model

In this model, bond angles are fixed, but rotation about bonds is possible. Rotation about a bond sweeps out a cone as shown below. The bond rotation angle is defined as  $\phi$ , and in the freely rotating model all values of  $\phi$  are assumed to be equally likely.

In the freely rotating chain model, the angle between adjacent bonds is fixed at certain angle, referred to here simply as  $\theta$  (without the subscripts). Adjacent bonds, *i.e.* those with  $i - j = 1$  or  $i - j = -1$ , have  $\langle \cos \theta_{ij} \rangle = \cos \theta$ . It can be shown that terms with  $i - j = 2$  or  $-2$  have  $\langle \cos \theta_{ij} \rangle = \cos^2 \theta$ , terms with  $i - j = 3$  or  $-3$  have  $\langle \cos \theta_{ij} \rangle = \cos^3 \theta$ , etc. The matrix of terms making up the summation to give  $\langle R^2 \rangle$  therefore has the following form:

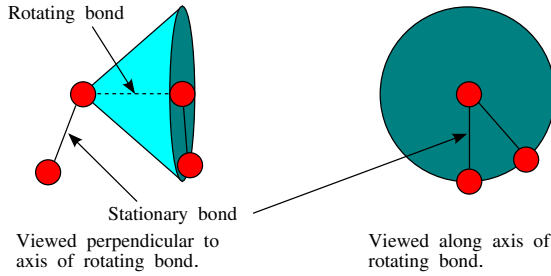


**Figure F.3:** Freely Rotating Chain Models with views perpendicular to the axis of the rotating bond and along the axis of the rotating bond

$$\langle R^2 \rangle = \ell^2 \left\{ \begin{array}{cccccc} 1 & + \cos \theta & + \cos^2 \theta & + \dots & + \cos^{(N_b-1)} \theta \\ + \cos \theta & + 1 & + \cos \theta & + \dots & + \cos^{(N_b-2)} \theta \\ + \cos^2 \theta & + \cos \theta & + 1 & + \dots & + \cos^{(N_b-3)} \theta \\ + \dots & + \dots & + \dots & + \dots & + \dots \\ + \cos^{(N_b-1)} \theta & + \cos^{(N_b-2)} \theta & + \cos^{(N_b-3)} \theta & + \dots & + 1 \end{array} \right\} \quad (F.8)$$

Of the  $N_b^2$  terms in the summation,  $N_b$  terms (the diagonal terms with  $i = j$ ) are equal to 1. There are  $N_b - 1$  terms with  $i - j=1$ , and an additional  $N_b-1$  terms with  $i - j=-1$ . There are therefore  $2(N_b-1)$  terms with a magnitude equal to  $\cos \theta$ . Similarly, there are  $2(N_b - 2)$  terms equal to  $\cos^2 \theta$ ,  $2(N_b - 3)$  terms equal to  $\cos^3 \theta$ , etc. The expression for  $\langle R^2 \rangle$  can therefore be written as follows:

$$\langle R^2 \rangle = \ell^2 \left\{ N_b + 2(N_b - 1) \cos \theta + 2(N_b - 2)(\cos \theta)^2 + \dots + 2(\cos \theta)^{N_b-1} \right\}$$

In the more compact notation, we have:

$$\langle R^2 \rangle = N_b \ell^2 + \ell^2 \sum_{i=1}^{N_b-1} 2(N_b - i) (\cos \theta)^i \quad (F.9)$$

Equation F.9 is an exact expression that is valid for any value of  $N_b$ . Unfortunately, it's not a very useful equation. Fortunately, we can get a greatly simplified expression that is very nearly exact for any reasonably large value of  $N_b$ . We are able to do this because  $\cos \theta$  is less than one, so that  $(\cos \theta)^i$  rapidly decreases as  $i$  increases. For example, for  $\theta = 71^\circ$  (the value corresponding to C-C single bonds),  $(\cos \theta)^i = 1.3 \times 10^{-5}$  for  $i = 10$ . For large values of  $N_b$ , we

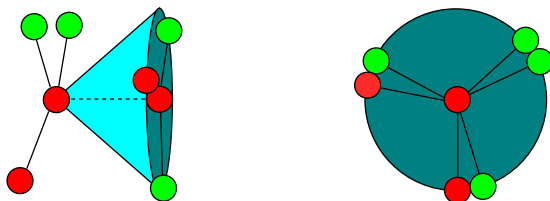


**Figure F.4:** Bond angle restrictions shown perpendicular and along the axis of rotation (Newman projection).

only need to consider contributions from values of  $i$  which are much smaller than  $N_b$ . A very good approximation is obtained by substituting  $N_b$  for  $N_b - i$  and extending the sum to  $i = \infty$ , which leads to the following:

$$\langle R^2 \rangle = N_b \ell^2 \left\{ 1 + 2 \sum_{i=1}^{\infty} (\cos \theta)^i \right\} \quad (\text{F.10})$$

At this point we are in a position to use the following standard sum, valid for any value of  $x$  with an absolute magnitude less than 1:

$$\sum_{i=1}^{\infty} x^i = \frac{x}{1-x} \quad (\text{F.11})$$

Use of this expression with  $x = \cos \theta$  gives (after a little algebraic rearrangement):

$$\langle R^2 \rangle = N_b \ell^2 \left\{ \frac{1 + \cos \theta}{1 - \cos \theta} \right\} \quad (\text{F.12})$$

For singly bonded carbon along the backbone,  $\theta = 71^\circ$  and  $\langle R^2 \rangle = 2N_b \ell^2$ .

## F.4 Bond Angle Restrictions

The freely rotating model is overly simplistic, because all bond rotation angles cannot be equally likely. At certain angles, functional groups attached to adjacent carbon atoms are too close to one another, as illustrated here.

Interferences between functional groups cause the free energy to vary as a function of the bond rotation angle,  $\phi$ , with an energy vs.  $\phi$  curve that looks

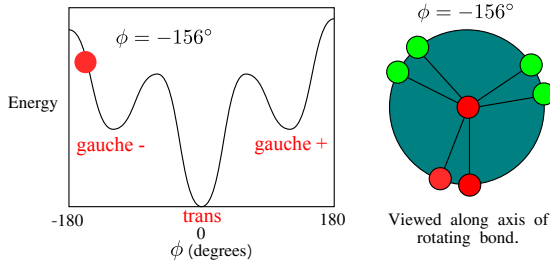


**Figure F.5:** Energy as a function of bond rotation angle.

like the one shown in Figure F.5. The **trans configuration**, where  $\phi = 0$ , has the lowest free energy, because the backbone carbon bonds are as far from each other as possible in this configuration. Secondary minima in the energy exist for  $\phi = \pm 120^\circ$ , where there is minimal overlap between the additional groups bonded to the carbon carbon molecules. These configurations are referred to as the **gauche configurations**.

We know that the freely rotating chain model must also be overly simplistic, because some bond rotation angles (those corresponding to the gauche and trans configurations, for example) are more likely than others. In this case  $\langle R^2 \rangle$  is given by the following expression, which we present here without proof.

$$\langle R^2 \rangle = N_b \ell^2 \left\{ \frac{1 + \cos \theta}{1 - \cos \theta} \right\} \left\{ \frac{1 + \langle \cos \phi \rangle}{1 - \langle \cos \phi \rangle} \right\} \quad (\text{F.13})$$

Here  $\langle \cos \phi \rangle$  is the average of  $\cos \phi$ , taking into account the fact that not all angles are equally likely. Note that  $\langle \cos \phi \rangle = 0$  for the freely rotating chain model, in which case Eq. F.13 reduces to Eq. F.12.

## F.5 Characteristic Ratio

The **characteristic ratio**,  $C_\infty$ , is defined as the ratio of the actual value of  $\langle R^2 \rangle$  to the value which would be obtained from the freely jointed chain model:

$$C_\infty \equiv \frac{\langle R^2 \rangle}{N_b \ell^2} \quad (\text{F.14})$$

Each model of chain dimensions has its own prediction for the value of  $C_\infty$ . For a chain with fixed bond angles, comparison to Eq. F.13 gives the following:

$$C_\infty = \left\{ \frac{1 + \cos \theta}{1 - \cos \theta} \right\} \left\{ \frac{1 + \langle \cos \phi \rangle}{1 - \langle \cos \phi \rangle} \right\} \quad (\text{F.15})$$



1) **Exercise:** What would the characteristic ratio be for polystyrene if 70% of the bonds were in trans configurations and the remaining 30% were in gauche configurations?

2) **Solution:** We use Eq. F.15 for  $C_\infty$ , with  $\theta = 71^\circ$ , the correct bond angle for singly bonded carbon, which we have along the polystyrene backbone. Gauche bonds have  $\phi = \pm 120^\circ$  ( $\cos \phi = -0.5$ ) trans bonds have  $\phi = 0$  ( $\cos \phi = 1$ ). With our assumed distribution of gauche and trans bonds we obtain the following for  $\langle \cos \phi \rangle$ :

$$\langle \cos \phi \rangle = 0.7(1) + 0.3(-0.5) = 0.55$$

This gives  $C_\infty = 6.9$ , which is actually a pretty reasonable value. Most polymers with singly bonded carbons along the backbone have a value for  $C_\infty$  that is between 6 and 10.

3) **Exercise:** How is the statistical segment length of a vinyl polymer related to  $C_\infty$ ?

4) **Solution:** The characteristic ratio and statistical segment length are both defined in terms of an expression for  $R^2$ . All we need to do is equate these two expressions (Eqs. 5.17 and F.14):

$$C_\infty N_b \ell^2 = N a^2 \tag{F.16}$$

The repeat unit for a vinyl polymer contains two C-C single bonds along the backbone, so  $N_b = 2N$ . Also, single bonds between carbon atoms have a bond length of 1.54 Å. The statistical segment length is therefore related to  $C_\infty$  as follows:

$$a = 2.18 \text{Å} \sqrt{C_\infty} \tag{F.17}$$

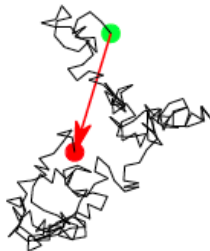


Figure F.6: Random walk diagram

## F.6 Self-Avoiding Random Walks

An isolated polymer molecule in a solvent no longer obeys random walk statistics. If the polymer is surrounded by solvent molecules, these surroundings no longer look the same as other parts of the same molecule. The chain will adopt shapes that avoid direct polymer/polymer contacts, and the end-to-end distance will be larger than the value predicted by random walk models. The rms end-to-end distance increases with the 0.6 power of the chain length, instead of the 0.5 power that was obtained for random walk statistics:

$$R_0 = a_s N^{0.6} \quad (\text{F.18})$$

Note: The value of  $a_s$  is not exactly the same as the statistical segment length describing chain dimensions in pure polymer melts, but it will be close to it.

## G Semicrystalline Polymers

Many polymers of commercial importance are able to crystallize to a certain extent. The most widespread crystallizable polymers are polyethylene and isotactic polypropylene. As we will see, crystallization is never complete, and there is always a certain amorphous fraction in any polymer. For this reason, many of the concepts which apply to amorphous polymers are still valid for semicrystalline polymers. For example, semicrystalline polymers are often quite brittle at temperatures below the glass transition temperature of the amorphous fraction.

In the following pages, we introduce some common semicrystalline polymers, and discuss their basic structural features, in addition to kinetic issues that are important in their processing.

### G.1 Structural Hierarchy in Semicrystalline Polymers

The structure of semicrystalline polymers is much more complex than the structure of amorphous polymers, and our discussion in the following pages is not as quantitative as our discussion of the random walk configurations of polymer chains in amorphous polymers. Instead, we illustrate the features of semicrystalline polymers by considering the following basic structural features:

- (a) Helices formed by individual polymer molecules
- (b) Perfect crystals formed by the lateral packing of these helices
- (c) Lamellar crystallites formed by folded helices
- (d) Semicrystalline regions formed by stacking of lamellar crystallites
- (e) Spherulitic morphologies formed by radial growth of lamellar crystallites

### G.2 The Structural Repeat Unit

The molecular structure is an important factor in the ability of a polymeric material to crystallize. One relevant parameter related to the structure of vinyl polymers is the number of backbone carbons per **structural repeat unit**, which is distinct from the **monomeric repeat unit** that is defined in terms of the structure of the monomer itself. Polyethylene, for example, can be viewed as a repeating string of  $\text{CH}_2$  units, so there is one carbon atom per structural repeat unit, although there are two carbon atoms per monomeric repeat unit. Tacticity needs

to be accounted for as well. Isotactic vinyl polymers have two backbone carbon atoms per structural repeat, because all non-hydrogen substituent groups are on the same side of the molecule. Syndiotactic vinyl polymers have four backbone carbon atoms per structural repeat, because the substituent groups alternate between different sides of the molecule.

**1) Exercise:** What are the structural repeats for each of the following polymers:

- (a) Poly(tetrafluoroethylene)
- (b) Syndiotactic Polypropylene
- (c) Isotactic Polypropylene
- (d) Atactic Polystyrene

**Solution:**

- (a) The repeating unit here is simply  $\text{CF}_2$  since I can reconstruct the polymer simply by connecting these units to one another.
- (b) The repeating unit here contains 4 backbone carbons and two methyl groups, since there is a methyl group on every other carbon, and these methyl groups alternate from one side of the backbone to the other.
- (c) In this case there are two backbone carbons and a single methyl group (a single propylene unit).
- (d) Since the polymer is atactic, it has an inherently disordered structure, with no structural repeat. This is why it is always amorphous.

### G.3 Helix Formation

The first step in understanding the structure of crystalline polymer is to understand the shapes that the polymer molecules take when they pack within the crystalline structure. The simplest situation is for a molecule like polyethylene, for which the molecules in the crystalline structure are all fully extended, with all of their bonds in the trans configuration as shown in Figure G.1.

The planar zigzag configuration is one special case of the shapes of polymers along the chain axis. In the more general case, the backbone carbon atoms all lie along the a helix that is formed about some central axis. Helices of vinyl polymers form by rotation about the C-C single bonds which make up the backbones of the molecules. The curved line in the side view of the planar

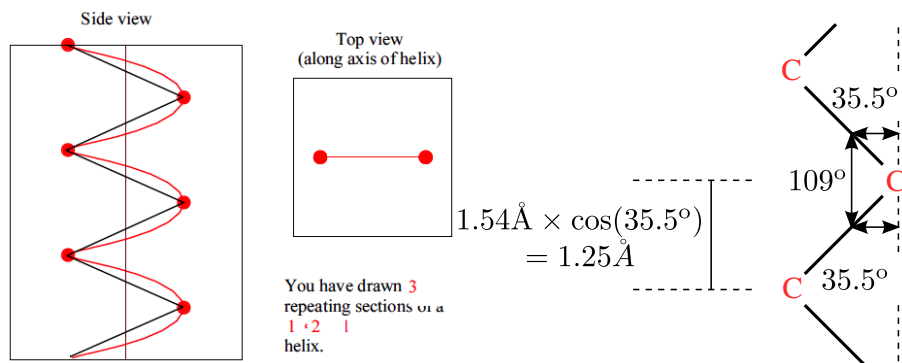


**Figure G.1:** Diagram of a planar zigzag (left), with the specific geometry for tetrahedrally bonded carbon (right). Note that the bond angles appear distorted in the leftmost portion of the figure because the horizontal and vertical scales are not necessarily equivalent.)

zigzag in Figure G.1 represents the helix that passes through each of the carbon atoms in a single molecule in the polyethylene crystal structure.

The general notation describing the helical structure is  $x * y/z$  where  $x$ ,  $y$  and  $z$  are defined as follows:

- $x$ : the number of backbone carbons in the structural repeat. This is the only number that we can get by looking at the molecular structure of the polymer itself. We need to know the crystal structure to know what  $y$  and  $z$  are.
- $y$ : the number of structural repeats per crystallographic repeat. This means that the product  $xy$  gives the number of carbon atoms that repeat along the chain direction within one unit cell.
- $z$ : the number of turns of the helix per crystallographic repeat.

The planar zigzag can be formally viewed as a 1\*2/1 helix, with 3 turns of the helix shown in Figure G.1. From the top view, we see that all of the backbone atoms of this helix are in the same plane. More complicated helices form because of steric interactions between the other substituents that are placed on the carbon backbones. It's easy for polyethylene molecules to adopt an all-trans configuration because the hydrogen atoms are small and don't interfere with each other when the polymer chain adopts this particular shape. Fluorine atoms are larger than hydrogens, however, so poly(tetrafluorethylene) (Teflon™) adopts a more complicated, 13/7 helix, which is shown below in Figure G.2.

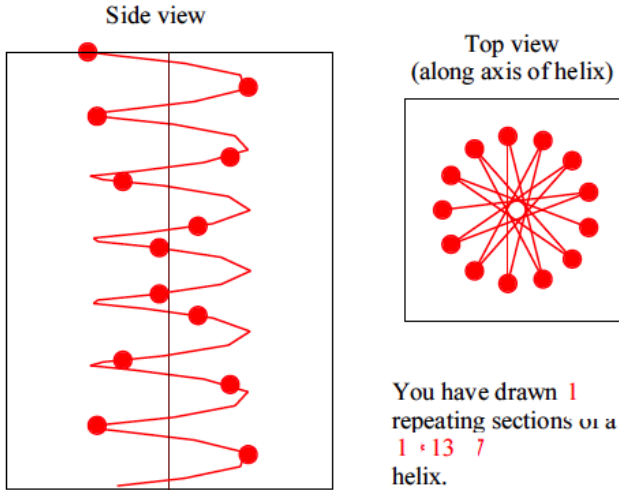


Figure G.2: Representation of a 13/7 helix.

2) **Exercise:** What is length of a polyethylene molecule with  $M = 10,000$  g/mole, if the molecule is in all-trans (planar zigzag) configuration.

3) **Solution:** For bond angle,  $\theta$ , for singly bonded carbon atoms are  $71^\circ$ , and the C-C bond length is  $1.54 \text{ \AA}$ . From the drawing below, we see that the projected length of this bond along the direction of the zigzag is equal to  $1.25 \text{ \AA}$ . We just need to multiply this length by the number of carbons in the polyethylene chain, which we get by dividing the molecular weight of  $10,000$  g/mole by the molecular weight of a single  $\text{CH}_2$  unit ( $14$  g/mole). This gives the following for the total length,  $L$ :

$$L = 1.25 \text{ \AA} \left( \frac{10,000 \text{ g/mole}}{14 \text{ g/mole}} \right) = 960 \text{ \AA}$$

## G.4 Crystalline unit cells

The structure of a perfect, three dimensional crystal, is defined by the lateral packing of polymer helices into repeating structure. As with any crystalline material, the structure is defined by the unit cell dimensions, and by the contents of the unit cell. The dimensions of the unit cell are defined by three lengths ( $a$ ,  $b$  and  $c$ ) and by three angles ( $\alpha$ ,  $\beta$  and  $\gamma$ ), as illustrated in Figure G.3.

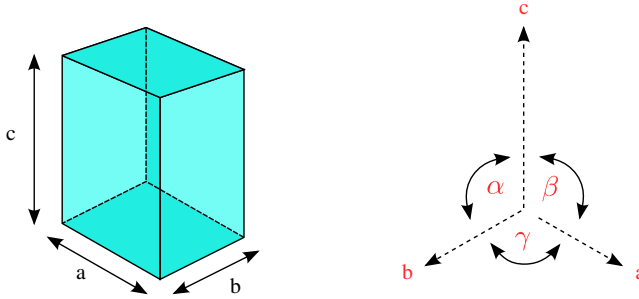


Figure G.3: Diagram of a crystalline unit cell.

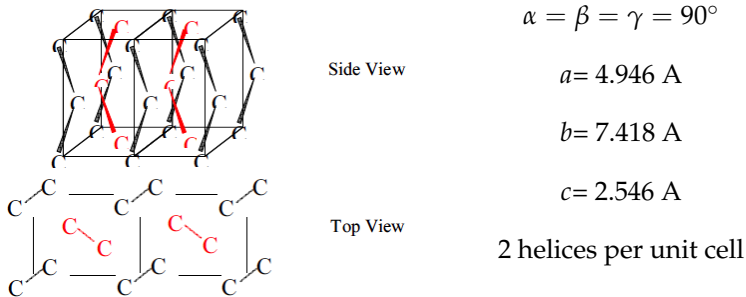


Figure G.4: Structure of polyethylene I.

The perfect crystal structure of a polymer is defined by the helix type, unit cell dimensions and by the packing of the helices in the unit cell. Polyethylene can exist in multiple crystal structures. One of these, referred to as polyethylene I, is illustrated in Figure G.4. This crystal structure has two  $1\frac{1}{2}/1$  helices packed into an orthorhombic unit cell ( $\alpha = \beta = \gamma = 90^\circ$ ). As is often the case, the helix axis corresponds to the  $c$  direction of the unit cell.

Polymer	Helix Type	a, b, c (Å)	$\alpha, \beta, \gamma$	structural unit- s/cell
polyethylene I	1*2/1	7.41, 4.95, 2.55	90, 90, 90	4
polyethylene II	1*2/1	8.09, 4.79, 2.53	90, 107.9, 90	4
poly(tetrafluoroethylene) I	1*1/1	5.59, 5.59, 16.88	90, 90, 113.3	13
polypropylene (syndiotactic)	4*2/1	14.50, 5.60, 7.40	90, 90, 90	8
polypropylene (isotactic)	2*3/1	6.66, 20.78, 6.50	90, 99.6, 90	12
PET	12*1/1	4.56, 5.96, 10.75	98.5, 118, 112	
Polyisoprene (cis 1,4)	8*1/1	12.46, 8.86, 8.1	90, 90, 90	8

**4) Exercise:** Calculate the density of perfectly crystalline polyethylene, given assuming the crystal structure from the previous page.

**5) Solution:** Density is mass/volume, so we just need to calculate the volume of a unit cell, and the total mass of material included in the unit cell:

1. Unit cell volume:  $a \cdot b \cdot c = 9.341 \times 10^{-23} \text{ cm}^3$

2. Mass: 14 g/mole =  $2.326 \times 10^{-23} \text{ g}$  per  $\text{CH}_2$  unit. Since there are 4  $\text{CH}_2$  units in a unit cell, mass per unit cell =  $4(2.326 \times 10^{-23} \text{ g}) = 9.302 \times 10^{-23} \text{ g}$ .

3. Density = mass/volume =  $0.996 \text{ g/cm}^3$ .

Note that the density is close to  $1 \text{ g/cm}^3$ , which is generally true for most polymers.

## G.5 Stiffness of Polymer Single Crystals

Single crystal polyethylene has the following calculated values for the modulus along the 3 crystal axes:

- $E=315 \text{ GPa}$  along c axis
- $E=8.0 \text{ GPa}$  along a axis
- $E=9.9 \text{ GPa}$  along b axis



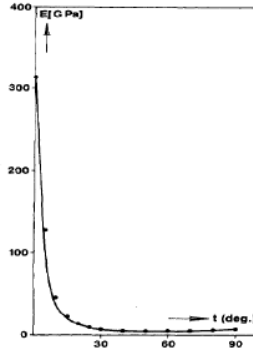


Figure G.5: Macromol. 23, 2365-2370 (1990).

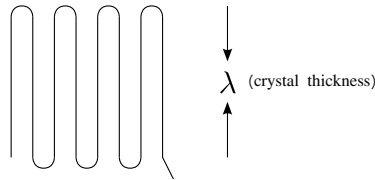


Figure G.6: Diagram of polymer chain folding

Amorphous fraction:  $E=0.001$  GPa

The actual modulus is almost always much lower than this because of imperfect crystal alignment, chain folding and the presence of an amorphous fraction. See the following pages for details.

## G.6 Chain Folding

The solid line in this animation represents the axis of a helix. As the polymer crystallizes, the helix folds back and forth on itself, producing a flat, plate-like lamellar crystallite. The chain folds are energetically unfavorable - the configuration with the lowest free energy would be for the helices to pack in a completely extended manner, with no chain folds at all. However, the chain-folded structure is favored kinetically. Thin crystallites (low values of the **crystal thickness**,  $\lambda$ ), are able to form much more quickly than crystallites with high values of  $\lambda$ .

### G.6.1 Models of chain folding

These drawings illustrate two extreme views of the structure of chain folded crystals. In the adjacent reentry model, the molecules are assumed to fold

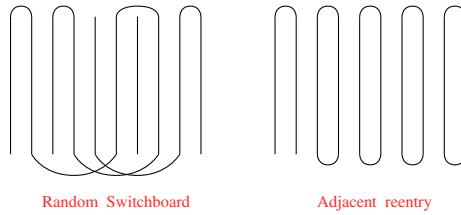


**Figure G.7:** Extreme views of chain folded crystals

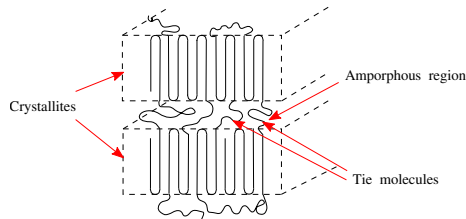


**Figure G.8:** Lamellar crystallites

back on themselves in a very well-organized way. In the random switchboard model, chains which leave the crystal at the tops and bottom surfaces reenter the crystal at random positions. Reality lies somewhere between these two extremes.

### G.6.2 Amorphous Fraction and Tie Molecules

Isolated **lamellar crystallites** can be obtained from polymers crystallized from dilute solution, but melt-crystallized polymers often have structures similar to what is illustrated here. The lamellar, platelike crystallites are separated by amorphous regions. Individual crystallites are bridged by **tie molecules**. These tie molecules span the amorphous region, and are incorporated into adjacent crystallites.

### G.6.3 Percent Crystallinity for Lamellar Crystallites

The amorphous fraction in a semicrystalline polymer resides between the lamellar crystallites as depicted here. If the crystallites are assumed to be perfectly crystalline, the percent crystallinity is given by the ratio of the **crystal thickness** ( $\lambda_c$ ) to the **crystal period** ( $d_c$ ). The crystal period is determined from x-ray scattering measurements. The overall percent crystallinity is determined by measuring the density of the sample.

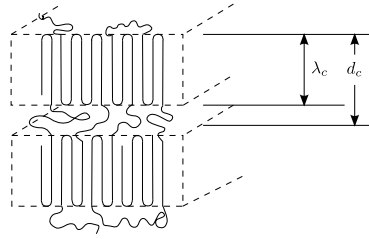


Figure G.9: Diagram of percent crystallinity of lamellar crystallites

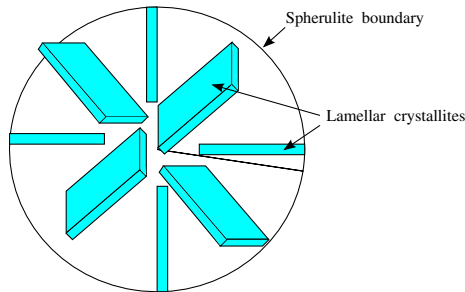


Figure G.10: A representation of a spherulite

## G.7 Spherulitic morphologies

A **spherulite** originates from the radial growth of lamellar crystallites from a central nucleation point. Not all semicrystalline polymers have spherulitic morphologies, but this morphology is quite common.

During crystallization, the spherulite grows radially outward, with each branch extending in the growth direction while maintaining a constant crystal thickness,  $\lambda_c$ .

This is the geometric requirement for addition of new lamellae; the additional space taken up by the spherulite as a whole is filled by new lamellae.

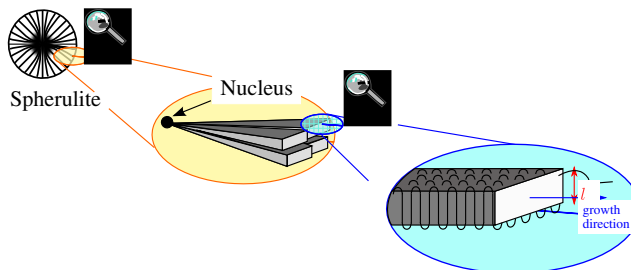


Figure G.11: Formation of a spherulite

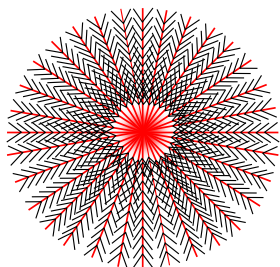


Figure G.12: Geometric representation of a spherulite

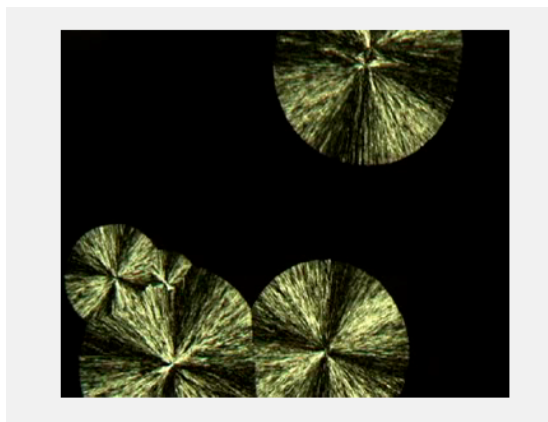


Figure G.13: Video of the formation of a spherulite

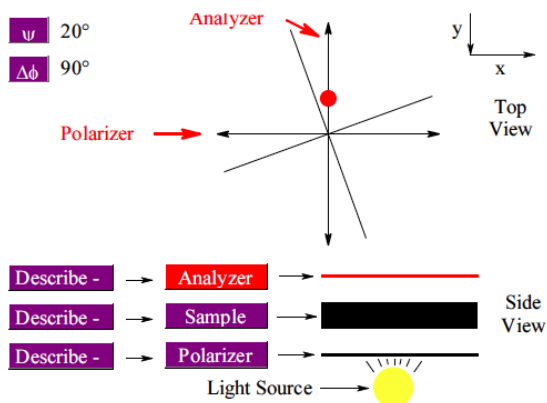


Figure G.14: Interactive model of birefringence

## G.8 Birefringence

- (a) Light emerging from the sample for  $\psi = 45^\circ$  and  $\Delta\phi = 90^\circ$  is said to be circularly polarized. Why is this a sensible description of the polarization state you observe under these circumstances?
- (b) For what values of  $\psi$  is no light at all transmitted through the analyzer?
- (c) The maximum light transmission through the analyzer is obtained for  $\psi = 45^\circ$  and  $\Delta\phi = 180^\circ$ . What fraction of the light emerging from the sample is transmitted under these circumstances?

### G.8.1 Birefringence and Radial Symmetry

<http://bly.colorado.edu/lcphysics/textures/>

If the object between the polarizer and analyzer has spherical symmetry, as is the case with these liquid crystalline droplets, the 'Maltese cross' pattern shown here will be obtained. Dark patches correspond to  $\Psi = 0$  and  $90^\circ$ , and the bright patches are obtained at  $\Psi = \pm 45^\circ$ .

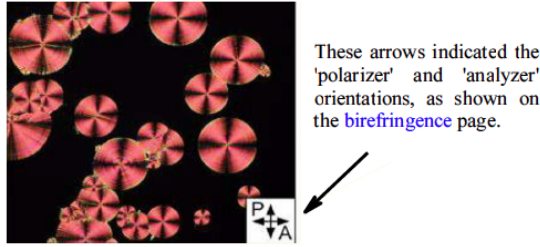


Figure G.15: Diagram showing birefringence

## G.9 Growth of a Lamellar Crystallite

The overall free energy change ( $\Delta F$ ) associated with the formation of a small crystallite has two components:

- (a) A surface energy component, which is always positive.
- (b) A bulk free energy component, which is negative for temperatures below the equilibrium melting temperature,  $T_m^0$ .

The bulk component can be written in terms of the undercooling ( $T_m^0 - T$ ) by writing the bulk free energy change per unit volume ( $\Delta f_c$ ) in terms of its entropic and enthalpic components:

$$\Delta f_c = \Delta h_c - T\Delta s_c \quad (\text{G.1})$$

Here  $\Delta h_c$  and  $\Delta s_c$  are the enthalpy and entropy of melting for a perfect crystal, normalized by the volume of the crystal. We can use the fact that  $\Delta f_c = 0$  when  $T = T_m^0$  to eliminate  $\Delta s_c$  from the equation and write  $\Delta f_c$  in terms of the enthalpy of melting and the undercooling,  $\Delta T$ , defined as  $T_m^0 - T$ :

$$\Delta f_c = -\frac{\Delta h_c \Delta T}{T_m} \quad (\text{G.2})$$

Note that we have used the following sign conventions (as is generally the case):

- $\Delta h_c$  is the enthalpy required to melt the crystal, and is always a positive number.
- From its definition,  $\Delta T$  is positive whenever the temperature is below the equilibrium melting temperature.

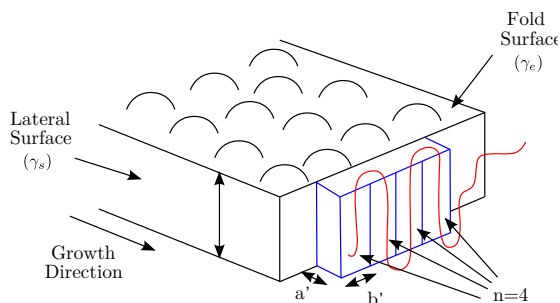


Figure G.16: Schematic representation of a growing lamellar crystallite.

- $\Delta f_c$  is the free energy difference between the crystal and the amorphous material, and is negative for temperatures below the equilibrium melting temperature.

The growth of a lamellar crystallite occurs by the addition of molecular strands (typically corresponding to the  $c$  axis of the crystalline structure) to the growing crystallite as illustrated in Figure G.16. In addition to the

If we account for the surface energies associated with the new crystal/amorphous interface that is created, the increase in free energy for adding  $n$  "strands" to the face of a lamellar crystallite is given by the following expression:

$$\Delta F = 2a'\lambda_c\gamma_s + 2na'b'\gamma_e + na'b'\lambda_c\Delta f_c \quad (\text{G.3})$$

If we assume that  $n$  is large we can neglect the term involving  $\gamma_s$ , so that  $\Delta F < 0$  when  $\Delta f_c < \frac{2\gamma_e}{\lambda_c}$ . With  $\Delta f_c$  given by Eq. G.2, we can rewrite the condition that  $\Delta F < 0$  in the following form:

$$\lambda_c > \frac{2\gamma_e T_m^0}{\Delta h_c \Delta T} \quad (\text{G.4})$$

A crystal will grow by the addition of additional strands when this criterion is met. Thick crystals (high  $\lambda_c$ ) are thermodynamically favorable, but thin crystals (low  $\lambda_c$ ) are kinetically favorable. In this model, the crystal thickness which is actually obtained is the lowest, thermodynamically possible value. The inequality from the previous page therefore becomes an approximate equality:

$$\lambda_c \approx \frac{2\gamma_e T_m^0}{\Delta h \Delta T} \quad (\text{G.5})$$

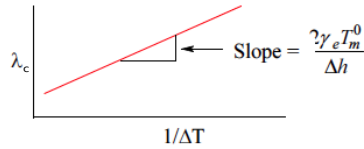


**Figure G.17:** Graphical representation of the crystal thickness prediction from Eq. G.5.

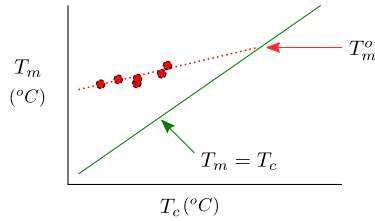


**Figure G.18:** Melting temp ( $T_m$ ) as a function of the crystallization temperature,  $T_c$ .

Because thick crystals are thermodynamically more stable than thin crystals, the thick crystals will melt at a slightly higher temperature than thin crystals. One therefore expects a relationship between the temperature at which the crystals will form, and the temperature at which the crystals will melt. Crystals crystallized at higher temperatures will also melt at higher temperatures. At an undercooling of zero the actual melting temperature,  $T_m$ , will be equal to the equilibrium melting temperature. For very low undercoolings, however, the crystallization rate becomes very slow, so crystallization will never take place at the exact equilibrium melting temperature. Values of the equilibrium melting temperature are obtained from measurements of  $T_m$  at higher undercoolings, and extrapolating to  $\Delta T = 0$  as illustrated in the following graph:

## G.10 Density of Semicrystalline Polymers

The percent crystallinity in a polymer sample is generally determined by measuring the density of the material. A linear relationship between density and percent crystallinity is assumed, so that the following relationship holds:

$$\% \text{Crystallinity} = \frac{\rho - \rho_{\text{amorphous}}}{\rho_{\text{crystalline}} - \rho_{\text{amorphous}}} \times 100 \quad (\text{G.6})$$



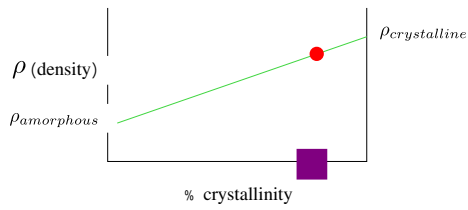


**Figure G.19:** Density vs percent crystallinity

## H Solutions and Blends

We now move from our discussion of the shapes of individual polymer molecules in a homogeneous, one component system, to the behavior of solutions and blends consisting of different types of molecules that have been mixed together. We are interested in studying these systems for many reasons, including the following:

- (a) Characterization: many of the properties of polymer molecules are determined by the properties of polymer solutions.
- (b) Processing: many applications of polymers involve require that the polymer molecules be dissolved in an appropriate solvent.
- (c) Improved materials: new materials with improved properties can often be formed by blending or "alloying" different polymers.
- (d) Recycling: polymers need to be separated before they can be recycled because the different polymers do not mix favorably.

The key quantity when discussing thermodynamics of polymer solutions (polymer + small-molecule solvent) and polymer blends (polymer A + polymer B) is the free energy of mixing. We therefore begin with a discussion of polymer solution thermodynamics. In general, we consider the case where we mix  $n_a$  A molecules with a degree of polymerization  $N_a$  with  $n_b$  B molecules with a degree of polymerization  $N_b$ . Polymer solutions will correspond to the case where one of the degrees of polymerization is very small (typically 1). We will make the assumption that the sizes of the repeat units for the components of the mixture are identical. This assumption is not as restrictive as it would initially appear, since one can always define "effective" repeat units with the desired volume. In this sense,  $N_a$  and  $N_b$  are determined by the relative molecular volumes of the components in the mixture, and are defined in terms of some reference volume.

**1) Exercise:** The room temperature densities of polystyrene and toluene are  $1.05 \text{ g/cm}^3$  and  $0.87 \text{ g/cm}^3$ , respectively. What reference volume,  $V_0$ , should we use to characterize the thermodynamics of polystyrene solutions in toluene? What degrees of polymerization would characterize a solution where the polystyrene molecular weight is 100,000 g/mole?

**2) Solution:** The obvious reference volume in this case is the volume of a toluene molecule, which we take as having  $N=1$ . This volume is obtained from the density and molecular weight of toluene. Toluene ( $\text{C}_6\text{H}_8$ ) has a molecular weight of 92 g/mole.

$$V_0 = \left( \frac{92 \text{ g}}{\text{mole}} \right) \left( \frac{\text{cm}^3}{0.87 \text{ g}} \right) = 106 \text{ cm}^3 / \text{mole}$$

Note that we have used the molar volume for  $V_0$ . This convention will be followed throughout our discussion.

The value of  $N$  for the polymer molecules will be given by the molecular volume, divided by the reference volume:

$$N_{\text{polystyrene}} = \left( \frac{100,000 \text{ g}}{\text{mole}} \right) \left( \frac{\text{cm}^3}{1.05 \text{ g}} \right) \left( \frac{\text{mole}}{106 \text{ cm}^3} \right) = 898$$

In our discussion of the thermodynamics of mixtures, we will refer to  $N$  as the number of "segments", defined in terms of a reference volume as described here. In some cases this reference volume will correspond to a repeat unit of the polymer, but this does not need to be the case in general.

## H.1 Chemical Potentials and Free Energy of Mixing

The chemical potential of  $A$  molecules,  $\mu_a$ , is defined as the free energy required to add an additional 'A' molecule to the system. Because all  $A$  molecules are equivalent, it is also equal to the free energy per  $A$  molecule in the system. The following expressions are helpful

$$F = n_a \mu_a + n_b \mu_b \quad (\text{H.1})$$

$$\left. \frac{\partial F}{\partial n_a} \right|_{n_b} = \mu_a$$

$$\left. \frac{\partial F}{\partial n_b} \right|_{n_a} = \mu_b \quad (\text{H.2})$$

The derivative with respect to  $n_a$  is taken with  $n_b$  held constant, and vice versa. Note that  $F$  is the total extensive free energy of the system, since it increases as the numbers of  $A$  and  $B$  molecules ( $n_a$  and  $n_b$ ) increases.

The chemical potentials of  $A$  and  $B$  molecules of the pure components are defined as  $u_a^0$  and  $u_b^0$ . The free energy of the two components before mixing is therefore given by:

$$F_{\text{unmixed}} = n_a \mu_a^0 + n_b \mu_b^0 \quad (\text{H.3})$$

The free energy of mixing is equal to the difference in the free energies of the mixed and unmixed systems:

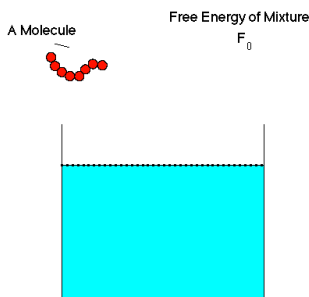


Figure H.1: Animation of the chemical potential of a molecule

$$\Delta F_{mix} = F - F_{unmixed} = n_a \mu_a + n_b \mu_b - (n_a \mu_a^0 + n_b \mu_b^0) = n_a (\mu_a - \mu_a^0) + n_b (\mu_b - \mu_b^0) \quad (\text{H.4})$$

Because we are only interested in changes in chemical potentials due to mixing, we can set the chemical potentials of the pure, unmixed components to zero ( $\mu_a^0 = \mu_b^0 = 0$ ).

By defining the chemical potentials of the pure components as zero, we obtain:

$$\Delta F_{mix} = n_a \mu_a + n_b \mu_b \quad (\text{H.5})$$

Equation H.5 is completely general, and valid for mixtures of molecules of any size. It's not that useful, however, because we generally don't write down values of  $n_a$  and  $n_b$  when we want to specify the composition of a multicomponent mixture. For mixtures of small molecules (metal alloys, for example), we commonly use mole fractions,  $X_a$  and  $X_b$ , to specify the composition:

$$\begin{aligned} X_a &= \frac{n_a}{n_a + n_b} \\ X_b &= \frac{n_b}{n_a + n_b} \end{aligned} \quad (\text{H.6})$$

This makes sense for metals because the molar volumes of the different components are not that different from one another. In polymer systems, however, we are often dealing with systems where the components have molar volumes that can differ by orders of magnitude. This is the situation if we are interested in the solubility of a high molecular weight polymer (which can have a molecular weight of several hundred thousand g/mole) in a solvent (which will typically have a molecular weight of  $\approx 100$  g/mole). Organic solutions are typically specified by the weight fractions of the different components. In

discussions of polymer solution thermodynamics it is more common to work in terms of volume fractions of the different components in the systems.

The concepts in this section can be easily extended to systems with more than two components, but we confine ourselves here to binary solutions of just two components: A molecules of length  $N_a$  and B molecules of length  $N_b$ . In our discussion of polymer thermodynamics it is important to keep in mind  $N_a N_b$  are not necessarily true degrees of polymerization as defined earlier in this text. Instead they are obtained by dividing the molar volumes of the different components by some reference volume,  $V_0$ . For polymer/solvent mixtures this reference volume is typically taken as the molar volume of the solvent, and for polymer/polymer mixtures it is typically taken as the volume per repeat unit for one of the polymers. The total volume,  $V$ , and volume fractions,  $\phi_a$  and  $\phi_b$  are given by the following expressions:

$$V = n_a N_a V_0 + n_b N_b V_0 \quad (\text{H.7})$$

$$\begin{aligned} \phi_a &= \frac{n_a N_a V_0}{V} \\ \phi_b &= \frac{n_b N_b V_0}{V} \end{aligned} \quad (\text{H.8})$$

The free energy of mixing per unit volume,  $\Delta f_{mix}$ , is obtained from  $\Delta F_{mix}$  by dividing by the volume of the system:

$$\Delta f_{mix} = \frac{n_a \mu_a + n_b \mu_b}{n_a N_a V_0 + n_b N_b V_0} = \frac{\mu_a \phi_a}{N_a V_0} + \frac{\mu_b \phi_b}{N_b V_0} \quad (\text{H.9})$$

By rearranging the equation at the bottom of the previous page we obtain:

$$\Delta f_{mix} V_0 = \frac{\mu_a \phi_a}{N_a} + \frac{\mu_b \phi_b}{N_b} \quad (\text{H.10})$$

The quantities  $\Delta f_{mix}$ ,  $\mu_a/N_a$  and  $\mu_b/N_b$  all depend on the composition of the material. The relationship between these quantities is illustrated by the tangent construction shown in Figure H.2, where the composition dependence of  $\Delta f_{mix}$  is plotted as a function of  $\phi_b$  for a hypothetical material. For a given composition (denoted  $\phi'_b$  in Figure H.2), the chemical potentials are obtained by first drawing a tangent to the free energy curve at  $\phi_b = \phi'_b$ . The value of  $\mu_a/N_a$  is determined by extrapolating this tangent line to  $\phi_b = 0$  and  $\mu_b/N_b$  is obtained by extrapolating the tangent line to  $\phi_b = 1$ . This result is consistent with Eq. H.10, which shows that normalized free energy of mixing at a

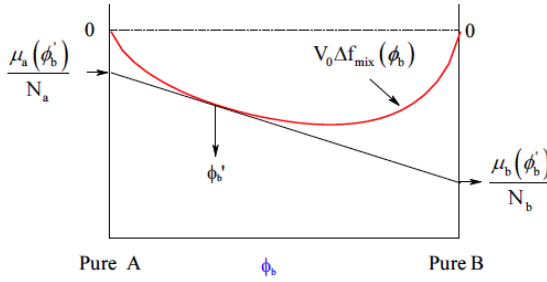


Figure H.2: Relationship of the free energy of mixing to the chemical potentials.

certain composition is determined by the weighted average of the normalized chemical potentials. As a result a straight line drawn between the normalized chemical potentials on the left and right axes must hit the free energy curve at  $\phi_b = \phi'_b$ .

To fully validate the tangent construction illustrated in Figure H.2 we still need to show that the straight line between the chemical potentials must be equal to the slope of the free energy curve. This can be done in formal terms by combining Eqs. H.2 and H.8, which after simplification leads to the following relationship:

$$\frac{\partial(\Delta f_{mix} V_0)}{\partial \phi_b} = \frac{\mu_b}{N_b} - \frac{\mu_a}{N_a} = - \frac{\partial(\Delta f_{mix} V_0)}{\partial \phi_a} \quad (\text{H.11})$$

The fact that the tangent must give the difference between  $\mu_b/N_b$  and  $\mu_a/N_a$  makes sense conceptually, because the only way changing the composition by some amount requires that an A segment be replaced by a B segment.

## H.2 Ideal Entropy of Mixing for Polymers

For small molecules the ideal free energy of mixing is given by the following expression:

$$\frac{\Delta s_{ideal} V_0}{R} = -X_a \ln X_b - X_b \ln X_a \quad (\text{H.12})$$

The quantity  $s_{ideal} V_0$  is the entropy of mixing per mole of molecules. If the molar volumes of the A and B molecules are the same, then we can simply

replace the mole fractions,  $X_a$  and  $X_b$  with the corresponding volume fractions,  $\phi_a$  and  $\phi_b$ . The entropy of mixing per molecule is independent of the size of the molecule. Therefore, the entropy of mixing per repeat unit is smaller than the entropy of mixing per molecule by a factor of  $N$ , where  $N$  is the degree of polymerization. In general, we have the following expression for the ideal free energy of mixing per volume for polymers with molar volumes of  $N_a V_0$  and  $N_b V_0$ :

$$\frac{s_{ideal} V_0}{R} = -\frac{\phi_a \ln \phi_a}{N_a} - \frac{\phi_b \ln \phi_b}{N_b} \quad (\text{H.13})$$

### H.3 Idealized Enthalpy of Mixing

The key result is that the entropy of mixing for a given volume is much smaller for large molecules than it is for small molecules. This result explains why different types of polymers almost never mix with one another in the liquid state. The driving force for two liquids to mix is normally the entropy of mixing, but this driving force is very low for mixtures of very large polymer molecules. In fact, the entropy of mixing for polymer mixtures is sometimes negative. While the ideal entropy of mixing must be positive, it is very small, and can be overwhelmed by non-ideal contributions to the entropy of mixing which can be positive or negative. Before discussing these effects, however, we will continue in our derivation of the Flory Huggins equation for the free energy of mixing. The Flory-Huggins theory combines the ideal free energy of mixing with a very simple form for the enthalpy of mixing. Unlike the entropy of mixing, the enthalpy of mixing is assumed to be independent of the size of the molecules. We can therefore use small molecules to illustrate the origins of the equation for the enthalpy of mixing.

In this example, the blue square is placed into an environment where one of its four nearest neighbors is blue, and three are red. Red-blue contacts have an energy (or enthalpy) of  $E_{ab}$ , red-red contacts have an energy of  $E_{aa}$ , and blue-blue contacts have an energy of  $E_{bb}$ . The enthalpy change,  $\Delta H$ , associated with the removal of the square from a pure blue phase on the left (4 blue neighbors) to the mixture on the right (1 blue neighbor and 3 red neighbors) is therefore given by the following formula:

$$\Delta H = 3E_{ab} + E_{bb} - 4E_{bb} = 3(E_{ab} - E_{bb}) \quad (\text{H.14})$$

How do we calculate the energy of a randomly mixed collection of A and B molecules? We begin by assuming that the energy of an A-A contact is  $E_{aa}$ , the

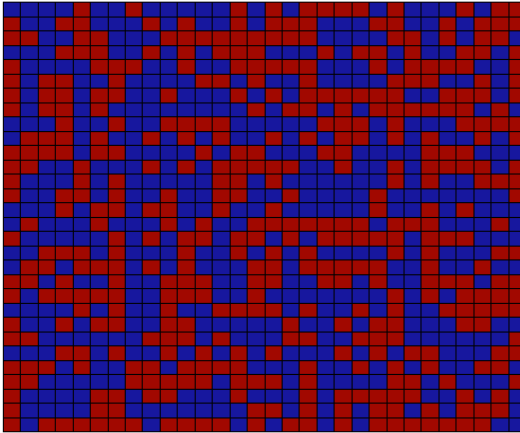


Figure H.3: An animated simulation of mixing



Figure H.4: Pictorial representations of mixing

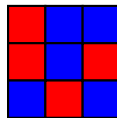


Figure H.5: Diagram showing contacts



energy of an B-B contact is  $E_{bb}$ , and the energy of an A-B contact is  $E_{ab}$ . Also assume that each molecule  $z$  nearest neighbors ( $z = 4$  for the 2-dimensional array of squares shown above.) The number of A-B contacts in a mixture of  $n_a$  A molecules and  $n_b$  B molecules is given by:

$$\begin{aligned}n_{aa} &= n_a z p_a / 2 \\n_{bb} &= n_b z p_b / 2 \\n_{ab} &= n_a z p_b\end{aligned}\tag{H.15}$$

where  $p_a$  is the probability that a nearest neighbor is an A molecule. The factor of 2 in the expressions for  $n_{aa}$  and  $n_{bb}$  is needed to avoid double counting. (For example, if  $n_a = 2$ , there is only one interaction between the two molecules, not 2.) Now we invoke the mean field (or random mixing) approximation, which is that  $p_a = \phi_a$ , and  $p_b = \phi_b$ . We obtain the following.

$$\begin{aligned}n_{aa} &= n_a z \phi_a / 2 \\n_{bb} &= n_b z \phi_b / 2 \\n_{ab} &= n_a z \phi_b\end{aligned}\tag{H.16}$$

The energy of the mixed state is obtained by multiplying the numbers of different contacts by their energy:

$$E_{mixed} = E_{aa}n_{aa} + E_{bb}n_{bb} + E_{ab}n_{ab}\tag{H.17}$$

Substitution for  $n_{aa}$ ,  $n_{bb}$  and  $n_{ab}$  gives the following:

$$E_{mixed} = E_{aa}n_a z \phi_a / 2 + E_{bb}n_b z \phi_b / 2 + E_{ab}n_a z \phi_b\tag{H.18}$$

The energy of the unmixed state is obtained in a similar fashion, remembering that in this state all A's are surrounded by other A's, and all B's are surrounded by other B's:

$$E_{unmixed} = E_{aa}n_a z / 2 + E_{bb}n_b z / 2\tag{H.19}$$

The energy change due to mixing is obtained by subtracting the energy of the unmixed state from the energy of the mixed state:

$$\Delta E_{mix} = E_{mixed} - E_{unmixed} = \frac{E_{aa}n_a z \phi_a}{2} + \frac{E_{bb}n_b z \phi_b}{2} + E_{ab}n_a z \phi_b - \frac{E_{aa}n_a z}{2} - \frac{E_{bb}n_b z}{2} \quad (\text{H.20})$$

This expression can be further simplified by recalling that  $n_a = \phi_a n$  and  $n_b = \phi_b n$ , where  $n$  is the total number of molecules ( $n = n_a + n_b$ ):

$$\Delta E_{mix} = nz \left[ \frac{E_{aa}\phi_a^2}{2} + \frac{E_{bb}\phi_b^2}{2} + E_{ab}\phi_a\phi_b - \frac{E_{aa}\phi_a}{2} - \frac{E_{bb}\phi_b}{2} \right] \quad (\text{H.21})$$

After some rearrangement we obtain the following expression:

$$\Delta E_{mix} = nz\phi_a\phi_b \left[ E_{ab} - \frac{E_{aa} + E_{bb}}{2} \right] \quad (\text{H.22})$$

Note that the mixing energy is positive if the energy of a-b contacts is larger than the average energy of a-a and b-b contacts. Because  $z$ ,  $E_{aa}$ ,  $E_{bb}$ , and  $E_{ab}$  are actually not measurable quantities, it is common to lump them together into a parameter called the **Chi parameter** represented by the Greek letter 'chi':

$$\chi \equiv \frac{z}{k_B T} \left[ E_{ab} - \frac{E_{aa} + E_{bb}}{2} \right] \quad (\text{H.23})$$

With this definition of  $\chi$ , the energy of mixing for A and B molecules (with the same size) is:

$$\Delta H_{mix} = \Delta E_{mix} = RT\chi n\phi_a\phi_b \quad (\text{H.24})$$

Strictly speaking, the 'enthalpy' and the 'energy' of a system are not the same thing. The Gibbs free energy involves the enthalpy, and is the appropriate thermodynamic quantity at a fixed temperature and pressure. The Helmholtz free energy involves the energy, and is the appropriate thermodynamic quantity at fixed temperature and volume. For compressible systems the two quantities differ slightly. We use the expression from the previous page for the extensive enthalpy of mixing, and divide by the volume of the system ( $nV_0$ ) to obtain the intensive enthalpy of mixing:

$$\Delta h_{mix} = \frac{\Delta H_{mix}}{nV_0} = \frac{RT\chi\phi_a\phi_b}{v_0} \quad (\text{H.25})$$

Normalizing as we did for the ideal entropy of mixing gives:

$$\frac{\Delta h_{mix}V_0}{RT} = \chi\phi_a\phi_b \quad (\text{H.26})$$

## H.4 Flory-Huggins Free Energy of Mixing

The most commonly used expression used to describe the free energy of mixing for polymer/polymer and polymer/solvent mixtures combines mean-field enthalpy of mixing with the ideal combinatorial entropy of mixing:

$$\Delta f_{mix} = \Delta h_{mix} - T\Delta s_{ideal} \quad (\text{H.27})$$

Combining these forms for the enthalpy and entropy gives the following expression, referred to as the Flory-Huggins free energy of mixing:

$$\frac{\Delta f_{mix}V_0}{RT} = \frac{\phi_a \ln \phi}{N_a} + \frac{\phi_b \ln \phi_b}{N_b} + \chi\phi_a\phi_b \quad (\text{H.28})$$

It is important to recognize that many assumptions went into the derivation of this equation, and that they can't possibly all be true. Nevertheless, this equation is very commonly used in polymer science, and needs to be understood. In fact, this equation is often used as a definition for  $\chi$ . Based on our earlier definition of  $\chi$  in terms of energetic parameters, one would expect that

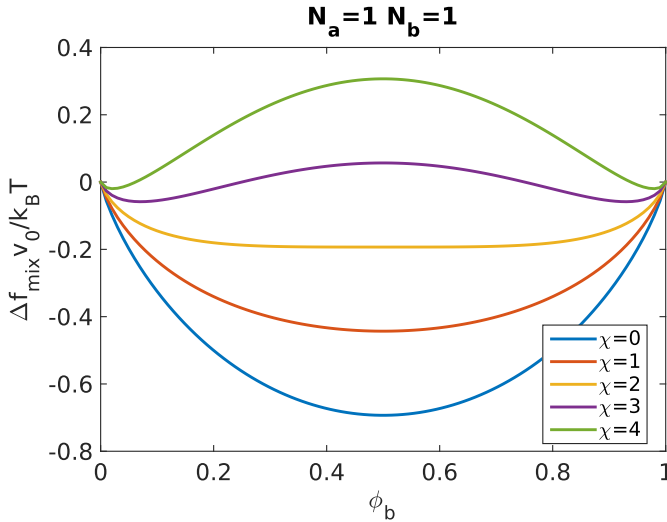


**Figure H.6:** Regular solution form for the free energy of mixing of small molecules.

its magnitude would decrease as the temperature increases. In fact, the actual free energy of mixing can have very different behavior, and the free energy of mixing is generally accurately described by the Flory-Huggins expression only when  $\chi$  is allowed to vary with temperature and composition. We begin on the next page by constructing phase diagrams, with the assumption that the free energy of mixing is adequately described by a value of  $\chi$  that is independent of composition. Free energy curves for  $N_a = N_b = 1$  are shown in Figure H.6 for  $\chi$  ranging from 0 to 4. For  $N_a = N_b = 1$ , the critical value of  $\chi$  is equal to 2. When  $\chi$  is larger than this critical value there will be a region of compositions where the free energy curve has a negative curvature in the free energy curve.

## H.5 The Coexistence (binodal) and Spinodal Curves

The critical value of  $\chi$  decreases as  $N_a$  and  $N_b$  increase. In addition, the free energy curves are no longer symmetric about  $\phi_b = 0.5$  when  $N_a \neq N_b$ . Both of these points are illustrated in Figure H.7, where we plot the Flory-Huggins free energy of mixing (Eq. H.28) for  $N_a = 200$ ,  $N_b = 500$  and  $\chi = 0.012$ . A two-phase region will exist for average compositions of the alloy that are between the compositions between  $\phi_1$  and  $\phi_2$ , the two compositions defined by the common tangent construction in Figure H.7. Because the tangent to the curve at these two compositions are identical, they have the same values of  $\mu_a$  and  $\mu_b$ , which is a requirement for equilibrium. In addition, the average free

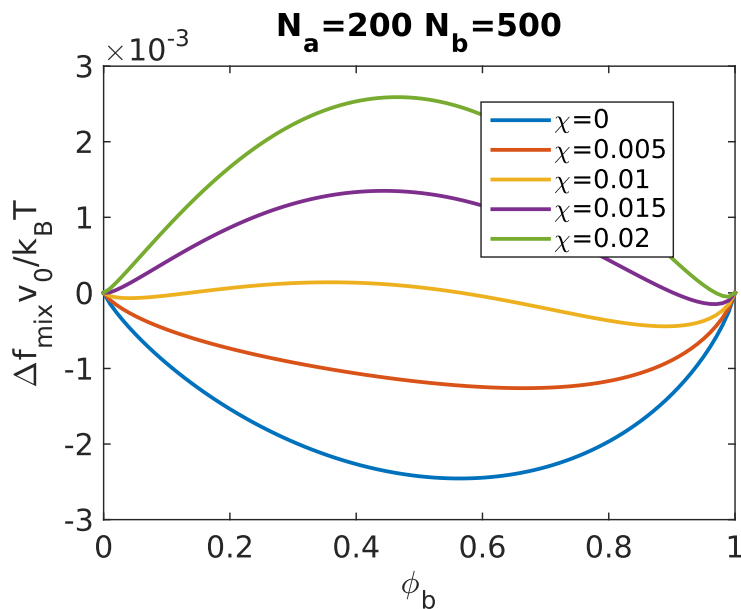


**Figure H.7:** Free energy of mixing for a system with asymmetric molecular sizes in the two phase regime.

energy for a mixture of these two phases (dashed line in Figure H.7) is less than the free energy for a homogenous phase of this average composition (solid line in Figure H.7). By plotting these two composition as a function of  $\chi$ , we obtain the binodal curve shown as the solid line in Figure H.8. The binodal curve is also referred to as the coexistence curve because it shows the compositions of the phases that are in equilibrium with one another in the two-phase region of the phase diagram.

The spinodal curve (or stability limit) represents the boundary in the phase diagram where the free energy of mixing changes from a positive curvature to a negative curvature. It occurs when  $\chi = \chi_s$ , where  $\chi_s$  defines the spinodal curve. For  $N_a = 200$  and  $N_b = 300$  the spinodal curve is shown as the dashed line in Figure H.8. The change in curvature from positive to negative values occurs when the second derivative of the free energy with respect to composition is equal to zero. We obtain the following expression for  $\chi_s$  by setting  $\phi_b = 1 - \phi_a$  in the free energy expression:

$$\frac{\partial^2}{\partial \phi_a^2} \left( \frac{\phi_a \ln \phi_a}{N_a} + \frac{(1 - \phi_a) (\ln 1 - \phi_a)}{N_b} + \chi_s \phi_a (1 - \phi_a) \right) = 0 \quad (\text{H.29})$$

Evaluating the second derivative leads to the following:

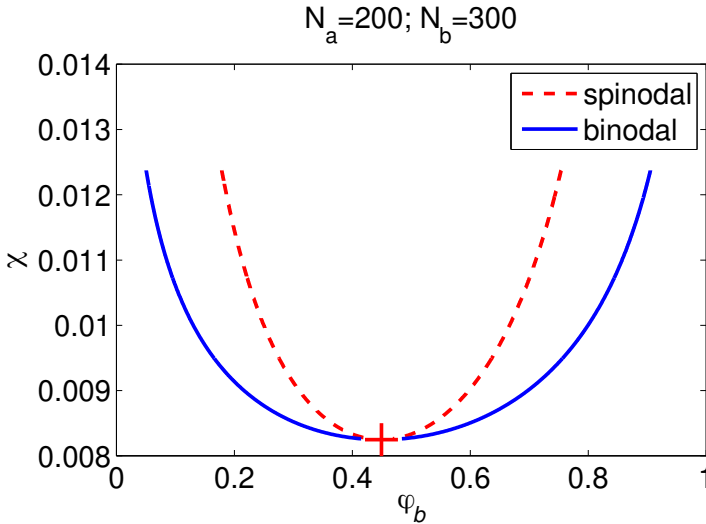


**Figure H.8:** Binodal and spinodal curves for  $N_a = 200$  and  $N_b = 300$ .

$$\frac{1}{\phi_a N_a} + \frac{1}{(1 - \phi_a) N_b} - 2\chi_s = 0 \quad (\text{H.30})$$

which can be rearranged to give the following for  $\chi_s$ :

$$\chi_s = \frac{1}{2\phi_a N_a} + \frac{1}{2\phi_b N_b} \quad (\text{H.31})$$

## H.6 Critical Point

The phase diagrams obtained from the free energy of mixing expression show under what conditions polymeric liquids are completely miscible, and under what conditions phase separation will occur. The critical point is the point on the phase diagram where a liquid is just beginning to undergo phase separation. Mathematically, the critical point corresponds to the point on the spinodal curve where  $\chi_s$  has the lowest possible value. We obtain this point by setting the derivative of  $\chi_s$  to zero:

$$\frac{\partial}{\partial \phi_a} \left( \frac{1}{2\phi_a N_a} + \frac{1}{2(1 - \phi_a) N_b} \right) = 0 \quad (\text{H.32})$$

The solution to this equation is given by  $\phi_a = \phi_{a,crit}$ , at which point  $\chi_s$  is equal to  $\chi_{crit}$ :

$$\phi_{a,crit} = \frac{\sqrt{N_b}}{\sqrt{N_b} + \sqrt{N_a}} \quad (\text{H.33})$$

$$\chi_{crit} = \frac{N_a + N_b + 2\sqrt{N_a N_b}}{2N_a N_b} \quad (\text{H.34})$$

**3) Exercise:** The value of  $\chi_s$  for blends of polystyrene (PS) and poly(methyl methacrylate) (PMMA) is 0.037 at 170 °C, based on a reference volume equal to the reference volume of a polystyrene repeat unit. Suppose monodisperse samples of PS and PMMA of equal molecular weights are mixed with one another. What range of molecular weights will be completely miscible with one another at 170 °C? (Assume the densities of the two polymers are identical).

**4) Solution:** First we calculate  $\chi_{crit}$ :

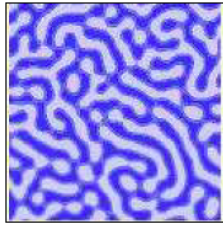
$$\chi_{crit} = \frac{N_a + N_b + 2\sqrt{N_a N_b}}{2N_a N_b} = \frac{2}{N} \quad (\text{H.35})$$

$$\text{for } N_a = N_b = N$$

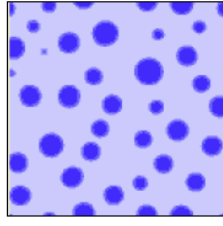
The polymers are completely miscible for  $\chi < \chi_{crit}$ , which occurs when  $N < 2/\chi$ . With  $\chi = 0.037$ , we have complete miscibility for  $N < 54$ . The repeat unit molecular weight for polystyrene is 104 g/mol, so the critical molecular weight below which the polymers are completely miscible is  $54 \cdot 104$  g/mol = 5616 g/mol.

## H.7 Spinodal Decomposition

"Spinodal Decomposition" is the mechanism of phase separation where small perturbations in the composition of the single phase grow because this decreases the overall free energy. This happens inside the spinodal curve defined previously. The microstructure is generally characterized by a well defined wavelength, as illustrated below.



Spinodal Microstructure



Nucleation and Growth

**Figure H.9:** Characteristic microstructures for phase separation by spinodal decomposition (left) and nucleation and growth (right).

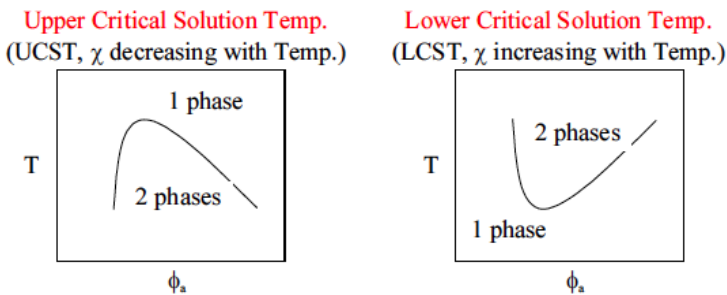


**Figure H.10:** Phase diagrams in temperature space.

## H.8 Phase Diagrams in Temperature Space

Actual values of  $\chi$  for real systems are generally obtained by fitting the Flory Huggins expression to the free energy of mixing to actual experimental data. This procedure can give actual values of  $\chi$  which either increase or decrease with increasing temperature. Smaller values of  $\chi$  (where mixing is favored) can therefore be obtained at either high or low temperatures, giving the following two types of phase diagrams:

**5) Exercise:** The following equation describes the temperature dependence of  $\chi$  for the PMMA/butanol polymer/solvent system:

$$\chi = 1.45 - 0.0115T \quad (\text{H.36})$$

Here  $T$  is expressed in  $^{\circ}\text{C}$ . For what range of temperatures will high molecular weight PMMA completely dissolve in butanol?



**6) Solution:** From the phase diagram, we see that the two components are completely miscible for  $\chi < \chi_{crit}$ . If the A phase is the solvent ( $N_a = 1$ ) we obtain the following for  $\chi_{crit}$ :

$$\chi_{crit} = \frac{1 + N_b + 2\sqrt{N_b}}{2N_b} \quad (\text{H.37})$$

As the polymer molecular weight becomes very large ( $N_b \rightarrow \infty$ ),  $\chi_{crit} \rightarrow 0.5$ . The temperature at which  $\chi$  is equal to this critical value of 0.5 for polymer solutions is called the **theta temperature**. It corresponds to the temperature at a theoretical polymer with an infinite molecular weight is just beginning to precipitate from solution. The general condition for complete miscibility for a polymer/solvent system, for the case where the polymer has a very high molecular weight, is given by the requirement that  $\chi < 0.5$ . For the data given for the PMMA/Butanol system, this occurs for  $T > 82.6^\circ\text{C}$ . Because  $\chi$  decreases with increasing temperature, this system exhibits an upper critical solution temperature (UCST).

**A cautionary note:** Note that the polymer volume fraction at the critical point is very low (i.e.,  $\phi_{a,crit}$  is very close to 1 for  $N_b \gg N_a$ ). The detailed predictions of the Flory Huggins theory will not be accurate in this regime, for reasons that are discussed more fully in the section on dilute solution thermodynamics.

## H.9 Chemical Potentials

Recall that the **Chemical Potentials** of species A is determined by differentiating the extensive free energy with respect to the number of A molecules in the system. The extensive free energy is obtained by multiplying the free energy density,  $f$ , by the volume of the system,  $V$ . For a binary mixture of A and B polymers we have:

$$\Delta f_{mix} = \frac{RT}{v_0} \left\{ \frac{\phi_a \ln \phi_a}{N_a} + \frac{\phi_b \ln \phi_b}{N_b} + \chi \phi_a \phi_b \right\} V \quad (\text{H.38})$$

Using the expressions for  $\phi_a$  and  $\phi_b$  (Eq. H.8) and  $V$  (Eq. H.7) we have:

$$\frac{\Delta F_{mix}}{RT} = \{n_a \ln \phi_a + n_b \ln \phi_b + \chi n_a N_a \phi_b\} \quad (\text{H.39})$$

We are now in a position to obtain expressions for the chemical potentials by differentiating the extensive free energy of mixing. We make the usual assumption that the chemical potentials of the pure components are equal to zero (activities of the pure components equal to one):

$$\mu_a = \frac{\partial \Delta F_{mix}}{\partial n_a} = RT \frac{\partial}{\partial n_a} (n_a \ln \phi_a + n_b \ln \phi_b + \chi n_a N_a \phi_b) \quad (\text{H.40})$$

In this way we obtain the following result:

$$\frac{\mu_a}{RT} = \ln \phi_a + \phi_b \left( 1 - \frac{N_a}{N_b} \right) + \chi N_a \phi_b^2 \quad (\text{H.41})$$

When discussing polymer/solvent mixtures we replace the 'a' and 'b' subscripts with 'p' (for polymer) and 's' (for solvent). In addition, we take  $N_s = 1$ . Formally,  $N_p$  is the ratio of the polymer volume to the solvent volume. With these substitutions, we obtain the following expression for  $\mu_s$ , the solvent chemical potential, which is valid for all concentrations:

$$\frac{\mu_s}{RT} = \ln(1 - \phi_p) + \phi_p \left( 1 - \frac{1}{N_p} \right) + \chi \phi_p^2 \quad (\text{H.42})$$

### H.9.1 Limiting case for high molecular weight polymer

For  $N_p \rightarrow \infty$  the solvent chemical potential reduces to  $\mu_s^\infty$ :

$$\frac{\mu_s^\infty}{RT} = \ln(1 - \phi_p) + \phi_p + \chi \phi_p^2 \quad (\text{H.43})$$

In addition the critical point from Eqs. H.33 and H.34 occurs at  $\phi_p = 0$  and  $\chi = 0.5$ . This means that for  $\chi > 0.5$  pure solvent will be in equilibrium with a phase that contains both polymer and solvent. The polymer volume fraction in this phase is determined from the requirement that the solvent chemical potential must be zero. In other words, if a chunk of high molecular weight polymer is immersed in a solvent, solvent diffuses into the polymer until  $\phi_p$  decreases to the point where  $\mu_s^\infty = 0$ . In general, this solution must be solved numerically. In Figure H.11 we plot the concentration dependence of  $\mu_s^\infty$  for  $\chi = 0$ ,  $\chi = 0.5$  and  $\chi = 1$ .

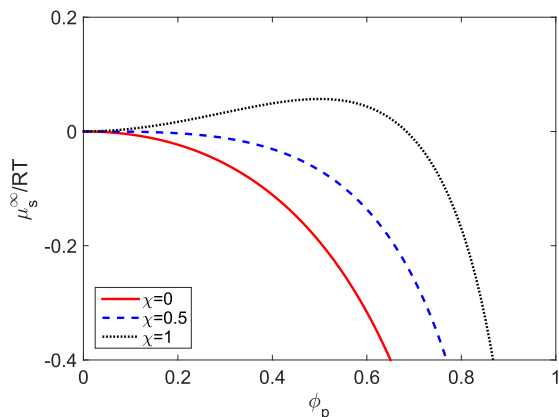


**Figure H.11:** Concentration dependence of the solvent chemical potential from Eq.H.43.

### H.9.2 Limiting case for dilute solutions

For small values of  $\phi_p$  the log term can be expanded as follows:

$$\ln(1 - \phi_p) = -\phi_p - \frac{\phi_p^2}{2} - \dots \quad (\text{H.44})$$

Retaining only the first two terms in the expansion gives the following for the solvent chemical potential:

$$\frac{\mu_s}{RT} = -\frac{\phi_p}{N} + (\chi - 1/2) \phi_p^2 \quad (\text{H.45})$$

**7) Exercise:** What is the polymer volume fraction for a polymer solution with a concentration of  $0.05 \text{ g/cm}^3$ ? Assume the solvent has a density,  $\rho_s$ , of  $0.85 \text{ g/cm}^3$  and the polymer has a density,  $\rho_p$ , of  $1.1 \text{ g/cm}^3$  and there is no volume change on mixing.

**8) Solution:** We just need to calculate the total weight of solution in a volume of  $1 \text{ cm}^3$ :

$$c = \phi_p \rho_p = 0.05(1.1 \text{ g/cm}^3) = 0.055 \text{ g/cm}^3 \quad (\text{H.46})$$

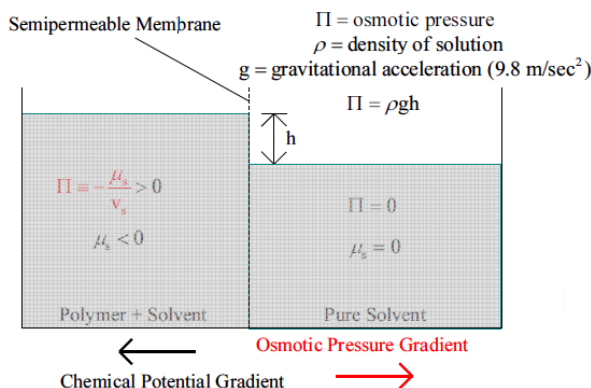


**Figure H.12:** Diagram demonstrating the principles of osmotic pressure.

Note: Actual solution concentrations are generally reported as weight of polymer per total volume of solution - the quantity that we refer to as  $c$ . From a theoretical standpoint, it is generally more convenient to use the polymer volume fraction,  $f_c$ . These quantities are linearly related to one another through the polymer density, as illustrated here. The solvent density is not needed for this calculation, although it is needed to determine the ratio of polymer to solvent.

## H.10 Osmotic Pressure

The concept of osmotic pressure can be illustrated by considering the operation of the membrane osmometer illustrated conceptually in Figure H.12. The device consists of a polymer/solvent mixture that is separated from a bath of pure solvent by a membrane that is permeable to solvent but impermeable to the polymer. The chemical potential of the pure solvent is zero, by definition. Because the solvent chemical potential in the polymer/solvent mixture is less than zero, there is a driving force for solvent to move into this side of the membrane from the pure solvent side. Solvent will continue to move into this side of the device until the hydrostatic pressure generated by the increased depth of the liquid layer provides counteracts the driving force associated with the chemical potential balance. This pressure is the osmotic pressure, and is obtained by dividing the chemical potential difference by the solvent volume:

$$\Pi = -\mu_s/V_s \quad (\text{H.47})$$

One important aspect of an osmotic pressure measurement is that it can be used to provide a direct measure of the number average molecular weight of the polymer. Osmotic pressure effects are important in many other situations

as well. For example, the osmotic pressure is the minimum pressure required to purify a solution by forcing it through a membrane. The osmotic pressure of aqueous solutions is also important in a wide variety of situations in biology. The height of many trees is limited by the maximum osmotic pressure that can be sustained in the leaves, since this is the driving force that draws water to the upper reaches of the tree. Here we explore these phenomena in more detail, and develop some quantitative descriptions of the osmotic pressure.

By combining the Flory-Huggins expression for the solvent chemical potential (Eq. H.42) with the definition of the osmotic pressure (Eq. H.47), we obtain the following expression for  $\Pi$ :

$$\Pi = \frac{RT}{V_s} \left( -\ln(1 - \phi_p) - \phi_p \left( 1 - \frac{1}{N_p} \right) - \chi \phi_p^2 \right) \quad (\text{H.48})$$

If  $N_p$  is large the osmotic pressure depends only on the polymer concentration, and not on the degree of polymerization. The following result is obtained for  $N_p \gg 1$ :

$$\Pi = \frac{RT}{V_s} \left( -\ln(1 - \phi_p) - \phi_p - \chi \phi_p^2 \right) \quad (\text{H.49})$$

### H.10.1 Osmometry for Molecular Weight Determination

The number average molecular weight can be obtained by measuring the osmotic pressure of a dilute polymer solution. Using the dilute solution form of the Flory-Huggins expression for the solvent chemical potential (Eq. H.45) gives the following for  $\Pi$ :

$$\frac{\Pi}{RT} = \frac{\phi_p}{N_p V_s} + (1/2 - \chi) \frac{\phi_p^2}{V_s} \quad (\text{H.50})$$

The polymer volume fraction and overall solution volume ( $V$ ) are given by the following expressions:

$$\phi_p = \frac{n_p N_p V_s}{V} \quad (\text{H.51})$$

Use of this expression for  $\phi_p$  gives the following for  $\pi$ :

$$\frac{\Pi}{RT} = \frac{n_p}{V} + (0.5 - \chi)N_p^2V_s \left(\frac{n_p}{V}\right)^2 + \dots \quad (\text{H.52})$$

Here it is helpful to rewrite  $n_p/V$  in the following way:

$$\frac{n_p}{V} = \left(\frac{w}{V}\right) \left(\frac{n_p}{w}\right) = \frac{C}{M_n} \quad (\text{H.53})$$

where  $c$  is simply the polymer concentration ( $\text{kg}/\text{m}^3$  in SI units,  $\text{g}/\text{cm}^3$  in the units that are more commonly used) and  $M_n$  is the number average molecular weight ( $\text{kg}/\text{mole}$  in SI units). The osmotic pressure is therefore related to the number average molecular weight and concentration as follows:

$$\frac{\Pi}{RT} = \frac{C}{M_n} + (0.5 - \chi)N_p^2V_s \left(\frac{1}{M_n}\right)^2 C^2 + \dots \quad (\text{H.54})$$

This expression is often written as a virial expansion in powers of the concentration:

$$\frac{\Pi}{RT} = \frac{C}{M_n} + A_2C^2 + A_3C^3 + \dots \quad (\text{H.55})$$

$A_2$  is the second virial coefficient, which describes effective two-body interactions between polymer segments within the solvent.  $A_2 = 0$  for  $\chi = 0.5$ , which means that the polymer chain does not 'see' itself under these conditions. For  $\chi = 0.5$ , the polymer chain behaves as a random walk, with chain dimensions very similar to what is obtained for the pure, amorphous polymer in the absence of solvent. For  $\chi > 0.5$ , polymer/polymer contacts are more favorable than polymer/solvent contacts. Under these conditions, high molecular weight polymers will not dissolve.

### H.10.2 Scaling Theory of Osmotic Pressure

The previous derivation of the expressions for the osmotic pressure are useful, but they are not packed with physical insight regarding the actual meaning of osmotic pressure. Some simple physical arguments are more useful in this

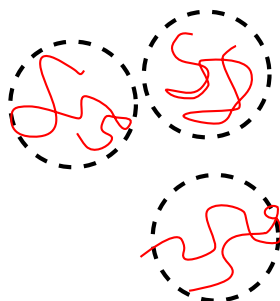


**Figure H.13:** Polymer solution at a concentration less than the overlap concentration,  $c^*$ . At  $c^*$  the spheres overlap and completely fill the space.

sense. We can start by making an analogy to the ideal gas law, which must be valid in the dilute regime. We start with the familiar ideal gas law:

$$PV = nRT \quad (\text{H.56})$$

If we replace the pressure,  $P$ , with the osmotic pressure,  $\Pi$ , and replace the number of moles of gas molecules,  $n$ , with the number of polymer molecules  $n_p$ . By equating  $n_p/V$  with  $C/M_n$  (Eq. H.53), we recover the leading term in virial expansion for the osmotic pressure (Eq. H.55):

$$\Pi = \frac{CRT}{M_n} \quad (\text{H.57})$$

In the dilute regime, molecular collisions are rare, and the pressure and free energy are dominated by the entropic penalty associated with confinement of the molecules into a fixed volume. Virial coefficients quantify the deviations from this ideal, dilute limit.

As the solution gets more and more concentrated, we eventually get to the point where the individual polymer molecules overlap with one another. If we treat the polymers as spheres with a volume equal to  $R_0^3$ , the concentration at which this happens, defined as the **overlap concentration**,  $c^*$ , is given by the average concentration in one of these spheres:

$$c^* \left( \text{g/cm}^3 \right) = \frac{M \left( \text{g/mole} \right)}{R_0^3 \left( \text{cm}^3 \right) N_{av} \left( \text{mole}^{-1} \right)} \quad (\text{H.58})$$

Below the overlap concentration, we can specify the polymer concentration by  $\zeta$ , the average distance between polymer molecules in solution, as illustrated

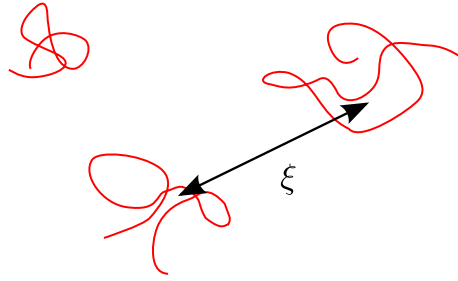


**Figure H.14:** Correlation length and dilute solutions

in Figure H.14. The concentration of polymer molecules (molecules per volume) is  $1/\xi^3$  and the osmotic pressure is given by the following expression:

$$\Pi = \frac{RT}{\xi^3} \quad (\text{H.59})$$

s

**9) Exercise:** What is the overlap concentration poly(methyl methacrylate) with  $M = 100,000$  g/mole in toluene?

**10) Solution:** We can combine Eq. H.58 for the overlap concentration with Eq. F.18 for  $R_0$  to obtain the following:

$$C^* = \frac{M}{R_0^3 N_{av}} = \frac{M}{a_s^3 N^{1.8} N_{av}} = \frac{M_0}{a_s^3 N^{0.8} N_{av}} \quad (\text{H.60})$$

Note that we have used the self-avoiding walk expression for  $R_0$ , which is the relevant expression for good solvent conditions ( $\chi < 0.5$ ). PMMA has  $M_0 = 100$  g/mole, so  $N = 1000$  for the polymer in our example. With these values of  $N$  and  $M_0$ , and an assumed value of  $7 \text{ \AA}$  ( $7 \times 10^{-8} \text{ cm}$ ) for  $a_s$ , we obtain  $c^* = 1.9 \times 10^{-3} \text{ g/cm}^3$ . The density of toluene is slightly less than  $1 \text{ g/cm}^3$ , so this corresponds to a polymer weight fraction of a couple tenths of a percent.

The basic assumption of scaling theory of osmotic pressure is that  $\Pi$  is still given by Eq. H.59 at concentrations above the overlap concentration, but that  $\xi$  has a different meaning in this regime. The approach works in the 'semidilute' solution regime where the overall concentration is still low ( $\phi_p < 0.25$ ),



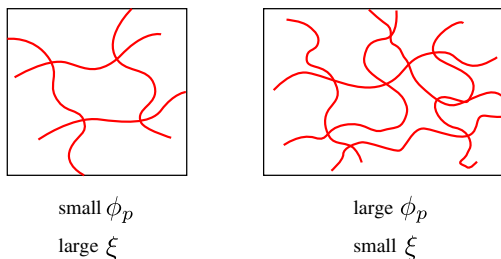


**Figure H.15:** Change in correlation length with solution concentration.

but where there is substantial overlap between polymer molecules. Each overlap point represents a constraint that contributes an entropic contribution of  $\sim k_B T$  to the free energy of the system. The osmotic pressure is therefore  $\sim k_B T$  times the concentration of overlap points, or  $k_B T / \xi^3$ , where  $\xi$  is the correlation length, or average distance between overlap points. As the solution gets more concentrated, the average distance between polymer contacts decreases, as shown schematically in Figure H.15.

To get the concentration dependence of the correlation length, we can start with the postulate that the corrections to the low-concentration form of the osmotic pressure must depend only on  $c/c^*$ , so that the osmotic pressure has the following form:

$$\frac{\Pi M}{CRT} = 1 + f(C/C^*) \quad (\text{H.61})$$

Here  $f(C/C^*)$  is some function that we still need to figure out. It's easy to sort out what this function must look like, because for  $C \gg C^*$  we don't expect that the molecular weight of the polymer to matter any more. At these concentrations the osmotic pressure is dominated by polymer/polymer contacts, and the solution at this local level does not depend at all on the molecular weight. The only way for the osmotic pressure to be independent of the concentration for high concentrations is for  $f(C/C^*)/M$  to be independent of the  $M$ . Because  $C^* \propto M^{-4/5}$ , this is only possible if  $f(C/C^*) \propto (C/C^*)^{5/4}$ . This means that for  $C > C^*$  we have  $\Pi \propto C^{9/4}$ , or equivalently,  $\Pi \propto \phi_p^{9/4}$ . The correlation length, which is related to the osmotic pressure through Eq. H.59, is then given by the following expression for  $C > C^*$ :

$$\xi = a_0 \phi_p^{-3/4} \quad (\text{H.62})$$

Here  $a_0$  is a typical monomer size, comparable in magnitude to the cube root of the molecular volume, or to the statistical segment length. This value for  $\xi$

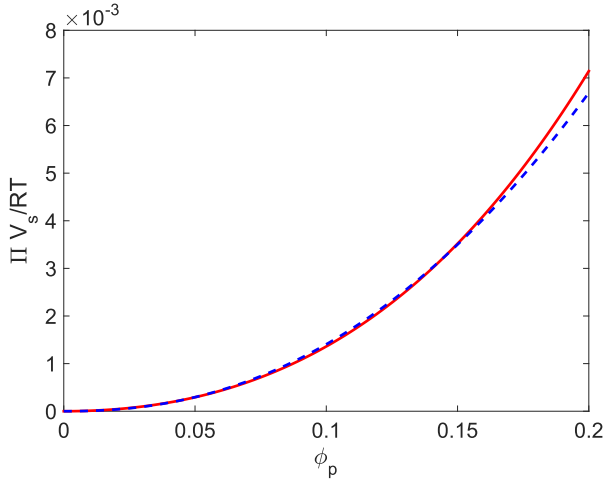


**Figure H.16:** Concentration dependence of the Flory-Huggins form for the osmotic pressure (Eq. H.49) with the semidilute scaling form (Eq. H.63), with  $\chi = 0.4$  and  $a_0^3 = 4v_s$ .

can then be combined with Eq. H.59 to give the following expression for the osmotic pressure in the semidilute concentration regime:

$$\Pi = \frac{k_B T}{a_0^3} \phi_p^{9/4} \quad (\text{H.63})$$

The full expression for the osmotic pressure for dilute and semidilute concentrations is obtained by using this value of  $\zeta$  for  $C > C^*$  and adding the osmotic pressure that dominates in the dilute limit:

$$\Pi = \frac{CRT}{M} + \frac{k_B T}{a_0^3} \phi_p^{9/4} \quad (\text{H.64})$$

While derived in completely different ways, Eqs. H.49 and H.63 actually behave similarly in the concentration regime where they both apply. This is illustrated in Figure H.16., where these two expressions are compared for a specific combination of  $a_0$  and  $\chi$ .

### H.10.3 Typical Magnitude of the Osmotic Pressure

The fundamental pressure scale for water is the thermal energy,  $RT$  divided by the solvent molar volume,  $V_s$ . For water, we have (at 25 °C):

$$V_s = \frac{18 \text{ g}}{\text{mole}} \frac{10^{-6} \text{ m}^3}{1 \text{ g}} = 1.8 \times 10^{-5} \text{ m}^3 = 18 \text{ cm}^3 \quad (\text{H.65})$$

$$\frac{RT}{V_s} = \frac{(8.314 \text{ J/mole} \cdot \text{K})(298 \text{ K})}{3.0 \times 10^{-29} \text{ m}^3} = 1.4 \times 10^8 \text{ Pa} \quad (\text{H.66})$$

This pressure is relatively large. The actual osmotic pressure is obtained by multiplying by a prefactor involving the Flory-Huggins interaction parameter and the polymer volume fraction. Osmotic pressures of many atmospheres (1 atm =  $10^5$  Pa) can easily be obtained.

**11) Exercise:** What is the osmotic pressure of seawater?

**12) Solution:** The osmotic pressure arises from all of the dissolved salts in seawater. Typical concentrations are tabulated below.[19] The total concentration of all dissolved salts is 1.12 moles/kg, which after multiplying by the density of seawater ( $1025 \text{ kg/m}^3$ ) gives an overall salt concentration of  $1150 \text{ moles/m}^3$ . The osmotic pressure is obtained by multiplying this concentration by  $RT$ :

$$\Pi = (8.314 \text{ J/mol} \cdot \text{K})(300 \text{ K}) \left(1150 \text{ mol/m}^3\right) = 2.8 \times 10^6 \text{ Pa}$$

Species	moles/kg
H <sub>2</sub> O	53.6
Cl <sup>-</sup>	0.546
Na <sup>+</sup>	0.469
Mg <sup>2+</sup>	0.0528
SO <sub>4</sub> <sup>2-</sup>	0.0282
Ca <sup>2+</sup>	0.0103
K <sup>+</sup>	0.0102
Br <sup>-</sup>	0.000844
Sr <sup>2+</sup>	0.000091
F <sup>-</sup>	0.000068
<b>Total Ions</b>	1.12

## H.11 Equilibrium Swelling of a Neo-Hookean Material

Suppose a crosslinked material is immersed in a solvent (or exposed to solvent vapor) so that it swells isotropically, increasing its volume from an initial volume of  $V_{dry}$  to a final volume of  $V_{wet}$ . The amount of swelling that we get is determined by the concentration of network strands, which also determines the elastic modulus. So by measuring the swelling we can also obtain a reasonably accurate estimation of the shear modulus of the dry, unswollen polymer, which we refer to here as  $G_{dry}$ . The modulus of solvent-swollen material, which we'll call  $G_{wet}$  is also of interest in many applications. We'll start by assuming that the material was crosslinked at equilibrium, with the network strands obeying random walk statistics, so that the strain energy density is given by Eq. 6.10, with  $\beta = 1$  and  $G_{dry} = k_B T \nu_{el}$ :

$$\Delta f_d = \left( \frac{V_{dry}}{V_{wet}} \right) \frac{G_{dry} \{ \lambda_x^2 + \lambda_y^2 + \lambda_z^2 - 3 \}}{2} \quad (\text{H.67})$$

The factor of  $V_{dry}/V_{wet}$  accounts for the fact that as the volume of the gel increases due to solvent swelling, the concentration of network strands decreases accordingly. The extension ratios appearing in Eq. H.67 are referenced to the undeformed, dry elastomer. To calculate the shear modulus of the solvent-swollen elastomer we need to consider a deformation process that occurs in two steps: isotropic expansion of the gel to an equilibrium solvent-swollen state and shear deformation of this isotropically deformed gel.

### H.11.1 Equilibrium Swelling of the Gel

The geometry of an experiment used to measure the solvent swelling is shown in Figure H.17. The polymer sample of interest is placed in a sealed container

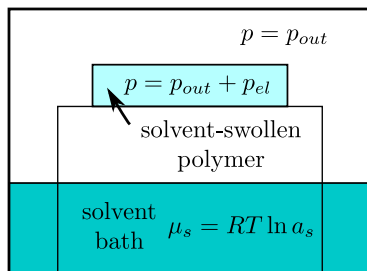


Figure H.17: Experimental geometry for obtaining the equilibrium swelling.

containing wither pure solvent (solvent activity,  $a_s$ , equal to 1), or a solvent diluted with soluble polymer to give  $a_s < 1$ . When water is the solvent the solvent activity is simply the relative humidity. Elasticity of the gel introduces an elastic pressure,  $p_{el}$  that limits the amount of solvent that is able to diffuse into the gel. To calculate this pressure we begin with the deformation free energy given in Eq. H.67, with the following values for the extension ratios and relative volumes of the dry and wet states:

$$\lambda_x = \lambda_y = \lambda_z \equiv \lambda_s \quad (\text{H.68})$$

$$V_{dry}/V_{wet} = \phi_p = \lambda_s^{-3} \quad (\text{H.69})$$

Here  $\phi_p$  is the volume fraction of polymer in the swollen gel.

A general expression for the equilibrium swelling is obtained by writing the deformation free energy for the swelling (step 1 in the previous subsection) in terms of the volume:

$$\Delta F_d = V_{wet} \Delta f_d = \frac{3V_{dry}}{2} G_{dry} \left\{ \left( \frac{V_{wet}}{V_{dry}} \right)^{2/3} - 1 \right\} \quad (\text{H.70})$$

The elastic pressure obtained directly from this expression by differentiating with respect to the sample volume:

$$p_{el} = \frac{\partial \Delta F_d}{\partial V_{wet}} = G_{dry} \left( \frac{V_{dry}}{V_{wet}} \right)^{1/3} = G_{dry} \phi_p^{1/3} \quad (\text{H.71})$$

The equilibrium polymer volume fraction in the gel is obtained by equating the solvent chemical potential in the solvent bath with the solvent chemical

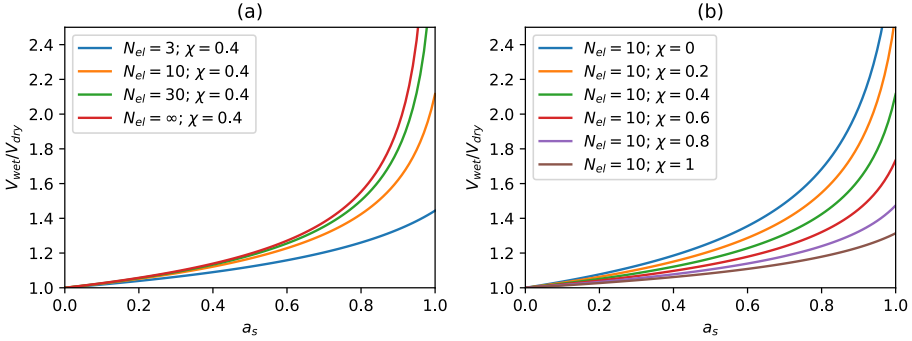


**Figure H.18:** Example swelling curves for a fixed value of  $\chi$  and different values of  $N_{el}$  (part a) and for a fixed value of  $N_{el}$  and different values of  $\chi$  (part b).

potential inside the gel, accounting for the elastic pressure,  $p_{el}$ . We illustrate the point here by using the Flory-Huggins expression for the solvent chemical potential, with  $N_p = \infty$ , since the polymer is crosslinked (see Eq. H.43):

$$\mu_s = RT \ln a_s = RT \left\{ \ln(1 - \phi_p) + \phi_p + \chi \phi_p^2 \right\} + p_{el} V_s \quad (\text{H.72})$$

The last term accounts for the fact that the pressure is larger inside the gel than outside the gel. This term involves the shear modulus of the dry material, equal to  $RT$  multiplied by the concentration of elastic strands in the network (Eq. 6.15, where we take  $\beta = 1$ ). This concentration can be expressed in terms of the average molar volume of a network strand,  $V_{el}$ . We further define  $N_{el}$ , an effective degree of polymerization of an elastic strand, as the ratio of  $V_{el}$  to  $V_s$ :

$$G_{dry} = v_{el} RT = \frac{RT}{V_{el}} = \frac{RT}{N_{el} V_s} \quad (\text{H.73})$$

Now we can combine Eqs. H.71, H.72 and H.17 to obtain an expression relating the solvent activity to  $\phi_p$ :

$$\ln a_s = \ln(1 - \phi_p) + \phi_p + \chi \phi_p^2 + \frac{\phi_p^{1/3}}{N_{el}} \quad (\text{H.74})$$

This equation can be solved numerically to obtain  $\phi_p$  (or its inverse, which gives the swelling ratio  $V_{wet}/V_{dry}$ ). Example curves of the swelling ratio obtained in this way are shown in Figure H.18.

### H.11.2 Shear Deformation of the Swollen Elastomer

Suppose that we now apply a shear strain to the swollen gel. The ,  $\gamma = \lambda_1 - \lambda_2$ , with  $\lambda_1\lambda_2 = 1$  and  $\lambda_3 = \lambda_s$  (see Section 6.1). For the swollen and sheared state we have  $\lambda_x = \lambda_s\lambda_1$ ,  $\lambda_y = \lambda_s\lambda_2$  and  $\lambda_3 = \lambda_s$ .

With these extension ratios we have the following expressions for volume ratio the free energy change from state 1 (the isotropically swollen state) to state 2 (the swollen and subsequently sheared state):

$$\Delta f_{1 \rightarrow 2} = \frac{G_{dry}}{2\lambda_s} \{ \lambda_1^2 - \lambda_2^2 + 2 \} = \frac{G_{dry}}{2\lambda_s} \{ \lambda_1^2 - \lambda_2^2 \} = \frac{G_{dry}}{2\lambda_s} \gamma^2 \quad (\text{H.75})$$

We differentiate twice with respect to  $\gamma$  (see Section 6.4) to obtain the shear modulus of the swollen elastomer:

$$G_{wet} = \frac{d^2}{d\gamma^2} (\Delta f_{1 \rightarrow 2}) = \frac{G_{dry}}{\lambda_s} = G_{dry}\phi_p^{1/3} \quad (\text{H.76})$$

Note that the elastic swelling pressure calculated from the previous section is equal to the shear modulus of the solvent-swollen polymer.

## References

- [1] Wikipedia, Matrix multiplication, [https://en.wikipedia.org/wiki/Matrix\\_multiplication](https://en.wikipedia.org/wiki/Matrix_multiplication)
- [2] B. McGinty, Coordinate Transforms, <http://www.continuummechanics.org/coordxfn.html>
- [3] Wikipedia, Mohr's circle, Wikipedia, the free encyclopedia.
- [4] Wikipedia, Speed of sound, [https://en.wikipedia.org/wiki/Speed\\_of\\_sound](https://en.wikipedia.org/wiki/Speed_of_sound).
- [5] Finite strain theory, Wikipedia.
- [6] Wikipedia, Torsion spring, Wikipedia, the free encyclopedia.
- [7] Laplace transform, Wikipedia.
- [8] Thermal Transitions of Homopolymers: Glass Transition & Melting Point, Tech. rep.
- [9] Differential Scanning Calorimetry, <https://www.pslc.ws/mactest/dsc.htm>.
- [10] K. Shull, Contact Mechanics and the Adhesion of Soft Solids, *Mat. Sci. and Eng. R.* 36 (2002) 1–45.
- [11] K. Johnson, *Contact Mechanics*, Cambridge University Press, Cambridge, 1985.
- [12] K. Johnson, K. Kendall, A. Roberts, Surface Energy and Contact of Elastic Solids, *Proceedings of the Royal Society of London* 324 (1558) (1971) 301–313.
- [13] X. Li, B. Bhushan, A review of nanoindentation continuous stiffness measurement technique and its applications, *Materials Characterization* 48 (1) (2002) 11–36. doi:10.1016/S1044-5803(02)00192-4.
- [14] A. T. Zehnder, *Linear Elastic Stress Analysis of 2D Cracks*, Vol. 62, Springer Netherlands, Dordrecht, 2012, pp. 7–32.
- [15] R. L. McSwain, K. R. Shull, Cavity Nucleation and Delamination During Adhesive Transfer of a Thin Viscoelastic Film, *J. Appl. Phys.* 99 (2006) 053533. doi:10.1063/1.2171770.
- [16] E. Kramer, Microscopic and Molecular Fundamentals of Crazing, in: *Adv. Polym. Sci.*, Vol. 52/53, 1983, p. 1.
- [17] H. F. Mohamed, E. Abdel-Hady, S. S. Mohamed, Temperature dependence of the free volume in polytetrafluoroethylene studied by positron annihilation spectroscopy, *Radiation Physics and Chemistry* 76 (2) (2007) 160–164. doi:10.1016/j.radphyschem.2006.03.026.
- [18] Teflon, Wikipedia, the free encyclopedia.
- [19] Seawater, Wikipedia, the free encyclopedia.



## Nomenclature

$\delta$	Compressive displacement.
$\delta_t$	Tensile displacement.
$\mathcal{G}$	Energy release rate
$\rho_c$	Crack tip radius of curvature
$A$	Contact area
$A_0$	Undeformed cross section
$b_c$	Minor axis of elliptical crack
$C$	Compliance
$C_0$	Flat punch compliance for a rigid punch with a circular cross section in contact with an elastic half space.
$d$	Distance from crack tip.
$E_r$	Reduced modulus
$f$	Reactive functionality - the number of times a given molecule can react in a step growth polymerization.
$G$	Shear modulus
$h$	Thickness of the compliant layer
$h_p$	Plastic zone size
$I$	Moment of inertia ( $\text{Kg}\cdot\text{m}^2$ )
$K_b$	Bulk modulus
$k_B$	Boltzmann's constant
$K_t$	Torsional stiffness
$P$	Compressive force.
$p$	Enumerate Reaction
$P_t$	Tensile force
$P_t$	Tensile force.
$W$	Work done on system
$T$	Absolute temperature

# Index

- Activation volume, 163
- Aromatic compounds, 191
- Atactic, 210
- Avogadro's number, 60
  
- Benzene, 191
- Berkovich tip, 109
- Birefringence, 244
- Block copolymers, 224
- Boltmann's Constant, 6
- Boltzmann superposition principle, 68
- Bulk modulus, 32
  
- Cauchy-Green deformation tensor, 28
- Chain Folding, 240
- Chain-Growth Polymerization, 202
- Characteristic ratio, 231
- Charpy impact test, 145
- Chemical potential, 250
- Chi parameter, 257
- Classification scheme, 186
- Considére construction, 130
- Copolymers, 223
- Correlation length, 272
- Covalent Bonding, 189
- Crack opening displacement, 142
- Crazing, 140
- Creep compliance function, 160
- Critical Point, 261
- Crosslinking, 211
- crystal period, 241
- Crystal Thickness, 240
- crystal thickness, 241
- Crystalline Unit Cells, 237
  
- Dashpot, 77
- Diblock copolymer, 224
- Dienes, 208
- differential scanning calorimetry, 92
- Double cantilever beam geometry, 119
- Dugdale Model, 142
  
- Eigenvalues, 22
- Elastomers, 187
- Energy release rate, 98
- Engineering stress, 8
- Entanglements, 71
- Epoxies, 193, 195
- Equilibrium Swelling, 275
- Extension ratios, 27
- Extent of reaction, 193
- Eyring model, 163
  
- Fiber torsion, 39
- Finger deformation tensor, 28
- Flory-Huggins Free Energy of Mixing, 258
- Fracture modes, 112
- Free Volume, 88
  
- Gauche configuration, 231
- Gel fraction, 197
- Gel point, 197
- gelation, 197
- Glass transition temperature, 88
- Glassy Polymers, 187
- Griffith model, 113
  
- Helix Formation, 235
- High impact polystyrene (HIPS), 142
- hydrolysis, 194
- Hydrostatic pressure, 23
- hydrostatic pressure, 32
- hyperbolic sine, 164
  
- Irwin model, 113
- Isotactic, 210
- Izod impact test, 145
  
- JKR equation, 109
  
- Kelvin-Voigt model, 83
- Kevlar, 220
  
- lamellar crystallites, 241

- Laplace transforms, 79  
 Lewis Diagrams, 189  
 Living Polymerizations, 210  
 Loss modulus, 67  
 loss tangent, 67, 75  
  
 Maltese cross, 244  
 Maxwell model, 70, 78  
     generalized, 82  
 Maxwell model - Generalized, 71  
 Modulus  
     reduced, 96  
 Mohr circle construction, 17  
 Mohr's circle  
     Strain, 30  
 Monomeric repeat unit, 234  
  
 Natural Rubber, 208  
 Neohookean model, 58  
 Neoprene, 216  
 Network, 197  
 Newman projection, 230  
 Non-Linear Step Growth Polymerization, 197  
 Nylon 6, 219  
  
 Occupied volume, 88  
 Osmotic Pressure, 267  
 Overlap concentration, 270  
  
 Poisson's ratio, 33  
 Poly(dimethyl siloxane), 222  
 Poly(ethylene oxide), 219  
 Poly(methyl acrylate), 215  
 Poly(methyl methacrylate), 215  
 Poly(phenylene oxide), 222  
 Poly(tetrafluoroethylene) (PTFE), 217  
 Poly(vinyl acetate), 218  
 Poly(vinyl chloride) PVC, 218  
 Poly(vinyl pyridine), 218  
 Polyamides, 193  
 Polybutene-1, 215  
 Polycaprolactam, 219  
 Polycaprolactone, 220  
 Polycarbonate, 221  
 Polychloroprene, 216  
  
 Polyesters, 193, 194  
 Polyethylene, 213  
 Polyethylene Terephthalate (PET), 221  
 Polyisobutylene, 216  
 Polypropylene, 214  
 Polystyrene, 217  
 prepolymer, 197  
  
 Random Walk in One Dimension, 46  
 Random Walk in Two Dimensions, 50  
 Reactive Functionality, 197  
 Reduced modulus, 96  
 Relaxation modulus, 65  
 Repeat units, 186  
 Rubber Elasticity, 54  
  
 Second virial coefficient, 269  
 Self avoiding Random Walks, 233  
 Shear modulus, 29  
 Shear viscosity, 63  
 Silicones, 222  
 Simple shear, 28  
 Sol fraction, 197  
 Sound velocity, 34  
 spherulite, 242  
 Spinodal curve, 260  
 Stability limit, 260  
 Stable Detachment, 100  
 standard linear solid, 82  
 Statistical copolymers, 224  
 Statistical segment length, 50  
 Step-Growth Polymerizations, 192  
 Storage modulus, 67  
 Strain, 24  
 Strains  
     Sample Displacements for Small Strains, 25  
     stress, 8  
     Stress intensity factor, 114  
     Stress invariants, 23  
     Structural repeat unit, 234  
     Syndiotactic, 210  
  
 Tacticity, 210  
 Teflon, 217  
 tensor, 9

Thermal expansion coefficient, 88  
Theta temperature, 264  
Tie molecules, 241  
time-temperature equivalence, 84  
Torsional Resonator, 75  
Trans configuration, 231  
Tresca yield criterion, 126  
True strain, 27

Ultem Polyetherimide, 222  
Undercooling, 245  
Unit cell, 237  
Unstable Detachment, 100

Vinyl polymers, 210  
Virial expansion, 269  
Viscoelasticity, 62  
Vogel equation, 72  
Von Mises stress, 127

Weibull distribution, 135  
Weibull modulus, 135

Young's modulus, 33

zero extension rate viscosity, 81  
zero shear rate viscosity, 81  
Zero shear viscosity, 70